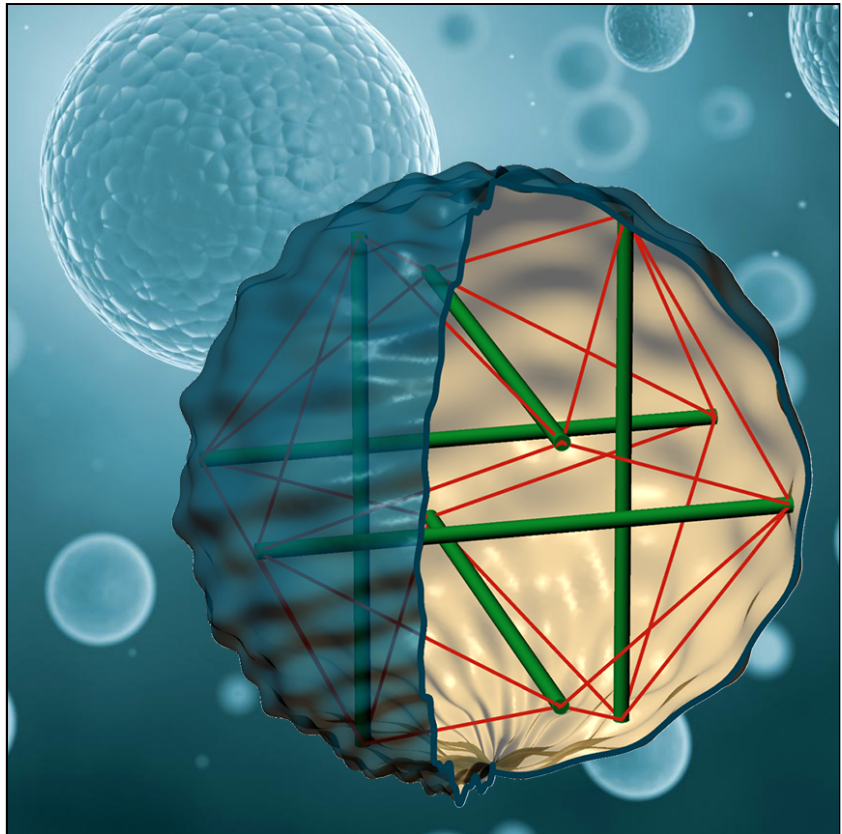




Stefania Palumbo

On the mechanical behavior of single-cell: from microstructural remodelling to macroscopic elasticity



Cells physical properties and functions like adhesion, migration and division are all regulated by an interplay between mechanical and biochemical processes occurring within and across the cell membrane. It is however known that mechanical forces spread through the cytoskeletal elements and reach equilibrium with characteristic times at least one order of magnitude smaller than the ones typically governing propagation of biochemical signals and biological phenomena like polymerization/depolymerization of protein microfilaments or even cell duplication and differentiation. This somehow allows to study as uncoupled many biochemo-mechanical events although they appear simultaneously and as concatenated. In this work, the complex machinery of the cell is hence deprived of its biochemical processes with the aim to bring out the crucial role that mechanics plays in regulating the cell as a whole as well as in terms of some interactions occurring at the interface with the extra-cellular matrix. In this sense, the single-cell is here described as a mechanical unit, endowed with an internal micro-architecture –the cytoskeleton– able to sense extra-cellular physical stimuli and to react to them through coordinated structural remodelling and stress redistribution that obey specific equilibrium principles. By coupling discrete and continuum theoretical models, cell mechanics is investigated from different perspectives, thus deriving the cell overall elastic response as the macroscopic projection of micro-structural kinematics involving subcellular constituents. Finally, some optimal arrangements of adherent cells in response to substrate-mediated elastic interactions with external loads are explored and compared with experimental evidences from the literature.

Stefania Palumbo earned Bachelor's and Master's degree in Biomedical Engineering at University of Napoli "Federico II" (Italy), in 2013 and 2015 respectively. She then continued her academic education by undertaking, in 2015, a Ph.D. program in Civil, Environmental and Mechanical Engineering at University of Trento (Italy), in collaboration with University of Napoli "Federico II". During the Ph.D. program, she spent a period (January-June 2016) at University of Pittsburgh and Carnegie Mellon University in Pittsburgh (PA, USA). Her research activity mainly focuses on Continuum Mechanics, Mechanics of Discrete Systems and Biomechanics, with particular attention to the theoretical modelling of the Cell Mechanics at different length scales.

UNIVERSITY OF TRENTO - Italy
Department of Civil, Environmental
and Mechanical Engineering



Doctoral School in Civil, Environmental and Mechanical Engineering
Topic 3. Modelling and Simulation - XXXI cycle 2015/2018

Doctoral Thesis - April 2019

Stefania Palumbo

**On the mechanical behavior of single-cell:
from microstructural remodelling
to macroscopic elasticity**

Supervisors

Prof. Luca Deseri - University of Trento (DICAM)
Prof. Massimiliano Fraldi - University of Napoli "Federico II" (DIST)



Except where otherwise noted, contents on this book are licensed under a Creative
Common Attribution - Non Commercial - No Derivatives
4.0 International License

University of Trento
Doctoral School in Civil, Environmental and Mechanical Engineering
<http://web.unitn.it/en/dricam>
Via Mesiano 77, I-38123 Trento
Tel. +39 0461 282670 / 2611 - dicamphd@unitn.it

ABSTRACT

Cells physical properties and functions like adhesion, migration and division are all regulated by an interplay between mechanical and biochemical processes occurring within and across the cell membrane. It is however known that mechanical forces spread through the cytoskeletal elements and reach equilibrium with characteristic times at least one order of magnitude smaller than the ones typically governing propagation of biochemical signals and biological phenomena like polymerization/depolymerization of protein microfilaments or even cell duplication and differentiation. This somehow allows to study as uncoupled many biochemo-mechanical events although they appear simultaneously and as concatenated. In this work, the complex machinery of the cell is hence deprived of its biochemical processes with the aim to bring out the crucial role that mechanics plays in regulating the cell as a whole as well as in terms of some interactions occurring at the interface with the extra-cellular matrix. In this sense, the single-cell is here described as a mechanical unit, endowed with an internal micro-architecture –the cytoskeleton– able to sense extra-cellular physical stimuli and to react to them through coordinated structural remodelling and stress redistribution that obey specific equilibrium principles. By coupling discrete and continuum theoretical models, cell mechanics is investigated from different perspectives, thus deriving the cell overall elastic response as the macroscopic projection of micro-structural kinematics involving sub-cellular constituents. Finally, some optimal arrangements of adherent cells in response to substrate-mediated elastic interactions with external loads are explored and compared with experimental evidences from the literature.

PUBLICATIONS

- M. Fraldi, **S. Palumbo**, A.R. Carotenuto, A. Cutolo, L. Deseri, N. Pugno. "Buckling soft tensegrities: fickle elasticity and configurational switching in living cells." In: *Journal of the Mechanics and Physics of Solids* 124 (2018).
- **S. Palumbo**, L. Deseri, D.R. Owen, M. Fraldi. "Disarrangements and instabilities in augmented one-dimensional hyperelasticity." In: *Proceedings of the Royal Society A: Mathematical, Physical and Engineering Sciences* 474 (2018).
- **S. Palumbo**, A.R. Carotenuto, A. Cutolo, L. Deseri, M. Fraldi. "Non-linear elasticity and buckling in the simplest soft-strut tensegrity paradigm." In: *International Journal of Non-Linear Mechanics* 106 (2018).
- **S. Palumbo**, A.R. Carotenuto, M. Fraldi. "Tensile integrity across the scales of the living matter: a structural picture of the human cell." In: *S&F_scienzaefilosofia.it* 19 (2018).
- **S. Palumbo**, A. Cugno, L. Deseri, M. Fraldi. "Nonlinear elasticity in 1D periodic structures with disarrangements." In: *AIMETA 2017 - Proceedings of the XXIII Conference of the Italian Association of Theoretical and Applied Mechanics*, L. Ascione, V. Berardi, L. Feo, F. Fraternali and A.M. Tralli (eds.).
- A. Cugno, **S. Palumbo**, L. Deseri, M. Fraldi, C. Majidi. "Role of Nonlinear Elasticity in Mechanical Impedance Tuning of Annular Dielectric Elastomer Membrane." In: *Extreme Mechanics Letters* 13 (2017).

CONTENTS

Abstract	vii
Publications	ix
Introduction	1
1 MECHANICAL PRINCIPLES OF LIVING CELLS BEHAVIOR	7
1.1 The cell as bio-chemo-mechanical unit	10
1.2 Whole-cell mechanics: tensile integrity rules cell structure	14
1.2.1 Remarks on tensegrity architectures	18
1.2.2 Cells as tensegrity systems	21
1.3 Cells orientation via cell-substrate elastic interactions . . .	29
1.4 Conclusion	34
2 TOWARD NONLINEAR SOFT-STRUT TENSEGRITIES FOR CELL MECHANICS	37
2.1 Hyperelastic models for deformable struts and cables . . .	39
2.1.1 Inconsistency of some linear constitutive models for highly deformable struts	39
2.1.2 Hencky-type cables and struts	44
2.1.3 Neo-Hookean cables and struts	46
2.2 The 2-element soft tensegrity paradigm	47
2.2.1 Characterization of the structure	48
2.2.2 Self-equilibria of the pre-stretched configuration . .	48
2.2.3 System's equilibria under off-axis perturbations . .	56
2.2.4 Further insights into the 2-element tensegrity mechanics	58
2.3 Conclusion	66
3 THE REVISED 30-ELEMENT CELLULAR TENSEGRITY PARADIGM	69
3.1 Equilibria at symmetry-preserving deformation states . .	72
3.1.1 Geometrical relations, compatibility and equilibrium equations	72
3.1.2 Internal (elastic) energies in symmetry-preserving configurations	77
3.1.3 Form-finding and energy storing in cell cytoskeleton	79
3.1.4 Symmetric responses of the cellular soft-tensegrity under external loading	82
3.2 Symmetry-losing equilibrium configurations	94

3.2.1	Competition of local buckling and global configura- tional switching in cellular tensegrity systems with bendable soft struts: form-finding and response to applied loads	96
3.3	Conclusion	101
4	MECHANOTROPISM OF ADHERENT CELLS VIA EXTERNAL POINT-LOADS	105
4.1	Boussinesq and Cerruti solutions for semi-infinite solids	107
4.2	Rationale and hypotheses underlying the model	110
4.3	Theoretical architecture of the model	112
4.4	Cell orientation guided by fences of normal point-loads	117
4.4.1	Effects of concordant perturbations	118
4.4.2	Effects of alternate perturbations	123
4.4.3	Remarks on the cell's pursuit of the maximum elon- gation	125
4.5	Conclusion	128
5	TOWARD MULTISCALE CYTOMECHANICS VIA STRUCTURED DEFORMATIONS	131
5.1	Fundamentals of structured deformation theory	135
5.1.1	Definition of structured deformation	135
5.1.2	Factorization of a structured deformation	136
5.1.3	Decomposition of stresses and constitutive assump- tions	137
5.2	SD-based paradigm of augmented 1D hyperelasticity	140
5.2.1	Bifurcation modes for the elementary system	143
5.2.2	Multi-modular structure under tensile load	146
5.2.3	Multi-modular structure under compressive load	157
5.3	Conclusion	163
	Conclusions	167
	 BIBLIOGRAPHY	 177

INTRODUCTION

Living cells are complex and dynamic systems constituting the units at the base of every biological organism [8, 19, 37]. Embedded in an entangled physical environment, *in vivo* animal cells are constantly subject to a wide variety of stimuli, including biochemical and mechanical signals and scaffolding alterations. However, while genetic informations and chemical factors have long been known to regulate cell behavior, only in recent decades mechanical cues and structural changes have been recognized to play an equivalent role in determining cellular biological processes, such as differentiation, proliferation, motility, apoptosis or even neoplastic mutations [8, 64, 106, 107, 146].

For example, it has been shown that *ex vivo* differentiation of stem-cells can be guided by the mechanical properties of the adhesion substrate [57, 62], that gradients of stiffness across the contact material can promote and direct adherent cells migration [124, 138, 197], as well as that the adhesion degree, the orientation and the collective organization of cells over deformable substrates can be sculpted as a combined effect of externally applied loads and medium mechanical properties [16, 57, 133, 176, 196, 197]. Since physical signals are easier to control and can be more permanent than biochemical or genetic manipulations, such observations are actually felt to pave the way to new methods and applications for regenerative medicine and tissue engineering. Also, particular interest has been registered in the literature for the measurement and the modelling of living cells mechanical properties, cell deformability moduli having been in fact recognized as indexes of the cell health state and the cell mechanotype having been identified as a label-free biomarker for diseases or cancer transformations related to alterations of the cell microstructure [23, 38, 84, 127, 156, 216, 217, 251]. On the other hand, solid tumours growth has been recently shown to be governed by microscopic cell-cell and cell-environment interactions whose dynamics are continuously affected by mechanical stress levels [27, 69]. All these findings seem then to allow to envisage new mechano-guided strategies for the therapy and the diagnosis of several pathologies and cancer diseases, different or complementary with respect to currently adopted biochemical and biomedical tools [68].

Despite significant qualitative and quantitative results provided by both experimental observations and theoretical modelling, the mechanical principles that govern the cellular feedback to physical input, thus moulding the cell development and functioning in a logic of dichotomy and complementarity with biochemical factors, are not fully understood yet. In this framework, the research activity described in the present thesis has been aimed to the theoretical study of some aspects of the cell mechanics at different length scales. This in fact represents an essential step to further investigate how the transmission and distribution of physical loads are eventually transduced into cascades of biochemical signals that in turn directly affect cell physiology and pathology [146].

As a matter of fact, *in vivo* cells continuously experience stresses and strains that, depending on the specific location and physiological environment, can occur in many different and combined forms, including shear, tension and compression, both of cyclic and static type [146, 213]. Additionally, adherent cells actively generate intracellular traction forces and transmit them to the surroundings at specific anchoring protein sites, in this way being able to probe and sense the environmental mechanical properties (e.g. elastic stiffness) [57, 88, 89, 101]. Under these mechanical stimuli, the cell firstly responds by shape deformation and stress modulation, according to structural and mechanical properties that it possesses as a physical entity [131, 147].

Among the several continuum and discrete models developed in literature [31, 106, 131, 147], the crossroad for properly describing such mechanical response and properties and for interpreting many underlying mechanisms regulating mechanotransduction dynamics of living cells [146, 239], has been offered in the 1980s by Donald E. Ingber's intuition, according to which cells might obey tensegrity principles [101, 104–106]. Tensegrity architectures are essentially discrete and elastic systems in self-equilibrium, made by floating (pre)compressed struts kept together by a continuous network of (pre)tensioned cables [149, 202]. Actually, several evidences have demonstrated that cell shape, structural stability and elastic stiffness are primarily provided by the cytoskeleton apparatus, which behaves like a tensegrity unit undergoing deformation and rearrangement of its elements (mainly actomyosin filaments and microtubules) and redistribution of internal forces when reacting to the mechanical stimuli coming from the extra-cellular microenvironment [101–103, 181, 210]. In static conditions, tensegrity-based cytoskeletal architectures have been previously studied by modeling actin filaments as linearly elastic tensed cables and microtubules as rigid [211] or as

elastic slender struts able to buckle under compression [35, 36, 232, 238]. However, experimental studies have shown that the cytoskeletal network can undergo nonlinear finite deformations and large displacements in the most of the cells physiological processes [74], such as spreading during adhesion and isolated or collective migration. In addition, recent works have highlighted the possibility that single as well as bundled actin filaments exhibit nonlinear constitutive behaviors [42, 136, 227, 228] and that intermediate filaments and other cytoplasmic proteins could act as lateral support for microtubules thus enhancing their capability to bear compression and delaying their buckling instability [17, 18, 129, 207]. Moreover, rough calculations lead to estimate discrepancies of less than one order of magnitude when comparing axial stiffness of actin filaments (cables) and microtubules (struts) [78, 106]. In the light of these observations, the present thesis addresses the modelling of novel hyperelastic and buckling soft-strut tensegrity systems, oriented toward a more faithful description of the cytoskeleton mechanical response under different types of (static) loading conditions and to the possible explanation of pre-stress-guided mechanisms exploited by cells for storing/releasing energy, for modulating their overall elasticity and shape and for directing instability-mediated configurational switching.

Together with the characterization of the whole-cell as a structural unit able to provide peculiar mechanical properties as well as inner remodelling and force redistribution under the direct action of external loads, essential element for understanding animal cells mechanobiology is to investigate the principles regulating their elastic interaction with environmental mechanical cues occurring at the interface with the extra-cellular matrix or with neighbouring cells [197]. Actually, as also highlighted above, adherent cells have been found to differently modulate morphology, arrangement and motility depending on the mechanical properties and on the stress and strain fields detected at the cell-environment interface, as an effect of their capability of active mechanosensing [29, 91, 176]. In this regard, several experiments have in particular revealed that orientation and positioning of *ex vivo* cells adhering to the surface of an elastic substrate, such as fibroblasts, can be guided by the application of selected external loads [32, 34, 134, 197, 213, 219, 234]. For example, it is commonly observed that uniaxial cyclic stretch/stress of the adhesion substrate induces cell reorientation along a direction nearly perpendicular to the loading one [219, 234], while static uniaxial solicitations generally promote the alignment of the cell axis with the loading direction [34, 134, 213]. However, despite several possible mechanisms and optimiza-

tion/homeostasis criteria have been supposed in the related scientific literature [14, 40, 41, 137, 194, 233, 249], the mechanobiological dynamics underlying the cell orientation process along preferred angles are still only partially understood. In this context, the present work provides a theoretical model exploring some optimal configurations assumed by adherent cells –described as dipoles of contractile forces– in response to substrate-mediated elastic interactions with *ad hoc* conceived regular patterns of external point-load solicitations. In this way a different strategy is also suggested for potentially driving the design of novel experiments aimed to investigate the mechanical principles of cell orientation.

Finally, in the research field about cell biomechanics and mechanobiology, the necessity of adopting multiscale and homogenization models has been largely recognized to the purpose of coherently and comprehensively describing cells mechanical properties and structural dynamics by overcoming some limitations related to classic continuum mechanics approaches [103, 181, 227, 252]. As a matter of fact, cell behavior arises as a result of complex kinematics and interactions occurring across hierarchical scale levels, from the one of the actomyosin cytoskeletal filaments undergoing sliding, folding/unfolding and disarrangement phenomena within their macromolecular structure [228, 252], up to the one of the overall cross-linked cytoskeletal network [73, 227, 252], in turn connecting all the other cellular sub-compartments like the plasma membrane and the nucleus. Based on these considerations, in this work, the theory of structured deformations [44, 47–49, 52, 159] is proposed as a possible instrument to effectively derive the macroscopic behavior of living systems as the projection of complex kinematics occurring at the lower scale of their microstructural components.

The present thesis is organized as follows. An overview on the research context of biomechanics and mechanobiology as well as on the mechanical principles underlying the cell behavior is provided in the chapter 1, together with a presentation of the aspects of the cell mechanics addressed here and of the related state-of-art. The chapter 2 is dedicated to the introduction of nonlinear and buckling soft tensegrity systems for applications to cell mechanics and to the adoption of these concepts for studying a 2-element tensegrity paradigm. The obtained results are then utilized in the chapter 3 for analyzing the mechanical properties and response exhibited by a revised 30-element cellular tensegrity paradigm, on the basis of that proposed by Ingber. Optimal orientations of an adherent single-cell, modelled as a force-dipole elastically interacting with special patterns of external forces, are explored in the chapter 4, while a first

model of augmented one-dimensional hyperelasticity with microstructural disarrangements, based on the structured deformations theory, is finally provided in the chapter [5](#) in the perspective of a multiscale modelling of the cell mechanics.

MECHANICAL PRINCIPLES OF LIVING CELLS BEHAVIOR

Human body is made of trillions of specialized eukariotic (i.e. provided with nucleus) cells, going from about 10 to 100 micrometers in size. These hierarchically organize and coordinate their physiological activities in order to form anatomically and functionally higher structures, namely tissues, which in turn form organs and, finally, whole individuals [37]. In this perspective, the single-cell can be seen as the structural and functional unit of the living (in particular, human) organisms [8, 19]. Therefore, the investigation of the mechanisms that determine the cellular behavior represents the cornerstone for the comprehension —and then, potentially, the prediction and the control— of biological phenomena occurring both at the cell scale, such as cell locomotion, proliferation, differentiation into specialized lines¹ or neoplastic mutations, and at the higher level of the assembled tissues, including morphogenesis, wound healing and diseases development.

As a matter of fact, research in cellular biology and medicine have been dominated by genetics and biochemistry for most of the past century, as long as, during its last (about) two decades, rapid developments in molecular biology techniques, DNA sequencing and mass spectrometry —widening the knowledge about genome and proteome— led to the realization that the DNA-encoded information was not sufficient to determine the final form of tissues and organs as well as that the cellular gene expression profiles and the action of biochemical cues (e.g. hormones or growth factors) could not explain alone how complex biological functions are carried out [8, 107]. Also, as a result of the advent of biophysical technologies enabling mechanical micromanipulation of cells and measurement of physical quantities at the cellular or even sub-cellular scales (e.g. micromanipulation with needles, magnetic bead twisting, traction force microscopy, optical tweezers, atomic force microscopy), it became increasingly evident that the mechanical interaction between a cell and its microenvironment, involving sensing and transmission of stress and strain signals, constitutes a crucial aspect in defining cell behavior and

¹ Cells can be classified into about 200 major types ranging from connective tissue cells through epithelial and muscle cells to nerve cells [19].

hence tissues and organs morphology, physiology and pathology [8, 46, 64, 86, 106, 107, 217].

The idea that physical forces can regulate tissue development was already articulated at the end of the nineteenth-century: in 1892, the surgeon and anatomist Julius Wolff first postulated that bone tissue adapts its structure to the mechanical environment and, in particular, to changes of the state of stress, based on the observation that trabeculae match the principal stress lines in bones caused by daily physical loading [64, 146]. This concept, known as Wolff's law, stands today as perhaps the earliest recognized example of the ability of living tissues to sense mechanical stress and respond by tissue remodeling. Also, at the beginning of twentieth century, in 1917, the mathematical biologist D'Arcy Thompson published his book *On Growth and Form* [223], in which he provided an archival description of how biological forms are shaped by developmental changes and correlated to mechanical phenomena.

Since these first insights, mainly oriented to the whole-tissue scale, the mechanical bases involved in organizational principles and regulatory mechanisms at the cellular level have been unveiled as primary and essential factors controlling biological functions [71, 146, 235]. Several works have indeed confirmed that the cell's structural arrangement and properties as well as the cell-material physical interface –including geometry, sensing of mechanical (e.g. elastic) properties and transmission of forces– contribute to determine living cells fate and tissue functioning as chemicals and genes and that the same biochemical signalling can have different effects on cells when their internal structure or the mechanical aspects of their environment are altered [29, 57, 196, 197]. The human cell has been thus progressively revealed as a complex biological entity whose behavior is the result of an interplay between biochemical and mechanical events developing across different spatial and temporal scales [64, 107].

In this context, *biomechanics* configures as the branch of science aimed to study the structural and mechanical aspects of biological systems at any scale, from whole organisms to organs, cells and cell organelles, by *de facto* using laws and methods of mechanics [37, 71]. Adjoining it, *mechanobiology* has recently emerged as a new discipline at the interface among biology, physics and engineering, dedicated to the study of how physical forces and changes in the mechanical and structural properties at the level of cells, extra-cellular matrix (ECM) and overall tissues impact a wide variety of biological processes across the hierarchical scales of

the human organism, from cell life-cycle to tissue remodelling and mass homeostasis, or complex inflammatory cascades [130, 148, 168, 186].

In particular, within these fields, novel nanotechnology techniques and experimental tools have been provided and several theoretical models have been proposed in recent years to the aim of gaining new insights into the *cytomechanics* and into the mechanical principles driving the so-called processes of cellular *mechanosensing* and *mechanotransduction*. These denote, together, the cell capability of sensing and responding to external mechanical properties and physical stimuli (namely surrounding stress and strain cues) by reorganizing its internal heterogeneous structure and distribution of forces, remodulating its physical properties and then transducing this reaction into a cascade of biochemical signals, in turn regulating cell functions or possibly inducing diseases and pathological alterations.

Examples of cellular mechanosensing and mechanotransduction and of their effect at the tissue level are provided, among disparate others, by the alignment of endothelial cells in the direction of stress, first observed in studies of arterial wall morphology [155] and later demonstrated in controlled *in vitro* experiments [55], by the calcification in the heart valve tissue in response to pathological solid and fluid cellular mechanical patterns and by the bone loss in microgravity [146]. Further examples are given by the migration of adherent cells induced by stiffness gradients in the contact medium [138], by the cells reorientation processes driven by static and cyclic mechanical forces applied to the adhesion substrate [28, 40, 197] as well as by the differentiation of stem cells towards specific lines as a function of the elastic or adhesive properties of the culture substrate [62] and of the sensed stress and strain distributions (e.g. mesenchymal stem cells differentiate into an osteogenic phenotype when subjected to low levels of strain [146, 199], but into a cardiovascular lineage at higher strains [146, 192]).

From a physical point of view, the capacity of mechanical sensing and controlled response to environmental signalling is related to the ability of cells to passively sustain mechanical forces by undergoing deformative processes but also to actively generate internal contractile forces and transmit them, upon adhesion, to the surroundings [64, 106, 197, 239]. Actually, the latter finding was first revealed in 1980s by Harris and coworkers with regard to fibroblasts from connective tissue that, cultured on soft polymer substrates, wrinkled the substrate surface [88, 89]. As a matter of fact, this represents a necessary requirement for the cells to interact with their microenvironment in a way to probe, by pushing

and pulling, its mechanical properties and stress/strain distributions: as an example, for rigidity sensing, the cell must actively strain the neighbourhood to test its elastic response in terms of deformability [57, 197].

The foundations of the cellular mechanical behavior and the structural and biochemical bases of the force generation and transmission in cells are briefly recalled in the next section [64, 146, 197].

1.1 THE CELL AS BIO-CHEMO-MECHANICAL UNIT

From the mechanical standpoint, independently of the specific cell line, human cells (schematized in figure 1.1A) are similar and provided with the same mechanically relevant components –i.e. the plasma membrane, the cytosol, the nucleus and the cytoskeleton– which together contribute to determine the cascade of mechanobiological events at the basis of the cellular behavior [8, 19, 37, 197].

In particular, the plasma membrane is an about $10nm$ thick and very deformable lipid bilayer (about $0.1-1 kPa$ in stiffness) surrounding the cell and acting both as its physical confinement and as site of interaction with the external environment, since it embeds transmembrane protein complexes that mediate the cell's outside-in and inside-out mechanical and biochemical signalling.

The cytosol is a viscoelastic gel-like matrix filling the inner cell volume where many intracellular signal transduction pathways develop; it imprisons the nucleus and the cytoskeleton as well as all the cell's proteins and organelles, the latter being generally membrane-bounded cellular subunits having specific functions, such as the mitochondria, the endoplasmic reticulum or the Golgi apparatus.

The nucleus is an highly specialized spherical-shaped organelle, with radius of the order of few micrometers depending on the overall cell size, in which much of the cell mass is concentrated; it can be identified as the control center of the cell's activities since it contains –surrounded by a nuclear membrane– the most of the genetic material (DNA) and hence regulates the gene expression that is the basis of the protein biosynthesis driving all cellular functions.

Finally, the cytoskeleton is a biopolymeric scaffolding architecture that extends throughout the cell and interconnects all the intracellular structures both mutually and, by binding to the proteins across the plasma membrane, to the extracellular material (see figure 1.1B). It *de*

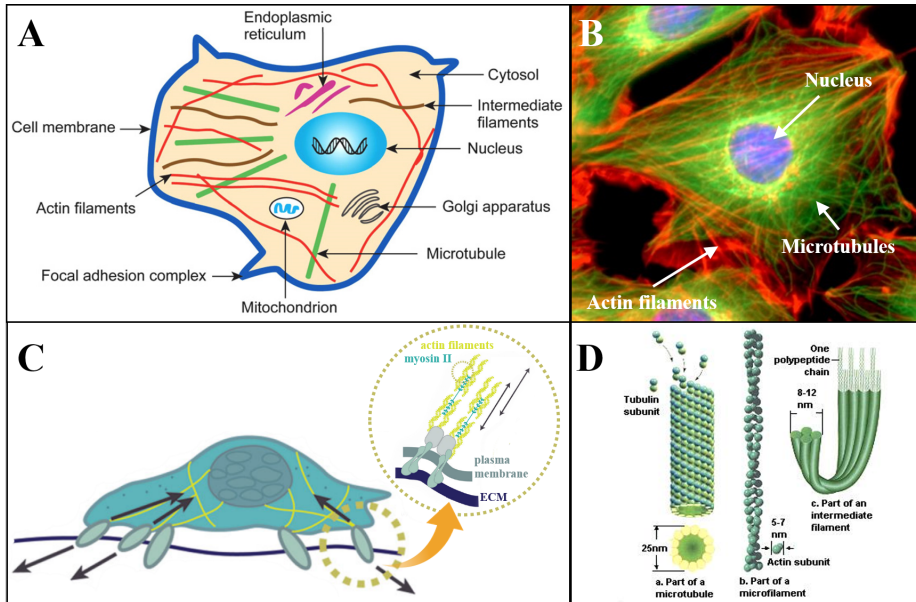


Figure 1.1: **A)** Schematic illustration of the subcellular structure of a typical eukaryotic cell. The image is reproduced from [217]. **B)** An immunofluorescence image of a 3T3 mouse fibroblast cell showing nuclear DNA (blue), cytoskeletal actin microfilaments (red) and alpha-tubulin forming cytoskeletal microtubules (green). The image is reproduced and adapted from [217]. **C)** Picture of a cell adhering to the extra-cellular matrix (ECM). The cell internally generates contractile forces by means of an ATP-driven sliding mechanism between actin filaments and myosin II protein motors and transmit them to the ECM via transmembrane protein complexes, known as focal adhesions. The image is reproduced and adapted from [86]. **D)** Schematic illustrations of the structures of the three basic components of the cytoskeleton of eukaryotic cells, namely microtubules, actin microfilaments and intermediate filaments from the left to the right.

facto represents the main load-bearing component of the cell-unit, primary governing its shape, structural integrity, mechanical stability and deformation response, and assumes a fundamental role in mechanosensing and mechanotransduction processes by actively generating cellular forces and by mediating force transmission both within the cell and at the cell-environment interface [101, 235].

More in detail, the cytoskeletal apparatus consists of an entangled viscoelastic network of filamentous biopolymers spanning large distances

within the cell, namely actin microfilaments, microtubules and intermediate filaments (see figure 1.1D), which mutually interconnect by means of various cross-linking proteins. By undergoing a continuous dynamic remodeling during which individual monomers can be added (polymerization process) and removed (depolymerization process), by interacting with motor proteins that can actively convert chemical energy into mechanical work (such as myosins, dyneins and kinesins) and by passively reorganizing in response to externally applied forces, these filaments regulate cell structural arrangement, mechanical integrity and properties as well as spreading and motility activities [103, 106, 177, 210, 217]. In particular, microtubules are polymers comprised of proteins called tubulins, which polymerize to form structures organized as hollow tubes of about 25 nm of outer diameter and about 14 nm of inner diameter, whose elastic modulus is on the order of 10^3 MPa [78, 106]. Vimentin, keratin and lamin protein monomers assemble instead to form intermediate filaments, which have typical diameters around 10 nm and can be regarded as the softest and most extensible of the cytoskeletal filamentous proteins, with 10^0 – 10^1 MPa in elastic stiffness, thus giving prominent contribution to the whole-cell elasticity only when cells are highly strained [106]. Finally, actin microfilaments are constructed from actin monomers polymerization and may be regarded as two parallel protofilaments wound together in a right-handed helix of diameter on the order of 7–9 nm and Young modulus on the order of 10^3 MPa [78, 106].

As a matter of fact, cellular contractile forces arise, both in muscle (cardiac, skeletal and smooth) and nonmuscle cells [146], from the interaction of the cytoskeletal actin microfilaments with the (predominant) class II of the myosin superfamily, i.e. myosin II (see figure 1.1C) [19, 86]. Specifically, when actin filaments physically associate with myosin motor proteins at their respective complementary binding sites, active tension is generated through a process that converts chemical energy into mechanical forces by means of a sliding mechanism of the myosin proteins heads along the actin filament, activated by hydrolysis of adenosine triphosphate (ATP). As a result of this action, the assembled actin-myosin contractile filaments make the cytoskeleton an actively pre-stressed structure, namely the force-generating apparatus of the cell [88, 101, 200]. It also worth to note that multiple actomyosin filaments generally align in parallel and assemble together –linked by actin binding proteins– during cell adhesion process, in this way forming increasingly thicker, oriented and stable bundles known as stress fibers, which have a much larger

diameter ($0.2\text{--}1\ \mu\text{m}$) but lower elastic modulus (order of $10^3\ \text{kPa}$) than individual actin filaments [42].

The pre-stress thus generated within both individual actomyosin filaments and stress fibers is then transmitted to the other entangled components of the cytoskeletal lattice (namely microtubules and intermediate filaments) and, in turn, from the whole cytoskeleton to all the cellular structures that it interconnects, from the plasma membrane to the sub-cellular organelles, including the nucleus [101]. Additionally, as well as being distributed throughout the cell, the cytoskeletal pre-stress is transmitted by the cell to the surroundings (see figure 1.1C) in the form of traction forces that act at specific cell anchoring sites across the cell membrane, known as focal adhesions [46, 75, 76, 195]. In fact, normal tissue cells –with the exception of blood cells– are anchorage-dependent [57], that is, they are not viable when suspended in a fluid and need to adhere to a solid. Therefore, in *in vivo* tissues, cells are generally coupled to an outside multicomponent gel-like network, named extra-cellular matrix (ECM), by means of transmembrane protein (principally integrin) adhesion receptors [3, 197]. These progressively assemble during cell adhesion process to form sufficiently large and stable clusters, namely the above-mentioned focal adhesions [7], which bind cytoskeletal actin filaments or bundles on the inner side of the cell membrane while outside anchor to specific (complementary) protein ligands, such as collagen or fibronectin, embedded by the ECM, in this way mediating the force exchange at the cell-environment interface [12, 75, 76].

By means of this active system of internal generation and inner as well as inside-out transmission of forces, the cell is able to mechanically probe the adjacent material and hence to sense its elastic properties and force and deformation fields (cellular mechanosensing [29, 57]).

Actually, together with internally and actively generated contractile forces, the cell also experiences a passive pre-stress and is subjected to stress and strain solicitations coming from the outside [14, 106, 197]. In particular, the first is essentially a result of the adhesion process, which leads the whole-cell from an approximatively round shape to a spread configuration in which the cytoskeleton is highly stretched, while the second can be for example due to traction forces exerted by neighbouring cells and sensed through the ECM, or related to physiological loading conditions, such as heart beating for cardiomyocytes, pulsating blood flow for epithelial cells in vessels, etc. As a consequence, an outside-in force transmission path also develops at the cell-environment interface through focal adhesions, which induces coordinated deformation and

structural rearrangement of the cytoskeletal network and a redistribution of the internal loads that in turn spread to the nucleus and to the other intracellular anatomical sites [101, 106].

As a result of the described cytoskeleton-orchestrated mechanisms of active generation and passive transmission of mechanical forces and of remodelling of its heterogeneous sub-compartments, the cell is able to exhibit an integrated mechanical behavior and peculiar physical properties (e.g. elastic and viscoelastic moduli) in response to changes of the external mechanical fields. Then, by means of mechanotransduction processes, the microstructural and mechanical response is transduced into cascades of biochemical signals that directly drive the cells functions, such as division, differentiation, motility or apoptosis: in this way, cell mechanics assumes an active and substantial role in determining cellular biology. In this regard, by way of example, it is worth to mention some of the known or hypothesized molecular mechanisms regulating mechanotransduction. Among them, thermodynamics shows that the events of polymerization and depolymerization of the cytoskeletal filaments [210] as well as the clustering of integrins into strong focal adhesion sites [7, 184] are influenced by the elastic stresses that these molecular systems support, an increase of tensile (compressive) forces in fact decreasing (increasing) their chemical potential relative to the molecular reservoir of free, non-assembled, monomers and thus promoting polymerization (depolymerization). Also, many of the postulated mechanisms for mechanotransduction rely on mechanically induced protein conformational changes or domains unfolding as promoters of phosphorylation, altered enzymatic activity or binding, or other biochemical events that can lead to activation of a biochemical signalling cascade [146]. Finally, direct effects of mechanical loads on nuclear mechanotransduction and gene expression [116, 230, 239] have also been considered: for example, distortion of ion channels within the nuclear membrane –induced by forces propagated from the cell surface to the nucleus by means of the cytoskeletal pathway and leading to an increase in pores dimension– stimulates calcium entry and induces associated gene transcription.

1.2 WHOLE-CELL MECHANICS: TENSILE INTEGRITY RULES CELL STRUCTURE

Biomechanics and mechanobiology of cells, tissues and organs have been extensively investigated in the last decades through both experimental

and theoretical approaches, with the aim to understand the principles and the dynamics according to which mechanical events and cascades of chemical signals evolve, correlate and transmit across the hierarchical scales of the living matter, thus determining every its physiological and pathological process, as highlighted above.

In this framework, the observation that transmission of mechanical forces throughout the cell and deformative responses occur with characteristic times that are at least one order of magnitude smaller than the ones typically governing diffusion of biochemical signals and biological events like polymerization/depolymerization of protein filaments or cell duplication and differentiation [197, 239], allows to study as uncoupled biochemical and mechanical processes in many cases. On these bases, the development and the application of physical and engineering models, having their roots in the theory of mechanics of materials and structures, have provided and still provide a great contribution to the investigation of complex biological behaviors characterizing the human organism at multiple length scales, both in health and disease, by complementing biochemical and biomedical know-how, models and methods. However, if tissue-level mechanics has achieved a relatively consolidate basis from many points of view, the same does not hold true with reference to the cellular scale, *de facto* the theoretical modelling of the single-cell mechanics still remaining an open issue [37, 71, 100, 197].

A crucial aspect towards the comprehension of the living cells mechanical behavior is represented by the qualitative and quantitative characterization of the whole single-cell as a physical unit able to provide specific mechanical properties and stress/strain responses when subject to stimulation and/or perturbation via direct action of external loads. This is an essential step both because shape and mechanics are involved in driving basically all the main cellular functions and because, under a hierarchical perspective, the mechanical response of individual cells contributes to determine the structural integrity and the physical properties of whole tissues. For example, diverse tissues provide different mechanical responses –compatible with the biological role for which they are designated within the organism– since they contain specific cell types exhibiting peculiar shapes and mechanical features, which assemble by observing certain supracellular organization and equilibria: e.g., for these reasons, brain tissue is softer than muscles and muscles are softer than skin [57].

Moreover, since the cells elastic and viscous responses mainly rely on the cytoskeleton structure and function as generator and conveyor

of forces, cellular deformability can be *de facto* regarded as a measure of the cytoskeleton integrity, connectivity and contractility status and, hence, of the cell physiology. Abnormalities in elastic stiffness of cells are indeed often recognized as signs of molecular and structural intracellular alterations related to pathological states of individuals cells or diseases in tissues, such as cancer [84, 216], inflammation and sepsis [188], asthma [66] and malaria [23, 143, 216]. For example, experimental studies recently performed on single cancer and healthy cells have demonstrated that the former are about 70% softer than the latter, regardless of the cell lines and the measurement technique used for determining the mechanical properties [38, 68, 114, 127]. It seems that the increase in cell deformability and flexibility is directly related to cancer progression, as observed in the case of a transformed phenotype from a benign (non-tumorigenic) cell to a malignant (tumorigenic) one, and that metastatic cells could be induced to become mechanically softer than healthy ones to the aim of passing through narrow rigid capillaries and gaining, in this way, improved migration capabilities that lead to the formation of new (dislocated) neoplastic foci and hence promote tumour expansion [114, 161, 172]. On these bases, cell mechanotype is emerging as a label-free biomarker for diseases pathogenesis and progression in cells and tissues and, in particular, as a potential biomechanical instrument for enhancing cancer diagnoses and therapy [156, 251]. In fact, at least in principle, the difference in cell stiffness might be exploited to create mechanical-based oncological targeting strategies for discriminating neoplastic transformations within human cell populations as well as for designing innovative tools –complementary to cell-specific molecular procedures– for the clinical treatment of cancer diseases [68].

Within the described context, numerous experimental techniques have been developed to measure single-cell mechanical properties (such as atomic force microscopy, micropipette aspiration and optical stretching) [8, 26, 63, 121, 156, 222, 251, 255] and a wide variety of theoretical models has been advanced in order to qualitatively and quantitatively explain the mechanical and mechanobiological cell response to alterations in shape and surrounding physical environment as emerging from the experimental results [147, 217].

Single-cell mechanical models can be principally distinguished between continuum-based and micro-/nano-structural (discrete) ones, the main differences between the two classes being essentially related to their respective purpose and length scale of interest.

As a matter of fact, the underlying assumption for treating materials—in this case, cells—as continua is that the smallest length scale of interest is significantly larger (at least one order of magnitude) than the dimensions of the microstructure, namely than the distance over which cellular structure and properties may vary. In such a case, averaged constitutive laws, generally derived from experimental observations, can be applied to the whole cell or to cellular compartments (e.g. cellular membrane, cytoplasm and nucleus) at the macroscopic level and the predictions of the model strictly depends on the suitability of the chosen stress-strain relations. Depending on the dynamic time scale of interest, such continuous stress-strain relations can be elastic, viscous or viscoelastic with different complexity. In particular, solid (elastic and viscoelastic) models, cortical shell-liquid core descriptions, fractional derivative approaches providing power-law structural damping (soft-glassy-material-like behaviors) as well as multiphasic (e.g. fluid-solid) models have been adopted in literature for theoretically catching stress and strain patterns induced within the cell by physiological or experimental perturbations (e.g. erythrocytes and neutrophils undergoing deformations while passing through narrow capillaries or as an effect of micropipette aspiration) and the mechanical properties of the whole-cell and its compartments. An extensive discussion about these models can be found, among other, in [131, 147].

However, while continuum approaches can be helpfully adopted at meso-/macroscopic scales, they appear less useful when one aims to investigate the way in which mechanical stresses and strains induced on cells are transmitted and channelled throughout its discrete cytoskeletal micro-architecture and distributed to sub-cellular components or if the interest is to understand how internal forces govern the cell behavior by modulating the pre-stress level in the cytoskeletal fibers and in turn influencing the overall cell actual stiffness, stored (internal) energy, adhesion and migration mechanisms as well as mechanotransduction signaling. In these cases, in which the length scale of interest is comparable to the structural features of the system under study, micro-/nano-scale and discrete models need to be implemented. In particular, these approaches allow to define specific molecular pathways for mechanical force transmission and sensation by recognizing in the cytoskeleton the main mechanical regulatory machine of the cell, governing its shape and stability by bearing (both passive and actively generated) pre-stress and guaranteeing to the cellular unit the ability to mechanically respond to external loads through a coordinated structural rearrangement of its biopolymeric elements [106, 221, 249, 250]. In this perspective, micro-

/nano-structural descriptions generally identify the overall cell with its cytoskeletal architecture, by modelling it as a discrete mechanical network. Several models have been proposed within this class, both for suspended and for adherent cells, which comprise open-foam cell examples, pre-stressed cortical membrane descriptions, tensed cable net and affine models and tensegrity-based characterizations, which are reviewed, for example, in [31, 106, 147]. Among these, models built on the idea that the cytoskeleton might configure as a tensegrity system to structure and stabilize itself and the whole-cell apparatus and to optimally sense and respond to physical forces [101, 104, 105], seem to have offered the crossroad for consistently interpreting and integrating several aspects of the mechanical behavior of living cells [101, 103–105, 238]. Therefore, in the following, the principles that underlay this form of architecture and its resulting features are summarized. Then, the evidences indicating the use of such building system by cells are provided, together with an introduction to the tensegrity-based cellular mechanical models available in literature.

1.2.1 *Remarks on tensegrity architectures*

The term *tensegrity* originates from the contraction of *tensional integrity* and was first coined by the architect Richard Buckminster Fuller in the early 1950s to describe structures that gain their stability and integrity through a pervasive tensional force, rather than through continuous compression as used in most manmade (e.g. brick upon brick) type constructions [20, 149, 202]. The same Fuller identified tensegrity systems as “islands of compression in an ocean of tension”. Starting from this description, tensegrity structures (see figure 1.2) can be more prosaically described as systems living in a stable *self-equilibrated* mechanical state resulting from the interaction of a discontinuous set of compressed components (*struts*) with a continuum of tensed elements (*cables*) [149, 202]. This concept hence implies that all the structural members already experience an internal state of stress –i.e. a state of *pre-stress*– before the application of any external force. Then, the amount of pre-stress stored by these architectures modulates –along with the intrinsic rigidity of the structural components– their overall stiffness and shape and, in turn, their response to external loads. In absence of pre-stress, these structures become instead unstable and collapse under mechanical solicitation, their intrinsic resistance to shape distortion vanishing in this case. Moreover,

since –according to tensile integrity principle– tension is continuously transmitted across all the structure, the application of a local force to one of the members results in an integrated geometric rearrangement and a coordinated change of internal stress of all the members, in a way to restore the global equilibrium of the system without compromising its physical integrity [106, 149, 202].

The simplest embodiment of a tensegrity force balance can be seen in the sculptures by Kenneth Snelson, the first to actually create a self-stabilizing "floating-compression structure", which are composed of a network of highly tensioned cables interconnected at the ends by a series of isolated (i.e. not touching) compressed struts in the form of free-standing metal columns (as in the examples given in figures 1.2A and 1.2B). Therein, the tension in the cables pulls in on the ends of each

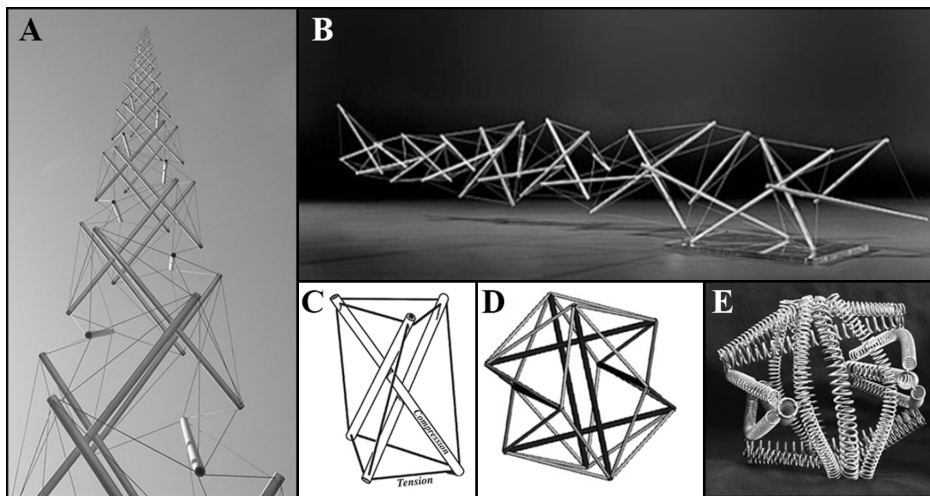


Figure 1.2: **A)** and **B)** Examples of tensegrity sculptures by Kenneth Snelson (known as the "Needle tower" and the "Easy-K", respectively) composed of rigid aluminum struts suspended by tensed stainless steel cables. These structures are composed of multiple tensegrity modules interconnected by similar rules. **C)** Schematic representations of the tensegrity force balance in a simple self-stabilizing tensegrity network composed of three compression struts interconnected by a continuous series of tensed cables. Finally, a spherical tensegrity configuration composed of 6 struts and 24 cables constructed with **D)** struts and cables, or **E)** using springs with different elasticities [146].

strut, thus compressing it, whereas the struts push out and tense the web of cables (see figure 1.2C). However, in general, rigid elements are

not strictly required, because similar structures can be constructed from flexible springs that simply differ in their elasticity arranged in a way to generate a stabilizing pre-stress in the entire network (see figures 1.2D and 1.2E) [106, 146]. It is also worth highlighting that having distinct tensile and compressive elements in a structure does not itself indicate that it is a tensegrity: a proper placement of the pre-stressed elements is in fact essentially required in order to determine a geometrical configuration in which synergy between tension and compression can be established in the sense that the subset of compression elements oppose and balance forces in the tension ones thus creating a stabilized system in the space.

The discrete geometrical configuration and the peculiar working principle confer to tensegrity systems remarkable properties [201] that make them suitable for applications in several fields, from civil engineering and architecture –from which they originate [20, 203]– to aerospace and robotics [24, 135, 166, 224]. As a matter of fact, by virtue of the specific relations among their components, tensegrities possess deployable capabilities and are able to support large displacements as a consequence of the floating spatial organization of the compressive elements, this feature offering advantages in portability, mobility and functionality. On the other hand, the pre-stress harboring throughout the structural network directly influences the overall stiffness and the stored elastic energy, this allowing to use it as a parameter that can be opportunely modulated to tune the mechanical behavior of the global system and to guarantee its adequate/desired response to static and dynamic external loads. Also, since tensegrity principles and properties largely rely on the geometrical arrangements of the elements, they are applicable from small- to large-scale units. This provides, among other, the possibility of combining multiple basic tensegrity modules by using similar rules (i.e. establishment of tensional integrity) to form more complex –eventually nested and hierarchically assembled– tensegrity structures, in which mechanical forces are transmitted along specific paths that extend across multiple size scales. In this way, while disruption of a single element in a minimal tensegrity can result in the destabilization of the entire structure, in these multimodular tensegrities, individual tensegrity components can be disrupted without compromising the integrity of the overall system. Furthermore, in multi-modular and hierarchical tensegrity structures, stress can be properly focused on selected distant sites according to the geometric forms of these discrete structures and force application to a single element results in a redistribution of forces and rearrangement of elements that can span across long distances and size scales throughout

the tensionally-integrated system, with an efficiency of the long-distance force transfer determined by the level of pre-stress [106, 181, 239].

As well as in man-made applications in the engineering field, the structural principles and the above-mentioned properties of tensegrities are exploited by several systems in nature, these including spider webs, gas-liquid foams, plant leaves and mammalian lungs [106, 202]. For example, in the case of foams, leaves and lungs, the pre-stress is provided by the pressure of the inflating fluid (the compression element in lieu of rigid struts) and is carried by lattice tension elements (e.g. liquid films in foams). In spider webs, the pre-stress is instead provided by discrete attachments to surrounding objects, such as tree branches, and is balanced by tension in web threads: in this case, the web and the tree branches represent the tension and the compression elements of an integrated mechanically stable whole, respectively.

Finally, tensegrity rules seem to play a fundamental role in governing the mechanical behavior of living systems, by driving the channelling of forces across the multiple size scales in the hierarchy of life –i.e. from whole (macroscopic) organisms to individual (nanoscopic) molecules and *vice versa*– and thus filtering the mechanotransduction processes. It is in fact known that tensile integrity principle is used in the way in which pulling forces generated in muscles and resisted by (compressed) bones produce isometric tension (i.e. muscle tone) that stabilizes the shape of our bodies. On the other hand, at the micro-scale, the cell cytoskeleton appears organized as a tensegrity whose pre-stress reservoir is used, as an example, to initiate the processes of cell remodelling and migration [101, 103, 106, 146, 210]. Also, these mechanisms are hierarchically connected at the sub-cellular (multi-molecular) scale, where the cytoskeletal actin filaments result themselves to behave as tensegrity chains, in which elastic energy and stress are released/accumulated in order to modulate contractility by means of depolymerization/polymerization reactions [141]. Finally, recent works also show how tensegrity units can be recognized at the level of individual molecules and atoms [106, 181].

1.2.2 *Cells as tensegrity systems*

The theory of tensegrity in molecular biology has been developed by the biologist and bioengineer Donald Ingber in the 1980s to explain the structural organization and the mechanical behavior of cells [101, 104, 105, 147]. He first proposed that living cells could behave as tensegrity architectures

based on the experimental observation that, just like a tensegrity, the cytoskeleton operates as a discrete network under mechanical pre-stress [88, 89], in this way stabilizing the shape and governing the mechanics of the overall cell system [237]. Pre-stress is in this case both actively and passively generated and maintained through the establishment of a complementary force balance among the cytoskeletal biopolymers and the extracellular tethering sites to the ECM (the focal adhesions) and to other cells [101, 103, 210].

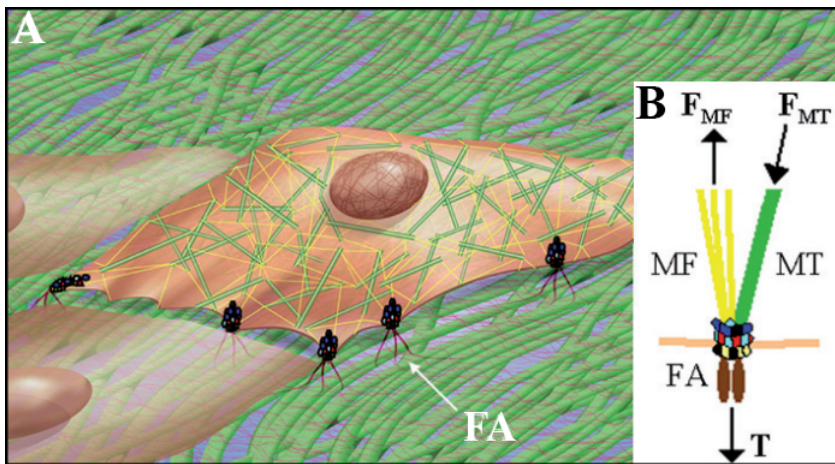


Figure 1.3: An artistic depiction of the cellular tensegrity model, designed by Matt Pickett and Donald E. Ingber, reproduced and adapted from [205]. **A)** The cytoskeleton is comprised of a continuous network of tensile actin filaments (yellow lines) and isolated microtubule struts (green). The cytoskeleton is linked to the extracellular matrix via focal adhesion (FA) molecular clusters. **B)** A schematic representation of the complementary force balance between tension (F_{MF}) in actin microfilaments (MF), compression (F_{MT}) of microtubules (MT) and traction forces (T) at the focal adhesion (FA) contacts.

More specifically, the pivotal idea of the cellular tensegrity model (see figure 1.3) is that the cytoskeletal actomyosin filaments act as the cables of a tensegrity network, by bearing tensile forces that are both actively produced through ATP-driven filament sliding processes (as actually illustrated in section 1.1) and partially passively induced through cell spreading on ECM and cytoplasmic swelling pressure. This tension is then resisted and balanced both inside the cell by compression-bearing microtubules –that hence play the role of the struts within a tensegrity– and, for an adherent cell, by the external traction forces exerted on it by

the neighbouring cells and by the ECM scaffold [106, 207]. In the latter case, the cytoskeleton of adherent cells and the ECM are together viewed as a unitary, synergetic and mechanically stabilized tensegrity system [147]. With reference to figure 1.3, at the level of a single focal adhesion, the force balance described above can be rendered as follows:

$$\mathbf{F}_{MF} = \mathbf{F}_{MT} + \mathbf{T}, \quad (1.1)$$

where \mathbf{F}_{MF} is the tension vector of actin filaments, \mathbf{F}_{MT} is the compression vector of microtubules and \mathbf{T} is the traction vector at adhesions to the ECM [205, 210].

Several experimental evidences and theoretical mechanical models have been provided in recent decades in support of the cellular tensegrity hypothesis [101, 106, 146, 147]. *In primis*, as discussed in section 1.1, it is actually well established that cytoskeleton carries pre-stress and that this is transmitted –via transmembrane cell-anchoring points– to adhesion substrates [46, 88, 89, 200]. Moreover, data obtained from *in vitro* biophysical measurements on isolated actin filaments and microtubules [78, 106] indicate that actin filaments are semiflexible, curved, of high tensile modulus (order of 10^3MPa) and of persistence length on the order of $10 \mu\text{m}$, while microtubules appear as straight tubes, of nearly the same Young modulus as actin filaments but of much greater persistent length, that is of the order of $10^3 \mu\text{m}$. Based on these observations, actin filaments should appear curved and microtubules should appear straight on the whole cell level if they were not mechanically loaded. However, immunofluorescent images of the cytoskeleton lattice of living cells show that actin filaments appear straight, whereas microtubules often appear curved [17, 147, 207, 238]. As a consequence, it follows that mechanical forces must act on these molecular filaments in living cells: conceivably, tension in actin filaments straightens them while compression in microtubules results in their bending (caused by buckling). In compliance with this, experimental findings support the existence of a mechanical coupling between tension carried by the actin network and compression of microtubules analogous to the tension-compression synergy characterizing the cable-and-strut tensegrity models. For example, it has been observed that microtubules of endothelial cells, which appear straight in relaxed cells, instead buckle following contraction of the actin network [238] as well as it has been shown that when migrating cultured epithelial cells contract, their microtubules in the lamellipodia region buckle as they resist the contractile force exerted on them by the surrounding actin filaments [240]. In addition, in cultured heart cells,

microtubules buckle with each beat (contraction) of the cell [17]. The possibility that compression in microtubules actually balances a substantial fraction of the contractile pre-stress in actomyosin network has been also corroborated by experimental and theoretical energetic analyses proving that disruption of cytoskeletal microtubules induces an increase in the traction forces transferred by an adherent cell to the culture substrate [207, 238]. Also, in compliance with the existence of a complementary force equilibrium as given in (1.1), it has been found that the contribution of microtubules to balance the tensile pre-stress of the cell and to its energy budget depends on the extent of cell spreading [99]: for example, experimental studies show that microtubules contribute to nearly 50% of cytoskeletal pre-stress in poorly adherent cells, whereas the proportion of forces borne by microtubules versus the ECM substrate reduces to an average of 14% as cells become extremely well spread on rigid ECM-coated substrates [210]. Finally, it has been observed that intracellular microtubules can support surprisingly high levels of compressive forces per microtubule when surrounded by the viscoelastic cytoplasm in comparison with results obtained for individual isolated elements and that these compressive loads can be even higher when *in vivo* microtubules are cross-linked within large bundles, as in nerve cells, or laterally tethered to other cytoskeletal filament systems that can function like guy wires (e.g. intermediate filaments) [17, 18, 129, 204].

Another important evidence in support of the cellular tensegrity model is the so-called pre-stress-induced variation of stiffness, typical of tensegrity systems (as previously described) and coherently detected in cells. As a matter of fact, it has been shown that mechanical, pharmacological and genetic modulations of the cytoskeletal pre-stress are paralleled by changes in cell stiffness and, in particular, advances in the traction cytometry techniques have made possible to quantitatively measure various indices of cytoskeletal pre-stress [21, 167] and thus to correlate an increase of this to an increase of an estimated index of cell stiffness [106].

Finally, it has been highlighted above that an interesting property of tensegrity architectures is the long-distance transfer of mechanical forces, which induces a global rearrangement of the entire structural lattice as a result of any local disturbance, a phenomenon that Ingber referred to as "action at a distance" effect [101, 147]. Actually, this is in accord with experimental studies about cells that confirm that forces applied to the external face of transmembrane integrin receptors (which are physically coupled to the inner cytoskeletal filaments on their other side) are channelled over long distances and concentrated at specific sites deep

inside the cytoplasm and nucleus [102, 210]. Such a phenomenon could not be explained by continuum models where local disturbances produce only confined responses, which dissipate inversely with the distance from the point of load application [239].

Within this framework, it is worth to highlight that, although the cytoskeleton seems to physically stabilize cell shape by following the equilibrium principles discussed so far, it is not a static but a highly dynamic structure that undergoes continual turnover, since the individual molecular constituents of its load-bearing filaments continuously assemble and disassemble by following chemical polymerization and depolymerization processes. These, however, occur without altering the total amount of filamentous biopolymers, in this way the cell being able to maintain its structural (tensional) integrity and to carry out robust mechanical behaviors over hours to days [210].

Despite its geometrical complexity, dynamic nature and combined inelastic and viscoelastic properties, the cytoskeleton is often modeled as a static and elastic cable-and-strut network of idealized geometry. Experiments indeed suggest that the hypothesis of elasticity can be properly adopted at least at early-time cell behaviors (i.e. up to tens of seconds), where cross-linkers among the biofilaments still guarantee the elastic response of the overall cytoskeleton to both internal and external forces and the transmission of the latter through cytoskeletal preferred pathways with velocities that are at least one order of magnitude greater than biochemical signalling [197, 210, 239]. In particular, several works have demonstrated that a 30-element regular (spherical) tensegrity structure, as the one shown in figures 1.4F–G, can be assumed as a good candidate for reproducing the cytoskeletal apparatus, able to account for a number of mechanical behaviors exhibited by cells. As a matter of fact, in his early conceptual studies [101], Ingber already showed that a spherical tensegrity, built with sticks and elastic strings, is essentially able to mimic cell spreading on the ECM/substrate by flattening without disrupting its structural integrity. Also, he asserted that such a system can reproduce the cell instantaneous (elastic) retraction and rounding observed when the cell–ECM/substrate adhesions are enzymatically dislodged as well as the cell ability to wrinkle an elastic substrate both during adhesion and withdrawal phases [88, 89]. On these bases, formal micro-structural analyses have been subsequently proposed in literature to the aim of tracing –qualitatively and, in some cases, quantitatively– mechanical properties of cells by means of the 30-element tensegrity module [35, 36, 122, 123, 170, 190, 208, 209, 211, 212, 215, 232, 242]. More in detail, this contains 6

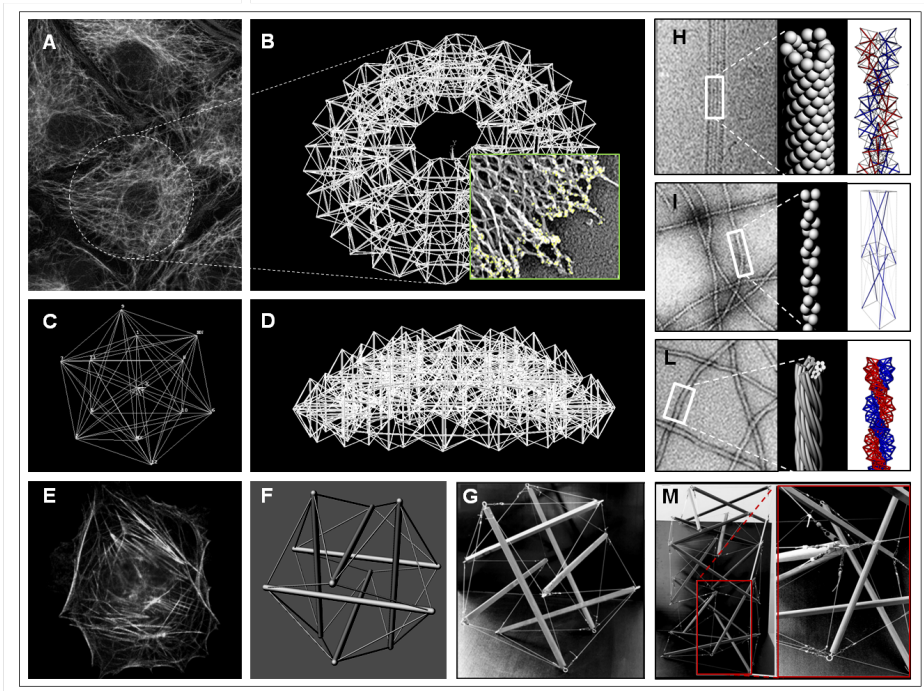


Figure 1.4: Synoptic panel illustrating how tensegrities can be met across the scales in cell structures. **A)** Standard microscope image of cells in which their cytoskeleton is highlighted. **B)** Possible tensegrity-based multi-modular model of a cell unit capable to replicate the complex geometry of the filaments network (green window) and **D)** lateral view of the model. **C)** Top view of a single cell finite element model made of an enriched icosahedral tensegrity whose nodes are all interlaced by filaments to capture details of **E)** the cytoskeleton architecture. **F)** 30-element tensegrity structure commonly utilized to idealize the cell mechanical behavior. **G)** Macroscopic hand-made toy system of a 30-element tensegrity structure. **H)** Microtubules, **I)** actin microfilaments and **L)** bundles of microfilaments whose structures can be modeled by means of piled tensegrity modules (shown on the right) such as the so-called *Snelson tower*, built up by repeating –and properly connecting– 30-element tensegrity units along a prescribed direction. **M)** Hand-made Snelson tower.

compression-bearing struts, taking the role of cytoskeletal microtubules, which are suspended in the space since sustained by interconnection (through frictionless pin joints) with a network of 24 tension-bearing cables, playing as actomyosin microfilaments, in a way to create a regular icosahedral shape.

The first actual attempt to mathematically model the cytoskeleton as a 30-element tensegrity was made by Stamenovic and colleagues in 1996 [211] and focused on a system containing 6 rigid struts connected to linearly elastic (i.e. Hookean) pre-tensed cables unable to bear compression, neglecting the nonlinear and viscoelastic nature of the cytoskeletal filaments for sake of simplicity [42, 108, 115, 136, 227]. By imposing uniaxial stretching, a structural stiffening of the overall tensegrity system was found when increasing the pre-stretch prescribed in cables and in most cases, at fixed pre-stretch, when growing the external stretching force, thus partially resembling trends observed in living cells [235, 236]. In [242], Wendling et al. somehow extended the previous results by studying the mechanical response of a similar system for three types of loading conditions, namely extension, compression and shear, and theoretically providing the nonlinearity of the stress-strain relationships characterizing cells. Among others, the works by Coughlin and Stamenović [35, 36] and by Volokh et al. [232] introduced in the 30-element tensegrity paradigm the flexural deformability experimentally observed for the cytoskeletal microtubules, by essentially modelling them as slender pin-ended Euler columns undergoing buckling while opposing the tensile forces coming from the network of (linearly elastic) cables. In this way, in [35] and [36] the response of the structure was evaluated under uni-axial stretch and under an external pulling force, respectively, while adhering to a rigid substrate, either in a round or in a spread configuration. Then, results by [232] predicted the possible existence of transient softening behaviors in living cells as a consequence of abrupt changes in the response of the individual members of the tensegrity assembly under shearing forces, namely the switching off of some unilateral (i.e. no-compression) microfilament-like cables and the buckling of microtubule-like struts. Also, in [190, 209], the 6-strut tensegrity unit was used as a model to quantitatively predict steady-state elastic properties of cells: in particular, on the basis of data reported in literature for mechanical properties of actin filaments and microtubules and by imposing uniaxial extension to the system, lower and upper bounds for the Young's modulus of the overall tensegrity were estimated by using an equivalent continuum approximation. In this way, a certain closeness was achieved with experimental values of cells elastic stiffness measures obtained with different experimental techniques and ranging between $10^{-1}kPa$ and 10^1kPa [8, 26, 68, 115, 206].

However, cells are also known to exhibit time- and rate-of-deformation-dependent viscoelastic behaviors [10, 68, 108, 115, 215, 231], which actually result of particular interest for predicting their response to dynamic

loads to which they can be exposed in their natural habitat (e.g. pulsatile blood flow in vascular endothelial cells, periodic stretching of the extracellular matrix in various pulmonary adherent cells, etc.). In this perspective, starting from models based on elasto-static tensegrity systems, there have been several attempts to trace cellular rheological properties by generally using similar tensegrity structures. Among others, some studies [22, 25, 215] essentially described the cell as a 30-element unit composed of 6 rigid bars connected to a continuous network of 24 linearly viscoelastic pre-stretched cables (e.g. Voigt elements with springs and dashpots in parallel) in order to analyze the role of the cytoskeleton spatial rearrangement on its viscoelastic response. In this way, it was possible to predict the dependence on the pre-stress level of both the elastic and viscous moduli of the cell as well as of the periodic geometrical rearrangement of the biofilament-like elements in response to sinusoidal loading, which is consistent with the oscillatory response of living cells [65, 106, 206]. Anyway, on the other hand, viscoelastic tensegrity models were less successful in explaining the observed power-law frequency-dependence of the material moduli of living cells, an effect that is instead theoretically taken into account by soft glass rheology theory [65, 106], so that some efforts for trying to reconcile tensegrity and soft glass rheology models of cells have also been made in literature [106, 205].

Finally, it is worth to highlight that, under a more general conception, the cellular tensegrity paradigm not only assumes that the cytoskeleton of the living single-cell behaves as a tensegrity structure, but it additionally presumes that cells may use tensile integrity principle to stabilize sub-cellular structures and multi-molecular complexes across multiple, hierarchical and interconnected size scales [103, 106, 181, 210], as shown in figure 1.4. As a matter of fact, the cortical cytoskeleton underlying the cell membrane, the shape stability of the nucleus, mitotic spindles, actomyosin stress fiber bundles and individual actin filaments [141], lipid micelles, viral particles, vesicles and single molecules, such as individual proteins or DNA molecules, could be both singularly and altogether described by using tensegrity models [106, 181]. The ability that such a complex and hierarchical pre-stressed network would have to channel mechanical forces over discrete molecular paths to sites deep inside the cell would then explain how local cell distortion or mechanical stress application to cell surface integrins result into coordinated structural changes of the entire cytoskeleton up to the nucleus and individual molecules at progressively smaller size scales, which in turn drive mechanotransduction processes by possibly inducing molecular unfolding or changes

of molecular and nuclear shapes that alter biochemical activities at the micro-/nanometre level [102, 210].

1.3 CELLS ORIENTATION VIA CELL-SUBSTRATE ELASTIC INTERACTIONS

As highlighted in the previous sections, mechanical response of adherent cells can arise as an effect of physical stimuli sensed by means of elastic interactions with the surrounding environment. Actually, when cultured on an elastic substrate, cells constantly probe it by pushing and pulling on it via traction forces induced by the contractility of the inner cytoskeleton and transmitted at the cell–substrate interface through transmembrane focal adhesions, which are internally coupled to the actin filaments network and externally anchored to the ligand-coated substrate [42, 46, 106, 167, 184, 210]. Hence, by means of its integrated active system of protein-based mechanosensors and mechanotransducers, the cell is able to mechanically interact with the adhesion medium, thus reading its elastic properties and stress and strain patterns –possibly induced by other adherent cells and/or by externally applied loads– and accordingly reacting to them by adjusting its shape, spreading and contractility level [28, 75, 76, 91, 197, 239]. As a consequence of this mechanical response, cell biological activities are, in turn, re-modulated [57, 138, 142, 146, 167]. As an example, microenvironment stiffness has been largely recognized to play a critical role in mechanosensing and mechanotransduction of tissue cells [138, 153, 167]. Stem-cell differentiation has been indeed found to be influenced by matrix rigidity [62], the most of the cellular types, such as fibroblasts, neurons, epithelial and muscle cells, have been shown to detect and respond distinctly to soft versus stiff substrates [57, 167, 176] and alterations of the cellular responsiveness to surroundings solidity have also been identified as symptom of diseases and pathologies [57].

In this context, wide attention has been paid in the last years to the study of the influence on adherent cells motility of substrate-mediated elastic interactions with extracellular mechanical stimuli. Processes of *mechanotaxis*, that is, of mechano-driven cell migration, have been for example detected, whose most consolidated evidence is represented by the stiffness-guided locomotion mechanism known as *durotaxis* [138]. This is a form of cell migration, occurring in the direction of greater stiffness in presence of rigidity gradients within the adhesion substrate, the most of the cells types (with the exception of the neural one) *de*

facto exhibiting the tendency to prefer stiff over soft regions [197]. This phenomenon is most likely explained with the assumption that contractile cells would effectively minimize the elastic energy invested in deforming their surroundings (i.e. the matrix/substrate) while exerting forces on them [14, 15], this minimization possibly being the result of evolution in producing optimized biological systems, since the energy that the cell invests in deforming its environment is not directly exploitable for its physiological activities [197].

As well as in the form of migration, mechano-guided cell motility can also arise in the form of alignment and reorientation of an adherent cell along a specific direction, as a coupled effect of the substrate's mechanical properties and of the forces that it senses, as shown in figure 1.5. In this regard, thanks to newly developed experimental techniques (mainly the traction force microscopy [7, 46, 174, 191, 195, 214]), quantitative measures of the cells mechanosensitivity have been obtained. It has been in particular observed that the level of traction forces generated and transmitted to an elastic substrate by the cell, the cell spreading area and aspect ratio as well as the area, the aspect ratio and the stability of the focal adhesions all increase with the stiffness of the substrate, these evidences thus contributing to unveil a matrix-rigidity-induced process of cellular polarization, that is, of cell shape elongation and alignment along a preferential axis [133, 176, 220]. More in detail, it has been demonstrated that adherent cells, e.g. fibroblasts, spread assuming highly elongated and stationary configurations on sufficiently rigid substrates (namely, substrates having stiffness of about $30kPa \div 2MPa$) while generally arrange into isotropic and motile forms over more compliant materials (see figure 1.5A), in the first case also exhibiting few, large, stable and preferentially oriented focal adhesions, which are instead numerous, small, dynamic and radially oriented in the second condition [176]. On the other hand, further experimental outcomes have highlighted that, along with the mechanical properties of the substrate, sensed extracellular mechanical forces and deformations also appear to play a concurrent critical role in this mechanism of cellular polarization as well as in driving the active reorientation and alignment of adherent cells along (non-random) preferred directions. It has been indeed observed that initially randomly oriented cells rotate and reorient themselves upon stretch or stress of the adhesion substrate, as for example shown in figure 1.5B [219, 233, 234, 249].

In the current research context of biomechanics and mechanobiology, understanding the mechanical principles at the basis of cell orientation represents an issue of crucial interest, since this phenomenon is

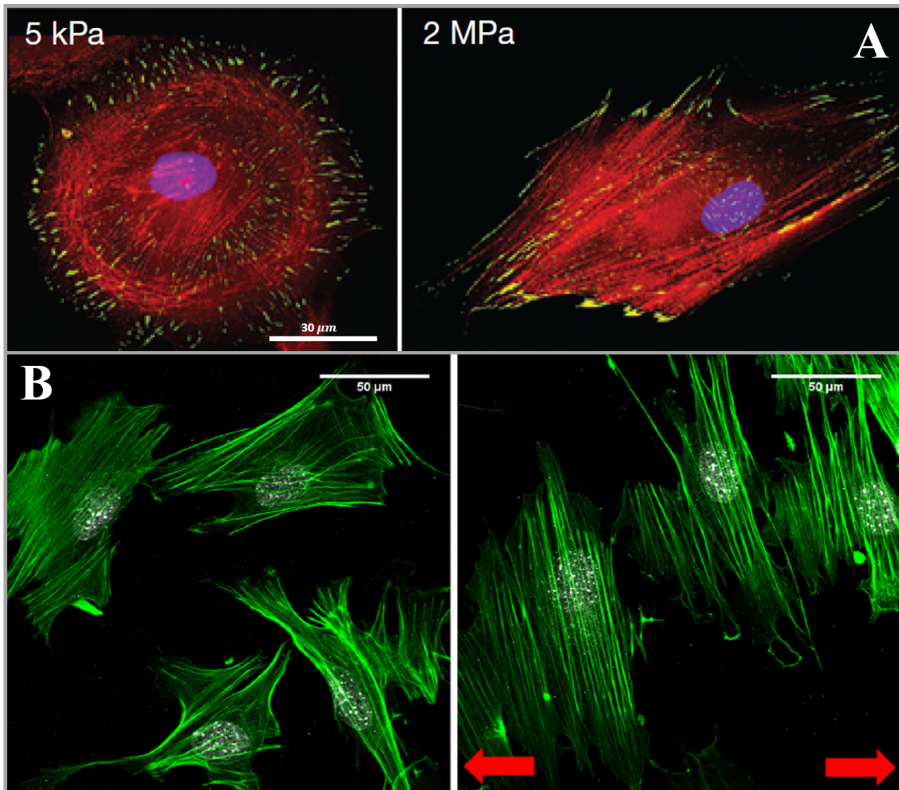


Figure 1.5: **A)** Images of isotropic and highly stretched configurations assumed by a cell when respectively plated on a compliant ($5kPa$) and on a stiff ($2MPa$) fibronectin-coated PDMS substrate. The image is reproduced from [176]. **B)** Images showing the orientation response to uniaxial cyclic strain (7% , $0.5Hz$) of mouse embryonic fibroblasts over a fibronectin-coated silicone membrane: cells and actin stress fibers (green), initially randomly arranged, orient almost perpendicularly to the strain direction (red arrows), a phenomenon known as strain avoidance. The image is reproduced from [219].

an integral part of the mechanisms of cellular organization that in turn determine the structural, morphological and functional character of assembled biological tissues. By way of example, active reorientation of cells deriving from the cell–matrix interaction plays an essential role in organisms development and maintenance, as cells progressively build up monolayers that then evolve to complex tissues with particular geometrical and physical features associated with specific functions. Also, cells arrangement is involved in many physiological processes, including

angiogenesis and wound healing. Motivated by this, several experimental and theoretical approaches have been proposed in literature for studying the spatial organization and, in particular, the preferential orientations adopted by stationary (i.e. stable and non-migrating) adherent cells as a consequence of the interplay with the network of neighbouring cells or the interaction with externally applied mechanical solicitations, occurring through elastic media [29, 197].

Many works have shown that cells adhering to a flat deformable substrate subject to pre-stretch or to static or cyclic stresses/stretching can rearrange from random to well defined angles through a sequence of disassembly and then reassembly of the cytoskeletal apparatus possibly combined with an actual rotation of the stress fibers [43], the final orientations depending on the type of mechanical test (e.g. uni-axial or bi-axial loading) and on the applied stretch/stress frequency, duration and amplitude, sometimes also evidencing threshold-activated behaviors in terms of frequency and/or magnitude [15, 28, 30, 40, 41, 137, 229, 233, 237, 249]. As an example, a rather common evidence is that, under uni-axial cyclic strains of the substrate, cells align nearly (but not exactly) perpendicular to the loading direction at proper frequencies ($\sim 1\text{Hz}$), presumably in a way to avoid the perturbations arising from passive deformations and therefore to follow the direction of minimal substrate strain, a phenomenon designated as stretch avoidance (see figure 1.5B) [90, 110, 219, 234]. On the other hand, the cellular responses to static or quasi-static stretches are less understood [197], in this case cells have been shown to principally arrange parallel to the stretching/force direction [34, 59, 134, 213, 249], despite some other experiments have found that they align randomly [110] and that static stretch is not as influential as cyclic stretching in directing cell alignment or changing cell morphology [79].

These experimental evidences, characterized by non-trivial variability of the response with the above-mentioned parameters of stimulation and by the observation of some discordant behaviors, pose substantial challenges to theoretical efforts aimed to understand the fundamental mechanisms at the basis of the relationship between cells orientation and the stress and strain fields acting on them. As a consequence, a number of different theoretical approaches and models have been elaborated to this aim [6, 28, 30, 41, 80, 137, 194, 197, 249]. In this regard, since the set of experimental outcomes *de facto* highlights that alignment on flat substrates can be seen as the result of a functional process implemented by the cells for achieving a certain optimal (non-random) condition, several possible

theoretical targets have been suggested to trigger such optimization mechanisms, such as optimal stress-, strain-, energy- or stability-driven conditions. Accordingly, different mechanical descriptions of the cell orientation have been provided, which range across different length scales, going from molecular approaches directly involving bio-chemo-mechanical processes at the level of the focal adhesion complexes to higher scale one-dimensional and bi-dimensional structural/continuum-based cellular models.

More in detail, widespread approaches predict that, under stretching of the substrate, cells re-align along angles that allow them to maintain an optimal strain or stress state, namely along the zero (or minimal) matrix strain directions [6, 41, 80, 233, 234], or in a way to retain a minimal or fixed (homoeostatic) stress level [6, 40, 41, 80, 229]. As an example, among the models proposed in literature, De et al. [40, 41] studied stress fibers re-orientation under both static and dynamic loading by supposing that cells tend to maintain an optimal (or set point) value of stress or strain in the adjacent matrix. In particular, motivated by experimental measurements of cellular traction patterns [21, 46, 195], they used a coarse-grained modelling of the cells approximated as single anisotropic force dipoles [194]. On the other hand, different models involving macromolecular or biochemical descriptions of cellular orientation and stress fibers rearrangement in response to applied forces have also been discussed [28, 30, 98, 112, 118, 197, 241]. In this framework, Chen et al. [28, 30] and Kong et al. [118] for example proposed a theoretical model based on the stability of the focal adhesions under cyclic loadings. On the other hand, recently, Xu et al. [249] also developed a planar cytoskeletal tensegrity models, by incorporating the molecular mechanisms of focal adhesion dynamics, the actin polymerization and the actin retrograde flow, to study the dynamics of cell reorientation on a substrate under biaxial static and cyclic stretches. Then, some other models recognize in the search for a minimum elastic energy configuration the driving mechanisms for cell rearrangement [15, 137, 194]. In particular, Livne and co-workers [137] developed a bi-dimensional model of the cell which takes into account both the passive elastic response of the cells to substrate deformation and the active remodelling of their actin cytoskeleton and focal adhesions, thus proposing that reorientation during cyclic stretching is driven by a dissipative process in which the passively stored elastic energy of the cell relaxes to a minimum through active realignment of the relevant molecular structures determining the final (optimal) orientation angle. Finally, Safran and co-workers [14, 15, 194], by employing a force dipole

model for the adherent single-cell, studied its interaction with the strain field induced on an elastic substrate homogeneously stretched along one axis under the assumption that cell orientation and positioning can be predicted by minimizing the interaction energy invested by the cell into straining its environment for a given level of force generation. The latter concepts were also used by the same authors to predict the collective response of contractile cells inside or over an elastic medium [14–16, 194], that is to study the preferred alignments of pairs or populations of elastically interacting (distant) cells in absence of externally applied loads, in this way highlighting the influence of the elastic properties of the contact medium (specifically, of the Poisson ratio in case of isotropic materials) on the coordinated multi-cellular orientation mechanisms [16].

1.4 CONCLUSION

In this first chapter, an introduction has been provided to the research context in which the present thesis integrates. In this regard, reasons and aims moving the fields of science known as *biomechanics* and *mechanobiology* have been highlighted with particular reference to the living cell and remarks about the bio-chemo-mechanical bases and the physical origins of the cellular behavior have been provided.

Then, attention has been paid on the theoretical modelling of the single-cell mechanics, by principally focusing –within this wide scientific context– on the aspects that are argument of the present work, by trying to define an essential picture of the related state-of-art. Actually, the problem of charactering the whole-cell mechanical properties and response has been addressed, by in particular selecting, among the several approaches proposed in literature, that based on the adoption of tensegrity models. The peculiar principles and properties of these special architectures, made by floating compressed struts kept together by a continuous system of tensioned cables, have in fact revealed them as the most effective mechanical paradigm for explaining most of the mechanisms regulating the structural and mechanobiological dynamics of living cells, by also overcoming some limitations provided by other models, such as the continuum-based ones, especially at early-times of the cell response when it can be assumed as elastic. With regard to this, in the chapters 2 and 3, the adoption of new tensegrity models, in which large strains and constitutive hyperelasticity of both cables and struts are involved and eventually combined with local or global instabilities, will be highlighted

as a necessity for the purpose of tracing mechanical behaviors consistent with the experimentally observed nonlinear cytomechanics. Hence, by introducing all these components, a 2-element tensegrity paradigm and a revised version of the Ingber's 30-element tensegrity model will be formulated.

On the other hand, some effects induced by environmental mechanical cues on adherent cells, deriving from their elastic interaction with the adhesion medium, have been pointed out. In particular, it has been highlighted that progressively elongated and stationary configurations are assumed by cells (such as fibroblasts) when adhering to the surfaces of substrates with increasing stiffness and that the orientation angle of such polarized cells is determined by the stress and strain fields that they sense by probing the deformable substrate. About this point, further theoretical efforts are required to explain results deriving from experimental observations, since the physical principles underlying the process of cell orientation along preferential directions are not fully understood yet. Thus, within this framework, a theoretical model will be implemented in the chapter 4, intended to contribute to the investigation of the mechano-induced directional response of an adherent cell mediated by elastic media and to suggest a possible strategy for driving novel related experiments.

Finally, in the chapter 5, an alternative approach will be proposed in the perspective of modelling the cell mechanics by taking into account the hierarchical and multiscale nature of its internal architecture and that its global mechanical response *de facto* arises as bottom-up integration of kinematics and structural interactions involving sub-cellular components at different length scales.

TOWARD NONLINEAR SOFT-STRUT TENSEGRITIES FOR CELL MECHANICS

On the basis of the arguments presented in section 1.2, tensegrity systems represent the most effective microstructural paradigm to trace the biomechanical behavior of the living cells [101, 106].

In the vast majority of the examples found in literature about the modelling of macroscopic tensegrity systems [70, 202] and tensegrity-based robot prototypes [135] as well as in the cases in which tensegrity structures are used to describe the mechanics of living cells [35, 36, 147, 209, 211, 232] or of their constituents [141], the constitutive laws of their structural components are treated as an ancillary issue. In fact, the hypotheses of linearly elastic (tensed) cables connected to rigid struts [151, 157, 211] or to elastic slender struts able to buckle under compression [35, 36, 182, 183, 209, 232] are commonly considered. Also, only geometrical nonlinearities –namely finite measures of strain– are generally employed for tracing large axial deformations that either the cables or both the cables and the struts (in the rare literature cases where the latter are axially deformable) can undergo as a consequence of the internal pre-stress and/or of an external loading [70, 82, 113, 183]. However, especially when tensegrities are used to describe the biomechanical behavior of living systems or to design newly conceived deployable devices in the field of bio-inspired soft-robotics, it is necessary to upgrade their modelling by introducing a fully (geometrical and constitutive) nonlinear characterization of their constituents and by involving the possibility of coupling axial deformability and elastic buckling for the compressed elements.

As a matter of fact, the cytoskeletal network undergoes large deformations and displacements as a consequence of the significant configurational changes associated to the most of the cells physiological processes [74], such as spreading, adhesion, duplication and isolated or collective migration. Furthermore, experimental studies have shown that single actin microfilaments as well as higher-order structures deriving from their assembling in bundles –namely the stress fibers– exhibit nonlinear stress-strain behaviors [42, 136] as a result of microstructural dynamics occurring at the level of the macromolecular composition of these filamentous protein systems [178, 227]. On the other hand, by estimating the

actual ratio between the experimental measures obtained for the axial stiffness of actin microfilaments and microtubules [78, 106], one finds that it can approach values tending to the unity or differing from it for less than an order of magnitude. Also, it has been observed that intracellular microtubules have considerably enhanced capabilities to resist buckling under compression in comparison with results of *in vitro* studies on isolated elements [17, 18]: this is probably due to the presence, throughout the *in vivo* surrounding cytoplasmic environment, of networked intermediate filaments, which could act, at certain levels of strains, as a tensed lateral support stabilizing compressed microtubules. As a consequence, especially when the cytoskeleton is extremely stretched –for instance during cell adhesion– relevant axial contractions of microtubules, possibly coupled with compressive buckling, might take place. All these observations thus suggest that large displacements and deformations, hyperelastic constitutive laws and struts axial deformability coupled with compressive buckling have to be all taken into account within tensegrity models aimed to more faithfully describe and predict the cytoskeleton mechanics.

In this regard, it is important to underline that tracing the (potential) high longitudinal contractions of microtubule-like struts also requires to abandon the combination of the linear (Saint Venant-Kirchhoff) constitutive law with the finite strain measures given by the Biot and the Green-Lagrange deformation tensors, which is generally adopted in literature for modelling the elements of standard tensegrity systems. This indeed leads to physically inconsistent results as moderately large axial contraction levels are attained under one-dimensional stress regime, in fact returning finite –rather than infinite– values of compressive nominal stress for vanishing longitudinal stretch when the Biot deformation tensor is adopted, while leading a non-monotonic stress-stretch curve under axial contraction when one employs the Green-Lagrange measure, in this way paradoxically giving null stress in the limit of zero stretch [95].

On these bases, the present and the next chapter of this work are dedicated to the introduction of nonlinear soft-strut tensegrity systems, oriented to the modelling of the cell mechanical behavior. In particular, to describe the mechanics of actin filament-like cables and microtubule-like soft (axially compressible and bendable) struts, hyperelastic models and large deformations are taken into account by exploiting Hencky's and neo-Hookean laws as described in the next section and by subsequently including concurrent buckling and contraction of the struts. In this context, starting from the paradigm of a 2-element soft-tensegrity structure

(studied in section 2.2), which can be thought as essential sketch of a single-microtubule/single-actin filament system, the equations governing the mechanical behavior of the 30-element cellular tensegrity paradigm proposed by Ingber are then re-formulated in the chapter 3.

2.1 HYPERELASTIC MODELS FOR DEFORMABLE STRUTS AND CABLES

In the present section, within the theoretical framework of the solid continuum mechanics at finite deformations, the above-mentioned physical inconsistencies produced at certain levels of axial contraction by the linear constitutive law when coupled with Biot and Green-Lagrange measures of strains are briefly pointed out to the aim of highlighting the need to abandon this coupling when dealing with soft-tensegrity structures under large strains. Then, the Hencky-type and the neo-Hookean isotropic strain energy functions are adopted to derive the mechanical behavior of both deformable struts and cables, modelled as hyperelastic cylindrical beams undergoing uni-axial stress regime. The relations thus obtained will be employed in the consecutive sections for studying the above-mentioned 2-element and 30-element tensegrity models.

2.1.1 *Inconsistency of some linear constitutive models for highly deformable struts*

By essentially recalling standard notions from the nonlinear continuum mechanics theory [13, 37, 85, 95], the deformation of an elastic continuum body \mathcal{B} from its reference (undeformed) configuration $\Omega_0(\mathcal{B})$ to a current (deformed) configuration $\Omega(\mathcal{B})$ –within the three-dimensional Euclidean space– can be entirely described, under a Lagrangian (or material) approach, by the smooth vector mapping $\chi \in C^2(\Omega_0)$:

$$\mathbf{x} = \chi(\mathbf{X}) = \mathbf{X} + \mathbf{u}(\mathbf{X}). \quad (2.1)$$

It one-to-one maps Ω_0 onto Ω by uniquely taking the material points $\mathbf{X} = X_i \hat{\mathbf{e}}_i$ –identifying the position vectors of the body particles in the reference configuration– to the spatial points $\mathbf{x} = x_i \hat{\mathbf{e}}_i$ –defining instead the current configuration– according to the smooth displacement vector field $\mathbf{u} \in C^2(\Omega_0)$. Herein, $\hat{\mathbf{e}}_i$ ($i = 1, 2, 3$) is the i -th unit vector of the right-handed orthonormal basis of the fixed reference frame, assumed as shared by the reference and the current configurations, with X_i and x_i indicating the corresponding (material and spatial) points components.

By differentiating equation (2.1) with respect to \mathbf{X} in order to exclude any rigid translations from the deformation process, the (second-order) *deformation gradient tensor* \mathbf{F} is obtained as

$$d\mathbf{x} = \mathbf{F}(\mathbf{X})d\mathbf{X}, \quad \mathbf{F} := \nabla_{\mathbf{X}}\boldsymbol{\chi} = \frac{\partial \mathbf{x}}{\partial \mathbf{X}} = \mathbf{I} + \mathbf{u} \otimes \nabla_{\mathbf{X}}, \quad (2.2)$$

where \mathbf{I} represents the identity second-order tensor, \otimes is the standard tensor (or dyadic) product between two vectors and $\nabla_{\mathbf{X}}$ is the nabla vector differential operator, its subscript indicating the coordinates with respect to which the differentiation is performed. The elements of \mathbf{F} are called *stretches* and give the relative change in length of an infinitesimal line element while going from the reference to the current configuration.¹

It can be shown that the deformation gradient can be multiplicatively decomposed into a pure rigid rotation contribution and a pure deformation, the latter being interpreted as change of the body shape not involving any rigid translations and rotations. This is made according to the *polar decomposition* reported below in its Lagrangean form:

$$\mathbf{F} = \mathbf{R}\mathbf{U}, \quad (2.3)$$

where $\mathbf{R} \in Orth^+$ is the orthogonal tensor (i.e. $\mathbf{R}^T\mathbf{R} = \mathbf{R}\mathbf{R}^T = \mathbf{I}$) representing the rotation, hence called the *rotation tensor*, while \mathbf{U} is the *right* (or *material*) *stretch tensor* giving the pure deformation contribution.

Then, to the aim of defining a strain measure that traces only the non-rigid part of the deformation process and also coherently vanishes

¹ It is worth to underline that, on the basis of the relations in (2.2), it can be proved that the deformation gradient also allows to interrelate infinitesimal volume elements in the change between the reference and the current configuration according to the following equation:

$$dv = JdV, \quad J := \det \mathbf{F}(\mathbf{X}) = \frac{dv}{dV},$$

where J is known as *Jacobian* of the deformation gradient and measures the local volumetric deformation. Since both the infinitesimal volumes dv and dV are positive quantities, the Jacobian must also be positive, namely $J > 0$, this implying that interpenetration of volume elements of the continuum body \mathcal{B} is excluded. On the other hand, the so-called *Nanson's formula*, reading as

$$d\mathbf{a} = J\mathbf{F}^{-T}d\mathbf{A},$$

rules the mapping of each infinitesimal material area element $d\mathbf{A} = dA\hat{\mathbf{N}}$ into an infinitesimal spatial area element $d\mathbf{a} = da\hat{\mathbf{n}}$, where such elements are defined by means of their surface dA and da , respectively, and by the normal outward vectors $\hat{\mathbf{N}}$ and $\hat{\mathbf{n}}$, respectively.

in absence of pure deformations, the general form of *strain tensor* \mathbf{E}_m , provided by the following so-called *Seth-Hill formula* [13, 93], can be adopted:

$$\mathbf{E}_m := \begin{cases} \frac{1}{m} (\mathbf{U}^m - \mathbf{I}) & m \neq 0 \\ \ln \mathbf{U} & m = 0 \end{cases}, \quad (2.4)$$

defined by starting from the right stretch tensor \mathbf{U} for every integer m .

With specific reference to the problem here addressed, in compliance with the structural definition of tensegrity –which considers the hypotheses of torqueless and frictionless spherical hinges as constraints between the rectilinear constituents– the generic element of a tensegrity system is modelled as an isotropic, homogeneous and hyperelastic cylindrical beam-like body undergoing uni-axial stress, namely uni-axial compression (strut) or tension (cable). In such a case, the deformation gradient tensor \mathbf{F} can be assumed in diagonal form as

$$\mathbf{F} = \lambda_L \hat{\mathbf{e}}_1 \otimes \hat{\mathbf{e}}_1 + \lambda_R (\hat{\mathbf{e}}_2 \otimes \hat{\mathbf{e}}_2 + \hat{\mathbf{e}}_3 \otimes \hat{\mathbf{e}}_3), \quad (2.5)$$

where $\hat{\mathbf{e}}_i$ ($i = 1, 2, 3$) is the i -th unit vector of the Cartesian reference frame having $\hat{\mathbf{e}}_1$ directed along the element axis and, accordingly, $\lambda_L = \lambda_1 = l/L$ is the principal stretch in the longitudinal direction while $\lambda_R = \lambda_{2,3} = r/R$ represents the principal stretch in the transverse –namely radial– direction, L and R denoting, in the order, the beam's length and radius in the reference (stress-free) configuration, while l and r identifying the corresponding deformed quantities in the current configuration, respectively.

Then, by considering the constitutively linear Saint Venant-Kirchhoff model, which represents one of the simplest hyperelastic material models and the direct three-dimensional continuous generalization of the linear (Hookean) elastic spring at large deformations, the following strain energy density can be adopted:

$$\Psi_{SVK}(\mathbf{E}_2) = \frac{1}{2} \mathbf{E}_2 : \mathbf{C} : \mathbf{E}_2 = \frac{E}{2(1+\nu)} \left[\text{tr}(\mathbf{E}_2^2) + \frac{\nu}{1-2\nu} \text{tr}(\mathbf{E}_2)^2 \right], \quad (2.6)$$

where \mathbf{C} is the (symmetric and positive definite) fourth-order tensor of the tangent elastic moduli, i.e. the *stiffness tensor*. This, by assuming an isotropic material, is given by $\mathbf{C} = 2\mu\mathbb{I} + \Lambda\mathbf{I} \otimes \mathbf{I}$, where \mathbb{I} is the fourth-order identity tensor while μ and Λ denote the first and the second Lamè

constants of the element, respectively, related to the Young modulus E and the Poisson ratio ν as $\mu = E / [2(1 + \nu)]$ and $\Lambda = E\nu / [(1 + \nu)(1 - 2\nu)]$. Also, therein $\mathbf{E}_2 := (\mathbf{U}^2 - \mathbf{I}) / 2$ is the *Green-Lagrange strain tensor*, selected from the Seth–Hill family in (2.4) for $m = 2$ and here explicitly given by

$$\mathbf{E}_2 = (\lambda_L^2 - 1) \hat{\mathbf{e}}_1 \otimes \hat{\mathbf{e}}_1 + (\lambda_R^2 - 1) (\hat{\mathbf{e}}_2 \otimes \hat{\mathbf{e}}_2 + \hat{\mathbf{e}}_3 \otimes \hat{\mathbf{e}}_3), \quad (2.7)$$

\mathbf{U} in fact coinciding with the deformation gradient \mathbf{F} given in (2.5) since no rigid rotation occurs in the present case (i.e. $\mathbf{R} = \mathbf{I}$ in (2.3)).

Hence, by employing the definition of hyperelastic material, the first Piola-Kirchhoff (nominal) stress tensor \mathbf{P} –expressing the stress relative to the reference configuration area elements– reads as:

$$\begin{aligned} \mathbf{P} &= \frac{\partial \Psi_{SVK}(\mathbf{E}_2)}{\partial \mathbf{F}} = P_L \hat{\mathbf{e}}_1 \otimes \hat{\mathbf{e}}_1 + P_R (\hat{\mathbf{e}}_2 \otimes \hat{\mathbf{e}}_2 + \hat{\mathbf{e}}_3 \otimes \hat{\mathbf{e}}_3), \\ P_{L,R} &= \frac{\partial \Psi_{SVK}(\mathbf{E}_2)}{\partial \lambda_{L,R}} = \frac{E}{2(1 + \nu)} \lambda_{L,R} \left[\lambda_{L,R}^2 - 1 + \frac{\nu}{1 - 2\nu} (\lambda_L^2 + 2\lambda_R^2 - 3) \right]. \end{aligned} \quad (2.8)$$

In compliance with the uni-axial (longitudinal) stress regime that struts and cables undergo, the transverse nominal stress must be vanishing, i.e. $P_R = 0$. As a consequence, the following relation between transverse and longitudinal stretches can be derived:

$$P_R = 0 \iff \lambda_R = \sqrt{1 + \nu(1 - \lambda_L^2)}, \quad (2.9)$$

whose substitution into the equation (2.8) provides:

$$P_L = \frac{E}{2} \lambda_L (\lambda_L^2 - 1). \quad (2.10)$$

On the other hand, when the Biot strain tensor \mathbf{E}_1 (the so-called engineering strain) is selected from the generalized Seth-Hill formula (2.4) as alternative finite measure of strain, one can write

$$\mathbf{E}_1 := \mathbf{U} - \mathbf{I} = \mathbf{F} - \mathbf{I} = (\lambda_L - 1) \hat{\mathbf{e}}_1 \otimes \hat{\mathbf{e}}_1 + (\lambda_R - 1) (\hat{\mathbf{e}}_2 \otimes \hat{\mathbf{e}}_2 + \hat{\mathbf{e}}_3 \otimes \hat{\mathbf{e}}_3). \quad (2.11)$$

Then, by adopting \mathbf{E}_1 in combination with the linearly constitutive law provided by the Saint Venant-Kirchhoff strain energy density Ψ_{SVK} in equation (2.6), the associated nominal stress tensor's components result:

$$P_{L,R} = \frac{\partial \Psi_{SVK}(\mathbf{E}_1)}{\partial \lambda_{L,R}} = \frac{E}{(1 + \nu)} \left[\lambda_{L,R} - 1 + \frac{\nu}{1 - 2\nu} (\lambda_L + 2\lambda_R - 3) \right]. \quad (2.12)$$

As above, to guarantee uni-axial stress along the element axis, it follows that:

$$P_R = 0 \iff \lambda_R = 1 + \nu(1 - \lambda_L), \quad (2.13)$$

which allows to obtain the following expressions for the strain energy function and the unique component of the nominal stress, respectively, also highlighting the direct analogy with the case of small strains in linear elasticity:

$$\Psi_{SVK} = \frac{1}{2}E(\lambda_L - 1)^2, \quad P_L = E(\lambda_L - 1). \quad (2.14)$$

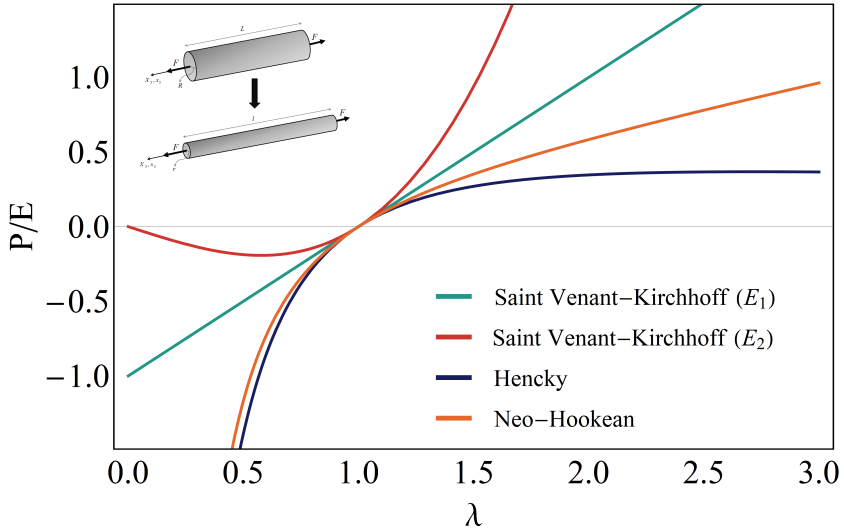


Figure 2.1: Longitudinal nominal stress P_L –normalized with respect to the Young modulus E – as a function of the longitudinal stretch λ_L in case of Saint Venant-Kirchhoff (linear) law combined with Biot (\mathbf{E}_1) and Green-Lagrange (\mathbf{E}_2) strain tensors and of Hencky’s and (incompressible) neo-Hookean models, for one-dimensional stress regime.

The stress-stretch relations obtained in equations (2.10) and (2.14)₂ are plotted in figure 2.1: although the two versions of the Saint Venant-Kirchhoff constitutive model converge to the linear case as the stretch tends to one (limit of small strains) and provide consistent results in case of extension as well as for moderate contractions, they both fail from

moderately high up to high contraction levels. In particular, the relation in (2.10) provides a non-monotonic stress-stretch curve in the interval $0 < \lambda_L < 1$, the stress starting to relax from the critical value $\lambda_L = \sqrt{1/3}$ and finally approaching zero as $\lambda_L \rightarrow 0$ [95], while the expression (2.14)₂ gives finite –rather than infinite– values of compressive nominal stress for vanishing λ_L . Therefore, despite the Saint Venant-Kirchhoff law has been often adopted in these forms to treat the mechanics of tensegrity structures [70, 202], the hypothesis of potentially highly axially deforming (contracting) struts obliges to adopt alternative models to avoid inconsistent results. In what follows, all the analyses of soft-strut tensegrity systems will be hence performed by making reference to consistent hyperelastic laws and in particular to Hencky’s and neo-Hookean models.

2.1.2 Hencky-type cables and struts

Here, the (Lagrangian) *Hencky strain tensor* \mathbf{H} , also known as *natural* or *true strain*, is adopted. It represents a logarithmic strain measure², obtained as limit case from the Settl-Hill formula (2.4), that is:

$$\mathbf{H} := \mathbf{E}_0 := \lim_{m \rightarrow 0} \frac{1}{m} (\mathbf{U}^m - \mathbf{I}) = \log \mathbf{U}. \quad (2.15)$$

² It is worth noting that, by referring to the one-dimensional case, the logarithmic strain $\varepsilon_H := \log \lambda$ can be directly introduced as natural measure of strain by considering the incremental deformation of a fibre of initial length l_0 up to the final length l , $\lambda = l/l_0$ representing the stretch of the fiber. In fact, an intermediate deformation between the two states can be described by a length l^* such that $l_0 \leq l^* \leq l$, in a way to define an incremental deformation as $d\varepsilon_H^* = dl^*/l^*$ and to finally obtain the total deformation as the sum of the next incremental deformations, that is:

$$\varepsilon_H = \int_0^{\varepsilon_H} d\varepsilon_H^* = \int_{l_0}^l \frac{dl^*}{l^*} = \log \frac{l}{l_0}.$$

Moreover, it can be verified that, at small strain, the fiber engineering strain is readily obtained, i.e. $\varepsilon_H \approx \lambda - 1$. The adoption of the logarithmic strain is in particular motivated by the possibility of additively decomposing deformations that are generally multiplicatively combined, by essentially exploiting the well-known properties of the logarithms. In the case of the fiber, for example, let the stretch λ be seen as the result of two superposed stretches, say $\lambda_* = l/l_*$ and $\lambda_0 = l_*/l_0$, where l_* depicts an intermediate configuration and the two stretches might be either elastic or inelastic. In this case, by employing the Hencky strain measure, the nonlinear multiplicative decomposition of the stretches $\lambda = \lambda_* \lambda_0$, widely used in finite thermoelasticity and plasticity or, in general, in presence of a harboring stretch, simply results in:

$$\varepsilon_H = \log \frac{l}{l_0} = \log \frac{l}{l_*} \log \frac{l_*}{l_0} = \log \lambda_* + \log \lambda_0.$$

In particular, the Hencky strain tensor associated to the deformation gradient \mathbf{F} given in equation (2.5) for kinematically describing the behavior of the generic tensegrity element under uni-axial stress, can be expressed as

$$\mathbf{H} = \log \lambda_L \hat{\mathbf{e}}_1 \otimes \hat{\mathbf{e}}_1 + \log \lambda_R (\hat{\mathbf{e}}_2 \otimes \hat{\mathbf{e}}_2 + \hat{\mathbf{e}}_3 \otimes \hat{\mathbf{e}}_3). \quad (2.16)$$

Then, recalling that the Hencky's strain finds in the *Kirchhoff stress* –say $\boldsymbol{\tau}$ – its work-conjugate stress tensor [13, 93, 95] when they are co-axial and no rotations occur (as in the present case) [93, 94, 171], with reference to the Hencky's strain energy function $\Psi_H(\mathbf{H})$ provided below:

$$\Psi_H(\mathbf{H}) = \frac{1}{2} \mathbf{H} : \mathbf{C} : \mathbf{H} = \mu \operatorname{tr}(\mathbf{H}^2) + \frac{\Lambda}{2} \operatorname{tr}(\mathbf{H})^2, \quad (2.17)$$

one can finally write [4, 171]:

$$\begin{aligned} \boldsymbol{\tau} &= \frac{\partial \Psi_H(\mathbf{H})}{\partial \mathbf{H}} = \mathbf{C} : \mathbf{H} = \tau_L \hat{\mathbf{e}}_1 \otimes \hat{\mathbf{e}}_1 + \tau_R (\hat{\mathbf{e}}_2 \otimes \hat{\mathbf{e}}_2 + \hat{\mathbf{e}}_3 \otimes \hat{\mathbf{e}}_3), \\ \tau_{L,R} &= \frac{\partial \Psi_H}{\partial (\log \lambda_{L,R})} = 2\mu \log \lambda_{L,R} + \Lambda \log J, \end{aligned} \quad (2.18)$$

where $J := \det \mathbf{F} = \lambda_R^2 \lambda_L$ describes the element's volumetric change. Then, imposing that the only not vanishing stress component is the longitudinal one implies the following relationship:

$$\tau_R = 0 \iff \lambda_R = \lambda_L^{-\nu}. \quad (2.19)$$

As a consequence, after simple algebraic manipulations, the determinant of the deformation gradient tensor and the axial component of the Kirchhoff stress take the forms:

$$J = \lambda_L^{1-2\nu} \quad \text{and} \quad \tau_L = E \log \lambda_L, \quad (2.20)$$

respectively. On the basis of these results, it is also possible to derive the first Piola-Kirchhoff stress tensor \mathbf{P} and the *Cauchy stress tensor* $\boldsymbol{\sigma}$, the latter being additionally known as *true stress tensor* since it provides the stress relative to the current configuration and the two measures *de facto* coinciding in the limit of infinitesimal deformations and rotations. The expressions of \mathbf{P} and $\boldsymbol{\sigma}$ are in general respectively related to $\boldsymbol{\tau}$ as

$$\boldsymbol{\sigma} = J^{-1} \boldsymbol{\tau} \quad \text{and} \quad \mathbf{P} = \boldsymbol{\tau} \mathbf{F}^{-T}. \quad (2.21)$$

Therefore, in the specific case, the only not vanishing (longitudinal) components of the two tensors are given by

$$\sigma_L = J^{-1}\tau_L = \lambda_L^{2\nu-1}E \log \lambda_L \quad \text{and} \quad P_L = \lambda_L^{-1}\tau_L = \frac{E \log \lambda_L}{\lambda_L}. \quad (2.22)$$

Finally, the direct integration of the strain energy density function $\Psi_H(\mathbf{H})$ over the undeformed volume Ω_0 of the cylindrical element in the reference configuration leads to estimate the total elastic energy that is stored during the deformation process as

$$\begin{aligned} U_H &= \int_{\Omega_0} \Psi_H(\mathbf{H}) \, d\Omega = \frac{1}{2} \int_{\Omega_0} \boldsymbol{\tau} : \mathbf{H} \, d\Omega = \frac{1}{2} \int_{\Omega_0} \tau_L H_L \, d\Omega \\ &= \frac{1}{2} EAL (\log \lambda_L)^2. \end{aligned} \quad (2.23)$$

where $AL = \text{Vol}(\Omega_0)$, A being the element's nominal cross-sectional area.

2.1.3 Neo-Hookean cables and struts

By following the same line of reasoning above, with reference to the strain energy density function $\Psi_{NH}(\mathbf{F})$ characterizing a generic neo-Hookean material [95, 185] as recalled in the equation below:

$$\Psi_{NH}(\mathbf{F}) = \frac{\mu}{2\beta} \left(J^{-2\beta} - 1 \right) + \frac{\mu}{2} \left[\text{tr}(\mathbf{F}^T \mathbf{F}) - 3 \right], \quad \beta = \frac{\nu}{1-2\nu}, \quad (2.24)$$

one can derive the nominal stress as $\mathbf{P} = \partial \Psi_{NH}(\mathbf{F}) / \partial \mathbf{F}$. In particular, by again imposing the uni-axial stress condition (i.e. $P_R = 0$), the same relationship between the transverse and longitudinal stretches as in (2.19)₂ is obtained and the longitudinal component of \mathbf{P} results:

$$P_L = \mu \left(\lambda_L - \lambda_L^{-(2\nu+1)} \right). \quad (2.25)$$

As a consequence, the not null components of the Cauchy and Kirchhoff stresses are

$$\sigma_L = J^{-1}P_L\lambda_L = \mu \left(\lambda_L^{2\nu+1} - \lambda_L^{-1} \right) \quad \text{and} \quad \tau_L = P_L\lambda_L = \mu \left(\lambda_L^2 - \lambda_L^{-2\nu} \right), \quad (2.26)$$

while the total elastic energy for the neo-Hookean element reads:

$$U_{NH} = \int_{\Omega_0} \Psi_{NH}(\mathbf{F}) \, d\Omega = \frac{\mu AL}{2} \left(\lambda_L^2 + \frac{\lambda_L^{-2\nu} - \nu - 1}{\nu} \right). \quad (2.27)$$

In the special cases in which the hypothesis of *incompressible* neo-Hookean material is adopted, as done in the next section with reference to the 2-element tensegrity paradigm, the above equations can be particularized by using for the Poisson's ratio the value $\nu = 1/2$. In this way, the following expressions can be obtained for the total potential energy and for the nominal stress state of the body, respectively:

$$U_{NH} = \frac{KL}{6} \left(\lambda_L^2 + 2\lambda_L^{-1} - 3 \right) \quad \text{and} \quad \mathbf{P} = \frac{E}{3} (\lambda_L - \lambda_L^{-2}) \hat{\mathbf{e}}_1 \otimes \hat{\mathbf{e}}_1, \quad (2.28)$$

herein being $K = EA$ the axial stiffness of the cylinder. As a consequence, the longitudinal force component results to be

$$F_L = \frac{K}{3} (\lambda_L - \lambda_L^{-2}). \quad (2.29)$$

2.2 THE 2-ELEMENT SOFT TENSEGRITY PARADIGM

The present section is aimed to the study of the simplest example of soft-strut tensegrity system involving nonlinear hyperelasticity and buckling instability. Actually, a 2-element tensegrity paradigm, constituted by a single hyperelastic tensed cable and a compressed axially deformable strut that can severely contract in combination with (locally) buckling, is here provided. A neo-Hookean hyperelastic law is adopted for both the elements to trace large deformation regimes, potentially related both to high values of pre-stretch at self-equilibrium and to the action of externally applied loads. Without loss of generality and with the aim of proceeding in the simplest way, the standard hypothesis of incompressible materials is also made, different choices not influencing the quality of the results. On this base, in what follows, the so-called form-finding problem is firstly addressed by investigating the pre-stressed equilibrium states of the 2-element tensegrity system in absence of external loading, in this way uncovering different configurations as a function of the geometrical and constitutive parameters. Then, to the aim of evaluating its mechanical response (e.g. in terms of tangent stiffness), the self-balanced architecture is *ad hoc* perturbed through the prescription of an orthogonal displacement, thus finding, also in this case, multiple peculiar behaviors depending on the combination of the structural parameters. Finally, the limit case of a rigid-strut tensegrity, the effects of geometrical imperfections on pre-stretched equilibria and the buckling response under compressive load are further examined.

2.2.1 Characterization of the structure

The soft-tensegrity paradigm here presented consists of two elements obeying the structural principle of tensegrity systems [149]: a strut and a cable, bearing pre-compression and pre-tension, respectively, are interconnected at their extremities in a way to ensure the self-equilibrium of the whole system (figures 2.2B and 2.2E). The elements are both axially deformable and equipped with a central internal hinge: in particular, the strut has, coupled with the hinge at its middle point, an elastic rotational spring, in this way enabling the possibility of activating compressive buckling [13], while the hinge of the cable is used to apply an external perturbation –here prescribed in terms of displacement– to test the structure in the direction orthogonal to its axis (figures 2.2A, 2.2C and 2.2F). A pointwise hinge and roller are then provided at the two ends of the overall system.

As anticipated above, to account for large deformations, the two constituents are modeled as incompressible neo-Hookean hyperelastic solids (as described in section 2.1.3) while the buckling is provided in discrete form by the change of relative slope –ruled by the internal rotational spring’s stiffness– between the two (contracted) strut’s segments, these preserving their rectilinear shape in each deformed configuration [13].

2.2.2 Self-equilibria of the pre-stretched configuration

As constituents of a tensegrity, the cable and the strut bear, in the potentially straight or buckled reference (self-balanced) configuration of the system (figures 2.2B and 2.2E), tensile and compressive pre-stress, respectively. Under the assumption of hyperelastic material, such pre-stress implies, for each element, an axial deformation, so that the cable is elongated with a pre-stretch $\lambda_c^* \in [1, +\infty[$ while the strut is contracted with a pre-stretch $\lambda_s^* \in]0, 1]$.

By considering a buckled configuration (Fig. 2.2E), the compatibility of the deformation gives the following geometrical relationship between the cable’s pre-stretched semi-length ($L_c^* = \lambda_c^* L_c$) and the strut’s one ($L_s^* = \lambda_s^* L_s$):

$$L_c^* = L_s^* \cos \phi^*, \quad (2.30)$$

ϕ^* denoting the inclination of the two strut’s segments with respect to the axial direction of the global system. By conveniently expressing the

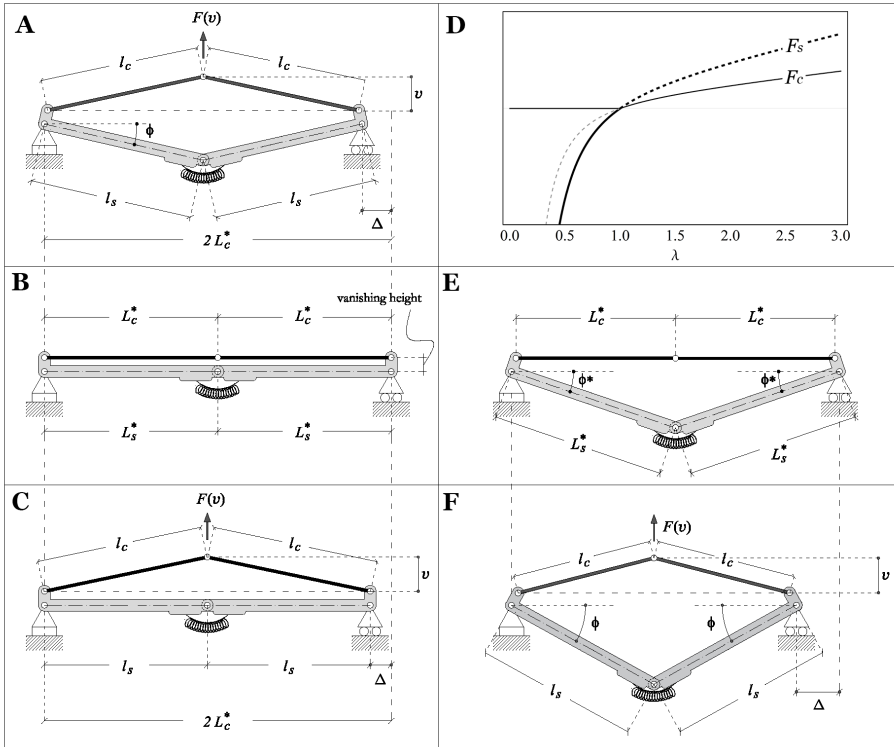


Figure 2.2: Sketch **B)** of the straight and **E)** of the buckled 2-element tensegrity in its (externally unloaded) pre-stretched self-balanced configuration. **A), C), F)** Sketches of the possible equilibrium configurations assumed by the tensegrity when perturbed by an off-axis displacement. **D)** Indicative trend of the (axial) force-stretch curves for incompressible neo-Hookean cable and strut. Solid lines identify the only tracts of the curves that can be actually experienced by the two elements, the strut being always compressed and the cable being assumed to support only tensile forces.

cable's rest semi-length L_c as a fraction of the strut's rest semi-length L_s , i.e.

$$L_c = \eta L_s, \quad (2.31)$$

with $\eta \in]0, 1]$ in order to guarantee that –in the pre-stretched state– the cable is actually tensed and the strut contracted, equation (2.30) returns:

$$\lambda_c^* = \frac{\lambda_s^* \cos \phi^*}{\eta}. \quad (2.32)$$

On the other hand, the equilibrium condition can be provided by standard arguments, namely by satisfying the principle of stationary total potential energy. In fact, with reference to the purely pre-stretched configuration, the total potential energy of the structure coincides with its internal elastic energy, which is given by:

$$U^* = 2(U_s^* + U_c^*) + U_k^*, \quad (2.33)$$

where U_s^* is –by virtue of symmetry– the elastic energy stored by each half-part of the strut, U_c^* is the aliquot associated to each half-cable, while U_k^* is the energy accumulated by the strut's rotational spring here written as

$$U_k^* = 2k(\phi^*)^2, \quad (2.34)$$

under the hypothesis of linear spring with rotational stiffness k . The strut's and the cable's halves are instead modeled as made of incompressible neo-Hookean beams undergoing uni-axial (longitudinal) stress (see section 2.1.3), whose elastic energies are thus given by

$$U_i^* = \frac{K_i L_i}{6} \left[(\lambda_i^*)^2 + 2(\lambda_i^*)^{-1} - 3 \right], \quad i = s, c, \quad (2.35)$$

where K_i represents the axial stiffness of each element. By substituting the expressions (2.34) and (2.35) into the equation (2.33), and by taking into account the compatibility condition (2.32), the total potential energy U^* results

$$\begin{aligned} U^*(\lambda_s^*, \phi^*) = & \frac{1}{3\eta\lambda_s^*} \left\{ L_s \left[K_c (\cos \phi^*)^2 + \eta K_s \right] (\lambda_s^*)^3 + \right. \\ & 3\eta \left[2k(\phi^*)^2 - (\eta K_c + K_s) L_s \right] \lambda_s^* + \\ & \left. 2\eta L_s (K_s + \eta^2 K_c \sec \phi^*) \right\}, \end{aligned} \quad (2.36)$$

where λ_s^* and ϕ^* are the kinematic variables of the system. Therefore, the equilibrium problem can be written in the classical form

$$\frac{\partial U^*}{\partial \lambda_s^*} = 0, \quad \frac{\partial U^*}{\partial \phi^*} = 0, \quad (2.37)$$

whose solution $(\bar{\lambda}_s^*, \bar{\phi}^*)$ is a function of the geometrical and constitutive parameters characterizing the structure. Additionally, suitable dimensionless parameters –say ζ and κ – are introduced:

$$K_s = \zeta k / (2L_s) \quad \text{and} \quad K_c = K_s / \kappa, \quad (2.38)$$

in this way $\zeta > 0$ denoting the ratio between the axial and the flexural rigidity of the strut and $\kappa > 0$ the corresponding ratio between the strut's and the cable's axial stiffness. As a consequence, the behavior of the system is entirely governed by the coefficients η , ζ and κ and the equilibrium equations (2.37) take the explicit form

$$\begin{aligned} \left[\eta\kappa + (\cos \phi^*)^2 \right] (\lambda_s^*)^3 - \eta (\kappa + \eta^2 \sec \phi^*) &= 0, \\ \zeta \sin \phi^* \cos \phi^* (\lambda_s^*)^3 - 12\eta\kappa\phi^* \lambda_s^* - \zeta\eta^3 \tan \phi^* \sec \phi^* &= 0. \end{aligned} \quad (2.39)$$

In particular, it can be proved that the (2.39)₁ gives the unique real root

$$\bar{\lambda}_s^* = \tilde{\lambda}_s^*(\eta, \zeta, \kappa) = \left[\frac{\eta (\kappa + \eta^2 \sec \phi^*)}{\eta\kappa + (\cos \phi^*)^2} \right]^{1/3}, \quad (2.40)$$

by which, upon substitution into the (2.39)₂, one can finally obtain a single governing equation that relates the angle ϕ^* to the structural parameters. This admits only the trivial solution $\bar{\phi}^* = 0$ as long as the pre-stress borne by the tensegrity's elements holds below a certain critical value, in this case the system preserving its straight configuration (figure 2.2B), fully characterized by

$$\bar{\phi}^* = 0, \quad \bar{\lambda}_s^* = \left[\frac{\eta (\kappa + \eta^2)}{\eta\kappa + 1} \right]^{1/3}. \quad (2.41)$$

Then, once the pre-stress achieves the critical threshold, bifurcation of the equilibrium occurs and the trivial solution coexists with a non-trivial one, say $\bar{\phi}^* = \tilde{\phi}^*(\eta, \zeta, \kappa)$, that, due to the nonlinearity of the equation at hand, has been numerically found with the aid of the computational software Mathematica[®] [244], in such a case the buckling mode (figure 2.2E) being completely described as

$$\bar{\phi}^* = \tilde{\phi}^*(\eta, \zeta, \kappa), \quad \bar{\lambda}_s^* = \left[\frac{\eta (\kappa + \eta^2 \sec \tilde{\phi}^*)}{\eta\kappa + (\cos \tilde{\phi}^*)^2} \right]^{1/3}. \quad (2.42)$$

More in detail, different pre-stretched configurations at equilibrium can be explored by taking the coefficient η as control parameter, since the pre-stress in the tensegrity's elements is simply decided by the difference between their two resting lengths, once L_s , ζ and κ are assigned. In particular, starting from the case $\eta = 1$, which identifies a structure with zero pre-stress, it is possible to progressively decrease η so as to

increase the internal pre-stress up to a critical value which induces the structure buckling (critical condition). Then, by further decreasing the cable's rest length, it is possible to follow the response of the tensegrity in the post-buckling phase.

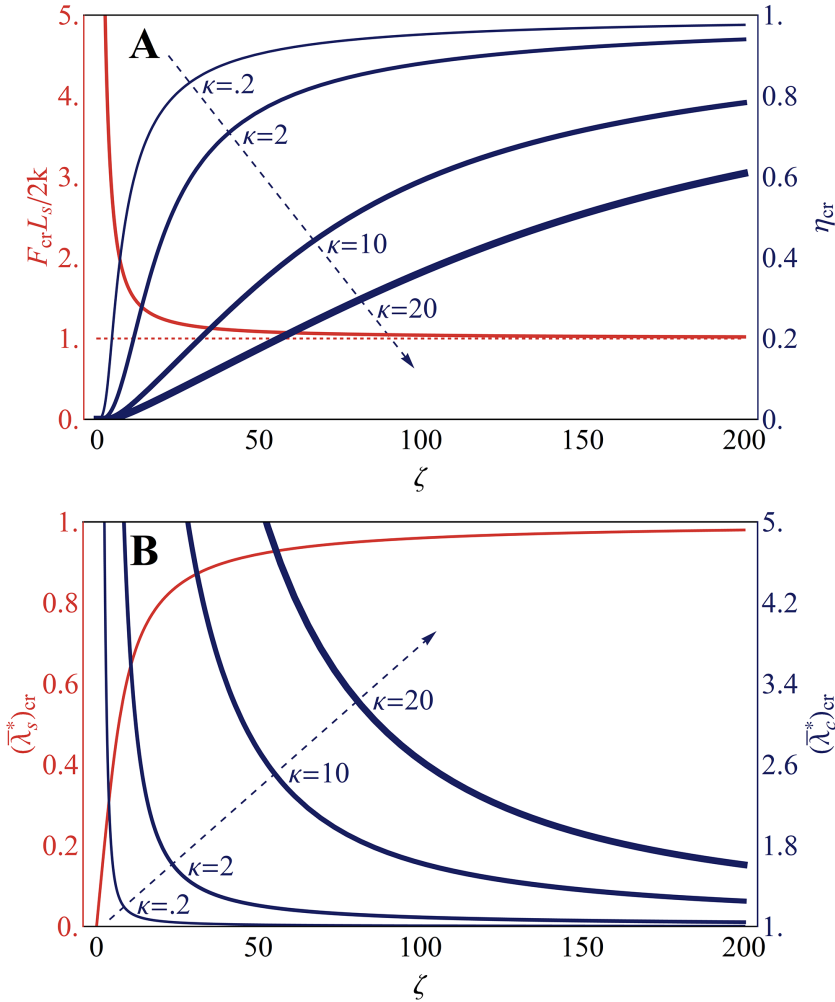


Figure 2.3: **A)** Critical force F_{cr} (red line) –normalized with respect to the limit value $2k/L_s$ that it assumes in case of inextensible strut– and critical ratio η_{cr} (blue lines), for varying values of ζ and κ . **B)** Trends of the critical strut's pre-stretch $(\bar{\lambda}_s^*)_{cr}$ (red line) and of the critical cable's pre-stretch $(\bar{\lambda}_c^*)_{cr}$ (blue lines), for varying values of ζ and κ .

The quantities of main interest, at the critical configuration of incipient buckling, are shown in figure 2.3, by making variable the parameters ζ and κ . Specifically, the red line in figure 2.3A describes the trend of

the critical load which, by taking into account both equilibrium and constitutive assumptions (see section 2.1.3), is given by

$$F_{cr} = \frac{K_i}{3} \left| (\bar{\lambda}_i^*)_{cr} - (\bar{\lambda}_i^*)_{cr}^{-2} \right|, \quad i = s, c, \quad (2.43)$$

herein being $(\bar{\lambda}_i^*)_{cr}$ the critical equilibrium pre-stretches defined as

$$(\bar{\lambda}_i^*)_{cr} = \bar{\lambda}_i^*|_{\eta=\eta_{cr}}, \quad \eta_{cr} : \tilde{\Phi}^*(\eta_{cr}, \zeta, \kappa) = 0, \quad (2.44)$$

where η_{cr} denotes the value of η at which buckling occurs, for given constitutive parameters. It is worth noticing that the instability event characterizing the system under study is actually related to the (compressive) buckling that the strut can undergo: *de facto*, the buckling of the global tensegrity occurs when the compressive stress within the strut reaches the critical value inducing the strut's local buckling, the cable–bearing tensile load– not experiencing any local instability. This means that the whole structure's critical load F_{cr} properly coincides with the one of the strut and, as a consequence, its value does not depend on the parameter κ , as observable in figure 2.3A. However, due to the geometry of the 2-element tensegrity, in which the constituents are pointwise connected at their extremities, equilibrium condition requires, at each stage, the equality of the axial –tensile and compressive– forces borne by the cable and the strut, respectively. Therefore, despite the value of F_{cr} is in principle imposed by the strut, by virtue of the equilibrium, it can be evaluated –according to the equation (2.43)– as the force borne indifferently by the strut or the cable when the critical ratio η_{cr} between the rest lengths of the two elements is reached, in this way it being independent from the index i , that indeed can be equally selected as s or c . On the other hand, it has to be highlighted that F_{cr} is strongly affected by ζ , since this parameter prescribes the ratio between the strut's axial and flexural stiffness so that the higher is ζ the more convenient is for the strut to buckle rather than to remain only axially contracted. Indeed, for high values of ζ , in particular when $\zeta \rightarrow \infty$, F_{cr} asymptotically approaches the critical load of a *standard* strut made of two *rigid* parts, that is $2k/L_s$ [13]. For smaller values of ζ , instead, the critical load is always higher than the standard case and, in the limit of $\zeta \rightarrow 0$, to avoid buckling results more convenient for the structure, i.e. $F_{cr} \rightarrow \infty$. Also, figure 2.3B reports the trend of the strut's critical pre-stretch $(\bar{\lambda}_s^*)_{cr}$, which corroborates the behavior described up to now, this pre-stretch converging to 1 when $\zeta \rightarrow \infty$ (buckling of the system anticipating any axial contraction) and to 0 for $\zeta \rightarrow 0$ (no buckling occurs). On the other hand, as illustrated in

figure 2.3A, it is found that the value of η_{cr} increases with ζ : in fact, the higher is ζ , the lower is the required critical load and, consequently, the lower is the difference between cable's and strut's rest lengths needed to induce buckling. Accordingly, the cable's critical pre-stretch $(\bar{\lambda}_c^*)_{cr}$, which allows to balance the critical load, also reduces as shown in figure 2.3B. Moreover, by increasing κ , at fixed ζ , it is possible to observe that η_{cr} decreases (figure 2.3A), this meaning that the instability event is delayed by prescribing an higher ratio between the strut's and the cable's axial stiffness. Accordingly, $(\bar{\lambda}_c^*)_{cr}$ increases with κ (figure 2.3B).

The obtained solutions (2.41) and (2.42) also lead to predict the different equilibrium states experienced by the system as η varies, in terms of pre-critical, critical and post-critical configurations, as illustrated in figure 2.4. More specifically, figure 2.4A shows the rotation angle $\bar{\phi}^*$ against the control parameter η (normalized with respect to its critical value) at the equilibrium, for assigned pairs of κ and ζ . Starting from a condition $\eta > \eta_{cr}$ –in which the tensegrity deforms by preserving its straight configuration so that $\bar{\phi}^* = 0$ – bifurcation of the equilibrium, with switching from the trivial to non-trivial solution's branches, is encountered as the critical value is reached, by progressively decreasing η . Also, the study of the Hessian of the total potential energy reveals that the trivial path is stable up to η_{cr} and unstable after it, while the stability of the non-trivial post-critical state depends on how the structural parameters combine. In figure 2.4, stable paths are represented by solid lines, while unstable ones by dashed lines: in detail, figure 2.4A reports both cases in which the pairs (κ, ζ) give an everywhere stable buckled solution and a possible scenario (the blue-petroleum curve) in which instead there exists a range of angles $\bar{\phi}^*$ within which the configuration becomes unstable. The inset in figure 2.4A shows the zoom of this particular scenario with the paths followed by a tensegrity that was lying in an unstable status between the points **b** and **d**: the system could be either in positions such as that denoted with the point **c**₁ –from which it could switch on a stable configuration by remaining on the non-trivial path by increasing/reducing its inclination– or in situations such as that of **c**₂, in which it can snap towards a stable buckled state (with increased rotation) as well as return to a straight configuration. In parallel, figure 2.4B shows the corresponding phase-portrait of the strut's and cable's equilibrium pre-stretches $\bar{\lambda}_s^*$ and $\bar{\lambda}_c^*$, obtained by decreasing η from 1 to 0: starting from $\eta = 1$ and following the trivial path up to η_{cr} (except the cases represented by the blue-petroleum curve that admit multiple solutions for some pre-critical values of η), $\bar{\lambda}_s^*$ decreases and $\bar{\lambda}_c^*$ increases so as to guarantee the equilib-

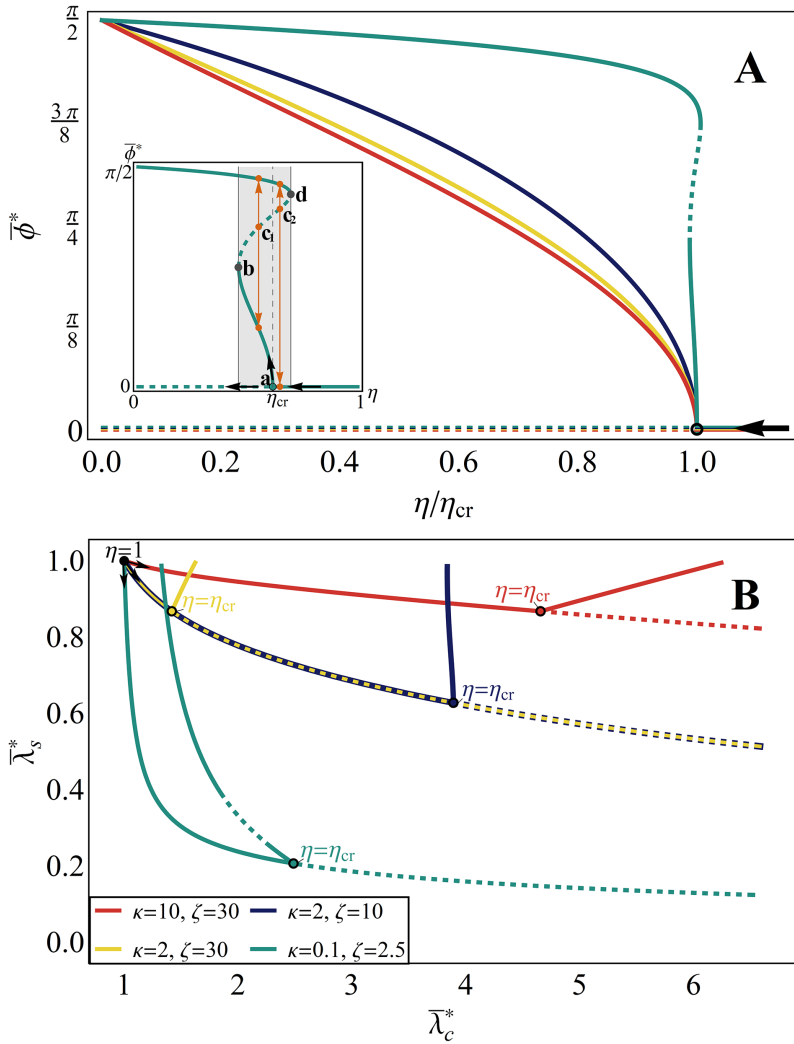


Figure 2.4: **A)** Bifurcation diagram showing the evolution of the angle $\bar{\phi}^*$, formed by the two half-parts of the strut with the axial direction of the whole system in the pre-stretched configuration, when decreasing the ratio η between the cable's and the strut's resting lengths, normalized with respect to its critical value η_{cr} . The inset gives a zoom over the unstable (dashed) tract of the blue-petroleum curve. **B)** Evolution of the strut's and cable's pre-stretches $\bar{\lambda}_s^*$ and $\bar{\lambda}_c^*$ when decreasing η from 1 to 0, plotted in the $\bar{\lambda}_c^*-\bar{\lambda}_s^*$ space. Both in **A** and **B**, the differently coloured curves are obtained for different pairs of constitutive parameters κ and ζ , while solid lines denote stable equilibrium paths and dashed lines represent unstable branches.

rium of the straight system. Then, the non-trivial configuration is always characterized by the strut re-elongation during buckling, that reports $\bar{\lambda}_s^*$ to 1 when $\eta \rightarrow 0$, while different behaviors can be observed for $\bar{\lambda}_c^*$: in fact, the cable's pre-stretch can either continue to increase or start to decrease as a function of the selected pair of parameters (κ, ζ) . Moreover, since the solution (2.41) is independent from the ratio ζ between the strut's axial and flexural stiffness, the trivial path –both in the pre-critical and post-critical conditions– is shared by tensegrity systems having the same κ but different ζ (see, as an example, the yellow and blue curves in figure 2.4B).

2.2.3 System's equilibria under off-axis perturbations

Let us consider a 2-element tensegrity with prescribed geometrical and constitutive parameters in its self-balanced pre-stretched configuration, undergoing the action of an off-axis external perturbation, say a pointwise displacement applied at the central hinge of the cable in the direction orthogonal to the reference axis of the overall system, as illustrated in figure 2.2. At the equilibrium, three different mechanical responses can be envisaged: *i*) the structure starts from a straight pre-stretched configuration (figure 2.2B) and the strut remains straight during the whole process (figure 2.2C); *ii*) the structure is initially straight (figure 2.2B), then the strut buckles as the prescribed displacement equates a certain critical value (figure 2.2A); *iii*) the structure (hence the strut) is already buckled in the self-balanced configuration (figure 2.2E) and the strut segments amplify their relative inclination as the external displacement magnitude grows (figure 2.2F). By analyzing the third situation –from which all the other cases can be recovered– and by fixing η , κ and ζ , the geometrical compatibility of the deformation produced by the prescribed displacement having magnitude v , requires that the strut's and cable's semi-lengths (l_s and l_c) in the current configuration respectively are

$$l_s = \frac{2L_s^* \cos \bar{\phi}^* - \Delta}{2 \cos \phi} \quad \text{and} \quad l_c = \sqrt{v^2 + l_s^2 (\cos \phi)^2}, \quad (2.45)$$

where $\phi = \bar{\phi}^* + \delta\phi$ is the current angle characterizing the buckling-induced rotation of the strut tracts, while $\delta\phi$ and Δ are respectively the strut's rotation and the overall system's axial displacement resulting from the applied perturbation, which also represent the two kinematic variables governing the problem at hand. Nondimensionalization of v

and Δ with respect to the resting length of the strut is then performed by setting:

$$v = 2L_s \varepsilon_v \quad \text{and} \quad \Delta = 2L_s \varepsilon_\Delta. \quad (2.46)$$

As a consequence, the total longitudinal stretches of the strut and the cable read as

$$\begin{aligned} \lambda_s &= \frac{l_s}{L_s} = \frac{\bar{\lambda}_s^* \cos \bar{\phi}^* - \varepsilon_\Delta}{\cos \phi} \quad \text{and} \\ \lambda_c &= \frac{l_c}{L_c} = \frac{\sqrt{4\varepsilon_v^2 + (\bar{\lambda}_s^* \cos \bar{\phi}^* - \varepsilon_\Delta)^2}}{\eta}. \end{aligned} \quad (2.47)$$

By following an analogous way to that giving the equation (2.33), the total potential energy of the tensegrity under the applied displacement can be written as sum of the internal energies of its constituents:

$$U = 2(U_c + U_s) + U_k, \quad (2.48)$$

where

$$U_k = 2k\phi^2, \quad (2.49)$$

while the energies of the neo-Hookean semi-strut and semi-cable lead to write

$$U_i = \frac{K_i L_i}{6} \left(\lambda_i^2 + 2\lambda_i^{-1} - 3 \right), \quad i = s, c. \quad (2.50)$$

By virtue of the nondimensionalization (2.46), the unknown functions $\delta\phi(\varepsilon_v)$ and $\varepsilon_\Delta(\varepsilon_v)$ univocally identify the deformed configuration related to the prescribed external displacement v and the equilibrium problem can be formulated as

$$\frac{\partial U}{\partial \delta\phi} = 0, \quad \frac{\partial U}{\partial \varepsilon_\Delta} = 0. \quad (2.51)$$

The resulting nonlinear system has been solved numerically, again with the aid of the symbolic code Mathematica[®][244], in this way providing the equilibrium states $(\bar{\delta\phi}, \bar{\varepsilon}_\Delta) = (\bar{\delta\phi}(\varepsilon_v; \eta, \kappa, \zeta), \bar{\varepsilon}_\Delta(\varepsilon_v; \eta, \kappa, \zeta))$. It is worth noting that, when the combination of geometrical and constitutive parameters is such that the tensegrity starts from a straight –rather than buckled– configuration (as for cases in figures 2.2A and 2.2C), the equations reported above hold true by assuming $\bar{\phi}^* = 0$. In this case, the

trivial solution with $\bar{\delta}\phi = 0$ represents the unique solution for the system (2.51) up to a critical value of the applied displacement, after which the equilibrium bifurcation occurs with the coexistence of the trivial path $\bar{\delta}\phi = 0$ and the non-trivial one $\bar{\delta}\phi = \bar{\delta}\phi(\varepsilon_v; \eta, \kappa, \zeta)$.

Figure 2.5A shows the response of the structure under the external perturbation in terms of current strut's inclination angle at equilibrium, namely $\bar{\phi} = \bar{\phi}^* + \bar{\delta}\phi$, and global tangent stiffness defined as

$$S = \frac{\partial^2 \bar{U}}{\partial v^2}, \quad (2.52)$$

$\bar{U} = U|_{(\delta\phi=\bar{\delta}\phi, \varepsilon_\Delta=\bar{\varepsilon}_\Delta)}$ being the energy associated to the deformed state of the structure at equilibrium. In addition, the plot of the results in the stretches' phases space is reported in figure 2.5B. Without loss of generality, the shown results have been obtained by fixing the resting lengths ratio ($\eta = 0.8$) and the cable-strut axial stiffness ratio ($\kappa = 2$), then considering three different values of ζ , chosen in a way to replicate –over the range $\varepsilon_v \in [0, 1.5]$ – all the three possible mechanical responses of the system (figures 2.2A, 2.2C, 2.2F). In fact, in the inset of figure 2.5A, it is possible to identify both the limit cases of tensegrity never undergoing buckling ($\zeta = 5$) and always buckled ($\zeta = 100$), respectively illustrated in figures 2.2C and 2.2F, as well as the intermediate situation of displacement-induced buckling ($\zeta = 40$), as the one in figure 2.2A. In figure 2.5A the trend of the (normalized) tangent stiffness has been obtained: in particular, with reference to the intermediate case ($\zeta = 40$), a downward jump produced by the instability event can be recognized. Correspondingly, the stretches $\bar{\lambda}_s$ and $\bar{\lambda}_c$ evolve as in figure 2.5B: by progressively increasing ε_v , $\bar{\lambda}_c$ grows while buckling, $\bar{\lambda}_s$ decreasing in pre-buckling and recovering in post-buckling. It is worth highlighting that, as consequence of the nondimensionalization, the overall trivial path associated to the initially straight tensegrity that undergoes displacement-induced buckling ($\zeta = 40$) actually coincides with the evolution followed by the structure in the case in which buckling never occurs within the range of values here considered for the external perturbation ($\zeta = 5$), both in terms of tangent stiffness and stretches.

2.2.4 Further insights into the 2-element tensegrity mechanics

In this subsection, the limit case of a rigid-strut tensegrity, the influence of a geometrical imperfection on the pre-stretched configuration and the effect of an externally applied compressive axial load are all analyzed,

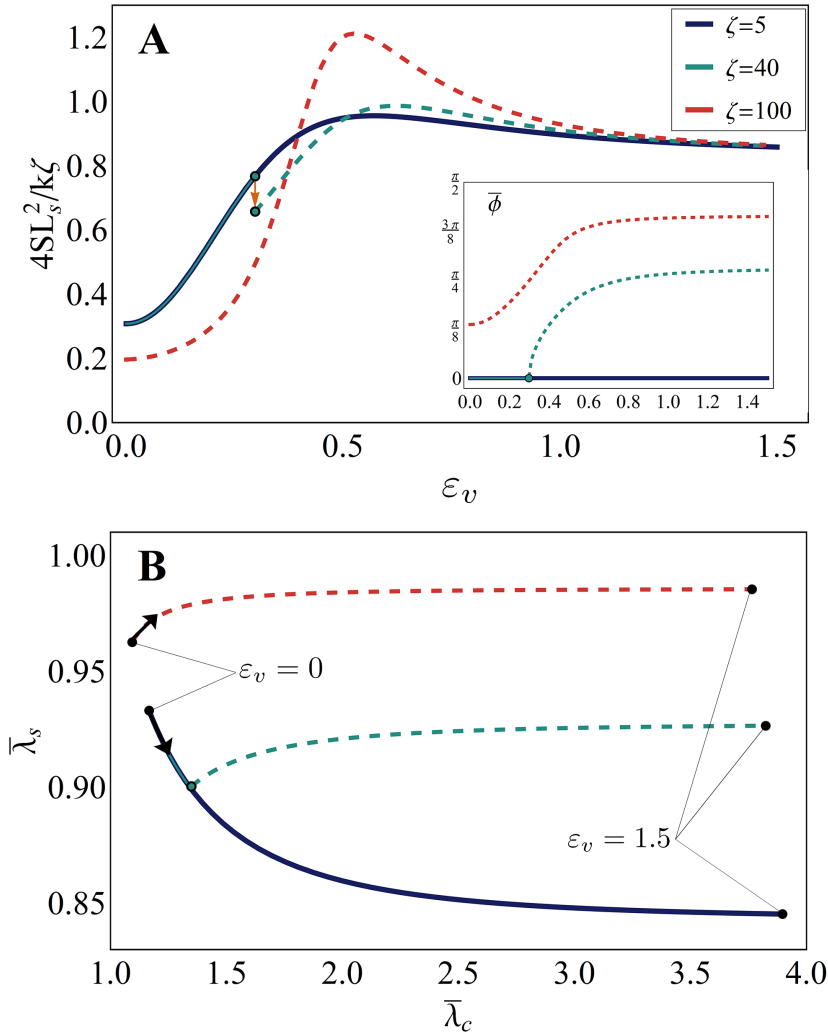


Figure 2.5: **A)** Normalized tangent stiffness exhibited by the 2-element tensegrity system when subjected to an external orthogonal displacement applied to the central internal hinge of the cable, for $\varepsilon_v \in [0, 1.5]$. In the inset, the inclination angle $\bar{\phi}$ described by the strut with respect to the system's axial direction in the current (perturbed) configuration, within the same range of ε_v . **B)** Trend of the strut's and cable's total (current) stretches $\bar{\lambda}_s$ and $\bar{\lambda}_c$ as varying ε_v within the considered range, plotted in the $\bar{\lambda}_c$ - $\bar{\lambda}_s$ space. All the plots have been obtained by setting $\eta = 0.8$ and $\kappa = 2$. The differently coloured curves are referred to different values of ζ , while solid lines are used to identify straight configurations and dashed lines denote the non-trivial buckled ones.

with the aim to obtain further insights into the mechanical behavior of the 2-element tensegrity paradigm.

2.2.4.1 Self-equilibrium states of a rigid-strut tensegrity

It has been already previously observed that, when the strut is composed by two rigid parts –namely its axial stiffness tends to infinity with respect to the one of the internal rotational spring ($\zeta \rightarrow \infty$)– the critical load F_{cr} in (2.43) asymptotically tends to the value classically found for an isolated axially rigid strut undergoing local buckling due to the application of an external compressive load [13], $(\lambda_s^*)_{cr}$ consistently tending to 1 (see figure 2.3A). With the aim to more deeply analyze the limit case of a 2-element rigid-strut tensegrity, one has to simplify equations (2.32) and (2.33) by imposing $\lambda_s^* = 1$, so that the cable's pre-stretch and the total potential energy of the whole purely pre-stretched (buckled) structure result respectively given by:

$$\lambda_c^* = \frac{\cos \phi^*}{\eta} \quad \text{and} \quad U^* = 2U_c^* + U_k^*, \quad (2.53)$$

with U_k^* and U_c^* provided by equations (2.34) and (2.35). By solving the only equilibrium equation for the present problem, that is $\partial U^* / \partial \phi^* = 0$, one finds the following analytical expression for the geometrical variable $\eta = \hat{\eta}(\phi^*; \alpha)$ describing the behavior of the system in the post-critical phase:

$$\hat{\eta} = \frac{-16\alpha\phi^* [1 + \cos(2\phi^*)] + 2^{1/3} [f(\alpha)]^2 \sin^{-1} \phi^*}{2^{5/3} \alpha f(\alpha)}, \quad (2.54)$$

where

$$\begin{aligned} \alpha &= 2K_c L_s / k, \\ f(\alpha) &= \left\{ (2 \cos \phi^*)^3 \sqrt{(\alpha \sin \phi^*)^3 [(\alpha \sin \phi^*)^3 + 256 (\phi^*)^3]} + \right. \\ &\quad \left. + [\alpha \sin(2\phi^*)]^3 \right\}^{1/3}, \end{aligned} \quad (2.55)$$

which also provides

$$\hat{\eta}_{cr} := \lim_{\phi^* \rightarrow 0} \hat{\eta} = \frac{-8 + 2^{1/3} (\alpha^{3/2} + \sqrt{256 + \alpha^3})^{2/3}}{2^{2/3} [\alpha^3 + \sqrt{\alpha^3 (256 + \alpha^3)}]^{1/3}} \quad (2.56)$$

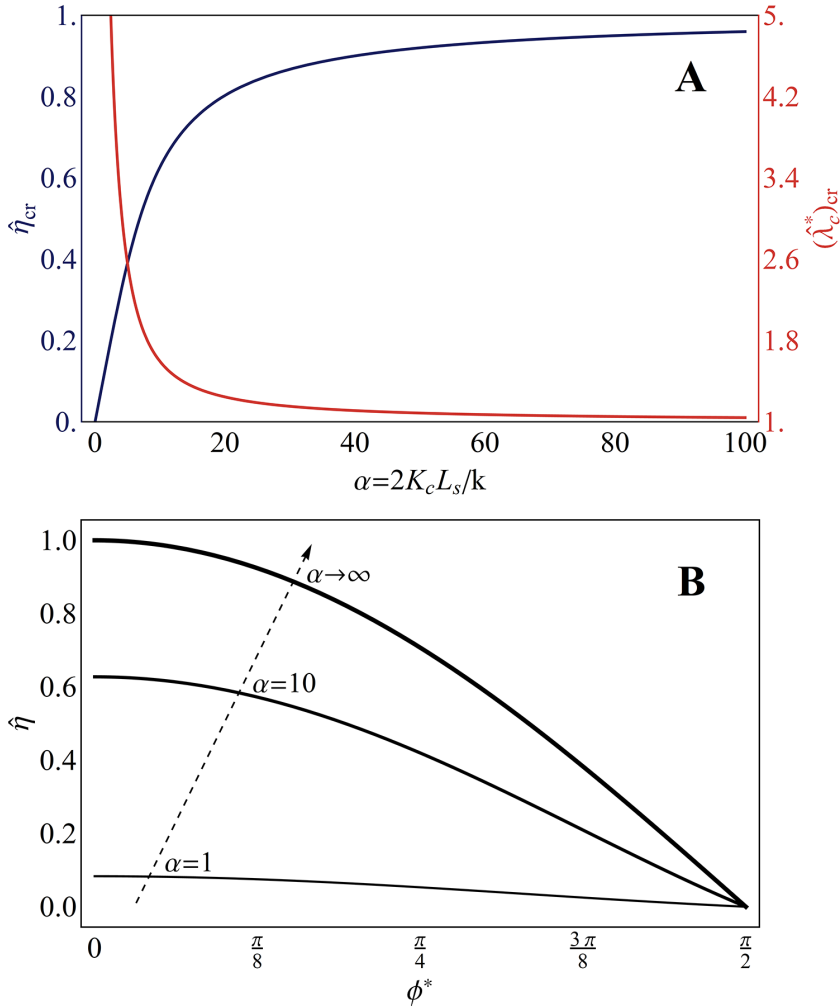


Figure 2.6: **A)** Critical ratio $\hat{\eta}_{cr}$ (blue line) and critical cable's pre-stretch $(\hat{\lambda}_s^*)_{cr}$ (red line) exhibited by the 2-element tensegrity in the limit case of rigid strut as functions of the parameter α . **B)** Plot of the geometrical ratio $\hat{\eta}$ required by the structure, in the case of rigid strut, to buckle with a certain angle ϕ^* , for selected values of the parameter α .

as threshold value inducing buckling of the self-balanced configuration, which in this case remains straight and globally axially undeformed as long as $\eta > \hat{\eta}_{cr}$, due to the axial rigidity of the strut. Then, the axial

force and the pre-stretch within the hyperelastic cable at the tensegrity's buckled stage are respectively given by

$$\hat{F} = \frac{2k\phi^*}{L_s \sin \phi^*}, \quad \text{with} \quad \hat{F}_{cr} = \frac{2k}{L_s} \quad (2.57)$$

and $\hat{\lambda}_c^* = \cos \phi^* / \hat{\eta}$, with $(\hat{\lambda}_c^*)_{cr} = (\hat{\eta}_{cr})^{-1}$.

Finally, the response of the analyzed rigid-strut structure is shown in figure 2.6 in terms of $\hat{\eta}_{cr}$ –with the related $(\hat{\lambda}_c^*)_{cr}$ – and $\hat{\eta}$, for varying α and ϕ^* .

2.2.4.2 Effects of a geometrical imperfection on the tensegrity self-equilibria

It is worth to analyze the self-equilibrium stages of the 2-element soft-strut tensegrity when it is characterized by a geometrical imperfection, e.g. an initial inclination ϕ_0 imposed to the two parts composing the strut at the pre-stretched configuration. In such a case, due to geometrical arguments, the upper value allowed for the ratio η between the lengths of the cable and the strut at rest, which defines the self-balanced stress-free condition for the assembled tensegrity structure, is given by $\cos \phi_0$ and coincides with 1 in the particular case of vanishing imperfection. Therefore, in general, in the case under study, it results $0 < \eta \leq \cos \phi_0 \leq 1$. Consistently, the total potential energy of the system can be still written as in equation (2.33), where the energy of the rotational spring, previously provided by the equation (2.34), has to be here replaced by

$$U_k^* = 2k(\phi^* - \phi_0)^2. \quad (2.58)$$

By then following a procedure analogous to that of the subsection 2.2.2, the same solution expressed in equation (2.42) is here found, although with a different form for $\tilde{\phi}^*$ –in this case depending also on ϕ_0 – which has been numerically determined and shown in figure 2.7A as a function of η . In particular, starting from the initial value ϕ_0 , corresponding to the unstressed tensegrity configuration in which $\eta = \cos \phi_0$, $\tilde{\phi}^*$ continuously increases up to $\pi/2$ while η decreases towards 0. Also, it can be observed that for a vanishing initial inclination of the strut (i.e. $\phi_0 = 0$), the buckling response of the perfect system is recovered. Finally, the phase diagram $\bar{\lambda}_c^* - \bar{\lambda}_s^*$ is shown in figure 2.7B, where the influence of a growing imperfection can be observed, in particular in the related lowering of the values assumed by both the cable's and strut's pre-stretches while η decreases.

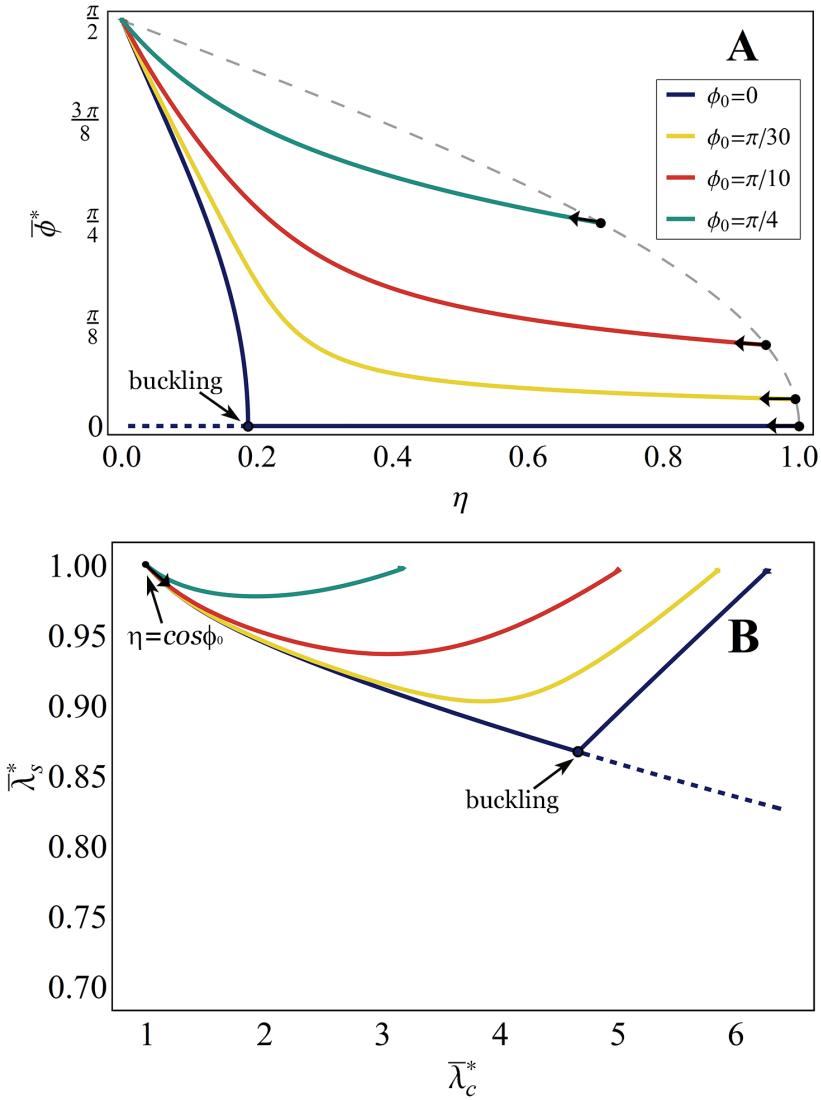


Figure 2.7: **A**) Plot of the inclination angle $\bar{\phi}^*$, formed by the two half-parts of the strut with the tensegrity axial direction, in the purely pre-stretched configuration, in presence of an imperfection ϕ_0 , against the ratio η . The grey dashed line identifies the curve limiting the value of η for each initial imperfection ϕ_0 –with $0 \leq \phi_0 < \pi/2$ – i.e. $\eta = \cos \phi_0$. **B**) Phase diagram of the strut's and cable's pre-stretches $\bar{\lambda}_s^*$ and $\bar{\lambda}_c^*$ while η decreases from $\cos \phi_0$ to 0 (from left to right). Both in **A** and **B**, the differently coloured curves are obtained for different values of the initial imperfection and for a selected pair of constitutive parameters κ and ζ : $\kappa = 10$, $\zeta = 30$. When $\phi_0 = 0$ the buckling response of the perfect system is recovered.

2.2.4.3 Buckling response under axial compressive load

Let us finally analyze the buckling response of an initially straight soft-tensegrity under the action of an external compressive load axially applied at the roller on the right end. As found in subsection 2.2.2, self-equilibria of a straight tensegrity are described by the solution in equation (2.41), with $\eta_{cr} < \eta \leq 1$. If one applies an axial compressive load having magnitude D to the self-balanced system, the updated (current) stretches of the cable and the strut can be respectively obtained as

$$\lambda_c^d = \frac{\bar{\lambda}_s^* - \varepsilon_d}{\eta} \quad \text{and} \quad \lambda_s^d = \frac{\bar{\lambda}_s^* - \varepsilon_d}{\cos \phi_d}, \quad (2.59)$$

herein being $\varepsilon_d = \Delta_d / (2L_s) - \Delta_d$ representing the global axial displacement induced by the applied force– and ϕ_d the corresponding rotation angle of the strut’s halves with respect to the horizontal direction. The internal elastic energy of the system U_d can be hence given in the same form provided in the equation (2.48), by properly re-writing the expressions of the rotational spring aliquot (2.49) and the ones of the hyperelastic elements (2.50) with reference to the rotation ϕ_d and to the total stretches in (2.59) obtained in this case, respectively. Then, the total potential energy can be provided as

$$W_d = U_d - D \Delta_d. \quad (2.60)$$

It is important to note that, differently from the problem analyzed in subsection 2.2.3, in which the geometry was such that the tension state of the cable was naturally preserved, the cable could here undergo compression both in the pre- and in the post-buckling phase under the effect of the axial load. Therefore, with the aim of modelling the inability of the cable to bear compression –a standard hypothesis for tensegrity systems– it is here assumed that the energy contribution of the cable vanishes when $\lambda_c^d \leq 1$. By then solving the equilibrium equations

$$\frac{\partial W_d}{\partial \phi_d} = 0, \quad \frac{\partial W_d}{\partial \varepsilon_d} = 0, \quad (2.61)$$

written with respect to the two kinematic variables of the system ϕ_d and ε_d , one finds the results shown in figure 2.8 in terms of critical and post-critical force, say \bar{D}_{cr} and \bar{D} respectively. Actually, due to the nonlinear but algebraic nature of the equations corresponding to the system (2.61), one can verify that such results can be also determined in closed-form if $\bar{D}(\phi_d; \eta, \kappa, \zeta)$ and $\bar{\varepsilon}_d(\phi_d; \eta, \kappa, \zeta)$ are chosen as unknowns; however, their explicit expressions are not reported here for sake of brevity.

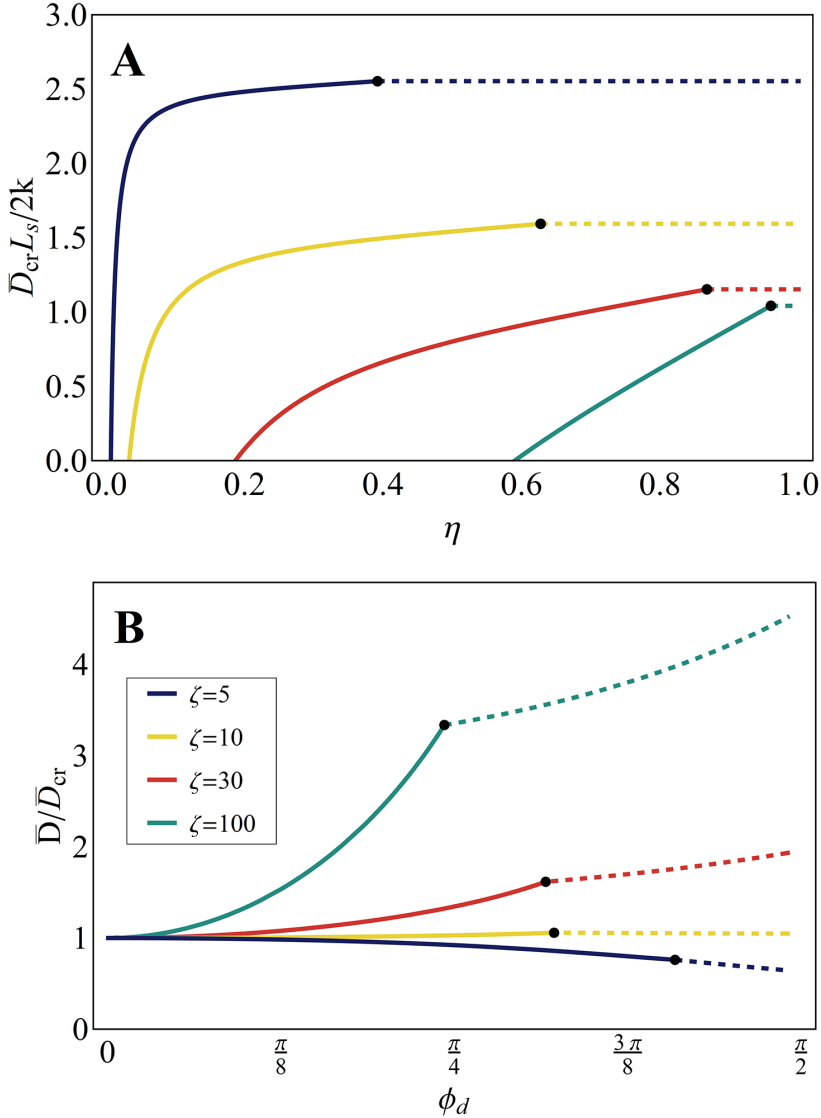


Figure 2.8: **A**) (Normalized) compressive critical load $D_{cr}L_s/(2k)$ obtained by varying η for a straight pre-stretched tensegrity configuration, for $\kappa = 10$ and the values $\zeta = 5, 10, 30, 100$. Dashed lines identify ranges of η such that the cable is inoperative at the buckling critical configuration while solid curves are obtained if the contribution of the cable is effective. **B**) Compressive post-critical load \bar{D} –normalized to its critical value– versus the rotation ϕ_d , for a tensegrity with $\kappa = 10$ and $\zeta = 5, 10, 30, 100$, the values of η being selected for each case in a way that the cable is still tensed at the buckling configuration: in the order, $\eta = 0.2, 0.4, 0.5, 0.7$. Dashed tracts of the curves identifies angles ϕ_d for which the cable would undergo compression due to the external loading.

2.3 CONCLUSION

In the sections of this chapter, the necessity of building up nonlinear and buckling soft tensegrity models for applications to cytomechanics has been highlighted. Then, hyperelastic models for deformable struts and cables undergoing large deformations have been introduced within the general framework of the nonlinear continuum mechanics. The obtained equations have been subsequently employed for providing a first paradigm of soft-tensegrity structure taking into account coupled nonlinear hyperelasticity and buckling of its elements. This consists in a 2-element pre-stressed system comprising a deformable strut, bearing compression, whose ends are linked to the ones of a tensed elastic cable. The structure has the possibility to both axially deform and buckle, as a result of the presence of a central hinge equipped with an elastic rotational spring within the strut. Firstly, in absence of external loads or applied displacement, the tensegrity form-finding problem has been addressed, by ascribing to the discrepancy of the resting lengths of cable and strut the pre-stress generated at self-equilibrium. This has allowed to explore the existence of both straight and buckled configurations with respect to different combinations of strut's axial stiffness, (elastic spring-mediated) strut's bending rigidity and cable's axial stiffness. Then, the tensegrity has been perturbed by applying an orthogonal displacement to the middle (hinge-like) point of the cable, thus revealing different possible mechanical responses depending on the selected key tensegrity parameters. Finally, the case of a rigid-strut system, the effects of geometrical imperfections and the behavior under compressive load have been investigated.

From the mechanical point of view, the 2-element system here addressed has been conceived as the first and simplest paradigm of tensegrity in which (large) axial and flexural deformability of the compression-bearing member(s) are coupled, also in combination with constitutive nonlinear hyperelasticity of all the elements. Despite the coexistence of these phenomena, thanks to its structural simplicity –essentially related to the small number of components (the least possible for a tensegrity) and to the prescribed local mode of buckling of the strut– such a system has allowed to set all the problems analytically and, in some cases, also to find closed-form solutions, without the necessity of resorting to numerical finite element models, which can be instead required for studying more complex architectures (as highlighted in the next chapter for a 30-element module). In this way, the model has provided the

possibility to perform a series of parametric analyses and, as a result, to gain qualitative insights into the wide spectrum of peculiar and fickle behaviors uniquely associated to soft tensegrity systems as a function of the specific combination of values of the structural (geometrical and constitutive) parameters, which in fact leads to the competition between axial (nonlinear) deformability and bendability of the strut.

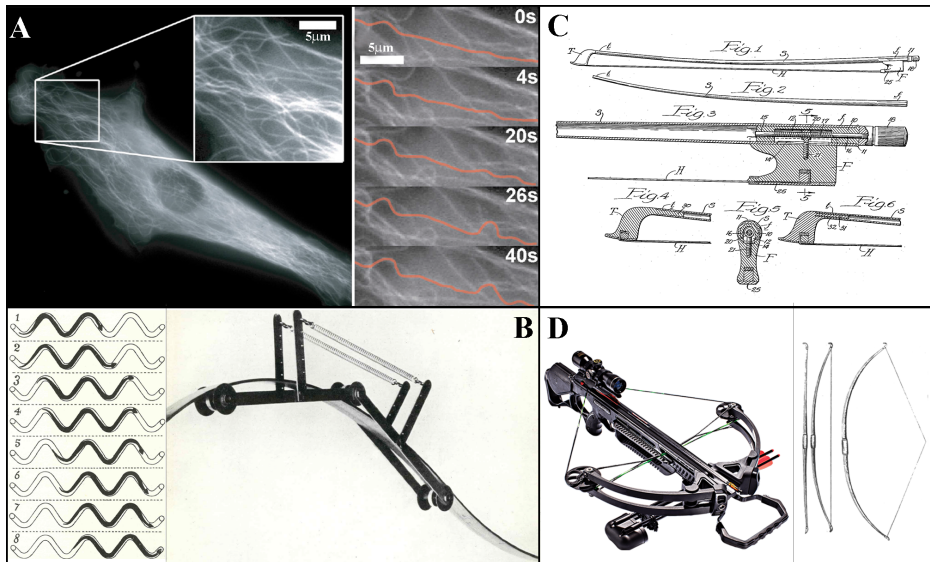


Figure 2.9: **A)** Buckling of a cytoskeletal microtubule caused by cell contractility (the image is reproduced from [17]). **B)** Model of snake's movement (the image is reproduced and adapted from [81]). **C)** Diagram of violin bow (image from [92]). **D)** Examples of crossbow (on the left) and longbow (on the right) mechanisms.

All these concepts establish the foundations for the construction of the cellular soft tensegrity model discussed in the next chapter and can be also used, already in the specific case of the 2-element structure, for tracing the working principle of a series of existing biomechanical and mechanical systems. As an example, in the main perspective of the present work, the 2-element soft tensegrity can be essentially read as the simplest cellular unit consisting in a single-microtubule/single-actin-microfilament system, which can be thus used for reproducing the behavior of cytoskeletal microtubules undergoing contraction and compressive buckling due to the stress deriving from the surrounding tensed actin network (figure 2.9A). Also, the structure can be utilized to replicate the working principle of the unit module of robotic skeletons

realized to simulate the mechanics of the snake locomotion (figure 2.9B) [33, 81, 111], as well as of manufactured instruments, such as the violin-bow (figure 2.9C) [92] and the crossbow/longbow (figure 2.9D).

THE REVISED 30-ELEMENT CELLULAR TENSEGRITY PARADIGM

The cytoskeleton is a moving, deforming and self-assembling architecture that plays a key role in any cell's biological process, by substantially providing structural stability to the cell, determining its shape and constituting the network filtering most of the relevant mechanotransduction signals that decide on the cellular physiological activities, such as adhesion, migration or division, as well as can be responsible of abnormal/pathological alterations, for example neoplastic mutations.

By briefly recalling concepts discussed in the section 1.2, the cytoskeletal apparatus is here seen as an interconnected system of actomyosin microfilaments and microtubules that distributes forces throughout the cell, continuously ensuring the balance of compression and tension of its pre-stressed biopolymeric elements by obeying the principles of tensegrity structures. As a matter of fact, among several models proposed in literature, the 30-element tensegrity suggested by Ingber represents the simplest and the most effective micro-structural paradigm to describe the cytomechanical behavior. It principally envisages that the internally stored pre-stress confers to the cell the needed shape and stability and the capability to adapt its overall elastic properties and the internal arrangement in response to physical and mechanical stimuli coming from the surrounding environment. More specifically, the structural components of the 30-element cellular tensegrity paradigm are placed in a way to determine a regular icosahedral geometry, in which 6 discontinuously distributed (i.e. not directly in contact) pre-compressed struts—representing the cytoskeletal microtubules—are interconnected at the ends through 24 pre-tensed cables, corresponding to the actin microfilaments.

In static conditions, this architecture has been studied in literature by modeling actin microfilaments as linearly elastic (tensed) cables and microtubules as rigid [211] or as elastic slender struts buckling under compression [35, 36, 232]. However, by following the rationale highlighted in the chapter 2 and on the heels of the simpler 2-element model studied in section 2.2, a 30-element soft-strut tensegrity is here *ad hoc* conceived for tracing the cell mechanics, by including both large deformations and

nonlinear elastic behaviors –coupled to possible instabilities– of the cytoskeletal biopolymers-like constituents, thus taking into account their actual axial and bending deformability. Standard hypotheses of torqueless and frictionless ball-joints as constraints connecting the discrete structural components are adopted and any stable tensegrity configuration in absence of external forces is classically assumed to be found in correspondence of a set of tensed members and compressed elements in self-equilibrium. On these bases, the form-finding problem is *ab imis* rewritten for the soft system and its response under elongation/contraction, shear and torsion conditions is then analyzed –in particular in terms of stored elastic energies, generalized stress-strain relations and associated varying stiffness– with the aim to qualitatively and quantitatively predict stiffness and energy measurements found through *in vitro* experimental tests and to resemble behaviors observed in cells. To overcome the intrinsic limitations of linear elastic constitutive models involving the classical Biot and Green-Lagrange strain measures at large deformations (namely at possible high contractions of the struts) and to the aim of catching the effects of constitutively nonlinear behaviors of the cellular tensegrity constituents, the adoption of two different hyperelastic models is investigated. These are the classical (compressible) neo-Hookean law and the Hencky’s model, the latter preserving the constitutive linearity but involving the true (logarithmic) strain measure, which is consistent for deformable struts and is also implemented in most of the commercial finite element codes when enabling large deformations. In this regard, by finally implementing a finite element model, the same above-mentioned boundary conditions are prescribed to the system by additionally activating the possibility to combine large axial deformations of cables and struts with buckling of the latter, so determining a variety of further responses involving instability and loss of shape symmetry actually characterizing the cellular behavior.

It is worth to highlight that, from the mechanical point of view, the competition among axial deformability of both cables and struts and bendability of the same struts can produce very different results in soft-tensegrity structures undergoing growing pre-stress levels or reacting to applied loads of increasing magnitude, as also found for the 2-element system in the previous chapter. Actually, this behavior takes coherently into account what observed in human cells, where the cytoskeleton is forced to continuously change its architecture and –with it– the effective ratios between axial stiffness and bending rigidity of its elements, as a consequence of polymerization/depolymerization processes and of the

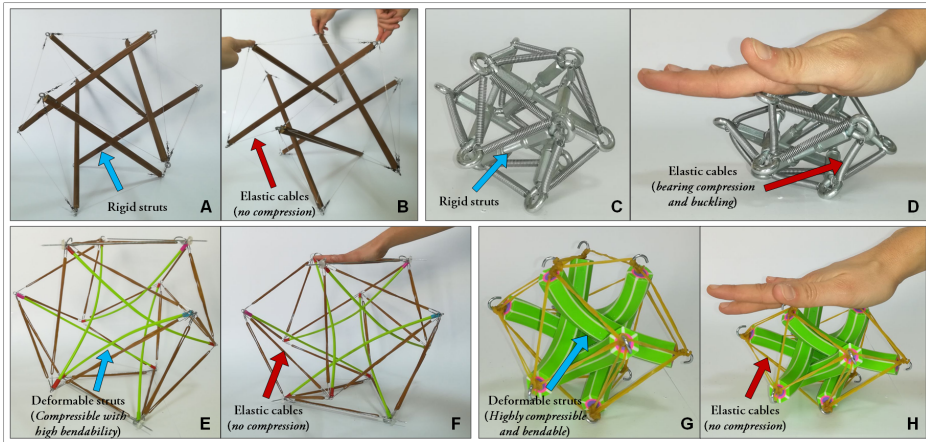


Figure 3.1: Four handmade 30-element tensegrity toy-systems in their natural (self-equilibrated and pre-stressed) reference configurations and some deformed (slightly crushed) ones, built up by using materials and elements such as to replicate all the relevant modulations of axial stiffness of cables and struts and bendability of struts. **A)** and **B)**: reference and deformed configurations of a standard 30-element tensegrity, with rigid bars and tensioned cables unable to bear compression; **C)** and **D)**: reference and deformed configurations of a quasi-classical 30-element tensegrity, with rigid steel struts and tensed metallic elastic springs, capable to support compression and to undergo buckling; **E)** and **F)**: reference and deformed configurations of a 30-element tensegrity with axially rigid but bendable struts and tensed rubber elastic cables; **G)** and **H)**: reference and deformed configurations of a *soft-strut* 30-element tensegrity made of axially deformable and bendable (rubber) bars and tensed elastic cables.

interactions with the ECM. As a result, these events can in fact make tip the scales in favor of structural configurations alternatively more prone to make prevalent the axial deformability than the bendability of the struts and *vice versa*. Motivated by these considerations, the form-finding and the behavior of the 30-element soft-tensegrity system under the selected loading conditions are analyzed below by separating its response in cases governed only by the axial deformation of cables and struts (say, high struts' bending stiffness) and those in which axial and flexural stiffness of the cytoskeletal elements compete (see, as an example, figure 3.1). This contributes to recognize two mechanically relevant classes of tensegrity deformations and associated equilibria. The first is here identified as the *symmetry-preserving* one, where both struts and cables can axially deform –also significantly– without violating the expected symmetries imposed

by the initial geometry and by the boundary conditions, the polyhedral regular shape of the tensegrity being kept preserved in absence of external loading. The second case is instead characterized by *loss of symmetry*, where buckling instability combined with axial deformability of struts and/or changing of the overall shape of the tensegrity can take place under applied loads as well as at increasing pre-stress in self-equilibrium states, thus leading to local or global configurational switching.

3.1 EQUILIBRIA AT SYMMETRY-PRESERVING DEFORMATION STATES

In the present section, the above defined symmetry-preserving class of equilibrium configurations of the 30-element cell-shaped tensegrity is theoretically explored, by hence properly excluding that –both in self-equilibrium and under applied loads– overall deformation shapes can deviate from states that respect geometrical and loading symmetries and by also assuming that the compressed struts can only contract without buckling (high bending stiffness).

3.1.1 Geometrical relations, compatibility and equilibrium equations

To idealize the cell cytoskeleton, let us consider a 30-element tensegrity system with a regular icosahedral geometry (figure 3.2A) and let us seek for the pre-stress conditions in cables and struts –and the correspondent compatible deformation states– ensuring self-equilibrium of the whole structure (as in the case of suspended or little adherent round-shaped cells). In such a configuration, the 6 struts –the cytoskeletal microtubules– have the same (pre-stretched) length L_t^* , while the 24 cables –the actin microfilaments– have (pre-stretched) length L_f^* . Geometrical arguments and symmetry require that these lengths obey the following equation:

$$L_f^* = \frac{\sqrt{6}}{4} L_t^*, \quad (3.1)$$

the subscripts f and t denoting (actin) filaments and tubules, respectively. Also, let us assume that the resting (undeformed) lengths, the initial cross-sections and the mechanical properties of all the cables are the same and that so happens for the struts, geometrical and constitutive parameters being in the successive calculations referred to those reported in literature and collected in table 3.1. Therein, the elastic moduli and the nominal cross-sectional areas have been chosen according to the experimental data

presented by Gittes et al. [78], while the resting microtubules' length has been estimated such that the mean cell's diameter –taken as the one of the smallest sphere circumscribing the polyhedral shape of the 30-element tensegrity, namely as $d^* = \sqrt{5}L_t^*/2$ – remains always within the range of 10–30 μm , consistently with the average sizes observed in many human cells in round or not highly stretched conditions.

Physical Parameter	Symbol	Value	Unit
MTs average nominal cross-sectional area	A_t	190	nm^2
μ Fs average nominal cross-sectional area	A_f	18	nm^2
MTs Young Modulus	E_t	1.2	GPa
μ Fs Young Modulus	E_f	2.6	GPa
MTs and μ Fs Poisson's ratio	ν	0.4	/
Resting MTs length	L_t	12	μm

Table 3.1: Values of geometrical and physical parameters used to simulate the mechanical behavior of tensegrity-based cell cytoskeleton [78, 106]. Herein, the acronyms MTs and μ Fs are employed to identify microtubules and actin microfilaments, respectively.

From the geometrical point of view, the topology of the system is defined by the vertices set, V_{TS} , and the edges set, E_{TS} :

$$\begin{aligned} V_{TS} &= \{1, 2, \dots, 12\}, \\ E_{TS} &= C_{TS} \cup S_{TS}, \quad C_{TS} = \{1, 2, \dots, 24\}, \quad S_{TS} = \{25, \dots, 30\}, \end{aligned} \quad (3.2)$$

where C_{TS} and S_{TS} denote the continuous set of cables and the disjointed set of struts, respectively. The configuration of the system is instead identified by the vector \mathbf{p} containing the coordinates \mathbf{p}_i , $i \in V_{TS}$, of the 12 nodes reported below, written with reference to a Cartesian coordinate system $\{x, y, z\}$ having the origin placed at the center of the above-mentioned sphere circumscribing the structure (see figure 3.2A). Because of the peculiar (regular) polyhedral symmetry exhibited by the 30-element tensegrity, the coordinates of all its nodes can be automat-

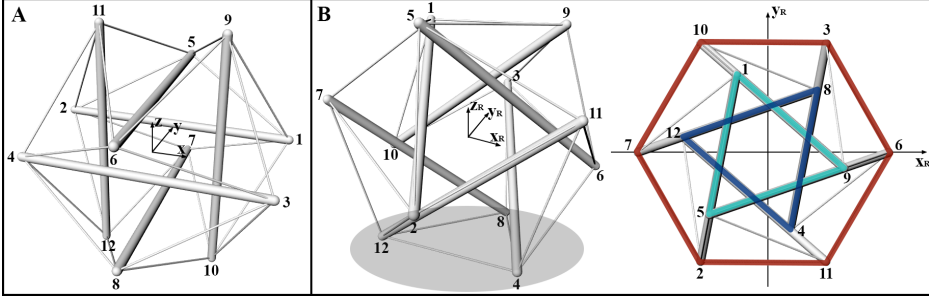


Figure 3.2: **A)** Perspective view of the 30-element tensegrity in the Cartesian coordinate system $\{x, y, z\}$. **B)** Three-dimensional (left) and top (right) views of the tensegrity system in the rotated Cartesian reference system $\{x_R, y_R, z_R\}$, with the latter representation highlighting the geometrical symmetries of the structure: two equilateral triangles –producing a star-shaped geometry– and a hexagon, all sharing the same center, are traced by the nodes of the system.

ically derived by starting from one of them, say \mathbf{p}_1 , by means of rigid transformations. With reference to the figure 3.2A, one then has:

$$\begin{aligned} \mathbf{p}_1 &= L_t^* \left(\frac{1}{2}, \frac{1}{4}, 0 \right)^T, & \mathbf{p}_2 &= \mathbf{R}_x \mathbf{p}_1, & \mathbf{p}_{5,6} &= \mathbf{P}_\pi \mathbf{p}_{1,2}, \\ \mathbf{p}_{9,10} &= \mathbf{P}_\pi \mathbf{p}_{5,6} = \mathbf{P}_\pi^2 \mathbf{p}_{1,2}, & \mathbf{p}_{3,4} &= \mathbf{R}_y \mathbf{p}_{1,2}, \\ \mathbf{p}_{7,8} &= \mathbf{P}_\pi \mathbf{p}_{3,4} = \mathbf{P}_\pi \mathbf{R}_y \mathbf{p}_{1,2}, & \mathbf{p}_{11,12} &= \mathbf{P}_\pi \mathbf{p}_{7,8} = \mathbf{P}_\pi^2 \mathbf{R}_y \mathbf{p}_{1,2} \end{aligned} \quad (3.3)$$

where \mathbf{P}_π is a permutation matrix corresponding to the permutation π , while \mathbf{R}_x and \mathbf{R}_y are reflection matrices with respect to the axes x and y , respectively given by:

$$\mathbf{P}_\pi = \begin{bmatrix} \hat{\mathbf{e}}_{\pi(x)} \\ \hat{\mathbf{e}}_{\pi(y)} \\ \hat{\mathbf{e}}_{\pi(z)} \end{bmatrix} = \begin{bmatrix} \hat{\mathbf{e}}_z \\ \hat{\mathbf{e}}_x \\ \hat{\mathbf{e}}_y \end{bmatrix} = \begin{bmatrix} 0 & 0 & 1 \\ 1 & 0 & 0 \\ 0 & 1 & 0 \end{bmatrix}, \quad \pi = \begin{bmatrix} x & y & z \\ z & x & y \end{bmatrix}, \quad (3.4)$$

$$\mathbf{R}_x = \mathbf{I} - 2\hat{\mathbf{e}}_x \otimes \hat{\mathbf{e}}_x, \quad \mathbf{R}_y = \mathbf{I} - 2\hat{\mathbf{e}}_y \otimes \hat{\mathbf{e}}_y,$$

herein $\hat{\mathbf{e}}_i$, $i = x, y, z$, denoting the unit vectors of the considered reference system. By using the nodal coordinates (3.3), it is also possible to verify the relationship (3.1). Furthermore, as already highlighted above, the

lengths L_t^* and L_f^* refer to the pre-stretched configuration and, therefore, keeping in mind that –at least in self-equilibrated states– the struts are all compressed and the cables all tensed, they can be related to the respective natural lengths, say L_t and L_f , through the relationships:

$$L_t^* = \lambda_t^* L_t, 0 < \lambda_t^* \leq 1 \quad \text{and} \quad L_f^* = \lambda_f^* L_f, \lambda_f^* \geq 1, \quad (3.5)$$

where λ_t^* and λ_f^* are the axial pre-stretches in struts and cables, respectively, these being here modeled as isotropic, homogeneous and hyperelastic cylinders undergoing one-dimensional stress regime, as described in section 2.1. However, the values of these pre-stretches cannot be independently assigned, since they have to ensure –mediated by the nonlinear elastic laws relating them to the stresses– equilibrium in the pre-stretched configuration. Hence, in absence of externally applied forces, the following equilibrium equations have to be verified at any node i :

$$\sum_j N_{ij}^* \frac{\mathbf{p}_j - \mathbf{p}_i}{\|\mathbf{p}_j - \mathbf{p}_i\|} = \mathbf{0}, \quad \forall i = 1, \dots, 12 \quad (3.6)$$

with the summation extended to all the nodes j connected to the node i by an element i - j , N_{ij}^* being the axial force pre-stressing that element. Also, the polyhedral symmetry of the tensegrity module and the hypothesis of equal resting lengths of struts and cables allow to assume that the pre-stretches –and the related pre-stresses– have the same values within each group of compressed and tensed elements, respectively. As a result, by indicating with N_t^* and N_f^* the axial forces brought, in the order, by tubules and filaments, the sole equation to be satisfied at each node is:

$$N_t^*(\lambda_t^*) = -\sqrt{6}N_f^*(\lambda_f^*), \quad (3.7)$$

found by imposing the equilibrium along the z direction, the equilibria along the x and y axes being instead automatically ensured –due to the geometrical symmetry– by the tensile forces of the four cables converging in any arbitrarily chosen node at the end of a strut. As a consequence, the equation (3.7) alone establishes the relationship that the pre-stretches defined in (3.5) must obey, the two forces being obtained by multiplying the related cross-sectional areas of the elements at rest –say A_f and A_t – and the nominal pre-stresses –say P_f^* and P_t^* – having expressions coming from one of the two different constitutive laws here hypothesized for describing the hyperelastic behavior of cables and struts, given in equation (2.22)₂ for the Hencky's model and in equation (2.25) for the

neo-Hookean one. The symmetry-preserving form-finding problem of the soft-tensegrity is therefore finally governed by the three compatibility relations given by equations (3.1) and (3.5), that is

$$L_f^* = \frac{\sqrt{6}}{4} L_t^* = \frac{\sqrt{6}}{4} \lambda_t^* L_t = \lambda_f^* L_f, \quad (3.8)$$

to which the equilibrium equation (3.7), written in terms of pre-stretches by accounting for the specific constitutive law, must be added. By following this way, the four equations (3.8) and (3.7) contain the six unknowns $L_f^*, L_t^*, L_f, L_t, \lambda_f^*, \lambda_t^*$ and thus the solution is obtained by treating two of them as parameters. In this case, the struts' natural length is fixed (at the value indicated in table 3.1) and the value of the cables' pre-stretch is parametrically varied in order to evaluate its influence –and consequently the influence of the pre-stress– on the mechanical response of the structure. In such a way, the limit case of inextensible (rigid) struts, frequently encountered in the literature [36, 70, 211], can be also traced back –for any possible pre-stressed self-equilibrated state– by making the elastic modulus of the struts significantly greater than the one of the cables (table 3.1), say up to the extreme case of rigid struts. In this limit situation, from equation (3.8), one in fact has that the relationship $L_f^*/L_t = \sqrt{6}/4$ holds true, the length of the rigid struts in the pre-stretched configuration clearly remaining fixed at the natural value while increasing the cables pre-stretch.

With the aim of analyzing the mechanical response provided by the cytoskeleton of cells adherent to the extra-cellular matrix and loaded by external forces, the structure is then assumed to stand on a (rigid) substrate and therein anchored through the nodes 4, 8 and 12, as in the configuration shown in figure 3.2B. From the operational point of view, it is convenient to rotate the reference system in a way that the new z -axis intercepts the centers of the equilateral triangles ideally formed by the nodes 1–5–9 and 4–8–12. In this new frame of coordinates, referred to as $\{x_R, y_R, z_R\}$ system, the nodes 1–5–9 form the upper triangle, while the lower one is defined by the vertices 4–8–12, which are thus fully constrained on the rigid substrate (see figure 3.2B). Also, the new $\{x_R, y_R\}$ plane is oriented in a way that the nodes 6 and 7 are identified by null y_R -coordinate. As a result, the considered rotation leads to define a new unit vector $\hat{\mathbf{z}}_R = (1/\sqrt{3}, 1/\sqrt{3}, 1/\sqrt{3})$, with the other two unit vectors being given by the relations:

$$\hat{\mathbf{x}}_R \cdot \hat{\mathbf{z}}_R = 0, \quad \hat{\mathbf{y}}_R \cdot \mathbf{p}_6 = 0 \quad (\hat{\mathbf{y}}_R \cdot \mathbf{p}_7 = 0), \quad \hat{\mathbf{y}}_R = \hat{\mathbf{z}}_R \times \hat{\mathbf{x}}_R. \quad (3.9)$$

This particular choice allows to exploit some symmetry properties (see the top view in figure 3.2B) in studying the mechanical response of the tensegrity experiencing the different deformation regimes of contraction/elongation, torque and shear as examined below, thus minimizing the number of the unknowns of the resulting problems and facilitating their formulation in analytical form. Therefore, in what follows, the above mentioned intrinsic symmetries and the peculiar choice of the reference frame are used when addressing the analysis of symmetry-preserving deformation modes in response to prescribed boundary conditions.

3.1.2 Internal (elastic) energies in symmetry-preserving configurations

Equilibria in pre-stretched configurations and at any stage of deformation induced by external loading can be classically determined by making the total potential energy stationary, thus minimizing the internal (elastic) energy minus the work done by the applied loads against the corresponding displacements. In order to determine the general form of the internal energy of the polyhedral soft tensegrity for both the nonlinear (hyper-elastic) behaviors to be here analyzed, one can start with the case of Hencky's materials described in subsection 2.1.2. In particular, according to equation (2.23), the energy of each k -th single-element (cable or strut) can be written as

$$U_k = \frac{1}{2} A_k E_k L_k (\log \lambda_k)^2, \quad k = 1, \dots, 30, \quad (3.10)$$

where the stretch λ_k is the result of the superposition of two stretches, namely the pre-stretch $\lambda_k^* = L_k^*/L_k$, ensuring self-equilibrium of the system, and a further elastic stretch due to a possible external loading that leads the element to the final length l_k , in a way that

$$\lambda_k = \frac{l_k}{L_k} = \frac{l_k}{L_k^*} \frac{L_k^*}{L_k} = \frac{l_k}{L_k^*} \lambda_k^*. \quad (3.11)$$

Herein, l_k turns out to be a function of the unknown nodal displacements, since it can be written as

$$l_k = \|\mathbf{p}'_i(u_i, v_i, w_i) - \mathbf{p}'_j(u_j, v_j, w_j)\|. \quad (3.12)$$

In this notation, i and j are the indices of the nodes connected by the k -th element, the prime referring to the nodes' coordinates in the current configuration, which depend on the nodal displacement vectors $\mathbf{u}_i = \{u_i, v_i, w_i\}$, $i = 1, \dots, 12$.

With reference to the Hencky's model, by taking into account equation (3.11) and by suitably exploiting the properties of the logarithmic function, the energy in (3.10) can be readily written as the sum of a term U_k^* representing the energy stored by the element due to the only pre-stretch—which is fixed, once the pre-stretch is provided—and a term, say ΔU_k , which accounts for the increase of elastic energy due to the external loading:

$$\begin{aligned} U_k &= \frac{1}{2} A_k E_k L_k \left(\log \lambda_k^* \frac{l_k}{L_k^*} \right)^2 = \frac{1}{2} A_k E_k L_k \left(\log \lambda_k^* + \log \frac{l_k}{L_k^*} \right)^2 \\ &= \frac{1}{2} A_k E_k L_k (\log \lambda_k^*)^2 + \frac{1}{2} A_k E_k L_k \left[\left(\log \frac{l_k}{L_k^*} \right)^2 + 2 \log \lambda_k^* \log \frac{l_k}{L_k^*} \right] \\ &= U_k^* + \Delta U_k. \end{aligned} \tag{3.13}$$

As a consequence, the total internal energy of the whole tensegrity can be obtained by summing up the energy aliquots of the single elements, say:

$$U_H = \sum_k U_k = \sum_k [U_k^* + \Delta U_k] = \sum_k U_k^* + \sum_k \Delta U_k = U^* + \Delta U. \tag{3.14}$$

Finally, by following the same line of reasoning, the total internal elastic energy for the 30-element tensegrity system constituted by neo-Hookean members can be computed as

$$\begin{aligned} U_{NH} &= \sum_k U_k = \sum_k \frac{\mu_k}{2} \left(\lambda_k^2 + \frac{\lambda_k^{-2\nu_k}}{\nu_k} - \frac{\nu_k + 1}{\nu_k} \right) A_k L_k = \\ &= \sum_k \frac{\mu_k}{2} \left[\left(\lambda_k^* \frac{l_k}{L_k^*} \right)^2 + \left(\left(\lambda_k^* \frac{l_k}{L_k^*} \right)^{-2\nu_k} - \nu_k - 1 \right) \nu_k^{-1} \right] A_k L_k. \end{aligned} \tag{3.15}$$

Such a result is found by modelling each cable or strut as illustrated in subsection 2.1.3 and accordingly adopting the expression given in equation (2.27) for any k -th energy contribution, with particular reference to the stretch multiplicative decomposition provided in equation (3.11). Note that, differently from the previous case, here no additive decoupling of the energies contributions related to the pure pre-stretching and to the external perturbation of the system can be used.

3.1.3 Form-finding and energy storing in cell cytoskeleton

As first, it is here analyzed the case of absence of external loads, say the form-finding problem of the idealized tensegrity-like cytoskeleton, in which the polyhedral shape of the structure is preserved and thus it can be seen as the configuration assumed by a suspended or little adherent round cell. To this aim, equilibrium equation (3.7) has to be particularized for the cases of elements obeying the Hencky's and the neo-Hookean laws, by also employing the compatibility relationships (3.8). Then, by considering the axial nominal pre-stresses, given by the expressions (2.22)₂ and (2.25) for the two models respectively, one finds that the pre-stretch in microtubules is driven by that in actin microfilaments according to the following balance relations:

$$E_t A_t \frac{\log \lambda_t^*}{\lambda_t^*} = -\sqrt{6} E_f A_f \frac{\log \lambda_f^*}{\lambda_f^*} \quad (3.16)$$

for Hencky-type elements, while

$$\mu_t A_t \left[\lambda_t^* - (\lambda_t^*)^{-(2\nu_t+1)} \right] = -\sqrt{6} \mu_f A_f \left[\lambda_f^* - (\lambda_f^*)^{-(2\nu_f+1)} \right] \quad (3.17)$$

for neo-Hookean ones, which, by introducing the values of the parameters given in table 3.1, provide the solutions plotted in figure 3.3A.

Also, in this purely pre-stretched/pre-stressed self-equilibrated state, the expressions of the energy stored by the tensegrity structure take the forms given by equation (3.14) in case of Hencky's model and by equation (3.15) in case of neo-Hookean elements, respectively simplified as

$$\begin{aligned} U_H^* &= 3A_t E_t L_t (\log \lambda_t^*)^2 + 12A_f E_f L_f (\log \lambda_f^*)^2 \quad \text{and} \\ U_{NH}^* &= 3\mu_t A_t L_t \left[(\lambda_t^*)^2 + \frac{(\lambda_t^*)^{-2\nu_t}}{\nu_t} - \frac{\nu_t + 1}{\nu_t} \right] \\ &\quad + 12\mu_f A_f L_f \left[(\lambda_f^*)^2 + \frac{(\lambda_f^*)^{-2\nu_f}}{\nu_f} - \frac{\nu_f + 1}{\nu_f} \right], \end{aligned} \quad (3.18)$$

these quantities increasing with λ_f^* as observable in figure 3.3B.

The results show that the introduction of hyperelasticity could more faithfully reflect the nonlinear way of a cell to accumulate elastic energy

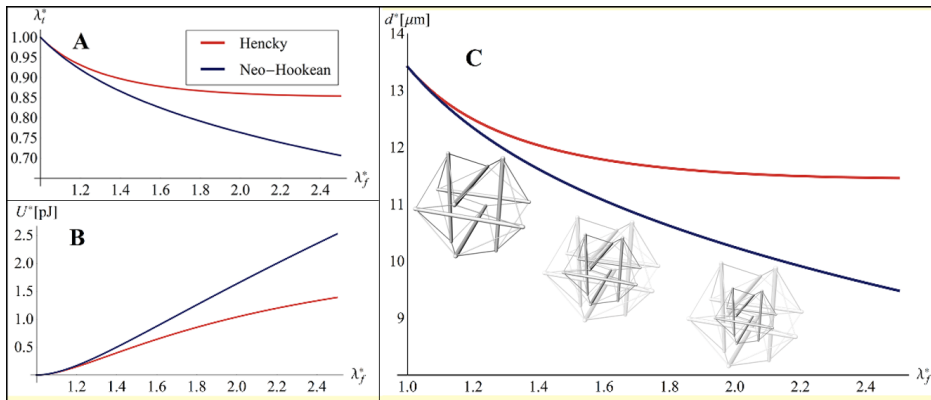


Figure 3.3: Change of **A)** microtubules's pre-stretch, **B)** globally stored elastic energy and **C)** average size (in terms of diameter of the circumscribing sphere) of the cell-tensegrity at the self-equilibrated pre-stretched state, while increasing the filaments' pre-stretch values from 1 to 2.5, both for Hencky's and neo-Hookean structural elements.

through the pre-stress of its protein filaments, here predicted to be of the order of a few units of pJ . Confirming this quantitative result is however not so easy. It is known that the main source of energy is allocated in cell proteins and other organic complexes and most part of it is spent to form molecules. As a function of the releasing times and of the provision needs the cell energy is stored at long term in lipids (e.g. triglycerides and adipocytes), at short term –say about 24 hour supply– in the liver (glycogen) and for immediate use as Adenosine TriPhosphate (ATP), the (chemical) energy currency of all living cells, generated by cellular respiration, stored in the bonds that held the atoms of molecule together and released by breaking into ADP (adenosine diphosphate) and inorganic phosphate, with the reaction catalyzed by ATPase enzymes. Despite all these mechanisms are known, obtaining a reliable estimate of the energy storage and of the energy rate production in human cells still remains a tricky task, these values strongly depending on the very different compositions, sizes, growth conditions and functions characterizing each cell line. It would be in fact sufficient thinking that, for instance, fibroblasts are significantly more active than the average human cell, thus requiring higher energy reserves to be used. Moreover, the major oxygen-consuming processes –e.g. protein synthesis, Na^+ / K^+ ATPase (responsible of maintaining the resting electric potential in cells) Ca^{2+} and actinomyosin ATPase (that drives muscle cells)– are found with extremely variable percentages in liver, heart, brain, skeletal muscle

cells and other human tissues [11, 187]. These differences might therefore call into question the accuracy of any estimate of stored energy per cell if one does not admit possible discrepancies of two (or more) order of magnitude when the average values are compared with experimental data related to a specific cell line. However, by using the rule of thumb and starting from a caloric intake of about 2000 kcal per day in an adult human of medium build, rough calculations lead to estimate an overall heat production at a rate of about one hundred watts (100 joules per second), corresponding to a few units of pico-watts per cell, if we consider about 3×10^{13} of cells which populate the human body [83]. Nevertheless, as already pointed out above, bottom-up analyses may conduce up to two order of magnitude greater values if selected cells are taken into account. Aware of this variability of data, the order of magnitude of the elastic energy storage predicted by the cellular soft-strut tensegrity unit here proposed seems to be however consistent with some estimates supported by experimental findings. By referring to [1, 97] for a more detailed discussion on the molecular basis of contraction and regulation in vertebrate and invertebrate muscles, it can be for example shown that the elastic energy storage in myofilament lattice depends on sarcomere length and, by comparing the energy input due to the consumption of ATP to the energy stored across all filaments and cross-bridges, values of energy stored by a single sarcomere were estimated not to exceed $1000 \text{ pN} \times \text{nm}$. By considering that a muscle fiber may contain about 10^5 sarcomeres, we can therefore calculate a stored elastic energy of about 10^{-1} pJ , that is in full agreement with the elastic energy accumulated by our tensegrity model when the pre-stretches in the filaments fall between 1.1 and 1.2, these values being consistent with the actual average strain ranging from 10% to 20% in a muscle fiber. A further confirmation of the capability of the proposed soft-strut tensegrity model to predict the order of magnitude of the energy storage in a cell can be also found by directly making reference to ATP. In fact, it can be demonstrated that in many eukaryotic cells, motility is driven by dynamic actin polymerization at a steady state cost of about 1 ATP hydrolysis per polymerizing actin monomer [2, 175]. Comparative studies show that an energy rate of $4 \times 10^5 \text{ ATP/s}$, associated to about 4000 filaments, is required to power cell movement [218]. On the other hand, the rule of thumb involving Gibbs free energy change due to ATP hydrolysis [189] and calculations of forces due to a molecular motor allow to predict that it would exert a force of roughly 5 pN [169] over a 10 nm [144], then doing a work of order $50 \text{ pN} \times \text{nm}$ which requires slightly more than $10 k_B \times T$ of energy

(k_B being the Boltzmann constant and T the absolute temperature), well within the range of what a single ATP can deliver [56]. Therefore, by converting the energy rate of 4×10^5 ATP/s in pico-joules per second, then multiplying this result for 8.64×10^4 seconds a day and dividing it by $36/4000$ (the ratio between the tensegrity elements and the total number of filaments on which the above energy amount has been estimated), one finally obtains about 15 pJ , consistent with the amount of elastic energy stored by the cellular tensegrity model, that hence would transform about 10% of the total chemical ATP in elastic energy.

Finally, figure 3.3C shows the evolution of the self-balanced architecture's average size in terms of the above-defined diameter d^* : under these conditions, it is found that the overall tensegrity module shrinks as the pre-stretch prescribed in the cables increases, by preserving its original symmetric shape. It is extremely worth noticing that this feature is strictly related to the soft (axially deformable) nature here envisaged for the struts, a similar behavior being instead absent in more standard rigid-strut tensegrities, which in fact preserves their size –dictated by the microtubules' resting length L_t – independently of the level of internal pre-stress. However, the possibility of tuning its global size by modulating the internally stored pre-stress identifies an important requirement for a (tensegrity) system aimed to trace the structural behavior of the cell cytoskeleton, since shrinking mechanisms represent a crucial capability exploited –as an example– by round as well as deforming cells for spreading, to sneak into blood vessels and to overcome micro-channel obstructions [198], or by cancer cells to gatecrash in remote districts so promoting metastasis [114, 161, 173]. Hence, also beyond any quantitative confirmation, the soft-strut 30-element model confers to the tensegrity-like cytoskeleton the capability to combine energy storing/releasing with cell size tuning as a result of the internal pre-stress modulation, in this way adapting the tensegrity paradigm to additional actual peculiar behaviors of living cells with respect to rigid-strut or small deforming models.

3.1.4 *Symmetric responses of the cellular soft-tensegrity under external loading*

Here, we consider that cells, by starting from their self-equilibrated pre-stressed configurations, deform under the action of external loads applied in terms of prescribed displacements at the three nodes 1, 5 and 9 placed at the top of the tensegrity structure (in the reference

Cartesian frame $\{x_R, y_R, z_R\}$), then impeding any degree of freedom at the corresponding three nodes 4, 8 and 12 at the basis of the system, assumed to be anchored to a rigid substrate (figure 3.2B). In this way, the total potential energy coincides with the internal energy U (provided either by U_H in (3.14) or by U_{NH} in (3.15)) and the equilibrium is found by making it stationary with respect to the vector collecting all the unknown nodal displacements components, say $\tilde{\mathbf{u}}_i$. The problem to be solved thus reduces to the following minimization:

$$\tilde{\mathbf{u}}_i : \min_{\tilde{\mathbf{u}}_i} U \Leftrightarrow \partial_{\tilde{\mathbf{u}}_i} U = \mathbf{0}, \text{ with } \mathbf{H}_{\tilde{\mathbf{u}}_i}(U) \text{ positive definite } \forall i \in \mathbb{I} \subset \mathbb{N} \quad (3.19)$$

where $\mathbf{H}_{\tilde{\mathbf{u}}_i}(U)$ is the Hessian of U , whose derivatives are calculated with respect to $\tilde{\mathbf{u}}_i$, and \mathbb{I} denotes the subset of the natural numbers collecting the indexes i such that the related nodes have at least one degree of freedom. Therefore, by recalling the expressions of the total internal energy given in (3.14) and (3.15), the following systems of nonlinear equations have to be solved to have equilibrium, in the cases of Hencky and neo-Hookean elements, respectively:

$$\begin{aligned} \partial_{\tilde{\mathbf{u}}_i} U_H &= \sum_k E_k A_k \frac{L_k}{l_k^2} \log \frac{l_k}{L_k} (\mathbf{p}'_i - \mathbf{p}'_j) = \mathbf{0}, \forall i \in \mathbb{I} \quad \text{and} \\ \partial_{\tilde{\mathbf{u}}_i} U_{NH} &= \sum_k \frac{\mu_k A_k}{l_k} \left[\frac{l_k}{L_k} - \left(\frac{L_k}{l_k} \right)^{2\nu_k+1} \right] (\mathbf{p}'_i - \mathbf{p}'_j) = \mathbf{0}, \forall i \in \mathbb{I}, \end{aligned} \quad (3.20)$$

with the summation extended to all the elements k having one endpoint in the i -th node. The non-algebraic and nonlinear structure of both these systems do not allow to solve them in closed-form. The minimization problems have been thus solved numerically, by exploiting the Newton's method implemented by the function *FindMinimum* provided by the code *Mathematica*[®][244] and double checking the results through an *ad hoc* implemented algorithm based on a random procedure. This involves the definition of a starting Gaussian-type distribution \mathfrak{N} with mean $Y = 0$ and standard deviation ω proportional to the value of the prescribed displacement (*p.d.*) according to

$$\mathfrak{N}(Y, \omega) = \mathfrak{N} \left(0, \frac{4}{10} (|p.d.| + 10^{-4}) \right) \quad (3.21)$$

from which the values to be initially assigned to the unknown displacements can be extracted (the constant 10^{-4} is added up to ensure that at

$p.d. = 0, \omega > 0$). Then, random values are extracted from the distribution (3.21) and assigned to the unknown displacements, by calculating the corresponding energy. This procedure is thus repeated a number of times much greater (at least three orders of magnitude) than the number of displacements to be determined (depending on the type of mechanical test to simulate) and successively, among all the energy values obtained, the minimum is extracted, together with the values of the unknown displacements in correspondence of which the minimum occurs. These values are then used as means of new Gaussian distributions –one for each displacement– whose standard deviation is halved than before. The random minimization step is so repeated and the values extracted from the distributions hence found to be closer to the minimum point. In the specific case, such operation has been iterated with, in particular, five repetitions. The double check has been then made by comparing the outcomes of the random procedure with those obtained by applying the function *FindMinimum* provided by the software *Mathematica*[®] and the very good agreement between the two outputs has been finally used as a measure of the reliability of the obtained results.

In the next sections, the results found by means of the strategy described here are provided for the specific cases of a self-balanced structure subjected to contraction/elongation, shear and torsion loading type conditions, these being able to somehow reproduce circumstances that cells can actually experience *in vivo* (as exemplified in figure 3.4) or *ex vivo* as an effect of experimental test aimed to measure their mechanical properties/response [8].

3.1.4.1 *Crushing and stretching of cells: contraction and elongation*

Let us start by analyzing the case of a cellular (soft-strut) tensegrity which simply contracts or elongates as downward or upward uniform vertical displacements are prescribed at the upper nodes 1, 5 and 9 of the structure, while the nodes 4, 8 and 12 at the basis are constrained, say anchored to the substrate (figure 3.2B). Hence, the unknowns of this problem are the Cartesian components of the displacements of the nodes at intermediate heights, ideally describing the middle hexagon highlighted in the top view of figure 3.2B, and the sole in-plane components of the upper nodes. To further reduce the number of unknowns, the symmetry of the structure and of the expected deformation (related to the specific solicitation mode) can be both exploited to impose that the nodes belonging to the above-mentioned hexagon and placed at the same height share

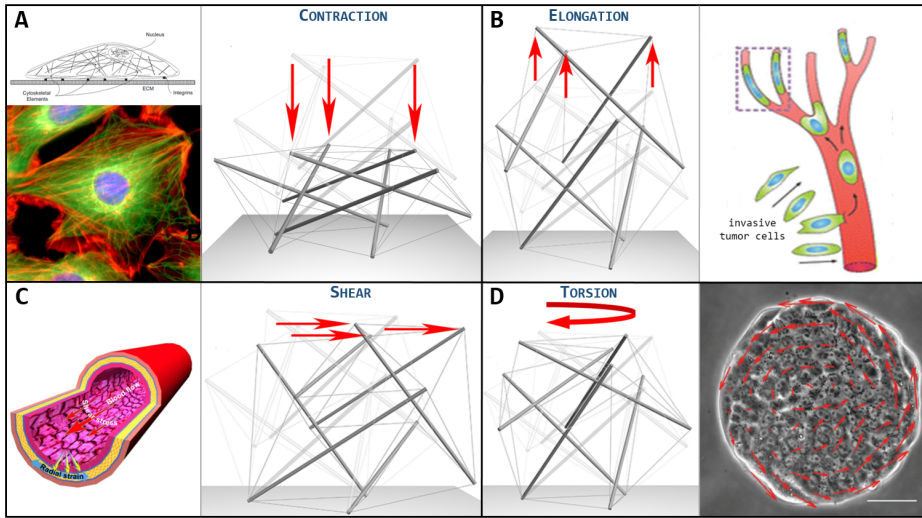


Figure 3.4: **A)** Cell stretched and flattened while adhering on a substrate (image reproduced from [217]). Beside, the 30-element tensegrity cell model deformed under contraction. **B)** Invasive tumor cells squeezing while migrating through blood vessels (image reproduced from [247]). Beside, the 30-element tensegrity cell model deformed under elongation. **C)** Endothelial cells coating the tunica intima of a blood vessel deform under the action of continuous flow-induced shear stresses (image reproduced from [39]). Beside, the 30-element tensegrity cell model deformed under shear. **D)** Collective migration of cells coupled with dynamic rotation (image reproduced from [58]). Beside, the 30-element tensegrity cell model deformed under torsion.

the same vertical displacement to preserve the geometrical symmetry. Therefore, the z_R -components of the displacement of the nodes 3, 7, 11 and of the nodes 2, 6, 10 have to satisfy the following equations and can be conveniently re-baptized as:

$$\begin{aligned} w_{HT} &:= w_3 = w_7 = w_{11}, \\ w_{HB} &:= w_2 = w_6 = w_{10}, \end{aligned} \quad (3.22)$$

where the subscript HT refers to the nodes belonging to the middle hexagon and placed at higher height, while the subscript HB is used to indicate the lower nodes. Additionally, symmetry implies that the radial and tangential displacements take the same values separately for the sets of nodes 3, 7, 11 and 2, 6, 10 of the hexagon, respectively, this holding true also for the nodes 1, 5 and 9. This means that a local two-dimensional reference system lying in the $\{x_R, y_R\}$ plane can be introduced for each

of these nodes, rotated in such a way that the new ordinate axis lies in the radial direction. Then, by indicating in the local frames the common radial and tangential displacements of the i^{th} node with d_{ri} and d_{ti} , the displacements u_i and v_i of such nodes along the axes x_R and y_R can be determined as follows:

$$\begin{bmatrix} u_i \\ v_i \end{bmatrix} = \mathbf{R}(\alpha_i) \begin{bmatrix} d_{ti} \\ d_{ri} \end{bmatrix}, \quad \text{with} \quad \mathbf{R}(\alpha_i) := \begin{bmatrix} \cos \alpha_i & \sin \alpha_i \\ -\sin \alpha_i & \cos \alpha_i \end{bmatrix}, \quad (3.23)$$

where $d_{ri} = d_{rUT}$ and $d_{ti} = d_{tUT}$ for $i = \{1, 5, 9\}$, $d_{ri} = d_{rHT}$ and $d_{ti} = d_{tHT}$ for $i = \{3, 7, 11\}$, $d_{ri} = d_{rHB}$ and $d_{ti} = d_{tHB}$ for $i = \{2, 6, 10\}$, while $\mathbf{R}(\alpha_i)$ is the clockwise rotation matrix defined in (3.23)₂ as a function of the angle α_i , defined with respect to the axis y_R and depending on the position of the specific node in the Cartesian frame:

$$\begin{aligned} \alpha_1 &= 2\pi - \arccos\left(\frac{5}{2\sqrt{7}}\right), & \alpha_2 &= \frac{7}{6}\pi, & \alpha_3 &= \frac{\pi}{6}, \\ \alpha_5 &= 2\pi - \arccos\left(-\frac{2}{\sqrt{7}}\right), & \alpha_6 &= \frac{\pi}{2}, & \alpha_7 &= \frac{3}{2}\pi, \\ \alpha_9 &= \arccos\left(-\frac{1}{2\sqrt{7}}\right), & \alpha_{10} &= \frac{11}{6}\pi, & \alpha_{11} &= \frac{5}{6}\pi. \end{aligned} \quad (3.24)$$

Under these considerations, the number of unknowns reduces to eight, namely d_{rUT} , d_{tUT} , d_{rHT} , d_{tHT} , d_{rHB} , d_{tHB} , w_{HT} and w_{HB} , while the vertical displacement W of the upper equilateral triangle is prescribed and the displacement components of the lower nodes set to be zero.

A view of the tensegrity deformation process is shown in figure 3.5, for cables' pre-stretch equal to 1.1 and a prescribed displacement up to $\pm h/3$ for both elongation and contraction, h being the height of the pre-stretched tensegrity, given by $h = \sqrt{3}L_t\lambda_i^*/2$. The results, obtained by means of Hencky's and neo-Hookean models, do not exhibit significant differences in terms of deformed configurations and therefore an unique plot is reported. In particular, during contraction, the tensegrity rotates counterclockwise and expands laterally, while clockwise rotation and lateral contraction occur in elongation. Noteworthy, this peculiar coupling of torsional rotation with axial and lateral deformations shown by the tensegrity undergoing contraction/elongation may have interesting implications in the analysis of some collective behaviors of cells. In fact, gastrulation during wound healing [245], as well as the experimentally observed geometrical confinement of cells into well-defined circles, that induces a persistent, coordinated and synchronized rotation of cells [58]

during their collective migration, are nowadays modeled through *top-down* macroscopic continuum descriptions based on the nematic liquid crystals theory by thus *a priori* imposing the peculiar kinematics. As a consequence, tensegrity models, that intrinsically relate torsion to lateral deformation, could helpfully contribute to construct, for example via homogenization, a rationale *bottom-up* way for deriving enriched continua for interpreting the above mentioned phenomena.

Other relevant results are illustrated in the figures 3.6A-B, that show the overall equivalent stiffness K_A of the structure as a function of the equivalent strain ε_{eq} (and the related nominal stress P_A versus the same strain in the insets), when different values of the cables' pre-stretch are considered, for both the cases of cytoskeletal elements obeying Hencky's and neo-Hookean laws. More in detail, the nominal stress P_A is here defined as the ratio between the equivalent reaction force F_A –obtained as derivative of the internal energy with respect to the applied displacement W – and the area of the upper equilateral triangle in the pre-stretched configuration, that is $P_A := F_A/A_{tr}^*$, with $F_A = \partial U/\partial W$ and $A_{tr}^* = 3\sqrt{3}L_t^2(\lambda_t^*)^2/32$. Moreover, the equivalent stiffness K_A is defined as $K_A := \partial P_A/\partial \varepsilon_{eq}$, where ε_{eq} is the ratio between the prescribed displacement and the height of the pre-stretched tensegrity, i.e. $\varepsilon_{eq} := W/h$. Figure 3.6A shows that the Hencky-type tensegrity exhibits a hardening, both in contraction and elongation, as the deformation level is increased at low values of λ_f^* , while a stiffening in elongation and a softening in contraction are registered for higher values of λ_f^* , with a trend that inverts this behavior as λ_f^* grows. The case of neo-Hookean tensegrity, in figure 3.6B, also provides a hardening by increasing the deformation level, both in contraction and elongation and for low values of λ_f^* , exhibiting instead always a stiffness increase in elongation and a stiffness decrease in contraction for higher values of λ_f^* , somehow qualitatively resembling the results very recently obtained by Fraternali et al. [70] for a simpler three-strut tensegrity with cables obeying the de Saint Venant-Kirchhoff law. Note that, in figures 3.6, grey tracts of the curves identify theoretical extrapolations corresponding to branches which *de facto* cannot be followed, since they would refer to cables bearing compression¹, a condition generally excluded in tensegrity

¹ Rigorously speaking, the tracts of the curves in grey indicate that at least one cable –or more likely a set of them– would undergo compression, this implying, in most of the cases examined, that the whole equilibrium is compromised or simply that the tensegrity should switch on other possible configurations no longer preserving the symmetry, in order to explore eventual different equilibria states. These possible alternative states, that could involve contraction and buckling of struts and/or global deviation of the

systems. Also, as a matter of fact, such a case is incompatible in cells where cable-like cytoskeletal contractile actin microfilaments absorb only tensile forces and the compressive stresses are supported by microtubules [165, 207, 238].

The previous results highlight that the two (neo-Hookean and Hencky-type) tensegrities exhibit different behaviors in elongation ($\varepsilon_{eq} > 0$) and contraction ($\varepsilon_{eq} < 0$), as well as very different trends –characterized by hardening/softening– for varying values of the pre-stretch. The response of the structure, in fact, strictly depends on the harboring pre-stress level which, in turn, governs the initial (tangent) stiffness of the tensegrity system, say $K_A^0 := K_A|_{\varepsilon_{eq} \rightarrow 0}$, as shown in figure 3.7A. In particular, both Hencky's and neo-Hookean models exhibit a non-zero tangent stiffness at early stage of contraction/elongation if a not vanishing pre-stress is present, the magnitude of this initial stiffness being closely related to the pre-stress value determined by the hyperelastic law chosen for the elements. However, the cell initial (tangent) stiffness is significantly different in the two cases considered (see figure 3.7): for the neo-Hookean case, it monotonically increases as the pre-stretch in the cables increases, as actually found in some theoretical predictions [236] and experimental results [237], while –for the Hencky's model– the initial stiffness shows a counterintuitive decreasing path from a selected threshold similar to that found by Coughlin and Stamenovic in their "round" tensegrity model comprising rigid struts [36, 211], that however seems to have not been experimentally observed so far. Moreover, from the quantitative point of view, it is worth to highlight that the values of the overall cell stiffness obtained by modeling the cytoskeleton as a soft-strut 30-element tensegrity, are of the order of magnitude of about $10^2 - 10^3 Pa$, while spanning over a reasonable wide range of pre-stretch, in line with the most commonly ascertained values of stiffness measured in the literature through several experimental techniques, for different healthy and cancer cell lines [68, 206].

Finally, by way of example, it can be useful to compare the initial (tangent) stiffness evaluated for the proposed soft tensegrity model with that provided by a classical rigid-strut one. To this end, figure 3.8A shows

deformed system from regular shapes, are investigated in the next section of the present work, just to analyze what happens in cases of symmetry losing. However, it should be emphasized that asymmetrical configurations are not a "safe harbor" where to find equilibria otherwise impossible. Also, they could compete with symmetry-preserving configurations in minimizing the tensegrity energy –in pre-stressed or under external loads– also if symmetry-preserving equilibrium states were possible.

that differences in stiffness increase, by reaching percentages up to about 25% and 17%, respectively for neo-Hookean and Hencky's constitutive laws, as the filaments' pre-stretch grows to 1.5. Coherently, a similar result in terms of proper frequencies is found by comparing standard and soft-strut models when oscillating by contracting/elongating around the tensegrity pre-stressed equilibrium position. By solving the *small-on-large* problem, the system's proper frequencies can be in fact determined as $f_A = \sqrt{(\partial F_A / \partial W) M_{cell}^{-1}}$, M_{cell} representing a rough estimate of the cell mass obtained by multiplying the volume of the equivalent sphere circumscribing the structure for the cytosol density, which is about the one of the water [68] (see figure 3.8B).

3.1.4.2 Shearing of the cell cytoskeleton

Cells experience shear stresses in many *in vivo* situations. Osteocytes inhabiting the lacunae across osteon lamellae regulate the bone mineral unit activity by sensing solid and fluid-induced shear stresses, so mediating the mechanical signaling to orchestrate the cell mechanobiology and the turnover of osteoblasts and osteoclasts [87]. Shear stresses are also sensed by endothelial cells forming the monolayer of the intima, the innermost tunica of an artery or a vein, the blood flow continuously stimulating them through tangential forces that are at the basis of important biomechanical processes [71], including vessel growth and remodeling [96, 152].

To simulate shear loading on a cell, the self-balanced tensegrity model is constrained at its basis and subjected to a uniform displacement in the $\{x_R, y_R\}$ plane (figure 3.2B), prescribed to the upper three nodes 1, 5 and 9 of the system in a way that:

$$\begin{aligned} U &:= u_1 = u_5 = u_9, \\ V &:= v_1 = v_5 = v_9, \\ w_{UT} &:= w_1 = w_5 = w_9, \end{aligned} \tag{3.25}$$

where the vertical component w_{UT} is unknown, while U and V are assigned along the axes x_R and y_R , respectively, and set equal to:

$$\begin{aligned} U &= D_S \cos \beta, \\ V &= D_S \sin \beta, \end{aligned} \tag{3.26}$$

where the displacement magnitude D_S in the $\{x_R, y_R\}$ plane and its direction with respect to the x_R -axis, said β , are data. The number of

unknowns for the case at hand is then 19. Differently from the previous contraction/elongation test, in case of shear this number cannot be further reduced, since there is no longer axial symmetry. The unknowns of the problem are thus $w_{UT}, w_2, w_3, w_6, w_7, w_{10}, w_{11}, u_2, v_2, u_3, v_3, u_6, v_6, u_7, v_7, u_{10}, v_{10}, u_{11}$ and v_{11} , as usual the subscript referring to the node number and u, v and w denoting the corresponding displacement components parallel to the axes of the Cartesian reference frame $\{x_R, y_R, z_R\}$.

The results, in terms of overall cell deformation, are shown in figure 3.5, for $\lambda_f^* = 1.1$, $\beta = \pi/2 - \alpha_8 = \arccos \sqrt{3/7}$ and for a prescribed shear displacement up to L_f^* . Possible sensitivity analyses by varying the value of the angle β are not reported, this being pointless since the geometrical symmetry of the structure would imply a periodicity of the shear response with period $2\pi/3$. The cell equivalent shear modulus $K_S := \partial P_S / \partial \gamma_{eq}$ and the nominal stress $P_S := (\partial U / \partial D_S) / A_{tr}^*$ are both represented as functions of the equivalent shear strain –here defined as $\gamma_{eq} := D_S / h$ – for different values of the pre-stretch in the cables and for both Hencky’s and neo-Hookean laws, as illustrated in figures 3.6C-D, respectively. The plots show a decrease of the shear stiffness as the strain level increases. As expected, also in this case, the value of the pre-stretch λ_f^* strongly affects the initial shear modulus $K_S^0 := K_S |_{\gamma_{eq} \rightarrow 0}$, which behaves very differently for the two hyperelastic models analyzed, exhibiting a stiffness decrease when the Hencky’s model is adopted –in analogy to the case of contraction/elongation– and an almost linear hardening in the neo-Hookean case, that is still in agreement with experimental and previous theoretical results [147, 209, 237] (see figure 3.7B). It is worth noticing that, in the present case, the results demonstrate that the curve K_S plotted against the equivalent shear strain cannot exhibit even a valid (reliable) tract if $\lambda_f^* = 1$ (indeed, it is entirely grey in figure 3.6C-D), not even for K_S^0 , that results not null at $\lambda_f^* = 1$. This is since, without an initial pre-stretch, some cables immediately would experience a not admissible compressive stress state, also leading to loss of equilibrium for the entire system at the early stage of shear.

3.1.4.3 Overall torque of cells

By considering that the cellular tensegrity model is virtually tested to torque, it is twisted by prescribing a growing torsion angle θ at the top of the structure through proper displacements imposed at the upper nodes 1,5 and 9 and by keeping the nodes at the basis locked (figure 3.2B). In

this case, to obtain the cell response, the updated (current) coordinates for the generic i -th node are conveniently written as

$$\mathbf{p}'_i = \left(R_i \cos \left(\frac{\pi}{2} - \alpha_i - \Delta\alpha_i \right), R_i \sin \left(\frac{\pi}{2} - \alpha_i - \Delta\alpha_i \right), z_i + w_i \right), \quad (3.27)$$

where R_i represents the radius of the circle passing through the tensegrity's nodes lying at the same height in the pre-stressed configuration, namely on a same plane parallel to the $\{x_R, y_R\}$ plane, in particular being $R_i = R_T$ for the nodes belonging to the upper and lower equilateral triangles, $R_i = R_{HT}$ for the nodes 3, 7, 11 of the middle hexagon and $R_i = R_{HB}$ for the nodes 2, 6, 10. Also, α_i is the angle that the i -th node forms with respect to the y_R axis (see equation (3.24)), while $\Delta\alpha_i$ describes the corresponding incremental angle (clockwise, whence the minus) due to the torsional rotation. Additionally, it is possible to assume that, for the nodes placed at the same height, the vertical displacements w_i are the same, so that, also in this case, the relations (3.22) and the (3.25)₃ hold true. Moreover, geometrical arguments allow to set:

$$\begin{aligned} \delta_{HT} &:= \Delta\alpha_3 = \Delta\alpha_7 = \Delta\alpha_{11}, \\ \delta_{HB} &:= \Delta\alpha_2 = \Delta\alpha_6 = \Delta\alpha_{10}. \end{aligned} \quad (3.28)$$

Therefore, since the basis of the structure is constrained, the unknowns of the problem finally reduce to the vertical displacements w_{UT} , w_{HT} and w_{HB} , the torsion angles δ_{HT} and δ_{HB} and the radii R_{HT} and R_{HB} .

The results are shown in figure 3.5 in terms of overall deformation, for $\lambda_f^* = 1.1$ and a prescribed torsion angle θ which varies up to $\pi/4$. The torsional stiffness $K_T := \partial M_T / \partial \theta'$, computed as first derivative of the twisting moment M_T with respect to the unit torsion angle $\theta' := \theta/h$, is shown in figures 3.6E-F for different values of the cables' pre-stretch and for both Hencky's and neo-Hookean laws. The corresponding twisting moment of the cell structure –obtained as $M_T := \partial U / \partial \theta$ – is plotted against θ in the insets. Similarly to the case of shear, a decrease of the torsional stiffness as the rotation increases is observed. In particular, it is still found that the tensegrity system whose elements obey the Hencky model exhibits a lowering of its initial (tangent) torsional stiffness, $K_T^0 := K_T|_{\theta \rightarrow 0}$, at large pre-stretches, the neo-Hookean tensegrity instead showing a significant stiffness increase for the same pre-stretch values, as also shown in figure 3.7C. As for the shear, it also here highlight that, if the system is initially characterized by a unit pre-stretch, torque would induce compression at the early stage of the prescribed torsional rotation in a number of cables such that the whole structure would no longer

be able to guarantee equilibrium, with the result that, in absence of pre-stress, the initial (tangent) torsional stiffness K_T^0 should be vanishing.

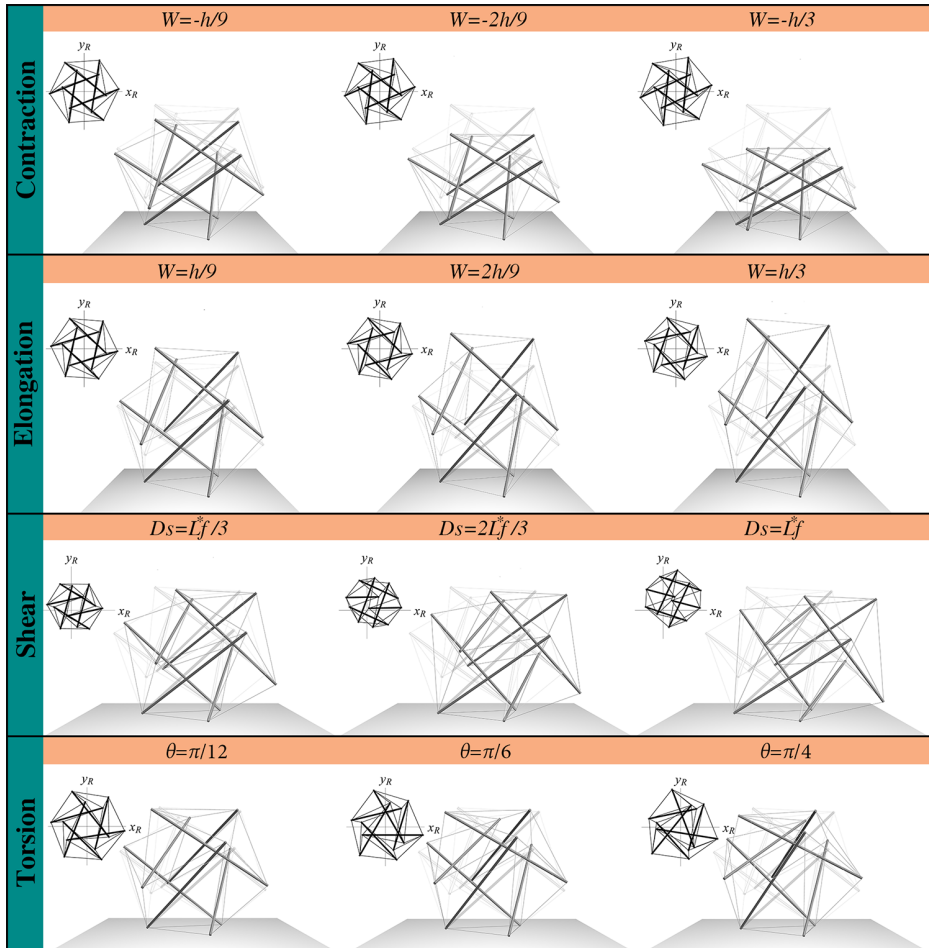


Figure 3.5: 3D front view –and top view (at the top left of each image)– of the deformation sequences of the cellular tensegrity model under the action of the prescribed mechanical conditions, for different values of the assigned displacements (contraction/elongation and shear) and rotation angle (torsion). Here, h and L_f^* are the tensegrity height and the cables length in the pre-stretched configuration, respectively, and in all the cases the value of cables' pre-stretch $\lambda_f^* = 1.1$ is set. Light-coloured on the background, each image shows the pre-stretched configuration. The values of the parameters used for the analysis are reported in table 3.1.

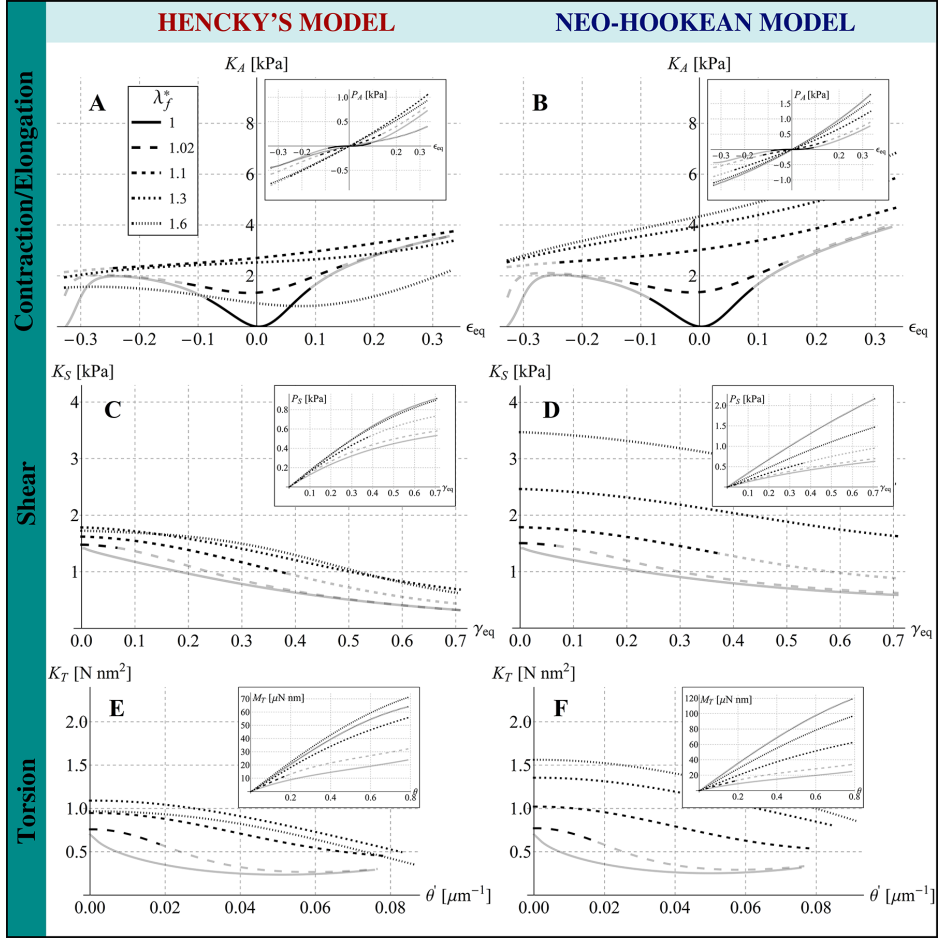


Figure 3.6: **A-B)** Equivalent axial stiffness K_A and, in the inset, nominal stress P_A against equivalent strain ϵ_{eq} , in case of contraction/elongation and for both Hencky and neo-Hookean models. **C-D)** Equivalent shear modulus K_S and, in the inset, nominal stress P_S versus the equivalent shear strain γ_{eq} , for Hencky and neo-Hookean elements. **E-F)** Equivalent torsional stiffness K_T and, in the inset, twisting moments M_T as functions of the unit torsion angle θ' and torsion angle θ , respectively, for the two hyperelastic laws hypothesized. The results are obtained for different values of cables' pre-stretch λ_f^* (1, 1.02, 1.1, 1.3, 1.6), by making reference to the cell physical parameters collected in table 3.1. In lighter gray the tracts of the curves theoretically extrapolated but unrealistic since therein cables would undergo compression.

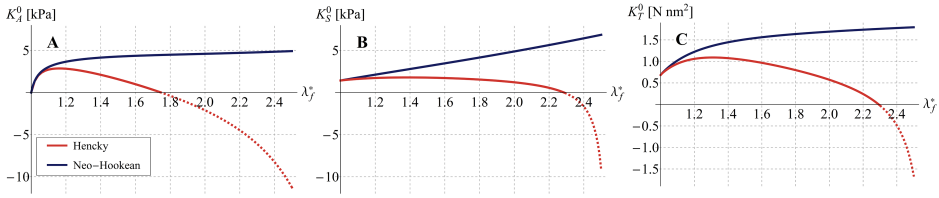


Figure 3.7: Tangent (initial) stiffness exhibited by the soft-strut 30-element tensegrity by varying the cables pre-stretch λ_f^* , for Hencky's and neo-Hookean models in cases of **A**) contraction/elongation, **B**) shear and **C**) torsion. Results are obtained for values of the cell physical parameters as reported in table 3.1. The dashed parts of the curves relative to the Hencky's model highlight negative stiffness values.

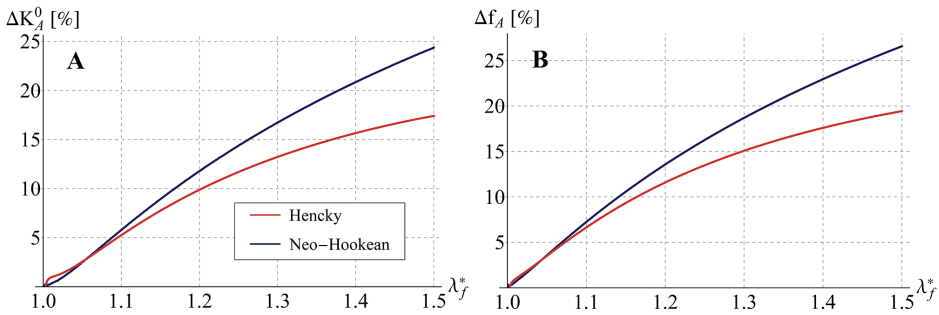


Figure 3.8: Percentage difference in terms of **A**) initial (tangent) stiffness and **B**) proper frequency obtained by comparing the presented soft tensegrity with a standard rigid-strut model, while prescribing growing filaments' pre-stretch, for a contraction/elongation loading type, under both the assumptions of Hencky's and neo-Hookean constitutive law.

3.2 SYMMETRY-LOSING EQUILIBRIUM CONFIGURATIONS

The previous section analyzes how the cell cytoskeleton would behave by expecting that its pre-stressed structure, modeled as a soft-strut tensegrity system, preserves geometrical symmetries in both self-equilibrated states (form-finding problem) and while undergoing deformations in response to applied loads. This implies that bending of microtubules under compression is there neglected, being instead enabled only their elastic shortening. Also, equilibria associated to global switching of the tensegrity towards possible not symmetrical configurations minimizing the elastic energy are so far not explored. Local loss of symmetry is

however not an unrealistic event in cells. In fact, according to table 3.1 and experimental measures [78], by considering the effective geometry of the cross-section of microtubules possessing a length L_t and a bending stiffness $B_t = 2.15 \cdot 10^{-23} \text{ N} \cdot \text{m}^2$, a critical axial load due to instability can be obtained as $N_c \simeq 1.5 \text{ pN}$. Such a value is compatible with the order of magnitude of the forces occurring in the struts both when the tensegrity is at self-equilibrium and when it is solicited by external loads, this legitimating the possibility that a post-buckling response cooperates with the purely axial contraction of the bars in influencing the actual cell mechanical behavior. As a matter of fact, buckling of cell microtubules has been observed experimentally [207, 238] and theoretically investigated in some literature works [35, 36, 232], by postulating the axial rigidity of the struts. More recent studies [17, 129] however highlighted that the critical load inducing buckling of *in vivo* microtubules, embedded in the cellular environment, would turn out to be significantly greater (from about two up to four orders of magnitude) than the one evaluated for the same isolated element *ex vivo*. This difference would occur due to the presence –*in vivo*– of the surrounding viscous/viscoelastic cytoplasm, which also comprises the elastic network of intermediate filaments. These, together with other intracellular protein structures of the gel-like cytosol, would therefore work as a tensed lateral support that stabilizes microtubules, in this way increasing their effective capability to resist buckling [17, 18, 129, 207] and in some cases forcing the microtubules to not buckle in a single-wave mode [204].

Local buckling of struts is however not the sole way for envisaging loss of symmetry in a cellular tensegrity structure. Equilibria could in fact be reached –at least in principle– during any deformation process in cells when prescribed levels of pre-stress, respectively in struts and cables, attain values such that the tensegrity is invited to deviate from its natural shape to follow minimal energy pathways. This is for instance the case of experimentally observed overall configurational switching of cells occurring during gastrulation [245] or in adhesion and migration phenomena, in occasion of which abrupt changes of the cytoskeleton organization are required to accommodate polymerization/depolymerization processes of protein filaments to respond to specific bio-chemo-mechanical stimuli resulting in reorientation/rearrangement of the stress fibers [112, 179, 180].

With all this in mind, in order to explore both situations of local and of global loss of symmetry in soft-strut cellular tensegrity systems, two hypothetical scenarios are analyzed in what follows, which *de facto* could

occur separately or as concomitant as a result of the interplay of axial deformability and bending stiffness of soft bars: the case of soft struts experiencing buckling and the case of minimum energy equilibrium states associated to overall deviations of the tensegrity from its expected (symmetrical) configuration. In this regard, by way of example, the responses of a handmade toy system are shown in figure 3.9 in comparison with results obtained by means of finite element analyses.

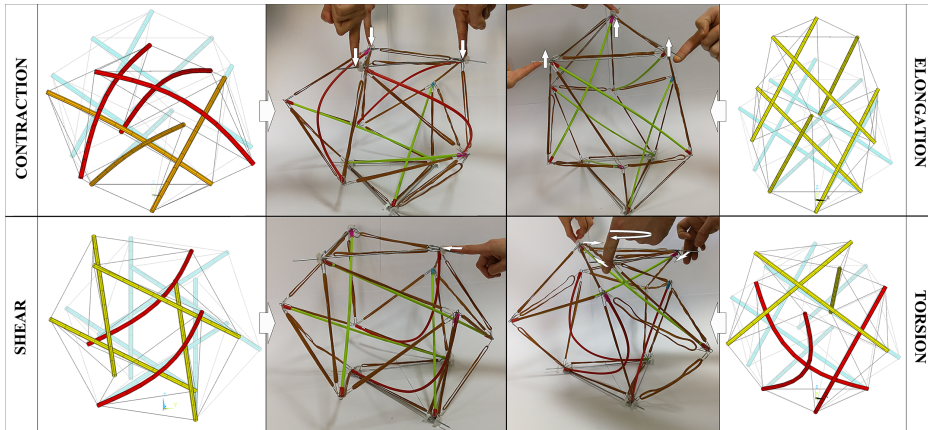


Figure 3.9: Experimental responses of handmade toy tensegrity systems with bendable struts experiencing elongation, contraction, shear and torsion, with comparison of deformations obtained from finite element analyses.

3.2.1 Competition of local buckling and global configurational switching in cellular tensegrity systems with bendable soft struts: form-finding and response to applied loads

As first step, the form-finding problem is here re-analyzed for a 30-element soft tensegrity system whose contracting struts are now enabled to also undergo bending. To make this coherently with experimental data and observations and to properly take into account the effect of the lateral confinement imposed by the cytoplasm, the intermediate filaments and other protein structures to microtubules of actual living cells, a fictitious amplification of the geometrical bending stiffness B_t up to 10^4 [17, 129] is *ad hoc* considered, leaving unchanged the cross-sectional area of the microtubules, responsible of their axial deformability. Higher values of the *effective* bending stiffness of the microtubules are then additionally

assumed, in this manner allowing the cell cytoskeleton, even though the axially soft struts are not prone to bend [204], to homotetically scale its polyhedral shape as a function of the increasing pre-stretch in the cables, or to switch asymmetrically on other –energetically more comfortable– configurations.

However, loss of symmetry no longer allows to proceed analytically and, therefore, this section makes reference to results obtained by means of finite element simulations. All the numerical analyses were performed by reconstructing the three-dimensional icosahedral 30-element tensegrity structure with the aid of the finite element commercial code ANSYS® [5], by uploading a progressively growing level of elastic pre-stretch to the tensed microfilaments (cables) and thus inducing a corresponding increasing of compressive pre-stress in the microtubules (struts). From the operational point of view, this was managed by properly tuning the natural (at rest) cables lengths on the basis of the geometrical relations involving stretches and resting lengths already established above for the polyhedral tensegrity. Non-linearly elastic bar-elements (LINK180) with no-compression and axially deformable and bending beams (BEAM188) were hence chosen to replicate respectively the behavior of actin filament-like cables and microtubule-like struts, by using for both the Hencky’s hyperelastic law [171] and assigning to them the corresponding geometrical and constitutive features according to the values reported in table 3.1. At the end, a mesh resulting in 84 elements and 66 nodes with translational and rotational degrees of freedom was generated. All the numerical analyses were conducted in finite strains and large displacements, by activating for all the elements the options of nonlinear geometry, standard step-by-step procedures and robust algorithms being furnished by the software to control and ensure the convergence. Moreover, a preliminary check was performed to verify that the model was capable to confirm the theoretical results, utilized as benchmark, already obtained for the case of symmetry-preserving deformations.

The solutions of the form-finding problem are synoptically shown in figure 3.10, in which all the possible self-equilibrated states that the tensegrity system can assume are uniquely represented by points in the phase space $\langle \lambda_f^* \rangle - \langle \lambda_t^* \rangle$, where $\langle \lambda_f^* \rangle$ and $\langle \lambda_t^* \rangle$ are the pre-stretch average values in filaments and tubules, respectively. In this phase space, by starting from slightly higher-than-one levels of average pre-stretch in the filaments, the corresponding average contractions almost proportionally grow in microtubules, at the early stage of the pre-stress showing that the soft-strut tensegrity overall contracts homotetically, preserving shape

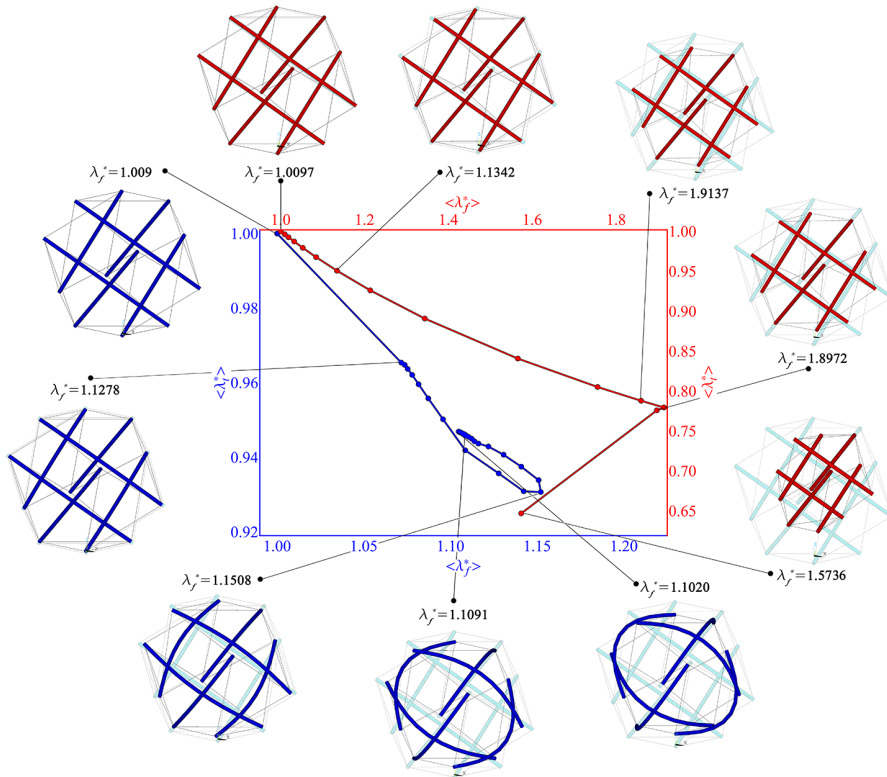


Figure 3.10: Self-equilibrium configurations of the soft-strut cellular tensegrity represented in the phase space $\langle \lambda_j^* \rangle$ - $\langle \lambda_t^* \rangle$. Blue points and (fitting) curves represent the states of self-equilibrium that the system gains for each pair of (average) elongation and contraction pre-stretches in its cables and struts, respectively, for the case in which the bending stiffness of the struts is assumed at values of 10^4 times [17, 129] the geometrical bending stiffness B_t experimentally measured for an isolated microtubule [78]. Red points and associated (fitting) curves represent instead the self-equilibrium states in case the tensegrity struts can axially deform but their bending stiffness $B_t \rightarrow \infty$. Note that, in both the cases, form-finding provides possible loss of symmetry: this happens, at the local level, with buckling of microtubules (deformed structures with blue struts) for bendable struts and with global configurational switching (tensegrities with red struts) if the bending stiffness of microtubules is forced to be extremely high. To synoptically show the two behaviors in the same phase space, two corresponding different axes scales and colors (blue and red) are coherently utilized for the axes.

and the original polyhedral symmetry. This behavior is exhibited by the system up to pre-stretches in filaments given by $\lambda_f^* \simeq 1.13$, for both the cases of bendable and flexurally stiff struts, in other words for an effective bending stiffness four orders of magnitude greater than the geometrical one, B_t , and for ideally unbendable struts, say $B_t \rightarrow \infty$. However, as the pre-stretch in the filaments increases, very different behaviors are exhibited by the system in the two cases of bendable and unbendable microtubules. In fact, in the first case, as filaments pre-stretch grows, struts elastically contract by increasing the compressive stress that they sustain, then suddenly undergo buckling while preserving part of the axial contraction and producing a sharp snap-back phenomenon at $\lambda_f^* \simeq 1.15$, at the end progressively relaxing the axial deformation level (see the blue curve in figure 3.10). However, the local buckling of the struts in this case occurs for all the compressed elements contemporaneously and this allows the tensegrity to maintain its overall symmetrical shape. In the other case, say when the microtubules' nominal bending stiffness is set to be high, the early stage of the deformation is still characterized by simple uniform scaling of the polyhedral tensegrity shape, up to a pre-stretch value in the cables of about $\lambda_f^* \simeq 1.9$, after which an abrupt global change of configuration is exhibited by the structure, which in fact switches on a deformed state associated with loss of symmetry (see the red curve in figure 3.10), then finding a stable equilibrium after a reversal in the phase space, by leaping up lower pre-stretch levels in microfilaments and higher contraction of microtubules.

To finally explore what happens if the effective (finite) bendability of the struts is taken into account also for soft tensegrity structures undergoing the same applied loads already theoretically (analytically) considered above in case of (imposed) symmetry-preserved situations, analyses for the entire set of loading conditions, say contraction, elongation, shear and torsion, were numerically replicated by performing finite element simulations. The results, in terms of overall deformation of the system, are illustrated for each of the four loading cases in figure 3.9, to the aim of highlighting the qualitative compatibility of the obtained deformed configurations with respect to those exhibited by handmade toy systems roughly loaded with the corresponding forces. More in details, quantitative results are reported –in terms of generalized stresses against associated overall strains– in figure 3.11. It is therein worth noticing that, as already found for the form-finding problem, a first phase of the mechanical response, characterized by an essentially perfect superposition of the numerical (finite element-based) results with the outcomes obtained

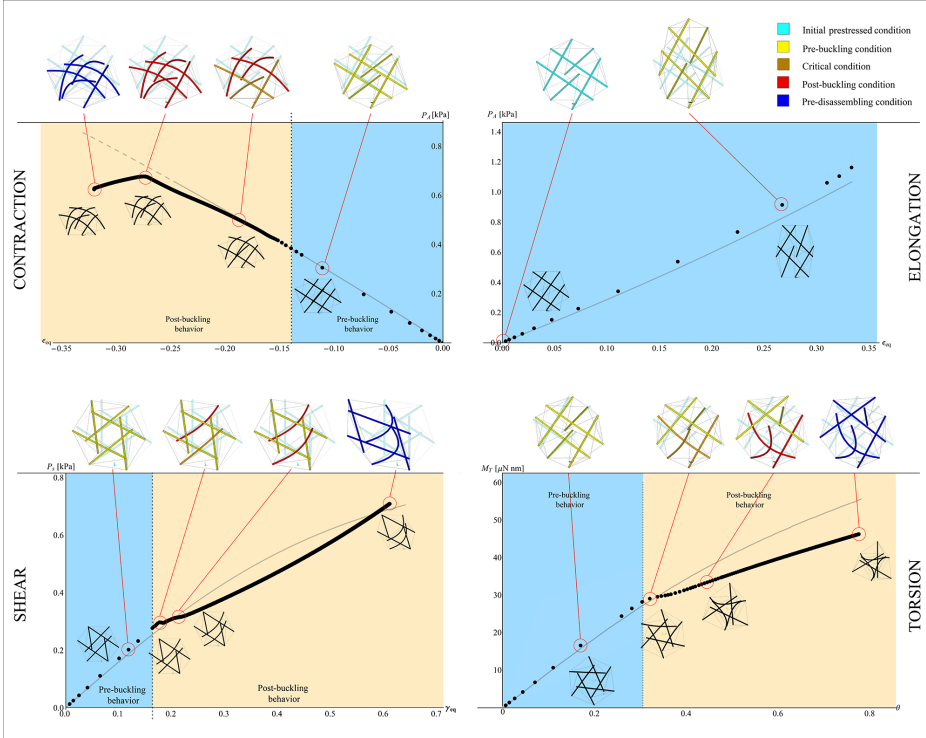


Figure 3.11: Numerical finite element-based (black dots) results for soft tensegrity systems with bendable struts in cases of contraction, elongation, shear and torsion, in terms of generalized stresses (axial forces, shear loads and torque) versus corresponding equivalent strains (overall contraction/elongation axial strains, shear deformation and global torsion angle). Grey curves recall the solution in the cases of preservation of the expected symmetries, as obtained from the theoretical analyses in absence of buckling struts in the sections above. Blue and flesh-coloured backgrounds allow to distinguish the so-called pre-buckling and post-buckling regions, respectively. The insets and the three-dimensional sketches on the top of each graphic show how tensegrities behave, in terms of deformation, as the loads increase.

theoretically, is traced until the pre-stress in cables and struts is such that the minimization of the total potential energy of the structure can be still attained for symmetry-preserving configurations. Then, a second phase can be registered, in which the tensegrity system progressively undergoes no longer symmetrical deformation states as the applied loads increase and induce both buckling of some strut elements and global rearrangement of the whole structures. In particular, with reference to

the overall deformation ranges considered in the analyses, except for the case of elongation, in all the other loading conditions, one can sharply separate a *pre-buckling* phase, recopying the already obtained analytical results related to symmetry-preserving equilibrium states (highlighted by blue background in the graphics), from a *post-buckling* behavior (denoted by the flesh-coloured background), characterized by a deviation of the numerical points (black dots) from the curve (grey line) that denotes the path ideally followed by the structure in case of absence of buckling of struts. The results are truncated at an end point in correspondence of which cables and struts are no longer able to sustain stresses for ensuring global equilibrium in the actual (deformed) configuration. To add geometrical information about what physically happens during the load's increase, insets with plane and three-dimensional views of the tensegrity systems, at any relevant stage of the deformation, are supplied in figure 3.11.

3.3 CONCLUSION

The cytoskeleton is a complex, continuously self-assembling and reorganizing network of interconnected microtubules and actin microfilaments, to which is assigned –among other– the role of bearing structure of living cells. In response to bio-chemo-mechanical stimuli, the cytoskeletal elements activate polymerization/depolymerization as well as micro-structural re-arrangement and disarrangement processes and undergo large deformations and displacements, accompanied by elastic pre-stretches. By following this way, they provide to the cell either stable configurations, thus governing adhesion and ensuring equilibrium of internal stresses and applied forces coming from cell-cell interactions or interactions of the cell with the ECM, or unstable shapes, for driving migration mechanisms, cell reorientation and duplication phenomena. At any of these stages, the cytoskeletal architecture contemporary guarantees energy storing and stiffness tuning and conveys selected signaling pathways across the cell membrane and towards the nucleus aimed to mechanotransduction.

By starting from the Ingber's pioneering idea of using tensegrity systems for describing the mechanical behavior of the cells and studying how equilibria evolve as its structural geometry changes, a new *soft-strut* tensegrity model of the cell cytoskeleton has been built up in the present chapter. With the aim to overcome some limits of previous models related

to intrinsic (constitutive and kinematical) assumptions, the hypothesis of linear elasticity for both cables and struts has been in particular removed, and the form-finding problem as well as the equations governing the elastic response to applied loads of a 30-element polyhedral tensegrity structure have been rewritten by including both axial deformability and bendability of struts, coherently with experimental measures –that highlighted close values of axial stiffness for single actin filaments and microtubules– and according to recent literature findings showing *in vivo* buckling of microtubules.

The analytical and numerical results provided by the soft tensegrity paradigm of the cell, as in detail described in the previous sections, have shown that rich families of nonlinear elastic responses of the cell cytoskeleton, presenting some previously unpredicted non-monotonic overall stress-strain curves and softening phenomena, can be derived by following its rearrangement under external actions. Also, the results found in the two cases of Henky-type and neo-Hookean elements have highlighted significant discrepancies in terms of both form-finding solution and global (equivalent) stiffness, even though the input physical parameters used for the modelling and borrowed from the experimental literature are the same, this corroborating the necessity to involve proper mechanical laws at the level of the tensegrity members for more faithfully describe –and predict– the overall cell response. Finally, finite element analyses have demonstrated that the loss of both local and global symmetry of the tensegrity structure can be found as a consequence of non-uniform buckling of its elements and configurational switching of the whole system on asymmetric shapes. All these transitions occur in correspondence of energy wells generated by a complex competition among bending stiffness and axial deformability of the struts, average pre-stress levels in filaments and microtubules and global structure instabilities.

It is worth noting that the presented model does not take into account additional aspects that could further enrich the description of the mechanical response of the tensegrity-based cytoskeleton. As an example, more complex (e.g. multi-modular) tensegrity-based architectures could be incorporated for more faithfully modeling the mechanical behavior of the cell cytoskeleton in terms of internal reorganization and redistribution of forces during the cell dynamics. Also, the model does not include the effects of the intrinsic viscoelasticity of the cell [10, 22, 108] as well as explicit biochemo-mechanical coupling driving the polymerization/depolymerization of the cytoskeletal filaments is not considered.

It is however felt that the proposed enhanced tensegrity model, allowing to quantitatively predict the order of magnitude of forces, stiffness and elastic energy amount stored by the pre-stressed cell cytoskeleton and being also capable to replicate both symmetry-preserving and instability-guided asymmetric configurations of the protein structural network, could contribute to move a further step towards an engineering modeling of mechanical behaviors and adhesion/migration mechanisms of single cells and to shed light on the underlying physics of many important phenomena not yet fully understood, involving abrupt changes of cytoskeleton configurations or cell morphology, such as gastrulations, extreme deformations occurring during duplication and modifications of elastic properties characterizing physiological cell processes and malignant transformations of cancer and metastatic cells [27, 69].

MECHANOTROPISM OF ADHERENT CELLS VIA EXTERNAL POINT-LOADS

As widely described in previous sections, processes of mechanosensing and mechanotransduction play a pivotal role in regulating –along with biochemical factors– main aspects of cells behavior [8, 107, 146]. As a matter of fact, necessary condition to the viability of the most cell lines (e.g. epithelial cells, fibroblasts, muscle cells) lies in their adhesion to a matrix able to offer an adequate stiffness to the continuous action of probing, by pushing and pulling, exerted by the single-cell via traction forces [12, 88]. These are generated by the internal actomyosin-based contractile cytoskeleton and transmitted outwards through transcellular structures consisting of tension-dependent micrometer-sized aggregates of proteins (primarily integrins) known as focal adhesions [42, 106, 184, 210]. There are several evidences that, through focal adhesions arrays, cells can recognize differences in the mechanical properties of the contact materials as well as sense the mechanical stimuli, namely forces and strains, coming from the surrounding environment and respond to them by altering their contractility level and structural organization, both locally (e.g. changes in stability and number of adhesion sites) and at a global scale by remodeling the cytoskeletal machinery [28, 75, 76, 91, 146, 239].

In particular, according to what discussed in detail in section 1.3, it has been observed that animal cells –assuming round shapes in suspension– stretch and flatten when adhering to an external surface, some cell types (e.g. fibroblasts) assuming highly elongated and stationary (i.e. stable and non-motile) profiles for sufficiently high values of the adhesion matrix rigidity [133, 176]. In addition, experimental outcomes have highlighted that the orientation of such adherent cells on deformable flat substrates under the action of external mechanical perturbations does not arise randomly, but seems instead the result of an optimization process implemented by the cells for achieving a preferential condition, whose mechanical principles are however not completely clear yet.

By keeping in mind the results provided by the previous experimental and theoretical related literature [29, 197], the present chapter is devoted to the analysis of a possible strategy for the identification of the

optimization mechanisms driving the orientation process of an adherent single-cell elastically interacting with external forces through the underlying (deformable) substrate.

The mechano-induced orientation mechanism is here referred to as *mechanotropism*. A tropism (from the greek word τροπος, tropos, "a turning") is a biological phenomenon indicating the turning movement (possibly accompanied by growth) of an organism, usually a plant, in response to an environmental stimulus. Phototropism, chemotropism or gravitropism are terms commonly adopted in biology for indicating the tendency of an organism to reorientate by responding to light, chemical and gravity stimuli, respectively. Accordingly, mechanotropism is here conceived as the process identifying the reorientation of a living system, in particular a cell, induced by mechanical solicitation, in this way also introducing a complementary behavior with respect to cell *mechanotaxis*, which instead refers to mechano-driven migration events [124, 138].

Then, this chapter proposes a theoretical model to study the mechanotropism of an adherent elongated single-cell under the perturbing effect of external static loads, conceived as patterns of concentrated forces acting orthogonally to the flat surface bounding an elastic and isotropic substrate of adhesion, at the vertexes of a n -sided regular polygonal fence surrounding the cell. It is in fact felt that this type of approach could be exploitable for designing novel possible experiments in which, once fixed the substrate's properties, the alignment of a cell would be sculpted through suitably selected configurations of applied loads (namely, proper forces' number n , pointing direction, magnitude and distance from the cell).

On the basis of experimental measurements of cellular traction patterns and of previous theoretical works [14, 194, 195, 197], the adherent polarized cell is here modelled as a stretched one-dimensional fiber-shaped body acting as a pair of contractile forces, i.e. as a force dipole, on the boundary of a semi-infinite elastic isotropic homogeneous solid. In this way, its mechanical interaction with the external fence of normal point-loads can be described by employing singular solutions of the linear elasticity theory [9, 243]. Cell's optimal orientations are then found by invoking as linchpin optimization principle the minimization of the work done by the cell to elastically deform the compliant substrate while retaining its traction forces level [14, 15].

It is worth highlighting that, despite the concept of anisotropic force contraction dipole has been already used in literature as paradigm for a bipolar-shaped cell [194, 197], it has been treated by following a course-

grained approach, namely by modelling the cell as a point defect in an elastic medium, thus assuming to observe it at a distance much larger than its spatial extent. Here, instead, the two contractile forces identifying the single-cell are assumed as acting at two distinct punctual sites of adhesion, in order to be able to take into account effects arising within an area more proximal to the cell, although preserving its simplified physical picture of force dipole.

4.1 BOUSSINESQ AND CERRUTI SOLUTIONS FOR SEMI-INFINITE SOLIDS

By considering an elastostatic displacement formulation that accounts for Saint-Venant's compatibility conditions and constitutive assumptions of homogeneous and isotropic material, equilibrium equations governing linear elasticity theory result in the following Navier-Cauchy equation [120]:

$$\mu \nabla^2 \mathbf{u} + (\lambda + \mu) \nabla \nabla \cdot \mathbf{u} + \mathbf{B} = \mathbf{0}, \quad (4.1)$$

where \mathbf{u} is the unknown displacement vector field to be determined by obeying the prescribed (Dirichlet- or Neumann-type) boundary conditions associated to the differential equations system, \mathbf{B} is the body force vector field, $\mu = E / [2(1 + \nu)]$ and $\lambda = 2\mu\nu / (1 - 2\nu)$ are the Lamé constants of the continuum body, E being its Young's modulus and ν its Poisson's ratio, while $\nabla^2(\bullet)$, $\nabla(\bullet)$ and $\nabla \cdot (\bullet)$ denote the Laplacian, gradient and divergence operators, respectively.

In the second half of the 1880s, Betti provided a first general method for the integration of such a system [139], founded on his reciprocal work theorem [225]. On these bases, Cerruti and Boussinesq subsequently developed solutions for the equilibrium problem in the particular case of concentrated forces acting –tangentially and normally, respectively– on the plane boundary of an isotropic elastic half-space [139]. Then, different derivations of such solutions have been given over the time [9, 109, 225], in particular Westergaard formulating an interpretation in terms of Galerkin vector [243]. In a general case, such vector allows to express the solution of the basic equations of linear elasticity (4.1) in the form:

$$2\mu \mathbf{u} = [2(1 - \nu) \nabla^2 - \nabla \nabla \cdot] \boldsymbol{\Gamma}, \quad (4.2)$$

where $\mathbf{\Gamma}$ is the Galerkin vector, that –by substitution into (4.1)– has to satisfy the equation:

$$\nabla^4 \mathbf{\Gamma} = -\frac{\mathbf{B}}{1-\nu}, \quad (4.3)$$

this meaning that, in case of negligible body forces, it has to be a biharmonic vector function.

Specifically, by considering a point-load acting normally to the boundary of a semi-infinite solid occupying the half-space $z \geq 0$, under null body forces ($\mathbf{B} = \mathbf{0}$), the Boussinesq's problem can be solved –by virtue of the superposition principle holding true in linear frameworks– through additive combination of the following Galerkin vectors $\mathbf{\Gamma}_1^B$ and $\mathbf{\Gamma}_2^B$, in a way that shear stresses vanish on the plane boundary $z = 0$ [243]:

$$\mathbf{\Gamma}_1^B = \frac{F_z}{2\pi} \rho \hat{\mathbf{e}}_z \quad \text{and} \quad \mathbf{\Gamma}_2^B \text{ s.t. } \nabla \cdot \mathbf{\Gamma}_2^B = \frac{(1-2\nu) F_z}{2\pi} \log(\rho + Z), \quad \nabla^2 \mathbf{\Gamma}_2^B = \mathbf{0}, \quad (4.4)$$

where $X := x - x_F$, $Y := y - y_F$ and $Z := z$, hence $\rho := \sqrt{X^2 + Y^2 + Z^2}$ is the distance of the generic point of the half-space, say $\mathbf{x} = x\hat{\mathbf{e}}_x + y\hat{\mathbf{e}}_y + z\hat{\mathbf{e}}_z$, from the point of application of the external force, namely $\mathbf{x}_F = x_F\hat{\mathbf{e}}_x + y_F\hat{\mathbf{e}}_y$, while $\hat{\mathbf{e}}_j$, with $j = x, y, z$, is the generic unit vector of the rectangular reference system and F_z is the sole non-vanishing component of the normal point-load $\mathbf{F}_B = F_z\hat{\mathbf{e}}_z$ acting at \mathbf{x}_F . Note that the harmonic scalar function $-\nabla \cdot \mathbf{\Gamma}_2^B$ is also known as strain potential and may be in general used, independently from the definition of Galerkin vector, for describing some purely irrotational deformation fields [9]. By then assuming $\mathbf{\Gamma} = \mathbf{\Gamma}_1^B + \mathbf{\Gamma}_2^B$ in equation (4.2), the displacement field that solves Boussinesq's problem is given by \mathbf{u}_B having the following scalar components:

$$u_x^B = \frac{F_z}{4\pi\mu} \left[\frac{XZ}{\rho^3} - (1-2\nu) \frac{X}{\rho(\rho+Z)} \right], \quad (4.5a)$$

$$u_y^B = \frac{F_z}{4\pi\mu} \left[\frac{YZ}{\rho^3} - (1-2\nu) \frac{Y}{\rho(\rho+Z)} \right], \quad (4.5b)$$

$$u_z^B = \frac{F_z}{4\pi\mu} \left[\frac{Z^2}{\rho^3} + \frac{2(1-\nu)}{\rho} \right]. \quad (4.5c)$$

On the other hand, Cerruti's problem –that concerns the complementary case of semi-infinite solid interesting the half-space $z \geq 0$ undergoing a

purely tangential concentrated load at $z = 0$, for negligible body forces—is solved by the superposition of the Galerkin vector

$$\mathbf{\Gamma}_1^C = \frac{1}{4\pi(1-\nu)} [\rho (F_x \hat{\mathbf{e}}_x + F_y \hat{\mathbf{e}}_y) + (1-2\nu) \log(\rho+Z) (F_x X + F_y Y) \hat{\mathbf{e}}_z] \quad (4.6)$$

with the strain potential

$$-\nabla \cdot \mathbf{\Gamma}_2^C = \frac{(1-2\nu)}{2\pi(\rho+Z)} (F_x X + F_y Y), \quad \nabla^2 \mathbf{\Gamma}_2^C = \mathbf{0}, \quad (4.7)$$

herein F_x and F_y being the non-null components of the tangential point-load $\mathbf{F}_C = F_x \hat{\mathbf{e}}_x + F_y \hat{\mathbf{e}}_y$ acting at \mathbf{x}_F [243]. As a consequence, analogously to the Boussinesq's previous problem, by substituting $\mathbf{\Gamma} = \mathbf{\Gamma}_1^C + \mathbf{\Gamma}_2^C$ into equation (4.2), the Cerruti's solution, guaranteeing null normal stress over the boundary, is given by the displacement field \mathbf{u}_C whose components read as:

$$u_x^C = \frac{1}{4\pi\mu} \left\{ \left[\frac{1}{\rho} + \frac{X^2}{\rho^3} + (1-2\nu) \left(\frac{1}{\rho+Z} - \frac{X^2}{\rho(\rho+Z)^2} \right) \right] F_x + \frac{XY}{\rho} \left[\frac{1}{\rho^2} - \frac{1-2\nu}{(\rho+Z)^2} \right] F_y \right\}, \quad (4.8a)$$

$$u_y^C = \frac{1}{4\pi\mu} \left\{ \frac{XY}{\rho} \left[\frac{1}{\rho^2} - \frac{1-2\nu}{(\rho+Z)^2} \right] F_x + \left[\frac{1}{\rho} + \frac{Y^2}{\rho^3} + (1-2\nu) \left(\frac{1}{\rho+Z} - \frac{Y^2}{\rho(\rho+Z)^2} \right) \right] F_y \right\}, \quad (4.8b)$$

$$u_z^C = \frac{1}{4\pi\mu} \left[\frac{Z}{\rho^3} + \frac{1-2\nu}{\rho(\rho+Z)} \right] (F_x X + F_y Y). \quad (4.8c)$$

Finally, by virtue of the linearity, the mechanical response of an elastic half-space in general undergoing combinations of normal and/or tangential point-loads can be obtained by employing the superposition principle [225] to couple displacements solutions of the types (4.5) and (4.8). In particular, superposed Boussinesq's and Cerruti's solutions are used in the present chapter with the aim to explore *optimal* orientations attained by a single-cell adhering to the boundary of a linear elastic substrate under the perturbing effects of externally applied point-loads.

4.2 RATIONALE AND HYPOTHESES UNDERLYING THE MODEL

It is known that stationary as well as migrating cells transmit traction forces to the substrate on which they lie through spatially localized focal adhesions complexes [46, 88, 89]. These in fact exhibit a strict correlation of their width and axis of elongation respectively with the magnitude and the direction of the force that they born [7, 184, 220], such properties also resulting a function of the stiffness of the underlying substrate [72, 77, 167, 176]. In many cases (e.g. for suitable values of rigidity of the support material [72, 133, 176]), stationary adhering cells, such as fibroblasts, assume highly elongated (polarized) configurations, characterized by focal adhesions principally located along the cell's rim and bearing significant forces only at the two extremities [195], as exemplified in figure 4.1. These have magnitude of the order of $10\text{-}30nN$ for each focal adhesion (corresponding to an average stress of about $5.5 \pm 2nN/\mu m^2$) and appear mainly oriented along the principal axis of the polarized cell, with a generally negligible projection along the direction orthogonal to the substratum surface [7, 12, 77, 195]. Moreover, the two tangent overall forces resulting, by superposition, at the opposite cell ends –actually directed along its polarization axis– appear to balance each other, in a way that, from the mechanical point of view, the whole adhering non-migrant cell can be treated as a dipole of equal contractile forces, each of the order of hundreds of nN [194, 195].

On the other hand, in conformity with the constitutive and geometrical properties of the materials commonly used for plating cells during experimental tests and with the related observations about smallness of displacements and strains induced by the cell tractions with respect to cell's length and to the thickness of the substrate, it is reasonable to model the latter as an isotropic linear elastic semi-infinite solid, as in fact commonly done in traction force microscopy techniques [7, 46, 174, 191, 194, 195, 214]. On these bases, the effects of a polarized cell adhering on the top of an elastic substrate are here evaluated by employing for each of its two contractile forces the solution (4.8) of the Cerruti's problem for tangential point-load acting over semi-infinite solids.

It is then envisaged that the steadiness of a so-modeled stationary cell-dipole is perturbed by the application of external concentrated loads contemporary acting normally on the top of the substrate. The influence of these forces is analogously studied by using superposed Boussinesq's solutions. In particular, peculiar patterns of perturbations are here considered, with the aim to build up a theoretical model that, on the one hand,

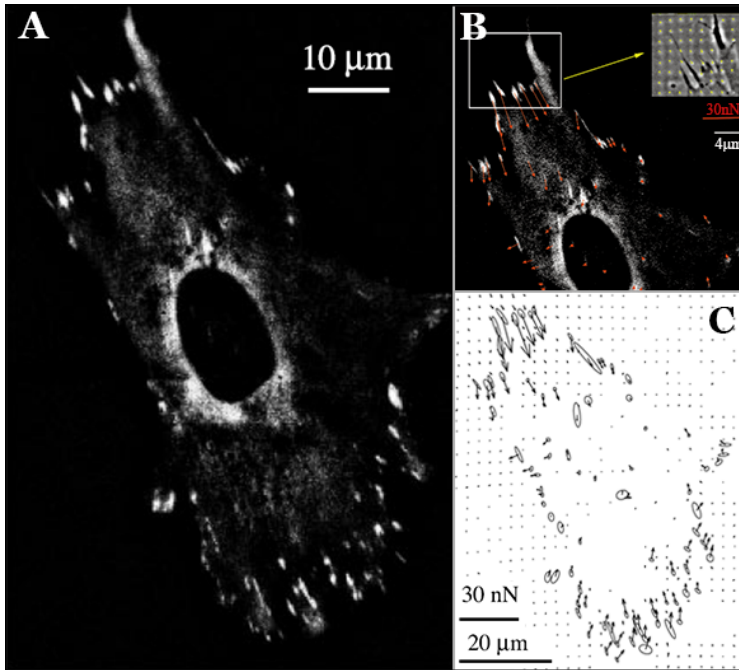


Figure 4.1: Illustration of the cell tractions distribution from a (stationary) human foreskin fibroblast adhering over a patterned elastomer (Young's modulus = $18kPa$). **A**) Fluorescence image of the fibroblast expressing green fluorescent protein (GFP)-vinculin, which localizes at focal adhesions (vinculin is indeed one of the major proteins of the sub-membrane plaque of focal adhesions). The image is reproduced from [195]. **B**) Focus on the alignment of the cell traction forces with the direction of elongation of large focal adhesions (red arrows in fact correspond to forces extracted from the displacements of the patterned elastomer). In the inset, phase-contrast image of the upper part of the cell, showing displacements of the small square pits constituting the pattern of the substrate. The image is reproduced from [7]. **C**) Reconstruction of the cellular force distribution, where arrows indicate the forces while ellipses are fits to the focal adhesions as marked by GFP-labelled vinculin. The image is reproduced from [195].

is sufficiently reach to lead insights into the mechanical principles driving the orientation of cell-dipoles and, on the other one, involves a limited number of variable parameters in order to be manageable both from an analytical point of view and for driving the design of possible experimental tests. Therefore, the rationale of investigating the effects produced by

fences of normal point-loads located at the vertexes of regular polygonal figures surrounding the cell is followed.

Finally, the response to such mechanical stimuli is studied by envisaging that adhering cells tend to align along specific directions that lead them to the minimization of the work spent in deforming the underlying substrate while transferring to it traction forces [15]. This assumption lies on the observation that cells need to preserve and exploit their energy to fulfil their own physiological activities and is encouraged by the well-established evidences of durotaxis [138], which is the cell migration towards directions of greater stiffness, namely towards less deformable regions.

4.3 THEORETICAL ARCHITECTURE OF THE MODEL

On the basis of what illustrated above, a stationary adhering single-cell is here modeled as a dipole of contractile tangential forces having equal magnitude (see figure 4.2A) and assumed to be essentially constant.

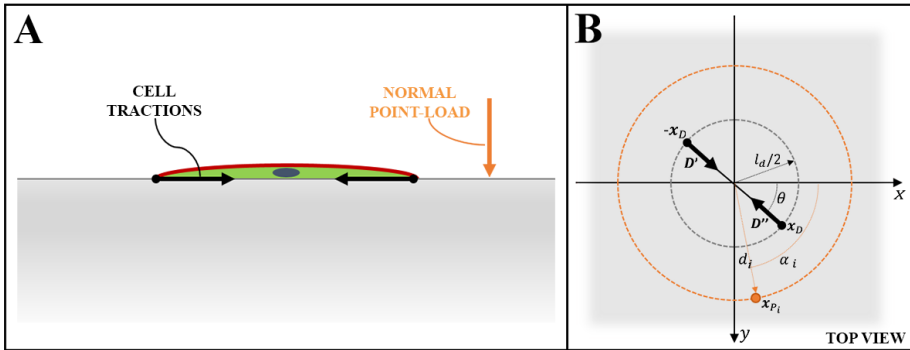


Figure 4.2: **A)** Sketch of an adherent stationary cell as a dipole of contractile forces acting tangentially on the top of the adhesion substrate, which also undergoes a generic -externally applied- normal point-load. **B)** A top view of the same elements embedded in a Cartesian frame reference as described throughout the main text.

In detail, as illustrated in figure 4.2B, the cellular dipole is envisaged to be centred at the origin of the Cartesian reference system $\{x, y, z\}$, so that its two contractile forces can be written as

$$D' = D, \text{ at } -x_D, \text{ and } D'' = -D \text{ at } x_D, \quad (4.9)$$

with

$$\mathbf{D} = (\cos \theta \hat{\mathbf{e}}_x + \sin \theta \hat{\mathbf{e}}_y) D \quad \text{and} \quad \mathbf{x}_D = (\cos \theta \hat{\mathbf{e}}_x + \sin \theta \hat{\mathbf{e}}_y) l_D / 2, \quad (4.10)$$

herein D indicating the magnitude of the dipole forces, l_D the dipole's length and, finally, the angle θ its (clockwise) orientation with respect to the x -axis which will be then used as cell's optimization parameter. On the other hand, the generic external point-load perturbation \mathbf{P}_i , applied at the point \mathbf{x}_{P_i} , can be given as

$$\begin{aligned} \mathbf{P}_i &= P_i [(\sin \phi_i \cos \gamma_i) \hat{\mathbf{e}}_x + (\sin \phi_i \sin \gamma_i) \hat{\mathbf{e}}_y + (\cos \phi_i) \hat{\mathbf{e}}_z], \\ \text{with } \mathbf{x}_{P_i} &= d_i (\cos \alpha_i \hat{\mathbf{e}}_x + \sin \alpha_i \hat{\mathbf{e}}_y), \quad i \in \{1, \dots, n\}, \end{aligned} \quad (4.11)$$

where n is the number of external perturbations, ϕ_i and γ_i represent the inclinations that the force \mathbf{P}_i describes with the z -axis and the x -axis, respectively, P_i is the i -th force's magnitude, while α_i is the angle that the position vector \mathbf{x}_{P_i} —defining the point of application of the perturbative force on the half-space boundary—forms with the x -axis and d_i the related distance from the axes origin.

The energy, say W , that the cellular force-dipole spends to deform the substrate on which it adheres in presence of a system of externally applied point-load perturbations can be written as the sum of two contributions—i.e. a *self-energy* W_D and an *interaction energy* W_{int} —as follows:

$$W = W_D + W_{int}. \quad (4.12)$$

Specifically, W_{int} identifies the amount of work that the cell forces perform through the displacements produced by the external perturbations and—by virtue of the Betti's theorem [225]—it reads as

$$W_{int} = \mathbf{D} \cdot \sum_{i=1}^n [\mathbf{u}_{P_i}(-\mathbf{x}_D) - \mathbf{u}_{P_i}(\mathbf{x}_D)] = \sum_{i=1}^n \mathbf{P}_i \cdot [\mathbf{u}_{D'}(\mathbf{x}_{P_i}) + \mathbf{u}_{D''}(\mathbf{x}_{P_i})], \quad (4.13)$$

where $\mathbf{u}_{P_i}(\pm \mathbf{x}_D)$ are the displacements due to the force \mathbf{P}_i at the extremities of the cellular dipole and, *vice versa*, $\mathbf{u}_{D'}(\mathbf{x}_{P_i})$ and $\mathbf{u}_{D''}(\mathbf{x}_{P_i})$ are the ones induced by the cell forces \mathbf{D}' and \mathbf{D}'' , respectively, at the point of application of the i -th perturbation. Note that, with reference to the first expression of W_{int} in (4.13), the sole in-plane displacement components produced by the external perturbations contribute to the interaction energy, since it is assumed that the cellular tractions have negligible normal component [195].

On the other hand, W_D indicates the work aliquot that the cell does *per se* to deform the underlying medium, regardless of the action of any other force, so that one has

$$\begin{aligned} W_D &= \frac{1}{2} \mathbf{D} \cdot [\mathbf{u}_{D'}(-\mathbf{x}_D) - 2\mathbf{u}_{D'}(\mathbf{x}_D) + 2\mathbf{u}_{D''}(-\mathbf{x}_D) - \mathbf{u}_{D''}(\mathbf{x}_D)] \\ &= \mathbf{D} \cdot [\mathbf{u}_{D'}(-\mathbf{x}_D) + 2\mathbf{u}_{D''}(-\mathbf{x}_D)], \end{aligned} \quad (4.14)$$

where $\mathbf{u}_{D'}(\pm\mathbf{x}_D)$ and $\mathbf{u}_{D''}(\pm\mathbf{x}_D)$ are the displacements produced by \mathbf{D}' and \mathbf{D}'' , respectively, at the two points of adhesion of the cell. By virtue of the antisymmetrical arrangement of the dipolar forces with respect to the selected reference system and of the substrate material homogeneity, one has $\mathbf{u}_{D''}(\pm\mathbf{x}_D) = -\mathbf{u}_{D'}(\mp\mathbf{x}_D)$, whence the last equality in the equation above.

However, it is known that the intrinsic limitation of the so-called singular (or fundamental) solutions of the linear elasticity theory –basically providing the response of elastic media to point-load solicitations– is to return divergent values of the resulting displacements, strains and stresses at the point where the load acts. Therefore, in the present case, due to the adoption of the Cerruti's singular solution to calculate the displacement field produced by each of the tangential contractile forces enlightened in equations (4.9)-(4.10), it is necessary to resort to an averaging operation to evaluate –for the purpose of calculating W_D through equation (4.14)– the displacement $\mathbf{u}_{D'}(-\mathbf{x}_D)$ produced by \mathbf{D}' at its own point of application. Without loss of generality, the following rationale has been pursued.

When fundamental solutions are adopted, due to their singularity at the point of application of the load, the possibility arises that there exist regions of space where the compatibility condition, given by the positiveness of the determinant of the deformation gradient tensor, is violated, that means:

$$J := \det(\mathbf{I} + \mathbf{u} \otimes \nabla) \simeq 1 + \nabla \cdot \mathbf{u} \leq 0. \quad (4.15)$$

With regard to the Cerruti's problem, the spatial domain in which the solution provided in equation (4.8) turns out to be inconsistent can be identified as follows

$$J_C := 1 + \nabla \cdot \mathbf{u}_C \leq 0 \quad \Leftrightarrow \quad \frac{F_x X + F_y Y}{\rho^3} \geq \frac{2\pi\mu}{1-2\nu}. \quad (4.16)$$

It can be shown that the radius of the smallest circular region –lying on the half-space boundary $z = 0$ and centred at the point of application of

the tangential force \mathbf{F}_C – which contains the planar domain $J_C|_{z=0} \leq 0$ is given by:

$$r_C = \sqrt{\frac{|\mathbf{F}_C| (1 - 2\nu)}{2\pi\mu}}. \quad (4.17)$$

This quantity assumes its maximum value when $\nu = -1/4$ and, in such case, its variability depends on the sole ratio between the magnitude of the applied force and the stiffness of the medium occupying the half-space $z \geq 0$, i.e.:

$$r_C|_{\nu=-1/4} = \frac{3}{2\sqrt{2\pi}} \sqrt{\frac{|\mathbf{F}_C|}{E}}. \quad (4.18)$$

With specific reference to the problem at hand concerning a cellular dipole, by considering the average values found in literature for the traction forces exerted by cells focal adhesions, for the length exhibited by polarized cells and for the stiffness of the substrates commonly used for experimental tests [7, 77, 176, 195, 214], it is possible to estimate the largest r_C by substituting into equation (4.18) the highest value of $|\mathbf{F}_C|$ –here coinciding with D – and the lowest of E : for a fibroblast exhibiting length $l_D \approx 50\text{-}60\mu\text{m}$, by assuming $|\mathbf{F}_C| = D = 1\mu\text{N}$ and $E = 10\text{kPa}$, it results $r_C^{\text{max}} \approx l_D/10$. On this basis, the compatibility of the displacement field due to \mathbf{D}' at a point $\mathbf{x}|_{z=0}$ of the substrate boundary can be assumed as guaranteed –for any cell traction magnitude, cell length and substrate’s stiffness within the ranges of interest– if the *safety* condition $|\mathbf{x}|_{z=0} - \mathbf{x}_F| = |\mathbf{x}|_{z=0} + \mathbf{x}_D| \geq r_C^{\text{max}}$ holds true¹. Starting from these considerations, the displacement $\mathbf{u}_{D'}$ ($-\mathbf{x}_D$) is here evaluated as arithmetic average between the displacements taken at the two points placed at a distance r_C^{max} from

¹ For sake of completeness, it is noted that: (i) due to what stated above, the displacement induced at each cell extremity by the force acting at the opposite end is guaranteed to lie within the *compatible* region of space, i.e. in which $J_C > 0$; (ii) similarly, when dealing with a perturbation acting normally to the substrate surface (Boussinesq’s solution in (4.5)), one might address the issue of evaluating the minimum distance from the cell ends at which the load should be applied to overcome the model’s limitations. *De facto*, in case of normal force, this kind of problem automatically vanishes, since it can be found that

$$J_B := 1 + \nabla \cdot \mathbf{u}_B > 0 \quad \Leftrightarrow \quad \frac{F_z Z}{\rho^3} < \frac{2\pi\mu}{1 - 2\nu},$$

a condition everywhere verified on the substrate surface $Z = z = 0$ since $\lim_{Z \rightarrow 0} (F_z Z) / \rho^3 = 0 \forall \{X, Y\} \neq 0$ and the right side of the inequality is strictly positive for any admissible Poisson ratio.

the action point of the cell force \mathbf{D}' (namely $-\mathbf{x}_D$) along the direction of the dipole, identified by the orientation θ , say:

$$\mathbf{u}_{D'}(-\mathbf{x}_D) := \frac{1}{2} [\mathbf{u}_{D'}(-\mathbf{x}_D - r_C^{max} \hat{\mathbf{x}}_D) + \mathbf{u}_{D'}(-\mathbf{x}_D + r_C^{max} \hat{\mathbf{x}}_D)] = \frac{5D}{\pi\mu l_D} \hat{\mathbf{x}}_D, \quad (4.19)$$

herein the hat denoting unit vectors and the second equality resulting from solution (4.8) particularized for the case at hand.

The same solution (4.8), can be instead directly applied to calculate $\mathbf{u}_{D''}(-\mathbf{x}_D)^2$ thus providing

$$\mathbf{u}_{D''}(-\mathbf{x}_D) = -\frac{D}{2\pi\mu l_D} \left(\cos\theta \hat{\mathbf{e}}_x + \sin\theta \hat{\mathbf{e}}_y + \frac{2\nu-1}{2} \hat{\mathbf{e}}_z \right). \quad (4.20)$$

By introducing equations (4.19) and (4.20) into (4.14), the cell self-energy W_D reads as

$$W_D = \frac{4D^2}{\pi\mu l_D}, \quad (4.21)$$

that –as expected due to the isotropy of the substrate material– does not depend on the particular orientation of the dipole. This, on the contrary, will evidently not happen for the complementary contribute related to the interaction energy, whose explicit expression –deriving from equation (4.13)– will depend on the selected pattern of applied perturbations and will be, in general, a function of the angle θ .

Then, by assuming –as anticipated above– that the sole degree of freedom for the considered stationary cell-dipole is represented by a

- 2 Upon calculation of the displacements $\mathbf{u}_{D'}(-\mathbf{x}_D)$ and $\mathbf{u}_{D''}(-\mathbf{x}_D)$, it is also possible to estimate the magnitude of the deformation (contraction) ε_D that the cell undergoes due to each of the two forces of adhesion to the substrate. This is in fact given by:

$$\begin{aligned} \varepsilon_D &= 1 - \frac{\|\mathbf{x}_D + \mathbf{u}_{D'}(\mathbf{x}_D) - (-\mathbf{x}_D + \mathbf{u}_{D'}(-\mathbf{x}_D))\|}{l_D} = \\ &= 1 - \frac{\|2\mathbf{x}_D - (\mathbf{u}_{D'}(-\mathbf{x}_D) + \mathbf{u}_{D''}(-\mathbf{x}_D))\|}{l_D} = 1 - \frac{\sqrt{4(2\pi\mu l_D^2 - 9D)^2 + (1-2\nu)^2 D^2}}{4\pi\mu l_D^2}, \end{aligned}$$

that, by considering again the limit case of high cell traction force and low substrate stiffness, namely $D = 1\mu N$ and $E = 10kPa$, assumes values from 0 to ~ 0.12 for ν respectively varying from -1 (auxetic material [119]) to $1/2$ (incompressible material), with $l_D \approx 50-60\mu m$. This actually corroborates the assumption of working in a linear deformation regime in which small changes of the dipole's length –and thus approximately constant cell tractions– can be considered.

rotational reconfiguration, aimed to minimize the intensity of the energy W spent to deform the underlying substrate, the statement of the problem at hand reads as

$$\min_{\theta} |W| = \min_{\theta} |W_D + W_{int}|. \quad (4.22)$$

At this stage, it is already possible to envisage that, depending on the specific attributes of the external perturbation system (e.g. number of perturbations, importance of their magnitude with respect to the cell traction forces, distance from the cell center, etc.), there could exist either configurations in which the cell-dipole is able to arrange itself in order to exactly nullify the total energy W by exploiting advantageous orientations leading to obtain $W_{int} \equiv -W_D$ or, on the contrary, configurations such that, although not being able to wholly cancel W , the dipole orients in a way to minimize its absolute value, by properly modulating –through θ – the interaction contribute. This means that, in general, the solution to the minimization problem (4.22) can be given by the angular points of the function $|W|$, represented by

$$\tilde{\theta} : W|_{\tilde{\theta}} = 0, \quad (4.23)$$

under proper conditions and, in complementary cases, by the stationary points

$$\tilde{\theta} : (\partial_{\theta}|W|)|_{\tilde{\theta}} = 0, \quad (\partial_{\theta^2}|W|)|_{\tilde{\theta}} > 0. \quad (4.24)$$

In what follows, the effects induced on cell's orientation by selected patterns of forces acting orthogonally to the substrate boundary are studied.

4.4 CELL ORIENTATION GUIDED BY FENCES OF NORMAL POINT-LOADS

Let us consider a fence of n point-loads having equal magnitude and acting normally to the plane boundary of a semi-infinite deformable substrate at the vertexes of a regular (n -sided) polygon centred at the origin of the reference system $\{x, y, z\}$, which coincides with the midpoint of the cell-dipole. In such case, the expressions in (4.11), defining the form of the generic i -th perturbation, can be particularized by assuming:

- $P_i = P$, $d_i = d$, $\alpha_i = (i - 1)2\pi/n$, $\forall i \in \{1, \dots, n\}$;

- $\phi_i = 0$ for i indicating a downward-pointing force (i.e. compressive force pointing towards the interior of the elastic half-space) while $\phi_i = \pi$ for i indicating an upward-pointing force (i.e. tensile force), since the z -axis is directed downwards.

This hence allows to write:

$$\mathbf{P}_i = \pm P \hat{\mathbf{e}}_z, \quad \mathbf{x}_{P_i} = d \left\{ \cos \left[(i-1) \frac{2\pi}{n} \right] \hat{\mathbf{e}}_x + \sin \left[(i-1) \frac{2\pi}{n} \right] \hat{\mathbf{e}}_y \right\}, \quad (4.25)$$

with *plus* and *minus* in (4.25)₁ evidently identifying downward-pointing (compressive) and upward-pointing (tensile) forces, respectively. For sake of clarity, from now on, signs –and hence pointing directions– will be taken into account by adopting the following notation: $P_d := +P$ and $P_u := -P$.

4.4.1 Effects of concordant perturbations

By employing the Boussinesq's solution given in (4.5) for each one of the n normal point-loads here considered and by invoking the superposition principle, in the case in which such loads are either all downward-pointing or all upward-pointing, it is found that the interaction energy (4.13) can be expressed in the following general form

$$W_{int} = \frac{DP_{d,u} (1+\nu) (1-2\nu) m 2^{2-m/n} [1 - \eta^m \cos(m\theta)]}{\pi E l_D [1 + \eta^{2m} - 2\eta^m \cos(m\theta)]}, \quad (4.26)$$

with $m = \begin{cases} n & n \text{ even} \\ 2n & n \text{ odd} \end{cases}$,

where the parameter $\eta := 2d/l_D$ has been introduced. Note that the assumption $\eta > 1$ is here embraced, this meaning that any perturbation acts beyond the circular domain that the cell could potentially span during its orientation process.

By adopting expressions in (4.21) and (4.26) for the energy amounts W_D and W_{int} , respectively, the minimization problem (4.22) results to be solved either by the angular points of the total work intensity $|W|$, that are:

$$\tilde{\theta} = \pm \frac{1}{m} \left\{ \arccos \left[\frac{2^{1+m/n} (1 + \eta^{2m}) D + m (1 - 2\nu) P_{d,u}}{\eta^m (2^{2+m/n} D + m (1 - 2\nu) P_{d,u})} \right] + 2k\pi \right\},$$

$k \in \mathbb{Z}$,

$$(4.27)$$

within ranges of the perturbations' parameters η and P such that:

$$\begin{aligned} 1 \leq \eta \leq \eta_c &:= \left| 1 + \frac{2^{-(1+m/n)} m (1-2\nu) P_{d,u}}{D} \right|^{1/m}, \\ \forall P_d \text{ and } P_u &< -\frac{2^{2+m/n}}{m(1-2\nu)} D, \end{aligned} \quad (4.28)$$

or, otherwise, by the following stationary points:

$$\tilde{\theta} = \begin{cases} \frac{2k\pi}{m}, & \text{when } \mathbf{P}_i = P_d \hat{\mathbf{e}}_z \forall i \\ \frac{(1+2k)\pi}{m}, & \text{when } \mathbf{P}_i = P_u \hat{\mathbf{e}}_z \forall i \end{cases}, \quad k \in \mathbb{Z}. \quad (4.29)$$

It is worth to note that the minimum significant domain for the variable θ (and thus for the solution $\tilde{\theta}$) can be restricted to the range of values $]-\pi/2, \pi/2]$, since orientations beyond such range describe equivalent configurations, due to the symmetry of the dipole.

It is interesting that in no case the solution is influenced by the stiffness of the substrate but it always depends on the number and the direction of the perturbations. On the contrary, the substrate Poisson's ratio, the magnitude of the applied loads with respect to the cellular force and, finally, the ratio η between the radius of the polygonal fence and the dipole (semi)length turn out to drive or not the cell orientation depending on whether this is provided by the solution in (4.27) or in (4.29), respectively.

By way of example, figure 4.3 shows, in the upper plots, the change of the intensity of elastic energy spent by a dipolar cell to deform the underlying substrate depending on its orientation angle θ , in presence of a single external point-load, either upward- or downward-pointing. It is worth noting how, by increasing η –for selected properties of the substrate (therein $\nu = 1/3$) and magnitude of the perturbation with respect to the cell force (therein $P_u/D = -40$ in order to verify the relation about P_u in (4.28) and $P_d/D = 15$)– one actually switches from a condition $\eta < \eta_c$ in which $|W|$ owns a null point corresponding to its minimum (e.g. points **A1** and **B1**) to a status $\eta > \eta_c$ in which the minimum value is reached at a (non-zero) stationary point (as for points **A3** and **B3**), by passing through the limit situation $\eta = \eta_c$ where the null point coincides with a stationary one (points **A2** and **B2**). In the bottom of the same figure, the optimal cell orientation $\tilde{\theta}$, verifying the minimization problem (4.22)

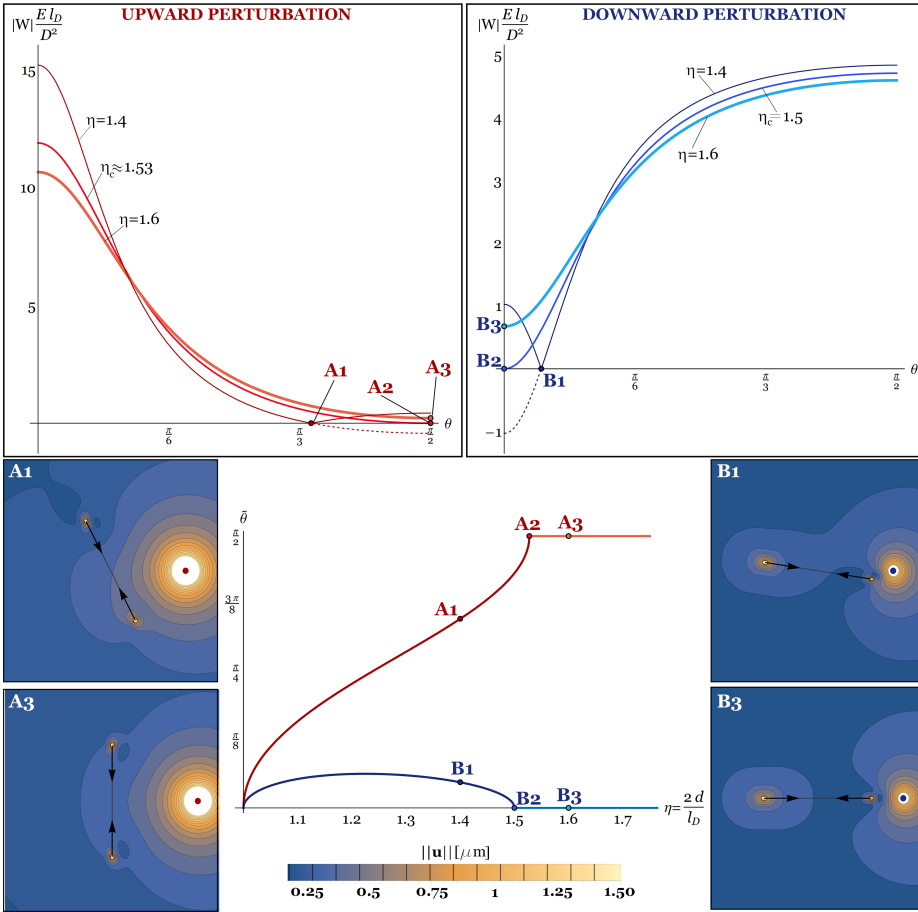


Figure 4.3: At the top, the normalized absolute value of the elastic energy spent by the cell-dipole to deform the substrate of adhesion, plotted against the orientation θ varying within the range $[0, \pi/2]$, for both the cases of upward-pointing (on the left) and downward-pointing (on the right) single perturbation. The curves have been obtained by setting $P = 40D$ for the former case while $P = 15D$ for the latter one, with $\nu = 1/3$. Moreover, different values of the distance parameter η have been considered in order to cover all the conditions $\eta \lesseqgtr \eta_c$ analyzed in the text. At the bottom, the solution $\bar{\theta}$, that minimizes the deformation energy $|W|$ when a single perturbation acts, is illustrated as function of η , through the red curve for upward-pointing load and the blue one for the complementary case. At the sides of such plot, there are focuses (top views) on the particular minimum energy configurations adopted by the cell-dipole (sketched as a couple of converging black arrows) at points **A1** and **B1** for which $\eta = 1.4 < \eta_c$ and points **A3** and **B3** characterized by $\eta = 1.6 > \eta_c$.

Figure 4.3: On the background, there are contour plots showing the intensity of the displacement field at the substrate's boundary, resulting from the interaction between the displacement amount induced by the adhering cell when optimally arranged and the one imposed by the normal perturbation (depicted as a red point if upward and as a blue one if downward). These results have been obtained by combining the values of ν , P and η mentioned above with the following ones: $D = 200nN$, $E = 50kPa$ and $l_D = 60\mu m$.

in the simplest case of single perturbation, is plotted as function of the distance parameter η , the shift from the solution in (4.27) to the one in (4.29) being evident for increasing η (points **A2** and **B2**). In particular, the solution (4.29) simplifies –in this situation of single point-load– as $\tilde{\theta} = 0$ for downward-pointing force and as $\tilde{\theta} = \pi/2$ for upward-pointing one. This means that the dipole arranges, in the former case, along a direction that contains the action point of the perturbation (placed in fact on the x -axis), while, in the latter one, in a way that such point lies –in the plane of the substrate– in the direction orthogonal to the dipole's one. Note that, since the even character exhibited by the function $|W|$ when a single normal perturbation is applied at a point of the x -axis and, hence, since the symmetry of the solution with respect to such axis, graphics in figure 4.3 are depicted by considering the restricted interval $[0, \pi/2]$ as reference domain for θ and $\tilde{\theta}$.

For a generic number n of concordant loads perturbing the cell-dipole orientation, the limitations in (4.28) allow to define –once fixed the Poisson's ratio of the substrate– regions of the P/D - η space within which the optimal cell configurations are provided by the solution in (4.27) annulling the deformation work W and out of which the dipole arranges, regardless of the substrate's and perturbations' properties, in accordance to the stationary points of $|W|$ given in (4.29). Figure 4.4 illustrates (at the center) such domains (grey-coloured) in the P/D - η plane for both upward- and downward-pointing externally applied forces, for selected $\nu = 1/3$ and $n = 1, 2, 3, 4$. As pointed out by equation (4.28), while the dipole can experience the possibility to nullify W for any ratio P/D under downward perturbations, on the contrary, it is necessary to apply forces with magnitude adequately higher than the cell's one to achieve the same result in the complementary case. Figure 4.4 shows in fact –for upward perturbations– a gap of values P/D for which the condition $\eta < \eta_c$ is never verified, whose width, by virtue of the last restriction about P_u

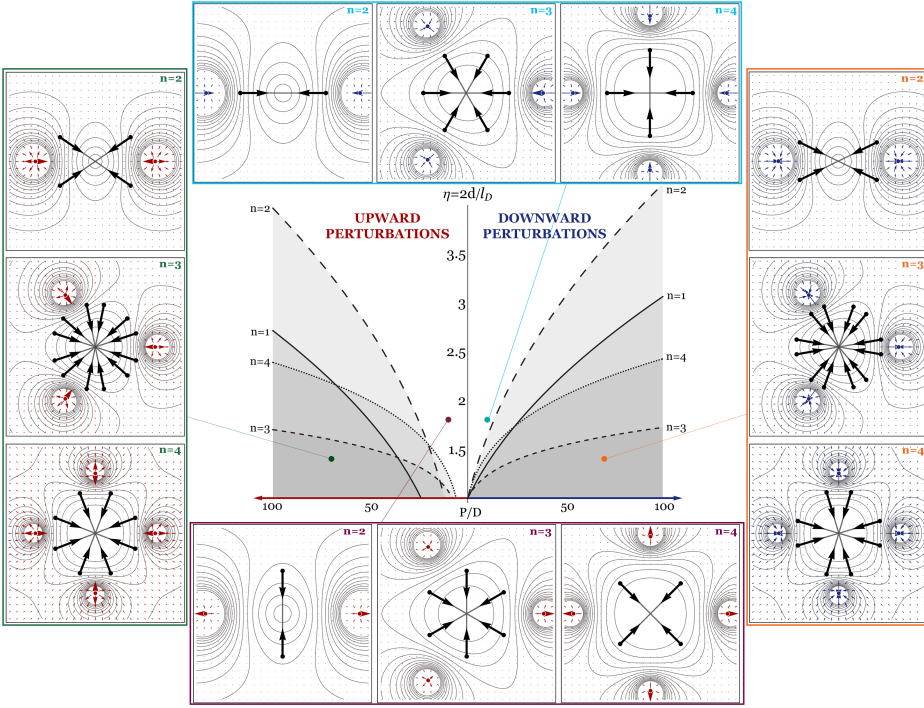


Figure 4.4: At the center, a plot illustrating, for both upward- and downward-pointing perturbations, the partition of the plane $P/D-\eta$ (whose each point identifies the properties of the n applied perturbations in terms of magnitude and distance from the dipole center) into domains (grey-coloured), defined by the limitations in equation (4.28), within which cell's optimal orientation are provided by solution in (4.27), and complementary regions where minimum deformation work configurations are given by (4.29). The size of such domains depends, in addition to the direction of the point-loads, on the substrate Poisson's ratio –here $\nu = 1/3$ – and on the specific number of perturbations –here $n = 1, 2, 3, 4$. At the four sides of the figure, there are sketches (top views) of the optimal configurations (multiple in some cases) that a cell-dipole would adopt when adhering on the top of a substrate having $\nu = 1/3$ where a fence of 2, 3 or 4 normal forces was applied. For both the possible directions of the perturbations, two pairs of parameters $P/D-\eta$ have been selected, that are $P/D = 70$ with $\eta = 1.4$ (green and orange points) and $P/D = 10$ with $\eta = 1.8$ (magenta and cyan points), in order to show all the circumstances under which the cell can be found for each considered n . In the sketches, the cell is depicted as a couple of converging black arrows, while on the background there are the level curves (grey solid lines) and the vector plot (red and blue arrows respectively for upward and downward perturbations) describing the displacement induced by the normal perturbations (represented as red points if upward and as blue ones if downward). The side plots have been obtained by also assuming $D = 200nN$, $E = 50kPa$ and $l_D = 60\mu m$.

in (4.28), is given by $2^{2+m/n} / [m(1-2\nu)]$. As an example, for both the possible directions of the perturbations, two pairs of parameters $P/D-\eta$ have been selected, that are $P/D = 70$ with $\eta = 1.4$ and $P/D = 10$ with $\eta = 1.8$, with the aim to respectively identify, for each considered n , a situation lying within the domain $\eta < \eta_c$ and a complementary one, thus showing the optimal configurations that the cell could assume in each case (see boundary plots in figure 4.4). As observed for a cell under the influence of a single perturbation, also when a greater number of loads is applied, there possibly exist multiple equivalent optimal directions –within the range $]-\pi/2, \pi/2]$ – along which the cell could indifferently align by undergoing the same energy expense. As a matter of fact, this happens since no dissipative effects are associated to the cell orientation process in the presented model and, as a consequence, the virgin direction in which the cell laid before the application of external perturbations (that, according to the substrate isotropy, should be here random) has no influence: as an example, it is envisaged that if a work quote related to drag forces was taken into account, the multiplicity of optimal configurations would disappear or, at least, would be reduced and the minimum energy solution would be conditioned by the original placement of the cell.

4.4.2 Effects of alternate perturbations

When an even number n of orthogonal perturbations is applied, it is possible to envisage patterns such that downward-pointing loads alternate with upward-pointing ones at the vertexes of the corresponding polygonal fence, their resultant being, in this way, overall zero. By employing again the superposition principle, displacement fields of the form (4.5) –particularized for each i -th perturbing normal force of which they are the result in the present context– can be combined and used into equation (4.13), thus obtaining a null interaction energy if $n/2$ is an odd number, while the following expression when $n/2$ is even too:

$$W_{int} = \frac{2PD(1+\nu)(1-2\nu)\eta^{n/2}(1-\eta^n)n\cos(n\theta/2)}{\pi El_D[1+\eta^{2n}-2\eta^n\cos(n\theta)]}. \quad (4.30)$$

Hence, in the current case of perturbations acting alternately in opposite (normal) directions with respect to the substrate's surface, by adding the interaction energy contribution to the cell's self-energy given in equation (4.21), one finds two significantly different results depending on whether n is a number multiple of 4 or not. In the latter event, since

$W_{int} \equiv 0$ and W_D does not depend on the specific orientation, as illustrated above, the cell has no possibility to exploit the presence of the strain field induced by the external fence of applied forces for reducing the work that it performs to deform the substrate, so that it could orient indifferently along any line passing through its center. On the contrary, in the complementary situation, that is $n/2$ multiple of 4, limited configurations could be helpfully adopted by the cell in order to satisfy the minimization problem (4.22). Indeed, by using the energies expressions in (4.21) and (4.30), one obtains that optimal dipole's orientations are represented by the solutions of equation (4.23), namely:

$$\tilde{\theta} = \pm \frac{2}{n} \left\{ \arccos \left[\frac{1}{32D\eta^{n/2}} ((1 - \eta^n)(1 - 2\nu) nP + \sqrt{[(1 - \eta^n)(1 - 2\nu) nP]^2 + [16D(1 + \eta^n)]^2}) \right] + 2k\pi \right\}, \quad k \in \mathbb{Z}, \quad (4.31)$$

under the following conditions concerning the perturbing forces:

$$1 \leq \eta \leq \eta_a := \left[\frac{(1 - 2\nu) nP + \sqrt{[(1 - 2\nu) nP]^2 + (8D)^2}}{8D} \right]^{2/n}, \quad \forall P \quad (4.32)$$

while, outside such domain, minimum energy placements are given by the solutions of equation (4.24), here reading as:

$$\tilde{\theta} = \frac{4k\pi}{n}, \quad k \in \mathbb{Z}. \quad (4.33)$$

Therefore, as well as for concordant perturbations, also for alternate ones (with even $n/2$), the P/D - η space can be divided into domains such that $1 \leq \eta \leq \eta_a$ (as an example, see grey-coloured regions in figure 4.5, obtained for $\nu = 1/3$ and $n = 4, 8$), whose points identify perturbations with properties allowing the cell to reach the most favourable condition $W = 0$, and outside which, on the contrary, the cell can minimize but not nullify the work spent through the deformation of the substrate. Moreover, it is worth to highlight also for the current problem, the dependence of its solution on the material and forces parameters ν , η and P/D , within the above-mentioned regions, and non-involvement of such parameters outside them, where, however, the sole n weights.

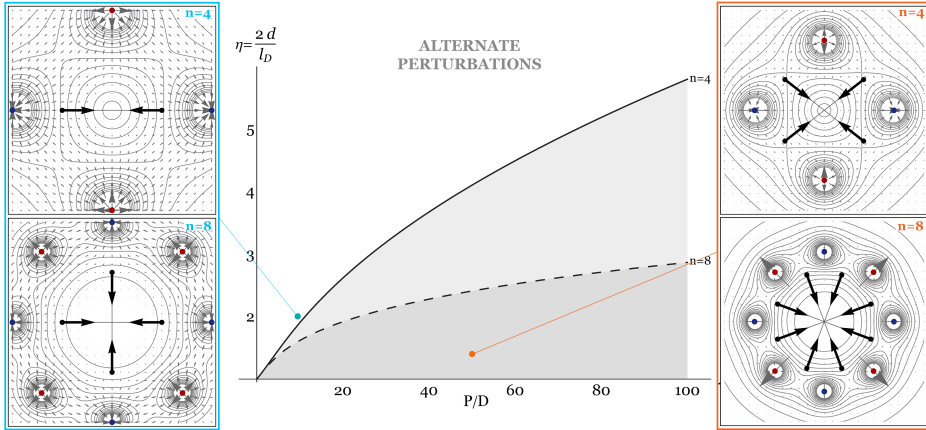


Figure 4.5: At the center, a plot illustrating, in case of perturbations with alternating directions, the partition of the plane $P/D-\eta$ into domains (grey-coloured), defined by the limitations in equation (4.32), within which cell's optimal orientations are provided by solution in (4.31), and complementary regions where minimum deformation work configurations are reached through solution (4.33). The size of such domains depends on the substrate Poisson's ratio –here $\nu = 1/3$ – and on the specific number of perturbations –here $n = 4, 8$. At the lateral sides of the figure, there are sketches (top views) of the optimal configurations (multiple in some cases) that a cell-dipole would adopt under the influence of 4 and 8 alternate perturbations when $\nu = 1/3$, $E = 50kPa$, $D = 200nN$ and $l_D = 60\mu m$, for a case in which $P/D = 50$ with $\eta = 1.4$ (orange point) and a case of $P/D = 10$ with $\eta = 2$ (cyan point), in order to fall respectively into and outside the domains described by (4.32). In the sketches, the cell is depicted as a couple of converging black arrows, while on the background there are the level curves (grey solid lines) and the vector plot (grey arrows) illustrating the displacement induced by the alternate normal perturbations (represented as red points when upward and as blue ones when downward).

4.4.3 Remarks on the cell's pursuit of the maximum elongation

It has been already highlighted above that cell's optimal orientations (4.29) and (4.33) –respectively attained in case of concordant and alternate loads directions when the substrate's and perturbations' properties are such that conditions (4.28) and (4.32) do not hold true– depend on the sole number of applied loads and, hence, on the specific polygon defining their spatial distribution. An outline of the results concerning such condition

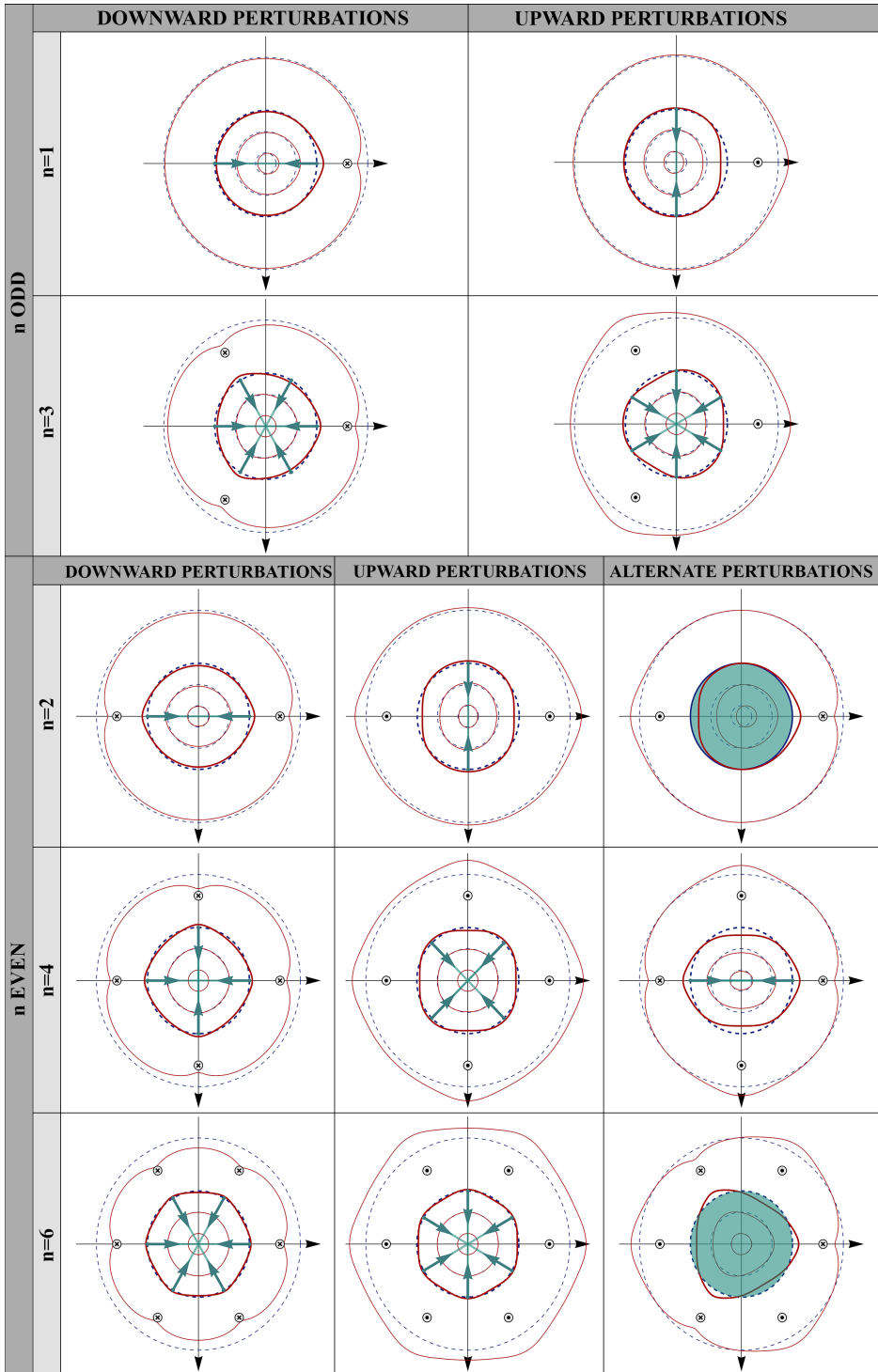


Figure 4.6: Synoptic table illustrating the cell-dipole’s optimal configurations given by the stationary points in equations (4.29) and (4.33), for concordant and alternate directions respectively, under the action of normal perturbations fences whose parameters P and η are such to fall outside the domains described by equations (4.28) and (4.32).

Figure 4.6: Here, the following values of the parameters have been setted: $\nu = 1/3$, $E = 50kPa$, $l_D = 60\mu m$, $D = 200nN$, $\eta = 1.6$ and $P = 5D$. In the upper part of the table the sole possible cases of all downward-pointing and all upward-pointing loads are shown for odd numbers of applied perturbations ($n = 1, 3$), while in the bottom part also the case of alternate loads directions is considered for even numbers of perturbations ($n = 2, 4, 6$). Top views of the dipoles are sketched through pairs of cyan converging arrows, while full cyan-coloured circles are used when there is no preferential orientation. Normal forces acting on the substrate are indicated with a cross when downward and with a circle when upward. Finally, there are shown the deformations undergone by the substrate points lying on the circumference to which the extremities of the dipole belong and on some concentric ones, due to the effect of the external perturbations. Dashed blue lines indicate circumferences in undeformed states while solid red lines their deformed configurations. To the aim of making the deformation detectable, an amplification of the displacement equal to 50 has been used.

is presented in figure 4.6, where polygonal patterns having both odd and even numbers of sides have been considered with the aim to further analyze the effects of concordant as well as alternate forces. According to what observed in presence of a single perturbation with reference to the bottom lateral sketches in figure 4.3, it is found that, for any n , the cell-dipole attains its minimum energy configurations by minimizing the distance of its direction from the points of application of downward loads and by maximizing the one from the vertexes in which upward forces act. Such behavior is explained by the fact that these orientations allow the cell to undergo the highest extension with respect to the ones achieved by all the other diametrical fibers of the circumference containing the cell's sites of adhesion, as evidenced in figure 4.6. The reason why optimal orientations (4.29) and (4.33) coincide with directions of maximum stretch is the following. From the expressions (4.26) and (4.30) of the interaction work spent by the dipole due to the presence of external forces with concordant and alternate directions respectively, one can find that there exists at least an angle $\theta \in]-\pi/2, \pi/2]$ such that $W_{int} = 0$. This means that, by spanning the whole range, such energy undergoes necessarily both positive and negative values, hence, when added to the positive and constant quote W_D , it provides a total energy either crossing zero values (as when conditions (4.28) and (4.32) are verified) or, as in the case here considered, remaining positive for all θ . In this latter case, the

stationary points (4.29) and (4.33), that hence minimize $|W| \equiv W$ by verifying equation (4.24), due to the independence of W_D from θ , match the minima of the sole interaction energy, whose corresponding values are necessarily negative for what illustrated above. This means –according to equation (4.13)– that the change of length induced on the cell at such optimal orientations occurs in the opposite direction with respect to the dipole forces one and produces the maximum extension. These results are in agreement with previous findings revealing the tendency of a bipolar-shaped single-cell to align along the direction of an external static tensile strain/stress or pre-stretch applied to the substrate [15, 32, 34, 134, 213, 249] as well as with the prediction about the formation of cells strings over elastic media [14, 15].

It is further worth to underline the duplex effect that can be observed for cases of orthogonal perturbations applied in alternate directions, which can be considered when n is an even number. In such situation the overall resultant load is null, but there exist forces configurations which do not have any effect on the dipole orientation –i.e. when $n/2$ is odd– and others such that the cell can however detect the presence of the perturbations and take advantage of it –namely when $n/2$ is even too. In the former event, as figure 4.6 shows for $n = 2, 6$, there arise pairs of normal loads pointing towards opposite directions and placed symmetrically with respect to the dipole center, whose action is not detectable by the cell since the coupled downward and upward forces mutually balance and annihilate their effects: in this way, the dipole does not undergo changes of length –and the interaction energy is null– for any orientation θ . On the other hand, in the parallel case, as illustrated in figure 4.6 for $n = 4$, the symmetric allocation of the external loads fence provides the formation of pairs of concordant loads at diametrically opposite vertexes that reciprocally reinforce their effects, thus interfering constructively rather than destructively and in this manner allowing the cell to sense and exploit their action by selecting the most convenient orientations in terms of elastic energy.

4.5 CONCLUSION

In this chapter, the mechanotropism (i.e. the mechano-stimulated directional response) of a polarized cell adhering to the surface of a deformable substrate undergoing assigned patterns of external forces has been theoretically explored. The elongated and stationary (non-migrating) cell

–e.g. a fibroblast– has been modeled as a dipole of contractile forces transmitted to the underlying elastic medium at two discrete points of adhesion, in a way to employ superposed Cerruti’s singular solutions to describe its effect in the linear deformation regime. On the other hand, combined Boussinesq’s solutions have been used to model the action of polygonal fences of normal point-loads surrounding the cell-dipole. By formulating a minimization problem involving as objective function the work done by the cell tractions to deform the substrate because of their own presence and of the external forces perturbing effect, optimal orientations of the dipole have been found, in fully analytical way. It has been highlighted that, depending on the specific combinations of the parameters describing the substrate’s material properties (specifically, its Poisson’s ratio) and the features of the pattern of externally applied loads (namely their number, direction, distance from the cell middlepoint with respect to the cell length and magnitude with respect to the cell tractions), essentially two different types of minimum energy configurations can be attained. In detail, under proper conditions, the cell can suitably exploit the strain field induced by the neighbouring forces for nullifying the energy spent against the substrate deformation: in such a case, optimal orientations result to be a function of the same above-mentioned parameters. Furthermore, there are complementary situations in which the cell is not able to reach the most favourable status of zero deformation work for any orientation, but can only align along preferential directions that however minimize the intensity of such work. In this latter case, it has been found that optimal solutions depend exclusively on the number and on the pointing directions of the perturbations and that, moreover, they equate the minima of the sole interaction energy’s contribute, thus also coinciding with the angles that provide the maximum extension for the cell.

These results suggest that, in principle, it would be possible to study the physical rules driving the orientation of single-cells adhering to deformable substrates through the application of *ad hoc* designed patterns of normal concentrated forces, by modulating a few number of parameters. On this basis, it is felt that the investigated approach could represent the starting point towards a powerful strategy for conceiving novel experimental set-up in which, once defined the material properties of the adhesion medium (both in terms of stiffness, which contributes to promote a sufficiently fiber-shaped arrangement of the cell, and of Poisson’s ratio, which participates to determine the optimal solutions), the cell’s orientation can be guided and thus examined by applying a properly se-

lected polygonal fence of normal point-loads. The quite simple feasibility of this method, related to the fact that it does not need neither the use of substrates with customized microstructures [132] nor the recourse to dynamics stimulations, allows to trace a potential way –to be hereafter more deeply explored– to gain new insights into the mechanics at the basis of the cellular arrangement and organization mechanisms and to then investigate the processes of wound healing, tissues morphogenesis and remodeling, which could find applications in regenerative medicine and tissue engineering.

TOWARD MULTISCALE CYTOMECHANICS VIA STRUCTURED DEFORMATIONS

Living cells are highly heterogeneous systems whose behavior derives from the mechanical and biochemical interaction of their constituents across multiple and hierarchical scales [103, 181, 252]. As a matter of fact, from the mechanical point of view, the cytoskeleton has been recognized as the architectural scaffold of the cell, physically interconnecting all the sub-cellular elements and thus guaranteeing coordination and continuous distribution of stress and deformation among them, namely from the plasma membrane to all the organelles within the cytosol, including the nucleus [106, 210, 239]. Also, the cytoskeletal network is itself the result of the assembly of thousands of individual as well as bundled macromolecular biofilaments, mainly actin filaments, interconnected by a variety of protein cross-linkers and mechanically acting in a coordinated manner [252]. As a consequence, the global mechanical properties and response of the single-cell emerge from the microstructural cooperation among all the heterogeneous sub-cellular components, each possessing specific mechanical features often related to their biological functions.

As highlighted in the previous chapters, this leads to the possibility to model the cell mechanics by following a variety of approaches and by focusing on different length scales [131, 147, 197]. Thus, in the chapter 4, with the aim of investigating single-cell optimal orientations upon adhesion over an elastic substrate under prescribed external forces, an highly elongated cell has been macroscopically depicted as a stretched one-dimensional fiber acting as a contractile force-dipole with length and magnitude selected in accordance with experimental data from the literature. Therefore, at this level, any constitutive relationship correlating the force level born by the cell and transmitted to the substrate with its actual length and stretch level, has been neglected. On the other hand, by following a microstructural (discrete) approach, in the chapter 3, the overall cell has been identified with its cytoskeletal network and thus modelled as a 30-element tensegrity unit whose cables and struts take the role of actomyosin filaments and microtubules, respectively. There, with the purpose of taking into account the nonlinear stress-strain relationships and the buckling responses that the cytoskeletal constituents

exhibit while bearing forces, the tensegrity elements have been described by adopting hyperelastic models and by including possible instability phenomena.

In this regard, it is however worth to underline that the (nonlinear) mechanical behavior of individual, bundled as well as networked biopolymeric (cytoskeletal) filaments [42, 74, 136] is in turn the result of structural mechanisms occurring at even lower length scales [178, 227, 252]. Therefore, understanding and faithfully involving the physics of such filament materials is critical for reaching a complete and integrated knowledge of the cell behavior at multiple scales. On these bases, particular attention has been paid in literature to the derivation of constitutive models for actin filaments, from single microfilaments to networks with cross-linkers and actin-associated proteins, by starting from their macromolecular structure [73, 178, 252, 253] and by adopting several theoretical approaches, as exemplified in figure 5.1 (e.g. molecular dynamics simulations [252], coarse-grained and continuum dynamics [253], statistical approaches [178], energetic models [178, 227, 228], tensegrity-based descriptions [141]). Actually, the thermodynamics of actin microfilaments, as in general of most protein materials, is the result of complex evolutions of their 'semicrystalline' multi-domain microstructures, which consist in chains of flexible protein macromolecules reinforced by strong and stiff crystals in the form of folded modules (each typically a few *nm* in size). When subjected to mechanical loading conditions, these protein chains undergo hard-soft transitions, due to the unravelling of the hard folded domains into soft unfolded ones, and thus globally exhibit typical nonlinear force-extension profiles [178, 228].

In this framework, the need arises for the development of multiscale models able to properly describe and explain the complex mechanical behavior of the living cell unit by effectively analyzing how its macroscopic response results from the material behavior at the meso-, micro- and nano-scales. Moreover, an analogous necessity could be certainly extended to higher length scales involving the modelling of cell clusters (e.g. solid tumour masses) or whole tissues, if one would take into account mechanobiological interactions at the cell-cell and cells-ECM levels [69, 117].

As well known, classic continuum mechanics represents a standard and consolidated instrument to describe the macroscopic response of a wide class of materials under several loading conditions [37, 67]. However, its basic assumption of uniform material distribution, stress and strain fields within an infinitesimal neighborhood of each material point,

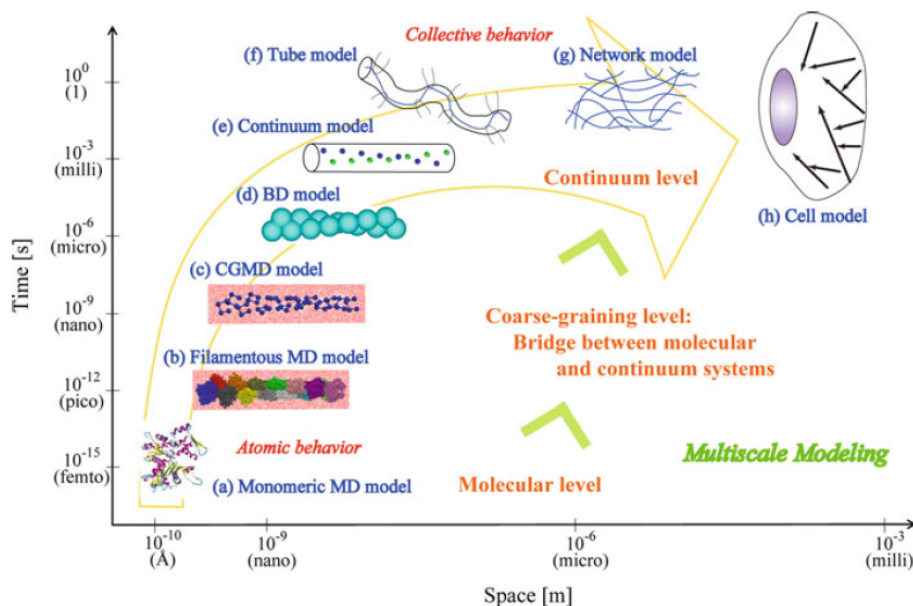


Figure 5.1: A schematic representation of various temporal and spatial scales of actin filament structures, in which some related modelling approaches adopted in literature are highlighted. Molecular dynamics (MD) approach is applied to the investigation of mechanical behaviors at the atomic scale, while continuum dynamics is invoked to investigate the collective behaviors of filaments. Many coarse-grained models (CG) and Brownian dynamics (BD) methods are instead proposed as techniques bridging between molecular and continuum systems. The image is reproduced from [252].

by definition, makes it inadequate for special cases in which material heterogeneities at the microscale, defects and/or effects of underlying microstructures, influence the overall response of the media and hence need to be somehow projected at the macroscopic level. Therefore, in recent years, many scientific efforts have been done to extend methods of nonlinear continuum mechanics with the aim to introduce multiscale analyses required for the description of the complex behavior of many biological materials [69, 227], as well as for the design of new bio-inspired materials [60]. This has brought an intense impulse in the development of homogenization techniques, deducing macroscopic constitutive laws starting from the meso-/microscopic material properties. By following analytical approaches or heuristic methods, homogenization theory [154] is in fact generally invoked to obtain functional relationships among overall contin-

uum fields of interest (i.e. macro-stress, macro-strain and elastic moduli) and microstructural parameters and properties of micro-constituents of the so-called representative volume elements. Nevertheless, standard homogenization theories sometimes do not allow to take into account some key correlation among kinematics that the biological matter undergoes at different scales, due to its hierarchical architectures.

A possible way to describe the macroscopic results of microstructural kinematics in complex continua is to adopt the theory of Structured Deformations (SDs) [44, 47–49, 52, 159]. This represents a field theory capable of modelling the dynamical evolution of nonlinear bodies that undergo *smooth* large deformations at the macroscopic (continuum) scale while can experience *piecewise-smooth* deformations at sub-macroscopic (discrete) levels, accompanied by localized *non-smooth* geometrical changes named *disarrangements*. As a consequence of these internal disarrangements, the considered bodies can not only store energy but can also dissipate it during such multiscale kinematics. By then deriving the mechanical fields of interest by means of a discrete-continuum (micro-macro) limit procedure, the SD theory *de facto* provides the formulation of an improved theory of elasticity with space-like disarrangements (such as slips or formation of voids), in which what happens at the body macroscopic scale is the result of deformations occurring at the lower level of its discrete infinitesimal constituents.

For the reasons above mentioned, it is felt that the SD theory could represent an effective tool for capturing the consequences of sub-macroscopic material structural kinematics on the macroscopic evolution of biological bodies. In particular, applied to living cells, SDs could represent a valid starting point towards the coupling of nonlinear elasticity, growth and remodeling phenomena [27, 69, 140, 152] with the additional advantage to eventually involve effects across the scales.

In order to introduce a first simple applicative example of the SD theory, the present chapter provides a first paradigm of SD-based one-dimensional (1D) mechanical model, conceived for laying the foundations on which to work for developing more complex and faithful models in the perspective of biomechanical applications. The system incorporates kinematics with disarrangements, defects, compressive and tensile buckling mechanisms [254] at the local level, which finally result in a hyperelastic (reversible) behavior, which can be properly modulated by prescribed microstructural parameters. It is in this way demonstrated that, with the sole weapon of few elemental degrees of freedom, instability phenomena and several nonlinear elastic laws, commonly observed at the macro-

scopic level in living systems, can be all obtained –in analytical way– as a result of ruling mechanisms concealed at lower scales.

5.1 FUNDAMENTALS OF STRUCTURED DEFORMATION THEORY

In the present section, essential concepts and equations of the SD theory are recalled with the aim of facilitating the comprehension of the analyses addressed in this chapter. For a detailed discussion about the SDs, the reader is referred to the works by G. Del Piero and D.R. Owen reported in bibliography [44, 45, 51, 158–160].

5.1.1 Definition of structured deformation

A (first order) SD [44, 45] of a body occupying a region \mathcal{A} of an Euclidean space \mathcal{E} with translation space \mathcal{V} is defined by the pair (\mathbf{g}, \mathbf{G}) of (sufficiently) smooth fields $\mathbf{g} : \mathcal{A} \rightarrow \mathcal{E}$, which represents the *macroscopic deformation*, and $\mathbf{G} : \mathcal{A} \rightarrow \text{Lin}\mathcal{V}$, named *deformation without disarrangements*, as it would coincide with the gradient of \mathbf{g} if no disarrangements occurred. In the hypothesis that the vector mapping \mathbf{g} is injective and that it and the tensor field \mathbf{G} satisfy the condition –known as accommodation inequality– that there exists a positive number m such that

$$m < \det \mathbf{G}(\mathbf{x}_0) \leq \det \nabla \mathbf{g}(\mathbf{x}_0) \quad \forall \mathbf{x}_0 \in \mathcal{A}, \quad (5.1)$$

the approximation theorem [44] assures that it is possible to find (at least) a sequence $\{\mathbf{g}_n\}$ of piecewise-smooth and injective functions –called approximating (or determining) sequences– defined on \mathcal{A} such that

$$\mathbf{g} := \lim_{n \rightarrow \infty} \mathbf{g}_n, \quad \mathbf{G} := \lim_{n \rightarrow \infty} \nabla \mathbf{g}_n, \quad (5.2)$$

in the sense of uniform convergence, L^∞ , where $\nabla(\bullet) = \partial(\bullet)/\partial \mathbf{x}_0 = (\bullet) \otimes \nabla$ represents the gradient of a vector function, being ∇ the nabla operator and \otimes the dyadic product. A relaxed, L^1 , convergence has also been shown to hold, thereby proving that \mathbf{g} and \mathbf{G} are obtainable as volume averages of \mathbf{g}_n and $\nabla \mathbf{g}_n$, respectively. Thus, according to the basic principle of the SD theory, the smooth deformations detectable at the macroscopic level can be interpreted as the result of a limit operation from the submacroscopic scale. There, on the contrary, discontinuities such as slips and separations –referred to as *disarrangements*– are permitted for the determining sequences. Because the limit \mathbf{G} in (5.2)₂ does not need to

represent the gradient of any deformation and, hence, it differs from the classic gradient of the macroscopic deformation \mathbf{g} in (5.2)₁, the tensor

$$\mathbf{M} := \nabla \mathbf{g} - \mathbf{G} \quad (5.3)$$

is introduced to account for the deformation amount relative to disarrangements, accordingly named *deformation due to disarrangements* or disarrangements tensor. It is worth noting that a very revealing identification relation is available for such tensor in terms of the discontinuities $\llbracket \mathbf{g}_n \rrbracket$ of the determining sequences introduced above, namely

$$\mathbf{M} = \lim_{\delta \rightarrow 0} \lim_{n \rightarrow \infty} \frac{1}{\text{vol} \mathcal{B}(\mathbf{x}_0; \delta)} \int_{\Gamma(\mathbf{g}_n) \cap \mathcal{B}(\mathbf{x}_0; \delta)} \llbracket \mathbf{g}_n \rrbracket(\mathbf{y}_0) \otimes \boldsymbol{\nu}(\mathbf{y}_0) \, dA_{\mathbf{y}_0}, \quad (5.4)$$

where $\mathcal{B}(\mathbf{x}_0; \delta)$ is a fixed ball of radius δ centered at $\mathbf{x}_0 \in \mathcal{A}$, $\boldsymbol{\nu}(\mathbf{y}_0)$ is the unit normal to the jump set $\Gamma(\mathbf{g}_n)$ at a point $\mathbf{y}_0 \in \Gamma(\mathbf{g}_n)$, while $\text{vol} \mathcal{B}(\mathbf{x}_0; \delta)$ is the volume of the ball previously introduced. The fact that here *first order* disarrangements as averages of jumps on the approximating functions \mathbf{g}_n are considered, while possible measures of the jumps on the gradients of such functions are not introduced in the analysis of the geometry of the continuum, allows to identify the pair (\mathbf{g}, \mathbf{G}) as *first order SD*.

5.1.2 Factorization of a structured deformation

Two (first order) SDs can be composed to give a third SD of the same kind according to the following rule [44]:

$$(\tilde{\mathbf{g}}, \tilde{\mathbf{G}}) \circ (\mathbf{g}, \mathbf{G}) := (\tilde{\mathbf{g}} \circ \mathbf{g}, (\tilde{\mathbf{G}} \circ \mathbf{g})\mathbf{G}), \quad (5.5)$$

where \circ denotes the operation of composition. From this definition, it follows that any SD (\mathbf{g}, \mathbf{G}) can be factorized as

$$(\mathbf{g}, \mathbf{G}) = (\mathbf{g}, \nabla \mathbf{g}) \circ (\mathbf{i}, \mathbf{K}), \quad (5.6)$$

with $\mathbf{i}(\mathbf{x}_0) := \mathbf{x}_0$ representing the identity mapping and $\mathbf{K} := (\nabla \mathbf{g})^{-1} \mathbf{G}$, for all $\mathbf{x}_0 \in \mathcal{A}$. This means that any given (first order) SD can be obtained as the succession of a purely sub-macroscopic SD, namely (\mathbf{i}, \mathbf{K}) , that maps the body from the *virgin* to the *reference configuration*, and a classic (purely macroscopic) deformation, namely $(\mathbf{g}, \nabla \mathbf{g})$, that maps the body from the *reference* to the *deformed configuration* (see figure 5.2). Therefore, a further –virgin– configuration is needed to be added to the well known

reference and deformed ones of the classic continuum mechanics, in order to take into account the distinction between the body before and after a deformation at the sub-macroscopic scale, not detectable macroscopically. An equivalent factorization reading as

$$(\mathbf{g}, \mathbf{G}) = (\mathbf{i}, \mathbf{H}) \circ (\mathbf{g}, \nabla \mathbf{g}), \quad (5.7)$$

being $\mathbf{H} := (\mathbf{G}(\nabla \mathbf{g})^{-1}) \circ \mathbf{g}^{-1}$, can be further performed, which allows to interpret the general (first order) SD (\mathbf{g}, \mathbf{G}) as the composition of a classic deformation, again $(\mathbf{g}, \nabla \mathbf{g})$, that maps the body from the virgin configuration to the *deformed configuration without disarrangements*, and a purely sub-macroscopic deformation, namely (\mathbf{i}, \mathbf{H}) , that maps the body from the deformed configuration without disarrangements to the deformed configuration (see figure 5.2). In observance of the condition (5.1), it follows that $0 < \det \mathbf{K} = \det \mathbf{H} \leq 1$.

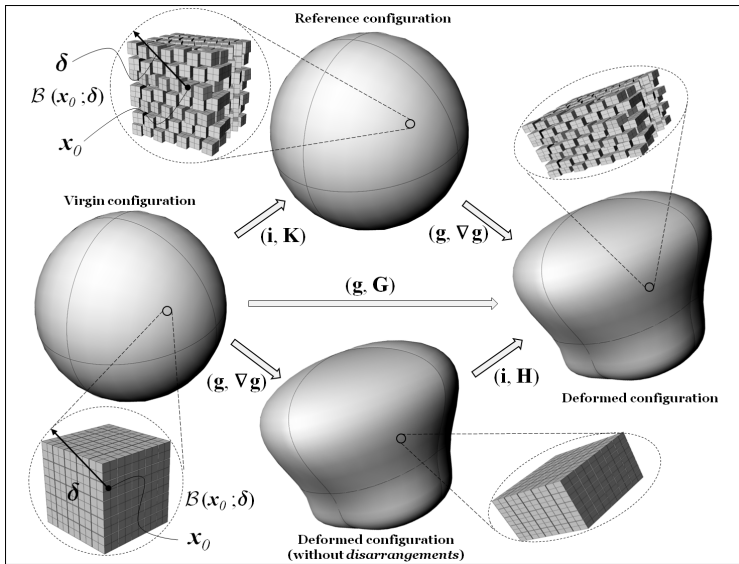


Figure 5.2: Sketch of the kinematics of a SD decomposed according its two possible factorizations (5.6) and (5.7).

5.1.3 Decomposition of stresses and constitutive assumptions

Balance laws (of forces and momenta) for a body undergoing a (first order) SD can be written in terms of a proper stress measure. The factorization (5.6) and the addition of the virgin configuration require a

refinement of such laws in order to take into account the presence of non-classical deformations. Specifically, the refined balance of forces expressed with reference to the virgin configuration reads as follows:

$$\nabla \cdot (\mathbf{S}\mathbf{K}^*) - \mathbf{S}\nabla \cdot \mathbf{K}^* + \nabla \mathbf{S} [(\det \mathbf{K}) \mathbf{I} - \mathbf{K}^*] + \mathbf{b}_v = \mathbf{0}, \quad (5.8)$$

where \mathbf{S} is the traditional first Piola-Kirchhoff stress tensor, $\mathbf{K}^* := (\det \mathbf{K}) \mathbf{K}^{-T}$ is the adjugate of \mathbf{K} and $\mathbf{b}_v := (\det \mathbf{K}) \mathbf{b}_r$ is the body force per unit volume in the virgin configuration, being \mathbf{b}_r the one in the reference configuration. By virtue of the identification [45, 158, 159] of the term $\nabla \cdot (\mathbf{S}\mathbf{K}^*)$ with the volume density of total contact forces without disarrangements and of the term $-\mathbf{S}\nabla \cdot \mathbf{K}^* + \nabla \mathbf{S} [(\det \mathbf{K}) \mathbf{I} - \mathbf{K}^*]$ with the volume density of total contact forces due to disarrangements, the quantity

$$\mathbf{S}_\setminus := \mathbf{S}\mathbf{K}^*, \quad (5.9)$$

that can be also interpreted as the stress relative to the virgin configuration, is defined as *stress without disarrangements*, while

$$\mathbf{S}_d := (\det \mathbf{K}) \mathbf{S} - \mathbf{S}_\setminus \quad (5.10)$$

is named *stress due to disarrangements*. The resulting additive decomposition of the stress:

$$(\det \mathbf{K}) \mathbf{S} = \mathbf{S}_\setminus + \mathbf{S}_d \quad (5.11)$$

has been proved to be unique and universal [53] and provides that the two amounts of stress $-\mathbf{S}_\setminus$ and \mathbf{S}_d are related through the *consistency relation*

$$\mathbf{S}_\setminus (\mathbf{K}^T - \mathbf{I}) = \mathbf{S}_d, \quad (5.12)$$

where \mathbf{I} represents the second-order identity tensor.

By taking into account that the SD theory permits energy to be stored by means of both smooth and non-smooth sub-macroscopic geometrical changes, a free energy function can be assigned as dependent on a pair formed by any combination of kinematic tensors chosen among \mathbf{G} , \mathbf{M} and $\nabla \mathbf{g}$ [51]. From an operational point of view, as pointed out in detail in [51] and [160], there are essentially two possible ways to analyze undergoing SDs within a body. A first one is to select a constitutive class, by prescribing constitutive equations for the stresses \mathbf{S}_\setminus and \mathbf{S}_d based on

a chosen free energy, then using the relation (5.12) to restrict the class of admissible processes for the system. A second way is instead to select a constitutive class by directly introducing a stress-strain law involving the total (Piola-Kirchhoff) stress \mathbf{S} , again based on a chosen free energy, and calculate \mathbf{S}_\setminus and \mathbf{S}_d through the definitions (5.9) and (5.10), respectively. This way to proceed does not put any restriction on the kinematical processes and identically verifies the consistency relation (5.12).

As an illustration of the first procedure, by writing the free energy in the form $\Psi(\mathbf{G}, \mathbf{M})$, the following constitutive assumptions can be made:

$$\mathbf{S}_\setminus = (\det \mathbf{K}) D_{\mathbf{G}} \Psi(\mathbf{G}, \mathbf{M}), \quad (5.13)$$

$$\mathbf{S}_d = (\det \mathbf{K}) D_{\mathbf{M}} \Psi(\mathbf{G}, \mathbf{M}), \quad (5.14)$$

where $D_{\mathbf{G}}$ and $D_{\mathbf{M}}$ indicate the partial derivatives with respect to \mathbf{G} and \mathbf{M} , respectively. The choice of the constitutive relations (5.13) and (5.14) reflects the identification of the stresses \mathbf{S}_\setminus and \mathbf{S}_d as "driving tractions" associated to the tensors of the deformation without disarrangements and of the deformation due to disarrangements, respectively. By referring to the literature for an extensive discussion ([49], [51]), it is here important to recall that the constitutive relations (5.13) and (5.14) provide, by substitution into (5.11), the total stress \mathbf{S} in the following form:

$$\mathbf{S} = D_{\mathbf{G}} \Psi(\mathbf{G}, \mathbf{M}) + D_{\mathbf{M}} \Psi(\mathbf{G}, \mathbf{M}). \quad (5.15)$$

This form clearly highlights that the free energy is *de facto* a generalized potential of the stress, as one would expect for a generalized hyperelastic material; in absence of disarrangements –that is when $\mathbf{M} = \mathbf{0}$, $\mathbf{K} = \mathbf{I}$ and $\mathbf{G} \equiv \nabla \mathbf{g}$ – it is immediate to see that (5.15) returns the classical equation for standard hyperelastic continua, provided that $D_{\mathbf{M}} \Psi(\mathbf{G}, \mathbf{0}) \equiv \mathbf{0}$.

As an illustration of the the second procedure, starting from the same free energy $\Psi(\mathbf{G}, \mathbf{M})$ as above, one may assume directly the constitutive relation (5.15) for \mathbf{S} and calculate from it, through equations (5.9) and (5.10), the stresses \mathbf{S}_\setminus and \mathbf{S}_d that, in general, will differ from (5.13) and (5.14). In this second procedure, the consistency relation (5.12) is identically satisfied in all motions of the body and, hence, does not provide a tensorial equation restricting the pair (\mathbf{G}, \mathbf{M}) or, equivalently, the pair $(\mathbf{G}, \nabla \mathbf{g})$. In this case, alternative restrictions can be provided through specific choices of determining sequences (e.g. see (5.33) in the examples below) and through a requirement of equilibrium at sub-macroscopic levels (e.g. see equation (5.26)).

5.2 SD-BASED PARADIGM OF AUGMENTED 1D HYPERELASTICITY

In what follows, the nonlinear elastic response of a multi-modular structure under tensile and compressive loads is analyzed, incorporating ten-

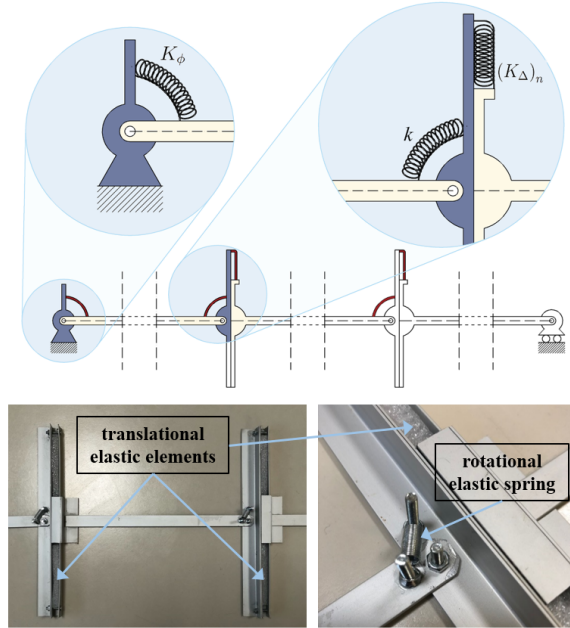


Figure 5.3: Sketch of the 1D periodic structure at the sub-macroscopic scale, with possible details of lateral hinge (at the left end of the system) equipped with a rotational elastic spring having stiffness K_ϕ and of the internal constraint able to respond both as a slider, enriched with a spring of stiffness $(K_\Delta)_n$, and as a hinge, equipped with a rotational spring of stiffness k . The pictures at the bottom show details of the actually realized multi-modular system: bars and sliders are made by standard aluminium profiles available in commerce; the hinges are endowed with elastic springs while the elastic elements of the sliders are obtained by embedding in them expanded poly-ethylene (EPE) rods.

sile and compressive buckling and possible imperfections at the discrete (micro-scale) level. The entire 1D structure results from the repetition of n units, each one comprising two rigid rods having equal lengths linked by means of a pointwise elastic constraint (see figure 5.3). At the extremities, the whole system is anchored to a hinge equipped with a

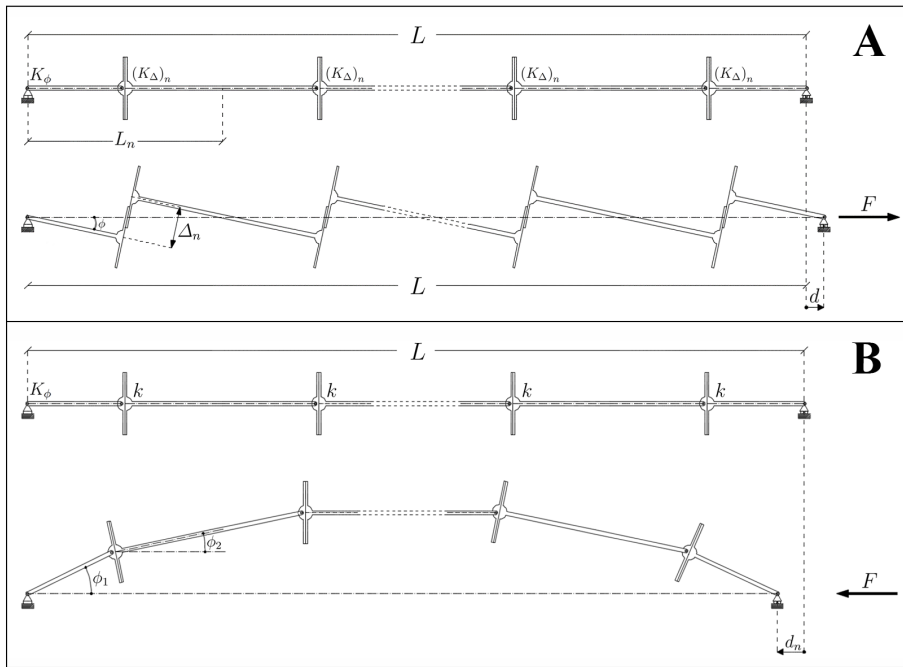


Figure 5.4: Sketch of the 1D underformed periodic structure and of its deformed configuration, observed at a sub-macroscopic scale, both under **A)** tensile and **B)** compressive dead loads. The structure, having whole length L , is made up of elemental moduli each having length L_n and consisting of two rigid rods interconnected by means of an internal constraint responding as a slider, with a spring of stiffness $(K_\Delta)_n$, under tension and as a hinge, with a rotational spring of stiffness k , under compression. A hinge –with a rotational spring of stiffness K_ϕ – and a roller bound the structure respectively at its left and right ends, the latter being the point of application of the external load F . In the deformed configuration under tensile load, Δ_n represents the sliding between the endpoints of each slider, ϕ the rotation angle and d the displacement of the left end. In the deformed configuration under compressive load, ϕ_i represents the i -th rotation angle and d_n the displacement of the left end.

rotational spring, at the left end, and by a roller on the right one, where either tensile and compressive external dead loads can be applied.

Under proper constitutive assumptions, it is found that –in case of tension (figure 5.4A)– the elastic hinges do not activate relative rotations and the intermediate constraints react only as sliders, by so replicating –as the number n of units tends to infinity and under prescribed constitutive

assumptions for the springs– the behavior of the elementary single-degree-of-freedom system presented in [254], the latter constituting the first example of structure undergoing buckling under tensile dead load. In the complementary situation, i.e. when a compressive load is applied (figure 5.4B), only the elastic hinges interconnecting the two parts of each unit are enabled to respond, the sliders remaining dormant and, as $n \rightarrow \infty$, the model giving back the classical buckled *elastica*.

In both the cases of tension and compression, reproduced through the toy system shown in figure 5.5, the deformation of the multi-modular structure is described by means of SDs, thus outlining a first 1D paradigm for this theory.

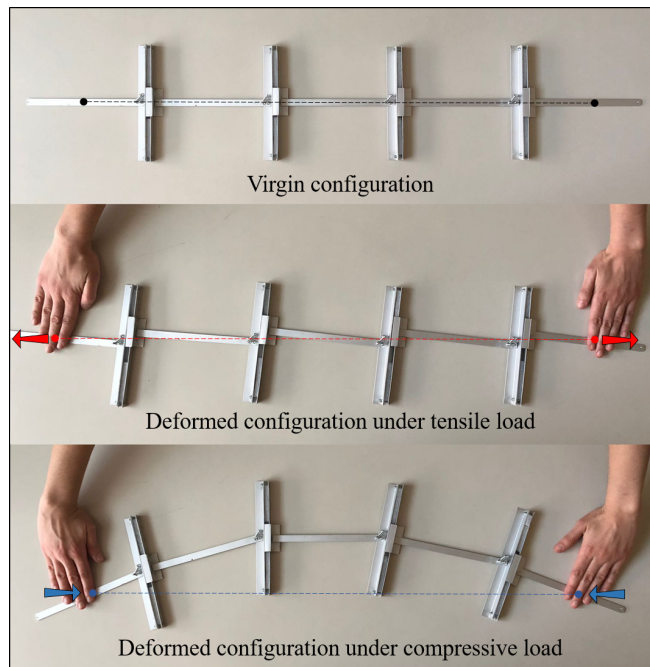


Figure 5.5: Prototype of the multi-modular structure under exam realized with aluminium bars, roughly loaded by tensile and compressive forces applied at the system ends. Note that, in both the cases, the sliders' orientations and the bars' slopes describe deformed configurations very close to those predicted by the proposed theoretical model.

5.2.1 Bifurcation modes for the elementary system

In the present subsection, the response of the structure's elemental unit (i.e. for $n = 1$), under both tensile and compressive dead loads, is briefly examined. In principle, by assuming finite value of stiffness for all the

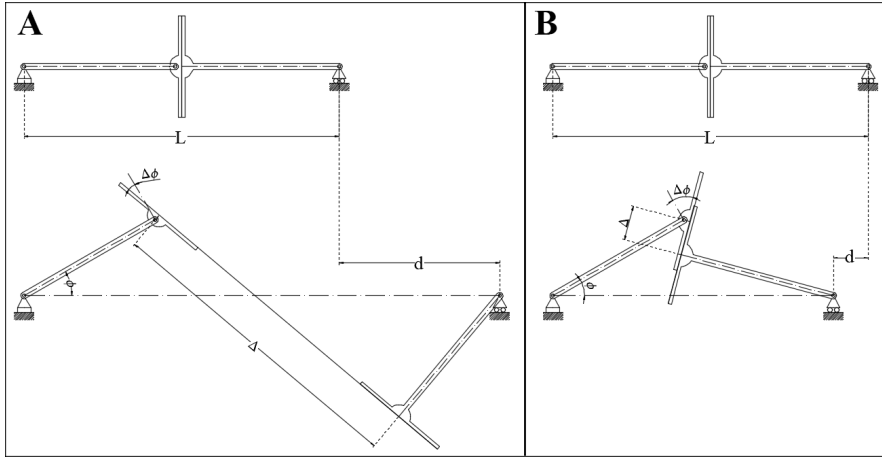


Figure 5.6: Sketch of the 1D underformed elementary (single-unit) structure and of its possible buckled configuration both under **A)** tensile and **B)** compressive dead loads.

elastic springs comprising the elementary system, a kinematics involving the contemporary opening of the slider and rotation of the central hinge would be admissible, both under traction and compression, as exemplified in figure 5.6. Therefore, by firstly considering the case of traction (see figure 5.6A), the most general expression of the internal energy U –which combines the elastic contributions of the transverse spring K_{Δ} stretching for a tract Δ , of the internal rotational spring k that rotates at an angle $\Delta\phi$ and, finally, of the lateral spring K_{ϕ} undergoing a rotation ϕ with respect to the undeformed condition– can be given as

$$U = \frac{1}{2} [K_{\phi}\phi^2 + k\Delta\phi^2 + K_{\Delta}\Delta^2], \quad (5.16)$$

$$\Delta = \frac{L}{2} [\tan(\phi + \Delta\phi) + \sin\phi \sec(\phi + \Delta\phi)],$$

L being the length of the single-unit system. Then, the total potential energy reads

$$W = U - Fd, \quad d = \frac{L}{2} [(1 + \cos\Delta\phi) \sec(\phi + \Delta\phi) - 2], \quad (5.17)$$

herein d being the displacement of the system's left end. It can be verified that the solution of the linearized equilibrium problem –standardly formulated by adopting the stationary total potential energy principle with reference to the kinematics variables ϕ and $\Delta\phi$ – provides the following linear relation between the two rotation angles in the first tract of the non-trivial post-buckling path (i.e. for small rotations ϕ and $\Delta\phi$):

$$\Delta\phi = \frac{\phi}{8k} \left\{ -4k + 2K_\phi + K_\Delta L^2 + \left[4 \left(4k^2 + 12kK_\phi + K_\phi^2 \right) + 4K_\Delta (6k + K_\phi) L^2 + K_\Delta^2 L^4 \right]^{1/2} \right\} \quad (5.18)$$

and a critical tensile load reading as

$$F_{cr} = \frac{1}{4L} \left\{ -4k - 2K_\phi + K_\Delta L^2 + \left[4 \left(4k^2 + 12kK_\phi + K_\phi^2 \right) + 4K_\Delta (6k + K_\phi) L^2 + K_\Delta^2 L^4 \right]^{1/2} \right\}. \quad (5.19)$$

An analogous procedure can be followed to study the buckling of the elementary structure under compression. In this case, the general expressions (5.16)₁ and (5.17)₁ for the internal and total potential energy, respectively, can be adopted with reference to the possible kinematics depicted in figure 5.6B, by writing

$$\Delta = \frac{L}{2} \sec(\Delta\phi - \phi) [\sin(\Delta\phi - \phi) - \sin\phi] \quad (5.20)$$

and

$$d = L \left[1 - \cos\left(\frac{\Delta\phi}{2}\right) \cos\left(\frac{3}{2}\Delta\phi - 2\phi\right) \sec(\Delta\phi - \phi) \right]. \quad (5.21)$$

By solving the linearized equilibrium problem, one again finds a linear law relating the two rotations in the first bifurcation mode, that is

$$\Delta\phi = \frac{\phi}{2(8k - K_\Delta L^2)} \left\{ 3(4k - 2K_\phi - K_\Delta L^2) - \left[4 \left(36k^2 + 28kK_\phi + 9K_\phi^2 \right) + 4K_\Delta (K_\phi - 2k) L^2 + K_\Delta^2 L^4 \right]^{1/2} \right\}, \quad (5.22)$$

associated to the lowest compressive critical force given by

$$F_{cr} = \frac{1}{4L} \left\{ 12k + 6K_\phi + K_\Delta L^2 - \left[4 \left(36k^2 + 28kK_\phi + 9K_\phi^2 \right) + 4K_\Delta (K_\phi - 2k) L^2 + K_\Delta^2 L^4 \right]^{1/2} \right\}. \quad (5.23)$$

The above results show how the critical loads and the specific bifurcation mode depend on the concurrent participation of all the spring-components according to their elastic constants, with both Δ and $\Delta\phi$ potentially contemporary non-vanishing. However, in such general conditions, it is not possible to find closed-form solutions without reducing the equilibrium problem to the linear form, even though the simplest case of the elementary (single-unit) structure is considered. Furthermore, if the units increased, the number of independent kinematic variables would be $2n$, thus forcing to use numerical strategies. On these bases, to the aim of studying analytically the mechanical response of the proposed 1D multi-modular architecture and to then provide a description in light of the SD theory, specific relationships are here assumed among the magnitudes of the springs' elastic constants, which guarantee the onset of bifurcation modes exhibiting expedient symmetries. In particular, under the specific assumption that the internal rotational springs behave as infinitely rigid, say $k \rightarrow \infty$ with respect to the elastic constants of the other springs, the tensile loading condition yields the post-critical deformation dynamics illustrated in figure 5.4A, with the sole opening sliders and frozen hinges, thus periodically reproducing the deformation response of the elementary paradigm presented in [254] for tensile buckling. Indeed, it is possible to not hardly verify that the central hinge rotation $\Delta\phi$ in (5.18) –found for the unitary system– results vanishing for any value of the angle ϕ when making k divergent, while the displacement d in (5.17)₂, the sliders' relative sliding Δ in (5.16)₂ and the tensile critical force F_{cr} in (5.19) assuming the same expressions that can be found in the next subsection 5.2.2 –for $n = 1$ – by postulating *ab initio* the non-participation of the internal hinges to the structure's elastic response under tension. On the other hand, the hypothesis that the sliders exhibit infinite stiffness K_Δ if compared to the one of the rotational springs, provides, under compression, the bifurcation mode shown in figure 5.4B for an exemplifying multi-modular structure, in which the sole internal relative rotations take place, without any sliding. For the simplest system examined in this section, one can find that the sliders' spring extension Δ in (5.20) actually vanishes when $K_\Delta \rightarrow \infty$, while the left end displacement in (5.21), the rods relative rotation $\Delta\phi$ in (5.22) and, finally, the critical compressive load in (5.23) coincide with the ones provided in subsection 5.2.3 –where the sliders are assumed to be rigid– when considering $n = 1$.

5.2.2 Multi-modular structure under tensile load

Let us consider a structure made of any number n of modular elements undergoing tensile dead load. With reference to the bifurcation mode illustrated in figure 5.4A, provided by infinitely stiff internal rotational springs, geometrical arguments lead to the conclusion that the whole compatible kinematics is ruled by the sole rotational degree of freedom represented by the rotation ϕ . As a consequence, the internal elastic energy –that the deforming structure stores through the sliders translational springs and the lateral rotational one– is given by

$$U_n(\phi) = \frac{1}{2} [K_\phi \phi^2 + n (K_\Delta)_n \Delta_n^2], \quad (5.24)$$

where $\Delta_n = L_n \tan \phi$ is the relative sliding between the two adjacent endpoints of each slider, $L_n = L/n$ being the length of each modular element and L the length of the whole structure, K_ϕ is the stiffness of the rotational spring associated to the hinge on the left end of the structure, while $(K_\Delta)_n$ is the stiffness associated to each one of the n internal transverse springs. Then, the total potential energy, formed by the internal energy of the whole system minus the work done by the external load, can be written as follows

$$W_n(\phi) = U_n(\phi) - Fd(\phi), \quad (5.25)$$

where F is the applied tensile load and $d(\phi) = L(\sec \phi - 1)$ is the corresponding displacement at the right end, independent of the number n of constituent moduli. Consequently, by making the total potential energy stationary, the solutions of the equilibrium problem are two, say the trivial solution $\phi = 0, \forall F$, and a non-trivial one, characterized by the following expression of the force, F_n , in principle depending on the number of units n :

$$\frac{\partial W_n(\phi)}{\partial \phi} = 0 \Rightarrow F_n = \frac{K_\phi \phi \cos \phi}{L \tan \phi} + \frac{(K_\Delta)_n L}{n \cos \phi}, \quad (5.26)$$

where the first term coincides with the solution obtained for the structure in [254], while the second one is due to the presence of the intermediate transverse springs. It is worth noting that $\phi = 0$ is a bifurcation path for equilibria. Indeed, upon evaluating (5.26) as $\phi \rightarrow 0$, one immediately finds the critical value $F_{cr,n}$ of the force as

$$F_{cr,n} = \frac{K_\phi}{L} + \frac{(K_\Delta)_n L}{n}. \quad (5.27)$$

As a matter of fact, the behavior of the system strictly depends on how the stiffness $(K_\Delta)_n$ scales with the number of units n . However, it is easy to verify that –by assuming that the sliders' stiffness scales by a power law, i.e. $\propto n^p$, $p \in \mathbb{R}^+$ – internal energy and forces at the equilibrium assume finite values for $0 \leq p \leq 1$, giving divergent results as $p > 1$. Therefore, without loss of generality, we analyze the two cases in which $p = 0$ and $p = 1$. More specifically, if one assumes that the sliders' stiffness is constant with n , that is $(K_\Delta)_n = K_\Delta$, the quantities in equations (5.24), (5.26) and (5.27) depend on n and converge respectively to the energy, the force and the critical load of the structure in [254] as $n \rightarrow \infty$, since the contribution of the internal springs converges to zero, i.e.:

$$\begin{aligned}
 U^{(1)} &:= \lim_{n \rightarrow \infty} U_n^{(1)} = \lim_{n \rightarrow \infty} U_n ((K_\Delta)_n \rightarrow K_\Delta) \\
 &= \lim_{n \rightarrow \infty} \frac{1}{2} \left(K_\phi \phi^2 + \frac{K_\Delta L^2 \tan^2 \phi}{n} \right) = \frac{1}{2} K_\phi \phi^2, \\
 F^{(1)} &:= \lim_{n \rightarrow \infty} F_n^{(1)} = \lim_{n \rightarrow \infty} F_n ((K_\Delta)_n \rightarrow K_\Delta) \\
 &= \lim_{n \rightarrow \infty} \frac{K_\phi \phi \cos \phi}{L \tan \phi} + \frac{K_\Delta L}{n \cos \phi} = \frac{K_\phi \phi \cos \phi}{L \tan \phi}, \\
 F_{cr}^{(1)} &:= \lim_{n \rightarrow \infty} F_{cr,n}^{(1)} = \lim_{n \rightarrow \infty} F_{cr,n} ((K_\Delta)_n \rightarrow K_\Delta) \\
 &= \lim_{n \rightarrow \infty} \frac{K_\phi}{L} + \frac{K_\Delta L}{n} = \frac{K_\phi}{L}.
 \end{aligned} \tag{5.28}$$

Upon assuming a different scaling between $(K_\Delta)_n$ and n , say $(K_\Delta)_n = nK_\Delta$, i.e. a stiffness proportional to the number of modular units composing the structure, the quantities in equations (5.24), (5.26) and (5.27) turn out to be independent of n :

$$\begin{aligned}
 U^{(2)} &:= \lim_{n \rightarrow \infty} U_n^{(2)} = \lim_{n \rightarrow \infty} U_n ((K_\Delta)_n \rightarrow nK_\Delta) = \frac{1}{2} (K_\phi \phi^2 + K_\Delta L^2 \tan^2 \phi), \\
 F^{(2)} &:= \lim_{n \rightarrow \infty} F_n^{(2)} = \lim_{n \rightarrow \infty} F_n ((K_\Delta)_n \rightarrow nK_\Delta) = \frac{K_\phi \phi \cos \phi}{L \tan \phi} + \frac{K_\Delta L}{\cos \phi}, \\
 F_{cr}^{(2)} &:= \lim_{n \rightarrow \infty} F_{cr,n}^{(2)} = \lim_{n \rightarrow \infty} F_{cr,n} ((K_\Delta)_n \rightarrow nK_\Delta) = \frac{K_\phi}{L} + K_\Delta L.
 \end{aligned} \tag{5.29}$$

In both the cases, the response of the system depends on the relationship between the values of stiffnesses K_ϕ and K_Δ , therefore a coefficient α is suitably introduced so that $K_\Delta = \alpha K_\phi / L^2$. It is found that, while the trivial solution is always stable up to the critical load and unstable after

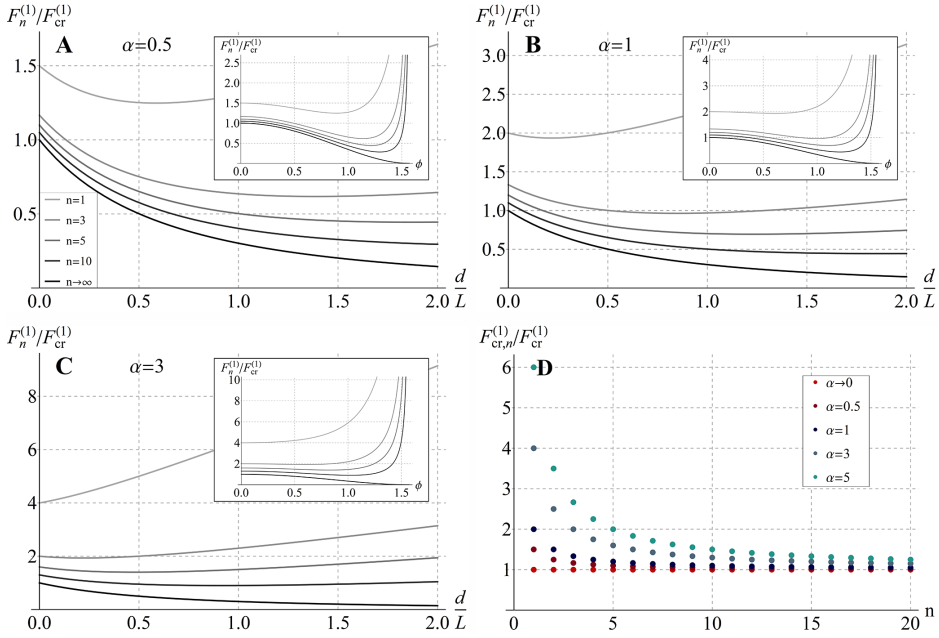


Figure 5.7: Tensile force $F_n^{(1)}$ –normalized with respect to the (limit) critical load $F_{cr}^{(1)}$ – as function of the boundary displacement normalized to the length of the whole structure d/L and of the rotation ϕ (in the insets) for increasing number of elemental moduli ($n = 1, 3, 5, 10$) up to the continuum limit $n \rightarrow \infty$, for different values of the ratio α between the translational and rotational springs stiffnesses: **A)** $\alpha = 0.5$, **B)** $\alpha = 1$ and **C)** $\alpha = 3$. **D)** Normalized tensile critical load $F_{cr,n}^{(1)}/F_{cr}^{(1)}$ as function of n , plotted for different values of α ($\alpha \rightarrow 0, \alpha = 0.5, 1, 3, 5$).

that value, the non-trivial post-critical behavior depends on α . Figure 5.7 shows the force $F_n^{(1)}$ –normalized with respect to the (limit) critical load $F_{cr}^{(1)}$ – both as function of the normalized displacement d/L (or overall engineering strain) and of the rotation angle ϕ , for different values of α and n . In particular, for the addressed case of $(K_\Delta)_n = K_\Delta$, analysis of the second derivative of the strain energy provides that the non-trivial post-bifurcation path is stable under the condition $\alpha > (5/3)n$ for any rotation angle ϕ (by way of example, see the curve obtained for $\alpha = 3$ and $n = 1$ in figure 5.7C). Otherwise, as also detectable from figures 5.7A,B,C, the system undertakes an unstable non-trivial post-critical behavior, that can reach stability at some finite deformation depending on the number of moduli n (see the rising tracts after initial softening in the insets of figure 5.7), with the exception of the limit case $n \rightarrow \infty$,

for which the structure remains unstable over the whole deformation range. An analogous behavior is found when $(K_\Delta)_n = nK_\Delta$, in this case the discriminating condition being given by $\alpha > 5/3$, as observable in figure 5.8, that shows the trend of the force $F^{(2)} \equiv F_n^{(2)}$ –again normalized with respect to the (limit) critical load $F_{cr}^{(1)}$ – as function of both the above defined normalized displacement d/L and the rotation angle ϕ , for different values of α . In figure 5.7D, the trend of the normalized critical load $F_{cr,n}^{(1)}/F_{cr}^{(1)} = (n + \alpha)/n$ as function of n , for different values of the ratio α , is also displayed, while the critical load $F_{cr}^{(2)}$ is simply given by $F_{cr}^{(2)} = (1 + \alpha)F_{cr}^{(1)}$, its expression thus coinciding with the previous case when $\alpha \rightarrow 0$.

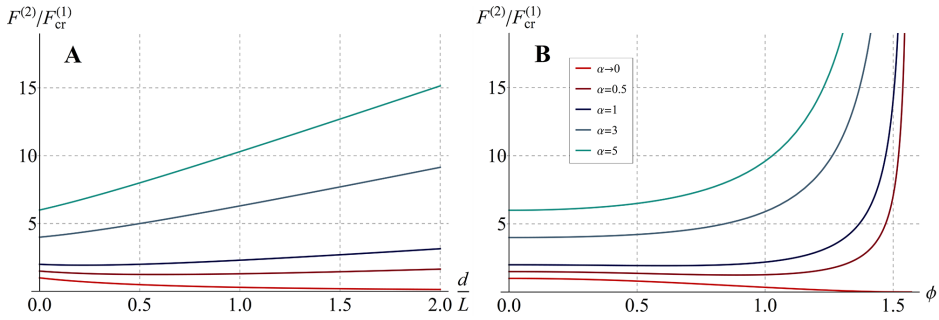


Figure 5.8: Tensile force $F^{(2)}$ –normalized with respect to the limit critical load $F_{cr}^{(1)}$ – as function **A**) of the normalized displacement d/L and **B**) of the rotation ϕ , for different values of the ratio α between the translational and rotational springs stiffnesses ($\alpha \rightarrow 0, \alpha = 0.5, 1, 3, 5$).

In analogy to what has been done in [254], it is of interest to evaluate the response of the system in the presence of an *imperfection*, i.e. a defect of the structure at the microscopic level, for instance assumed to be an initial inclination ϕ_0 of the rods. In this case, the total potential energy can be written as follows:

$$W(\phi; \phi_0) = \frac{1}{2} \left[K_\phi (\phi - \phi_0)^2 + \frac{(K_\Delta)_n L^2}{n} (\tan \phi - \tan \phi_0)^2 \right] - FL (\sec \phi - \sec \phi_0), \quad (5.30)$$

consequently giving the force-rotation equilibrium relationship as

$$F_n = \frac{K_\phi (\phi - \phi_0) \cos \phi}{L \tan \phi} + \frac{(K_\Delta)_n L}{n} \left(\frac{1}{\cos \phi} - \frac{\tan \phi_0}{\sin \phi} \right), \quad (5.31)$$

so that equations (5.28)₂ and (5.29)₂ can be now respectively replaced with:

$$F_n^{(1)} = \frac{K_\phi(\phi - \phi_0) \cos \phi}{L \tan \phi} + \frac{K_\Delta L}{n} \left(\frac{1}{\cos \phi} - \frac{\tan \phi_0}{\sin \phi} \right),$$

$$F^{(1)} := \lim_{n \rightarrow \infty} F_n^{(1)} = \frac{K_\phi(\phi - \phi_0) \cos \phi}{L \tan \phi}$$

and $F^{(2)} \equiv F_n^{(2)} = \frac{K_\phi(\phi - \phi_0) \cos \phi}{L \tan \phi} + K_\Delta L \left(\frac{1}{\cos \phi} - \frac{\tan \phi_0}{\sin \phi} \right).$

Figure 5.9 shows the normalized force $F_n^{(1)}/F_{cr}^{(1)}$ as function of the normalized displacement d/L –for the present case being $d = L(\sec \phi - \sec \phi_0)$ – and of the rotation ϕ , for different values of n and α , as well as for two initial values of the imperfection ϕ_0 . Similarly, figure 5.10 shows the trend of $F^{(2)}/F_{cr}^{(1)}$ as function of d/L and ϕ , for several α and for the same values of the initial imperfections.

5.2.2.1 SD-based formulation for tensile loads

The kinematics that the system experiences when it is subjected to tensile load, specifically in the considered non-trivial post-buckling phase (figure 5.4A), can be suitably described by means of the (first order) SD theory. In particular, the generic material point of the studied body in the virgin configuration (in which, by definition, it is neither macroscopically nor sub-macroscopically deformed) can be identified by a position vector $\mathbf{x}_0 = x_0 \hat{\mathbf{e}}_1$, with $x_0 \in [0, L]$ and $\hat{\mathbf{e}}_i$, $i \in \{1, 2\}$, indicating the unit vectors of two-dimensional Cartesian coordinate system. The approximating functions, that map each point \mathbf{x}_0 to the deformed configuration (in which the body is both macroscopically and sub-macroscopically deformed) at the sub-macroscopic scale, can be expressed as

$$\mathbf{g}_n^h(\mathbf{x}_0) = \mathbf{x}_0 + \mathbf{u}_n^h(\mathbf{x}_0), \quad (5.32)$$

where, by virtue of geometrical arguments, the displacement \mathbf{u}_n^h reads

$$\mathbf{u}_n^h(\mathbf{x}_0) = [x_0(\cos \phi - 1) + hL_n(\sec \phi - \cos \phi)] \hat{\mathbf{e}}_1 - [(x_0 - hL_n) \sin \phi] \hat{\mathbf{e}}_2,$$

$$\forall x_0 \in \left] \frac{L_n}{2}(2h - 1 + \delta(h)), \frac{L_n}{2}(2h + 1 - \delta(h - n)) \right[,$$

(5.33)

where $h \in \{0, 1, \dots, n\}$ is a translation index and $\delta(h - p)$ the Kronecker delta function taking the value 1 when $h = p$ and 0 otherwise.

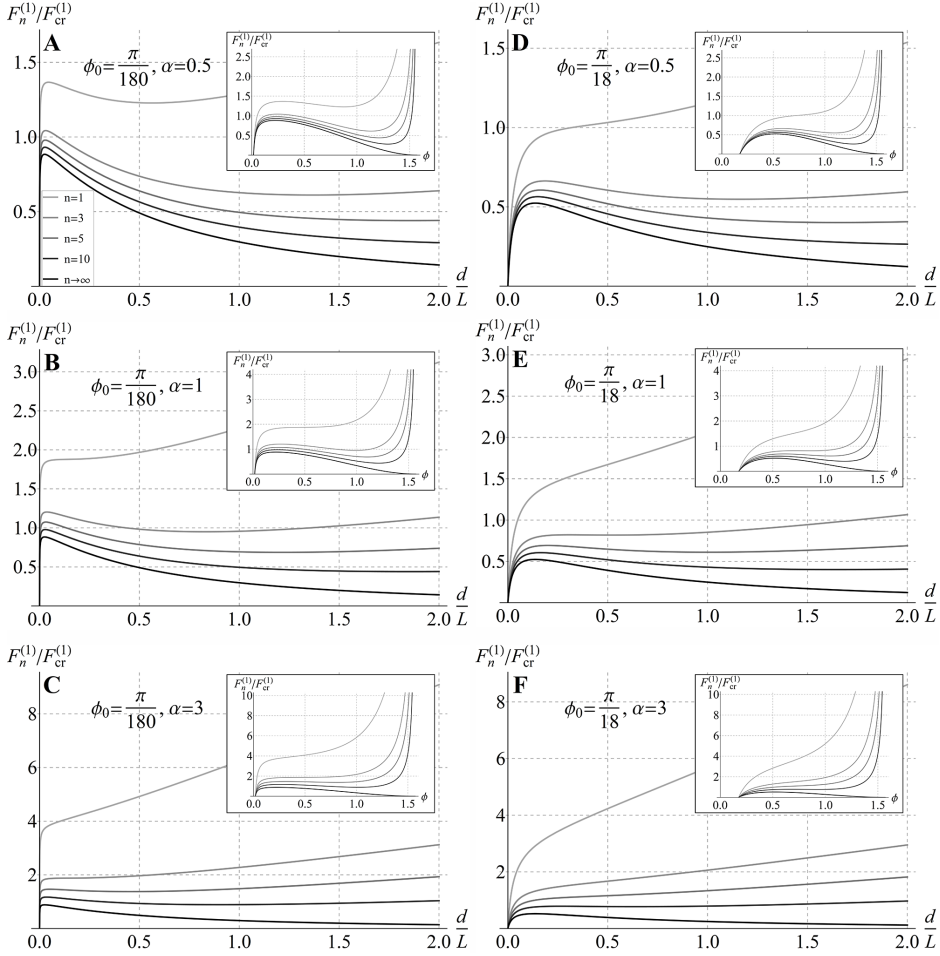


Figure 5.9: Tensile force $F_n^{(1)}$ –normalized with respect to the limit critical load $F_{cr}^{(1)}$ – against normalized displacement d/L and rotation ϕ (in the insets) for increasing number of elemental moduli composing the structure ($n = 1, 3, 5, 10$) up to the continuum limit $n \rightarrow \infty$, for different values of the imperfection ϕ_0 and of the ratio α between translational and rotational springs stiffnesses: **A**) $\phi_0 = \pi/180, \alpha = 0.5$, **B**) $\phi_0 = \pi/180, \alpha = 1$, **C**) $\phi_0 = \pi/180, \alpha = 3$, **D**) $\phi_0 = \pi/18, \alpha = 0.5$, **E**) $\phi_0 = \pi/18, \alpha = 1$, **F**) $\phi_0 = \pi/18, \alpha = 3$.

Then, the deformation gradient associated to the approximating sequence takes the form

$$\nabla \mathbf{g}_n^h = \mathbf{I} + \nabla \mathbf{u}_n^h = \cos \phi \hat{\mathbf{e}}_1 \otimes \hat{\mathbf{e}}_1 - \sin \phi \hat{\mathbf{e}}_2 \otimes \hat{\mathbf{e}}_1 + \hat{\mathbf{e}}_2 \otimes \hat{\mathbf{e}}_2 \equiv \mathbf{G}, \quad (5.34)$$

which, since not depending on n , naturally provides also the deformation without disarrangements \mathbf{G} (see equation(5.2)₂). Herein, $\mathbf{I} =$

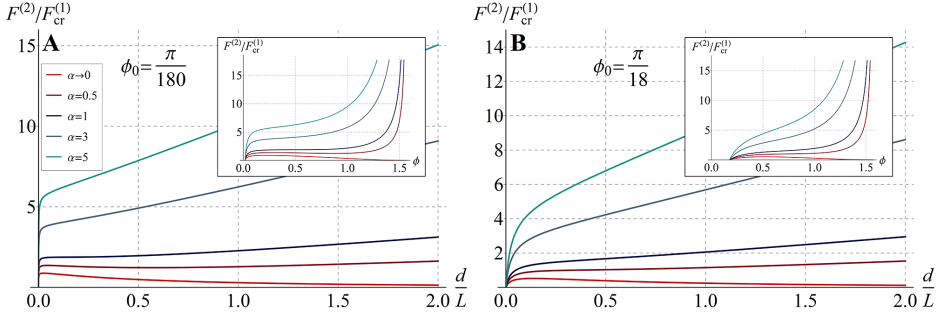


Figure 5.10: Tensile force $F^{(2)}$ –normalized with respect to the limit critical load $F_{cr}^{(1)}$ – versus normalized displacement d/L and rotation ϕ (in the insets) for different values of the ratio α between translational and rotational springs stiffnesses ($\alpha \rightarrow 0, \alpha = 0.5, 1, 3, 5$) and values of the imperfection ϕ_0 : **A**) $\phi_0 = \pi/180$ and **B**) $\phi_0 = \pi/18$.

$\hat{\mathbf{e}}_1 \otimes \hat{\mathbf{e}}_1 + \hat{\mathbf{e}}_2 \otimes \hat{\mathbf{e}}_2$ is the identity tensor. On the other hand, $\mathbf{g}_n^h(\mathbf{x}_0)$ uniformly converges to the macroscopic deformation $\mathbf{g}(\mathbf{x}_0) = \mathbf{x}_0 + \mathbf{u}(\mathbf{x}_0)$, with

$$\mathbf{u}(\mathbf{x}_0) = \lim_{n \rightarrow \infty} \mathbf{u}_n^h(\mathbf{x}_0) = (\sec \phi - 1) \mathbf{x}_0, \quad (5.35)$$

and, consequently, the related classical deformation gradient is

$$\nabla \mathbf{g} = \mathbf{I} + \nabla \mathbf{u} = \sec \phi \hat{\mathbf{e}}_1 \otimes \hat{\mathbf{e}}_1 + \hat{\mathbf{e}}_2 \otimes \hat{\mathbf{e}}_2. \quad (5.36)$$

It is worth highlighting that the tensor \mathbf{G} obtained in equation (5.34) satisfies the requirement of inextensibility of the single constituent rods –a direct consequence of the assumption of rigidity– as $|\mathbf{G}\hat{\mathbf{e}}_1| = 1$. Additionally, the result of the geometry above entails $\mathbf{G} \neq \nabla \mathbf{g}$, the studied 1D model thus revealing the presence of sub-macroscopic *disarrangements*. As a matter of fact, at the macro-scale, the non-classical nature of the deformation considered for the system under study turns out to produce a threshold-activated pure axial elongation whose magnitude is ruled by the disarrangement degree at the sub-macroscopic level (see equation (5.35)), for all the values of the angle ϕ in the range of interest $[0, \pi/2[$. The corresponding overall constitutive response can be deduced by plotting force *versus* displacement as shown in figure 5.7 for the limiting case $n \rightarrow \infty$ and in figure 5.8 as a function of the choice made about the stiffness of the internal sliders springs. Also, it has to be highlighted that –within the whole range– the fields \mathbf{g} and \mathbf{G} satisfy the so-called accommodation inequality (5.1).

The presence of disarrangements is taken into account by the disarrangements tensor, that in this case is given by

$$\mathbf{M} = \sin \phi (\tan \phi \hat{\mathbf{e}}_1 \otimes \hat{\mathbf{e}}_1 + \hat{\mathbf{e}}_2 \otimes \hat{\mathbf{e}}_1), \quad (5.37)$$

while the tensor \mathbf{K} , related to the purely sub-macroscopic deformation, takes the form

$$\mathbf{K} = \cos^2 \phi \hat{\mathbf{e}}_1 \otimes \hat{\mathbf{e}}_1 - \sin \phi \hat{\mathbf{e}}_2 \otimes \hat{\mathbf{e}}_1 + \hat{\mathbf{e}}_2 \otimes \hat{\mathbf{e}}_2. \quad (5.38)$$

Also, by exploiting the one-dimensional nature of the stress regime related to the uni-axial applied external load, the equilibrium allows one to write the first Piola-Kirchhoff stress tensor in the form

$$\mathbf{S} = \frac{F}{A} \hat{\mathbf{e}}_1 \otimes \hat{\mathbf{e}}_1, \quad (5.39)$$

where A is the transverse area of the structure in the reference configuration and F is given by $F^{(1)}$ or $F^{(2)}$, depending upon the choice made on $(K_\Delta)_n$. Thus, according to their definitions, the stress without disarrangements and the stress due to disarrangements turn out to be respectively

$$\mathbf{S}_\setminus = \frac{F}{A} (\hat{\mathbf{e}}_1 \otimes \hat{\mathbf{e}}_1 + \sin \phi \hat{\mathbf{e}}_1 \otimes \hat{\mathbf{e}}_2) \quad (5.40)$$

$$\text{and } \mathbf{S}_d = -\frac{F}{A} \sin \phi (\sin \phi \hat{\mathbf{e}}_1 \otimes \hat{\mathbf{e}}_1 + \hat{\mathbf{e}}_1 \otimes \hat{\mathbf{e}}_2). \quad (5.41)$$

Finally, from the kinematical point of view, the SD describing the deformation of the system when characterized by an imperfection ϕ_0 , namely (\mathbf{z}, \mathbf{Z}) , can be seen as the composition of two SDs according to the definition (5.5), that is:

$$(\mathbf{z}, \mathbf{Z}) = (\mathbf{g}, \mathbf{G}) \circ (\mathbf{g}_0, \mathbf{G}_0)^{-1} = (\mathbf{g} \circ \mathbf{g}_0^{-1}, \mathbf{G} \mathbf{G}_0^{-1}), \quad (5.42)$$

being, by virtue of the invertibility of the tensor \mathbf{G} in the range of interest for ϕ , $(\mathbf{g}_0, \mathbf{G}_0) = (\mathbf{g}, \mathbf{G})|_{\phi=\phi_0}$ and $(\mathbf{g}_0, \mathbf{G}_0)^{-1} = (\mathbf{g}_0^{-1}, \mathbf{G}_0^{-1})$ its inverse.

5.2.2.2 Consistency of discrete and SD-based approaches: an argument in support of augmented hyperelasticity

By regarding the multi-modular structure under study as a 1D continuum and by looking at the limiting quantities obtained through both the relations (5.28) and (5.29) for constant and proportional to n sliders'

stiffness, respectively, it appears evident that the limiting energies per unit volume (e.g. divided by the cross sectional area A of the structural arms and the overall length L of the system) are not potentials for the stress, the sole nonzero component $S_{11} = F/A$ being in fact not obtainable as derivative of the energy with respect to any standard strain measure coming from the deformation gradient. This would force one to admit that—at least within the classical framework of continua— as $n \rightarrow \infty$, the resulting 1D continuum material cannot be thought of as hyperelastic. To be convinced of the need to use SDs, the naturally arising question is then whether or not SDs give a way to find a generalized potential for \mathbf{S} , for instance in the form (5.15).

With this in mind, it is remarked that, in the case at hand, the geometry is known, namely both the macroscopic deformation (5.35) and the limit of the gradients of its approximating sequence (5.34) have been found, and, furthermore, the stress is statically determined. However, these two pieces of information do not suffice to ensure that the resulting continuum behaves as an augmented (generalized) hyperelastic material, that is the stress obeys the (5.15). To demonstrate that it is the case, one has in fact to seek a *free energy* ψ such that *i*) it is a generalized potential for the stress \mathbf{S} and *ii*) no dissipation is found for the resulting limiting material (i.e. as $n \rightarrow \infty$). With reference to the request *ii*), it is in fact worth to recall that, in general, the overall presence of disarrangements neither requires nor rules out the possibility of having *dissipation* during loading [47, 49, 52]. Nonetheless, because the underlying parent discrete systems, discussed above, do not exhibit dissipation behaving as purely elastic at the local scale, it is expected that the effective continuum and its resulting constitutive properties do not entail dissipation.

In order to establish if *i*) can be fulfilled, upon analyzing the geometrical changes described by (5.33) for the tensile case, one first can note that the discrete system undergoing an imposed axial displacement achieves its balance thanks to the change in configuration of each arm, captured through $\nabla \mathbf{g}_n^h$ in (5.34) acting on $\hat{\mathbf{e}}_1$, caused by pulling above the critical load and to the energy stored within the sliders because of the openings Δ_n arising at each of such sites due to the rotations. Somehow, in the limit $n \rightarrow \infty$, the effective continuum mimics a body whose internal fibers reorient according to what happens only in the direction $\hat{\mathbf{e}}_1$. In the limit, the features just highlighted are in fact embodied in the first invariant (i.e. the trace) of the tensors $\mathbf{G}\hat{\mathbf{e}}_1 \otimes \mathbf{G}\hat{\mathbf{e}}_1$ and $\mathbf{M}\hat{\mathbf{e}}_1 \otimes \mathbf{M}\hat{\mathbf{e}}_1$. This suggests to

represent the target effective free energy density per unit volume of the continuum limit in the form

$$\psi = \Psi(\mathbf{G}, \mathbf{M}) = \tilde{\Psi}(tr(\mathbf{G}\hat{\mathbf{e}}_1 \otimes \mathbf{G}\hat{\mathbf{e}}_1) + tr(\mathbf{M}\hat{\mathbf{e}}_1 \otimes \mathbf{M}\hat{\mathbf{e}}_1)). \quad (5.43)$$

From this assumption, by considering the forms of the tensors \mathbf{G} and \mathbf{M} given in equations (5.34) and (5.37) for the problem at hand, one can find:

$$\begin{aligned} D_{\mathbf{G}}\Psi(\mathbf{G}, \mathbf{M}) &= 2\tilde{\Psi}'\mathbf{G}\hat{\mathbf{e}}_1 \otimes \hat{\mathbf{e}}_1 = 2\tilde{\Psi}'(\cos\phi\hat{\mathbf{e}}_1 \otimes \hat{\mathbf{e}}_1 - \sin\phi\hat{\mathbf{e}}_2 \otimes \hat{\mathbf{e}}_1) \quad \text{and} \\ D_{\mathbf{M}}\Psi(\mathbf{G}, \mathbf{M}) &= 2\tilde{\Psi}'\mathbf{M}\hat{\mathbf{e}}_1 \otimes \hat{\mathbf{e}}_1 = 2\tilde{\Psi}'[(\sec\phi - \cos\phi)\hat{\mathbf{e}}_1 \otimes \hat{\mathbf{e}}_1 + \sin\phi\hat{\mathbf{e}}_2 \otimes \hat{\mathbf{e}}_1], \end{aligned} \quad (5.44)$$

that, by substitution into (5.15), provide the following expression for the first Piola-Kirchhoff tensor:

$$\mathbf{S} = 2\tilde{\Psi}'\sec\phi\hat{\mathbf{e}}_1 \otimes \hat{\mathbf{e}}_1, \quad (5.45)$$

where the apex indicates the derivative of the function with respect to its argument, here equal to $tr(\mathbf{G}\hat{\mathbf{e}}_1 \otimes \mathbf{G}\hat{\mathbf{e}}_1) + tr(\mathbf{M}\hat{\mathbf{e}}_1 \otimes \mathbf{M}\hat{\mathbf{e}}_1) = \sec^2\phi$. This Piola-Kirchhoff stress tensor, derived by proper constitutive assumptions and according to the SD theory, has to coincide with the one obtained by means of equilibrium arguments, given in equation (5.39). The imposition of this condition leads to the following differential equation for the free energy density:

$$\tilde{\Psi}' = \frac{F(\phi)}{2A}\cos\phi. \quad (5.46)$$

The integration of both the members of this equation with respect to the argument of the unknown function $\tilde{\Psi}(\sec^2\phi)$ would return a general expression for $\tilde{\Psi}$. As an example, to show the form that $\tilde{\Psi}$ could assume at equilibrium for a particular choice of the structural constitutive parameters, the case in which the stiffness of the sliders springs scale proportionally to n , i.e. $(K_{\Delta})_n = nK_{\Delta}$, is taken into account, so that the response of the system is described by the quantities in (5.29). Also, for sake of simplicity, it is assumed that no lateral rotational spring is present, namely $K_{\phi} = 0$. Under these conditions, the force at equilibrium is given by $F = K_{\Delta}L\sec\phi$, so that $\tilde{\Psi}'$ turns out to be constant with respect to its argument and the integration of (5.46) can be easily performed:

$$\tilde{\Psi}'(\sec^2\phi) = \frac{K_{\Delta}L}{2A}, \quad \tilde{\Psi}(\sec^2\phi) = \frac{K_{\Delta}L}{2A}\sec^2\phi + C. \quad (5.47)$$

The value of the constant of integration C is then found by imposing vanishing energy as rotation approaches zero, so that:

$$C = -\frac{K_{\Delta}L}{2A} \Rightarrow \tilde{\Psi} = \frac{K_{\Delta}L}{2A} \tan^2 \phi. \quad (5.48)$$

It is possible to observe that the elastic energy that one obtains by multiplying $\tilde{\Psi}$ in (5.48)₂ by the volume of the continuum body, AL , actually matches the expression of $U^{(2)}$ in (5.29)₁ written for $K_{\phi} = 0$, thus revealing the full consistency of the SDs modeling strategy with the discrete approach. It can be verified that such a conclusion is not influenced by the specific choice made about the system's parameters and can be therefore generalized to different cases. Furthermore, for seek of completeness, if interested in retrieving the stress also before it reaches its critical value, one should properly introduce a Lagrangean multiplier for taking into account the rigidity constraint due to the axial inextensibility of the structure. In the present case, this can be trivially determined from the boundary conditions. However, for a detailed discussion about the stress decomposition in presence of reactive components, the reader is referred to [160].

It is also worth noticing that, differently from classical elasticity theory, where continua store energy during isothermal processes involving smooth finite deformations, the constitutive assumptions employed in the SDs framework allow the body both to store and dissipate energy while undergoing geometrical changes across the scales, due to the presence of disarrangements [47, 49, 51, 52]. In particular, the second law of thermodynamics requires that any SD satisfies the following *dissipation inequality*:

$$\dot{\psi} \leq \mathbf{S} \cdot (\nabla \mathbf{g}), \quad (5.49)$$

which classically claims that the rate of change of the density of Helmholtz free energy does not exceed the density of stress-power (the dot over the variable indicating its time derivative and the dot as superscript denoting time derivative of the whole content in the parentheses). By virtue of the additive decomposition provided in equations (5.3) and (5.15), such inequality reads

$$\dot{\psi} \leq D_{\mathbf{G}}\Psi \cdot \dot{\mathbf{G}} + D_{\mathbf{M}}\Psi \cdot \dot{\mathbf{M}} + D_{\mathbf{G}}\Psi \cdot \dot{\mathbf{M}} + D_{\mathbf{M}}\Psi \cdot \dot{\mathbf{G}}. \quad (5.50)$$

It can be recognized that the sum of the first two terms on the right side of this equation recovers the rate of change of the free energy density

$\dot{\psi}$. This means that the sum of the two last terms, in the SD theory referred to as *mixed (stress) power*, represents the rate of work done by the stress components due to disarrangements and those not associated to disarrangements against the reciprocal kinematics counterparts, being the difference between the free energy rate and the stress-power. Therefore, the *internal dissipation* is given by

$$Y := \mathbf{S} \cdot (\nabla \mathbf{g})^\cdot - \dot{\psi} = D_{\mathbf{G}} \Psi \cdot \dot{\mathbf{M}} + D_{\mathbf{M}} \Psi \cdot \dot{\mathbf{G}} \geq 0. \quad (5.51)$$

As a consequence, (5.51) yields a decomposition of the stress-power into a non-dissipative part and a non-negative dissipative part:

$$\mathbf{S} \cdot (\nabla \mathbf{g})^\cdot = \dot{\psi} + Y. \quad (5.52)$$

Then, with reference to the above mentioned request *ii*), it can be observed that the specific SD characterizing the multi-modular system under tensile load provides a fully reversible deformation process, because the dissipation Y vanishes. Indeed, by employing the relations (5.44) in (5.51) and by explicitly calculating the rate of change of the kinematic tensors \mathbf{G} and \mathbf{M} as:

$$\begin{aligned} \dot{\mathbf{G}} &= -\dot{\phi} (\sin \phi \hat{\mathbf{e}}_1 \otimes \hat{\mathbf{e}}_1 + \cos \phi \hat{\mathbf{e}}_2 \otimes \hat{\mathbf{e}}_1) \quad \text{and} \\ \dot{\mathbf{M}} &= \dot{\phi} [\sin \phi (1 + \sec^2 \phi) \hat{\mathbf{e}}_1 \otimes \hat{\mathbf{e}}_1 + \cos \phi \hat{\mathbf{e}}_2 \otimes \hat{\mathbf{e}}_1], \end{aligned} \quad (5.53)$$

where it is considered that the unit vectors $\hat{\mathbf{e}}_1$ and $\hat{\mathbf{e}}_2$ are time-invariant, it is possible to verify that the dissipation Y vanishes for any rotation ϕ .

5.2.3 Multi-modular structure under compressive load

In this subsection, the complementary case of a compressive load applied to the examined multi-modular structure is analyzed, under the hypothesis of infinitely stiff internal transverse springs and, as a consequence, not opening sliders. The activation of the hinges under this type of loading makes possible, in principle, a kinematics characterized by independent rotations for each element, according to the constraints imposed at the endpoints. The effective value of such rotations, i.e. the effective bifurcation mode of the structure, will be then determined by solving the equilibrium problem. Without loss of generality, the stiffness of the lateral rotational spring K_ϕ is here assumed as much lower than the one of the internal hinges, k . In this case, the contribution associated with K_ϕ to the internal energy stored by the structure while undergoing

compression can be neglected. Therefore, by virtue of this consideration and of the assumption of rigidity for the constituent rods, the internal energy can be given as

$$U_n(\phi_1, \dots, \phi_n) = \frac{1}{2}k \sum_{i=1}^n (\phi_i - \phi_{i+1})^2, \quad (5.54)$$

where ϕ_i , $i = \{1, \dots, n+1\}$, are the angles that the $n+1$ constituent rods form with respect to the horizontal direction (taken positive when clockwise), with

$$\sin \phi_{n+1} = -\sin \phi_1 - 2 \sum_{i=2}^n \sin \phi_i \quad (5.55)$$

in order to respect the geometrical constraint on the right endpoint. Then, the total potential energy can be expressed as

$$W_n(\phi_1, \dots, \phi_n) = U_n(\phi_1, \dots, \phi_n) - Fd_n(\phi_1, \dots, \phi_n), \quad (5.56)$$

where

$$d_n(\phi_1, \dots, \phi_n) = L - L_n \left(\frac{\cos \phi_1 + \cos \phi_{n+1}}{2} + \sum_{i=2}^n \cos \phi_i \right) \quad (5.57)$$

is the displacement at the boundary and F the compressive external load.

To solve the linearized equilibrium problem in case of small rotations, one can first obtain a generalized McLaurin's series expansion of the equilibrium equations $\nabla_{\phi_1, \dots, \phi_n} W = \mathbf{o}$ up to the first order and then solve the system $[\nabla \nabla(W)|_{\phi_i=0}] (\phi_1 \dots \phi_n)^T = \mathbf{o}$, where $\nabla(\bullet)$ and $\nabla \nabla(\bullet) = \nabla \otimes \nabla(\bullet)$ represent the gradient and the Hessian operators, respectively. One can hence verify that, among all the possible bifurcation modes, the one associated to the lowest critical load is that corresponding to the symmetrical configuration, as exemplified in figure 5.4B. Also, by following physical arguments, the structure that at early stages deforms according to this symmetry is then assumed to preserve it when undergoing large rotations¹. Therefore, the total potential energy can be

¹ Rigorously speaking, this kinematical assumption would neglect the possibility of other modes (say *zig-zag* as well as localized V-shaped ones) as the deformation grows approaching larger rotations. However, as highlighted in the text, despite these other modes were here not taken into account, numerical calculations confirmed that minimal energy values were only attained by the hypothesized symmetrical kinematics. Nevertheless, it is not excluded that, for example in presence of imperfections –such as slight discrepancies among the bar lengths, springs' stiffness etc– the system could in principle activate not-symmetrical modes more prone to reach lower energy levels.

accordingly simplified by considering as independent variables the sole rotations characterizing the left half of the structure, that is

$$W_n(\phi_1, \dots, \phi_{a_n}) = U_n(\phi_1, \dots, \phi_{a_n}) - Fd_n(\phi_1, \dots, \phi_{a_n}), \quad (5.58)$$

with

$$U_n(\phi_1, \dots, \phi_{a_n}) = k \left[\sum_{i=1}^{a_n-1} (\phi_i - \phi_{i+1})^2 + (2 - b_n)\phi_{a_n}^2 \right] \quad (5.59)$$

$$\text{and } d_n(\phi_1, \dots, \phi_{a_n}) = L - L_n \left(\cos \phi_1 + 2 \sum_{i=2}^{a_n} \cos \phi_i + b_n \right), \quad (5.60)$$

where:

$$a_n = \begin{cases} n/2 & n \text{ even} \\ (n+1)/2 & n \text{ odd} \end{cases} \quad \text{and} \quad b_n = \begin{cases} 1 & n \text{ even} \\ 0 & n \text{ odd} \end{cases}. \quad (5.61)$$

By explicitly writing the equilibrium equations $\partial_{\phi_i} W = 0$, $\forall i = \{1, \dots, a_n\}$, after some algebraic manipulations, one obtains

$$\begin{cases} \frac{\phi_2 - \phi_1}{L_n/2} + \frac{F}{k} \sin \phi_1 = 0 & i = 1 \\ \frac{\phi_{i+1} - 2\phi_i + \phi_{i-1}}{L_n^2} + \frac{F}{kL_n} \sin \phi_i = 0 & i = 2, \dots, a_n - 1 \\ \frac{(b_n - 3)\phi_{a_n} + \phi_{a_n-1}}{L_n^2} + \frac{F}{kL_n} \sin \phi_{a_n} = 0 & i = a_n \end{cases} \quad (5.62)$$

where the discrete version of the problem of the Euler's elastica under compressive load [13] can be recognized. Specifically, the equations (5.62)₂ and (5.62)₃ take the place of the well-known second order differential equation

$$\phi'' + \frac{F}{B} \sin \phi = 0 \quad (5.63)$$

and can be exactly identified with it if $n \rightarrow \infty$, by properly setting $k = B/L_n$, where B would represent the bending stiffness of the continuum system. Also, with such a stiffness value, the equation (5.62)₁, as $n \rightarrow \infty$, provides the elastica boundary conditions $\phi'(0) = \phi'(L) = 0$.

As a matter of fact, one finds that the curves F versus ϕ_1 , obtained by solving the equilibrium problem (5.62), quickly converge to the elastica solution as n increases. Indeed, by substituting $k = B/L_n$, from equations (5.62)₁ and (5.62)₂, it is possible to derive each rotation as a function of both the angle at the origin $\phi_1 = \phi(0)$ and the external force, that is

$$\phi_2 = \phi_1 - \frac{FL_n^2}{2B} \sin \phi_1 \text{ and } \phi_{i+1} = 2\phi_i - \phi_{i-1} - \frac{FL_n^2}{B} \sin \phi_i, i = 2, \dots, a_n - 1. \quad (5.64)$$

The substitution of these expressions into (5.62)₃ provides the equation, here numerically solved, that relates ϕ_1 and F , finally finding the result shown in figure 5.11A. Furthermore, by solving the linearized equilibrium problem, one obtains the trend of the bifurcation loads as function of n (see figure 5.11B).

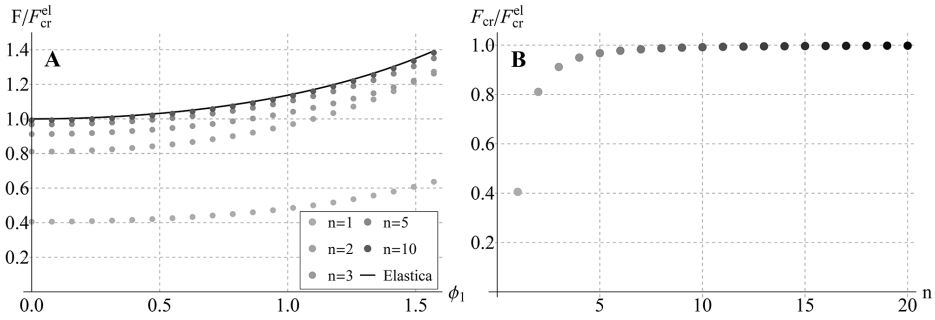


Figure 5.11: **A)** Compressive load F –normalized with respect to the elastica critical load F_{cr}^{el} [13]– as function of the initial rotation $\phi_1 = \phi(0)$, for increasing number of elemental moduli composing the structure ($n = 1, 2, 3, 5, 10$) up to the limit $n \rightarrow \infty$ coinciding with the continuum case of the elastica. **B)** Critical compressive load F_{cr} –normalized with respect to the elastica critical load F_{cr}^{el} [13]– as function of n .

5.2.3.1 SD-based formulation for compressive loads

As for the case of tension, the kinematics of the structure subject to compressive axial load can be described in light of the theory of (first order) SDs. Specifically, an approximating sequence properly describing

the geometry that characterizes the deformation in this case (figure 5.4B) can be written as follows:

$$\begin{aligned}
\mathbf{g}_n^h(\mathbf{x}_0) = & \left\{ H(a_n - 1 - h) \left[(x_0 - c_n) \cos \phi_{h+1} + L_n \left(e_n \cos \phi_1 + \sum_{i=2}^h \cos \phi_i \right) \right] \right. \\
& + b_n \delta(h - a_n) \left[x_0 - c_n + L_n \left(e_n \cos \phi_1 + \sum_{i=2}^{a_n} \cos \phi_i \right) \right] \\
& + H(h - a_n - b_n) \left[(x_0 - p_n) \cos \phi_{n-h+1} \right. \\
& \left. + L_n \left(b_n + f_n \cos \phi_1 + 2 \sum_{i=2}^{a_n} \cos \phi_i - \sum_{i=2}^{n-h+1} \cos \phi_i \right) \right] \left. \right\} \hat{\mathbf{e}}_1 \\
& + \left\{ H(a_n - 1 - h) \left[(x_0 - c_n) \sin \phi_{h+1} + L_n \left(e_n \sin \phi_1 + \sum_{i=2}^h \sin \phi_i \right) \right] \right. \\
& + b_n \delta(h - a_n) \left[L_n \left[\frac{1}{2} \sin \phi_1 + \sum_{i=2}^{a_n} \sin \phi_i \right] \right] \\
& \left. + H(h - a_n - b_n) \left[(p_n - x_0) \sin \phi_{n-h+1} + L_n \left(t_n \sin \phi_1 + \sum_{i=2}^{n-h+1} \sin \phi_i \right) \right] \right\} \hat{\mathbf{e}}_2, \\
\forall x_0 \in &]c_n, p_n + 2L_n t_n[,
\end{aligned} \tag{5.65}$$

where $H(h - p)$ is the Heaviside function taking value 1 when $h \geq p$ and 0 otherwise, and the functions c_n, p_n, e_n, f_n and t_n are introduced, for sake of simplicity, as $c_n = L_n (2h - 1 + \delta(h)) / 2$, $p_n = L_n (2h - 1 + \delta(h - n)) / 2$, $e_n = (1 - \delta(h)) / 2$, $f_n = (1 + \delta(h - n)) / 2$ and $t_n = (1 - \delta(h - n)) / 2$. Consequently, the related gradients are

$$\begin{aligned}
\nabla \mathbf{g}_n^h = & [H(a_n - 1 - h) \cos \phi_{h+1} + b_n \delta(h - a_n) \\
& + H(h - a_n - b_n) \cos \phi_{n-h+1}] \hat{\mathbf{e}}_1 \otimes \hat{\mathbf{e}}_1 + \\
& + [H(a_n - 1 - h) \sin \phi_{h+1} - H(h - a_n - b_n) \sin \phi_{n-h+1}] \hat{\mathbf{e}}_2 \otimes \hat{\mathbf{e}}_1, \\
\forall x_0 \in &]c_n, p_n + 2L_n t_n[.
\end{aligned} \tag{5.66}$$

By considering that the approximating sequence in (5.65) represents the solution of the problem at hand, described by the system in (5.62), and by recalling that such a *discrete* problem tends to the differential Euler's elastica problem as $n \rightarrow \infty$, it can be deduced that –in the limit $n \rightarrow \infty$ – the approximating sequence above also tends to the solution

of the Euler’s elastica, i.e. to the well-known macroscopic deformation describing its deformed shape:

$$\mathbf{g}(\mathbf{x}_0) = \left\{ -x_0 + \frac{2}{\Lambda} \left[E(am(x_0\Lambda + K(\sin \frac{\phi_1}{2}), \sin \frac{\phi_1}{2}), \sin \frac{\phi_1}{2}) - E(am(K(\sin \frac{\phi_1}{2}), \sin \frac{\phi_1}{2}), \sin \frac{\phi_1}{2}) \right] \right\} \hat{\mathbf{e}}_1 + \left. - \frac{2}{\Lambda} \sin \frac{\phi_1}{2} cn(x_0\Lambda + K(\sin \frac{\phi_1}{2})) \hat{\mathbf{e}}_2, \right\} \quad (5.67)$$

where $\Lambda = \sqrt{F/B} = 2K(\sin(\phi_1/2))/L$, $K(\bullet, \sin(\phi_1/2))$ and $E(\bullet, \sin(\phi_1/2))$ are the elliptic integrals of the first and second kind, respectively, while $am(\bullet, \sin(\phi_1/2))$ and $cn(\bullet, \sin(\phi_1/2))$ are the Jacobi amplitude and the Jacobi cosine amplitude functions. This is graphically illustrated in figure 5.12, where the deformed configuration of the structure is plotted for an increasing number of modular elements in comparison with the elastica (the continuum limit), for different values of the initial rotation. On the

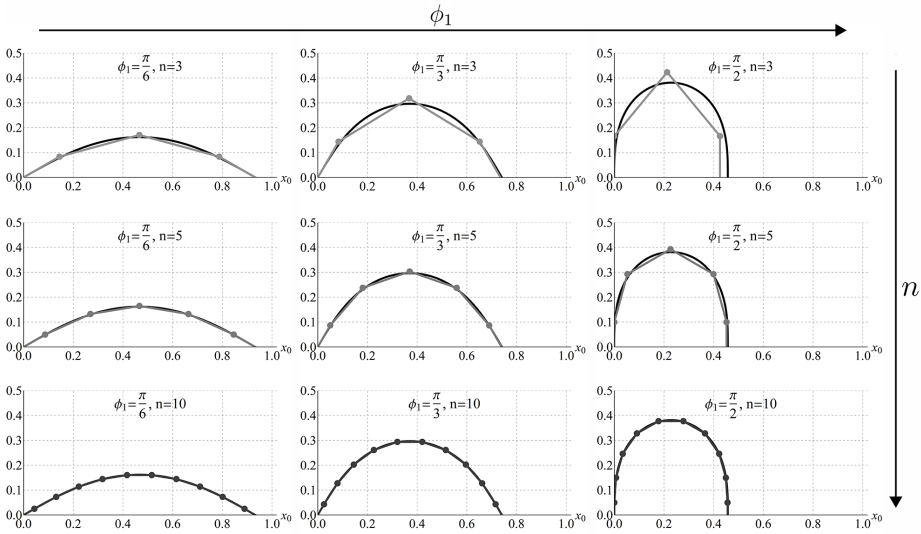


Figure 5.12: Progressively deformed configurations of the discrete structure under compression for increasing values of initial rotation ($\phi_1 = \phi(0) = \pi/6, \pi/3, \pi/2$, from left to right), with increasing number of modular elements ($n = 3, 5, 10$, from top to bottom), in comparison with the elastica continuum limit. Grey dots and segments denote deformed configurations of the discrete systems while black solid lines indicate the corresponding ones of the continuous (elastica).

other hand, with regard to the deformation without disarrangements \mathbf{G} , one obtains from equation (5.66) that

$$\mathbf{G} = \lim_{n \rightarrow \infty} \nabla \mathbf{g}_n^h = \cos \phi(\mathbf{x}_0) \hat{\mathbf{e}}_1 \otimes \hat{\mathbf{e}}_1 + \sin \phi(\mathbf{x}_0) \hat{\mathbf{e}}_2 \otimes \hat{\mathbf{e}}_1, \quad (5.68)$$

which exactly coincides with the gradient $\nabla \mathbf{g}$ of the macroscopic deformation \mathbf{g} in (5.67), thus showing that the considered SD is, in fact, a *classical* deformation, with no sub-macroscopic disarrangements. In compliance with the absence of such disarrangements, the tensor \mathbf{M} introduced in (5.4) turns out to be equal to $\mathbf{0}$, while the tensor \mathbf{K} , accounting for the purely sub-macroscopic quote of a first order SD, is the identity tensor and, hence, the virgin configuration coincides with the reference configuration. As a consequence, the stress due to disarrangements \mathbf{S}_d vanishes and the component of stress without disarrangements \mathbf{S}_\setminus is exactly equal to the first Piola-Kirchhoff stress tensor $\mathbf{S} = F/A \hat{\mathbf{e}}_1 \otimes \hat{\mathbf{e}}_1$.

In conclusion, it is important to note that, while disarrangements arising from discontinuities in the sequence \mathbf{g}_n^h of deformations are absent in this case, the sequence of the gradients $\nabla \mathbf{g}_n^h$ in (5.66) is characterized by discontinuities. This is also shown in figures (5.5) and (5.12) where, obviously, slopes of neighboring modules of the compressed discrete structure exhibit different constant slopes as the whole system contracts, this implying that second gradients $\nabla \nabla \mathbf{g}_n^h$ are identically zero for the case at hand. These properties of approximating sequences render this geometry a special case of coherent sub-macroscopically affine motions, analyzed in [160] for studying elasticity with gradient disarrangements.

5.3 CONCLUSION

In the present chapter, the nonlinear elastic response of a one-dimensional multi-modular structure under compressive/tensile dead loads has been analyzed, both for a finite number of constituents (discrete structure) and infinite elemental units (continuum structure), in the latter case providing, for the first time, a 1D paradigm of the SD theory and demonstrating the need to invoke this approach for naturally obtaining *augmented* hyperelastic models, often required for the accurate description of multiscale biological systems.

In particular, with regard to the compressive loading, it has been found that the first bifurcation mode exhibited by the structure replicates, in a discrete form, the solution of the *Euler's elastica* problem, converging to the classical elastica in the continuum limit. On the other hand, the

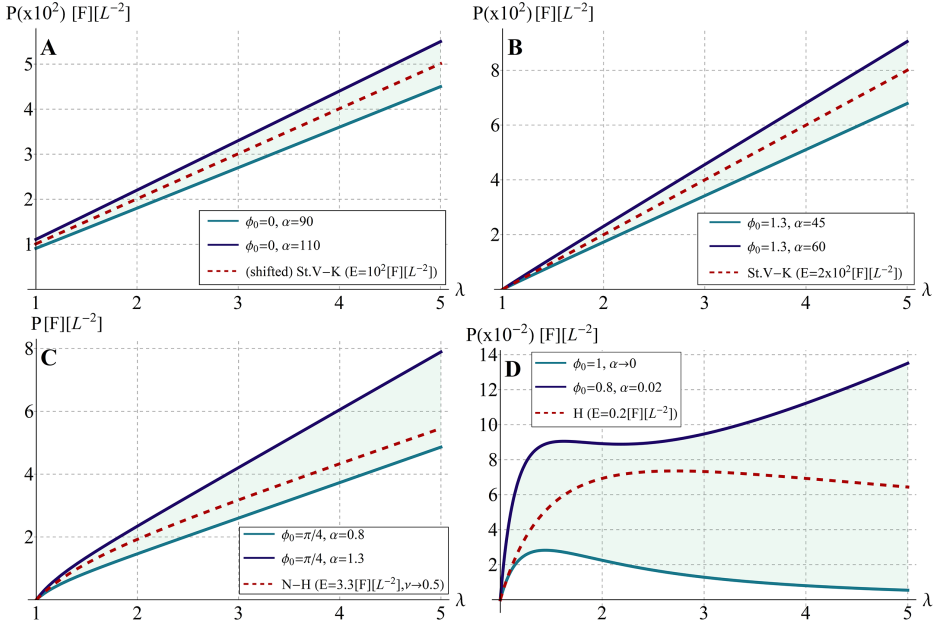


Figure 5.13: Comparison (in terms of first Piola-Kirchhoff stress P versus axial stretch λ) between standard hyperelastic models (dashed lines) and the macroscopic responses given by the 1D structure studied in the present work –in the *continuum* limit of $n \rightarrow \infty$ – by properly setting the values of its internal parameters ϕ_0 (initial imperfection) and α (ratio between translational and rotational springs stiffnesses): **A)** *shifted* Saint Venant-Kirchhoff model (St.V-K), **B)** Saint Venant-Kirchhoff model, **C)** neo-Hookean model (N-H) and **D)** Hencky's model (H), with the upper curve (in blue) a typical balloon-like trend.

behavior of the structure under tensile load –that can be further enriched with the introduction of an initial imperfection– results to be influenced both by the stiffness of the springs associated with the internal sliders (i.e. by their dependence on the number of elemental moduli) and by the ratio between the values of such stiffness and of the rotational spring at the left end. It has to be highlighted that, in the compressive case, the description in terms of SDs reveals that, as $n \rightarrow \infty$, the relative rotations at the nodes endowed with elastic springs tend to vanish, thus reproducing the classical deformation mode of the continuum without disarrangements. On the contrary, this does not occur under tensile load, where the associated deformation converges to a macroscopic (threshold-activated, for the case of a perfect system) uni-axial elongation, storing

sub-macroscopic disarrangements which a standard continuum theory would not have traced.

Additionally, it is interesting to note the plurality of behaviors that the structure provides under tensile load (see figures 5.7-5.10), by tuning internal properties such as the ratio between the springs stiffnesses and/or the initial imperfection. In fact, by modulating these ratios, various classical nonlinear constitutive models can be derived as the result of a consistent bottom-up procedure incorporating SDs. To show this in detail, a focus on the macroscopic behavior of the 1D continuum structure (i.e. $n \rightarrow \infty$) is here considered by in particular setting the stiffness of the sliders' springs proportional to the number of units n . For this case, figure 5.13 illustrates that one can reproduce at least four commonly adopted hyperelastic constitutive models, therein plotted in terms of first Piola-Kirchhoff stress versus axial (macroscopic) stretch. In particular, if the system is *perfect* ($\phi_0 = 0$), one finds a *threshold-activated* Saint Venant-Kirchhoff model [13] (written with reference to the Cauchy strain measure derived from the Seth-Hill formula [13, 93], for small strain giving the classic linear Hooke's law [225]). On the other hand, in the case of *imperfect* system, by properly playing on the microstructural parameters ϕ_0 and α , one can obtain a wider class of hyperelastic curves including the neo-Hookean law [95] and responses providing softening such as the Hencky's model [4, 248] and the non-monotonic behavior recognized in inflated balloons, in terms of pressure-radius relation [150]. Figure 5.14 then combines the responses of the multi-modular structure under the examined loading condition types, that is for tensile and compressive external applied forces, accounting for the complementary constitutive assumptions respectively made in the two cases in the previous subsections. In particular, figure 5.14A shows the response of a structure which can deform only under tensile load –with or without a threshold behavior, according to the absence or to the presence of sub-macroscopic imperfections, respectively– offering instead infinite stiffness to compression ($k \rightarrow \infty$). On the other hand, figure 5.14B illustrates the complementary case of a system which undergoes deformation only under compressive load, being infinitely stiff to tension ($K_\Delta \rightarrow \infty$).

In conclusion, it is foreseen that the presented SD-based strategy could be in future generalized to two- and three-dimensional structures, in this way widening the range of applicable loading conditions and the richness of the potential resulting microstructural and global mechanical behaviors. Moreover, it is envisaged that dissipation –irreversible and time-dependent– phenomena could be also involved, for example through

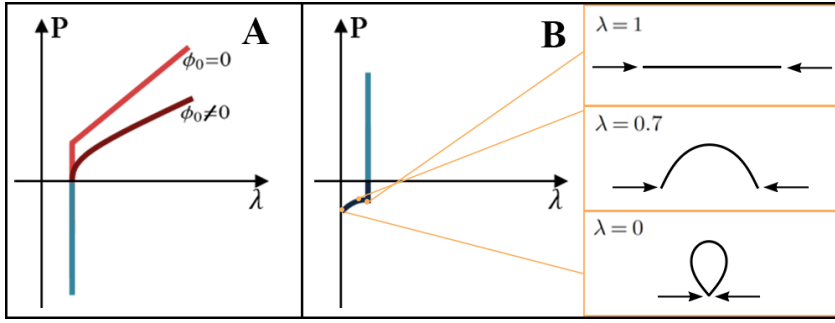


Figure 5.14: Whole (i.e. both under compressive and tensile regime) *macroscopic* response of the structure in terms of first Piola-Kirchhoff stress *versus* axial stretch, for the two complementary constitutive assumptions made in the sections above: **A**) structure deforming only under tensile load –with or without a threshold behavior according to the absence or presence of sub-macroscopic imperfections, respectively– offering infinite stiffness to compression ($k \rightarrow \infty$); **B**) structure deforming only under compressive load, offering infinite stiffness to tension ($K_{\Delta} \rightarrow \infty$). In the latter case, the apparently inconsistent finite value of the stress as the macro-stretch λ goes to zero —a condition unseen in standard continua— is here in principle admissible as a consequence of the fact that such stretch measures the actual distance between the 1D element endpoints, that in case of compression could coincide —or even invert their position so producing negative stretches— for extremely large deformation of the elastica. In this regard, the inset on the right side reports illustrative sketches of the deformed macroscopic system for decreasing value of λ .

the integration of dashpot elements, thus possibly including the chance of reproducing as special cases classical models of linear viscoelasticity (e.g. Maxwell as well as Kelvin-Voigt models). In this way, valuable homogenized models could be then obtained, which would allow to both interpret complex macroscopic behaviors of biological or bioinspired hierarchically organized materials, from living single-cells to tissues, and trace back some relevant physical phenomena by means of localization procedures.

CONCLUSIONS

The single cell can be thought as a unitary element embedded in a complex physical space, able to continuously receive and respond to external biochemical and mechanical signals. Recently, wide interest has been addressed to the role played by the cell mechanics in mechanosensing and mechanotransduction processes, which seem to regulate many important cell biological functions by means of viscoelastic properties variations as well as of mechano-driven morphological changes and forces transmission [64, 107, 146, 197].

In this framework, the research work presented in this thesis deals with the study of the single-cell mechanical behavior. With in mind experimental evidences, microstructural kinematics steering the macroscopic elasticity of the living cell and guiding some key mechanisms implicated in cellular adhesion, motility and mechanotransduction, have been modelled by means of a theoretical approach. Also, to consider the cell-environment interaction, the physical principles governing the behavior of adherent cells when perturbed by mechanical stimuli, such as external stress/strain fields, sensed through an elastic substrate, have been investigated.

Starting from the idea that the mechanical response of the cell is mainly provided by its cytoskeleton that obeys tensile integrity principles [149, 202] in ensuring overall structural stability, morphology and elastic stiffness [101, 106], both hyperelastic and buckling soft-strut tensegrity models have been here proposed as enhanced paradigm for describing single-cell mechanics. Recent experimental evidences highlight large deformations and nonlinear behaviors exhibited by the whole cytoskeleton and by its individual and bundled actin constituents [42, 74, 136, 227, 228] and suggest the possible coupling of severe axial contractions and buckling of *in vivo* microtubules [17, 18, 129, 207], this motivating the need of overcoming the standard adoption of cellular tensegrity units comprising (pre)tensed linear elastic actin-filament-like cables and (pre)compressed rigid or purely buckling microtubule-like struts [35, 36, 211, 232, 238].

In the light of these observations, a first 2-element soft-tensegrity paradigm, which includes (neo-Hookean) finite hyperelasticity for cable and strut, with the latter potentially undergoing both contraction and localized buckling, has been analyzed at each pre-stressed equilibrium

stage and under the action of applied loads. In this way, it has been shown that constitutive properties and geometrical parameters contribute to determine competition between axial deformability and buckling instability of the system, thus providing multiple form-finding results and peculiar overall mechanical responses (e.g. elastic stiffness) to external solicitation already in this essential single-microtubule/single-actin-filament structure.

By following an analogous approach, the 30-element spherical tensegrity model firstly proposed by the scientist Donald E. Ingber and commonly adopted in literature as structural paradigm of the single-cell [101, 106] has been here re-formulated. The pre-stressed self-equilibria of the system and its response under contraction/extension, shear and torsion have been analyzed by removing the usual hypothesis of axially rigid struts, in order to introduce their compressibility coupled to bendability. The theory has been then accordingly rewritten to simultaneously take into account large deformations and nonlinear hyperelasticity of both cables and struts, modelled as either Hencky-type or neo-Hookean materials. In this way, some quantitative confirmations have been found both in terms of energy (order of $10^{-1} \div 10^0 pJ$) elastically stored by the cell and for example transferred –upon adhesion– to external elastic media in the form of contractile forces [7, 194, 195], and of elastic stiffness (order of $10^{-1} \div 10^1 kPa$) actually measured for different cell lines and by means of several techniques [8, 68]. In addition, qualitative and sometimes counter-intuitive mechanical behaviors, characterized by nonlinear and non-monotonic elastic responses and hardening/softening phenomena, have been theoretically predicted, by tracing some experimentally observed mechanisms that seem to be exploited by cells for storing/releasing energy, for resisting to applied loads and for deforming by modulating their overall elasticity and shape through pre-stress changes and instability-guided configurational switching.

On the other hand, motivated by the laboratory evidences that the orientation of *in vitro* adherent cells is influenced by the stress/strain distributions that they sense through the elastic interaction with the substrate [32, 34, 134, 197, 213, 219, 234], a novel strategy has been also theoretically presented in this thesis to investigate the optimization principles ruling the cell mechano-induced directional response.

More in detail, based on experimental measurements of cellular traction patterns on deformable substrates [194, 195], the adherent and stationary (i.e. non-motile) single-cell has been modelled as a dipole of contractile forces and its preferential orientations have been theoretically explored

under the effect of regular fences of point-loads acting normally to the substrate (flat) boundary and surrounding the cell. Then, by employing singular solutions of the linear theory of elasticity, angles of optimal orientation have been analytically found as the directions along which the cell-dipole can exploit the strain field induced by the external forces to minimize the elastic work that it spends to deform the underlying substrate while retaining its own contractile force level. In particular, depending on the combination of substrate Poisson's ratio and applied forces features (namely their number, pointing-direction, magnitude and distance from the cell), two different classes of preferential arrangements have been found, one leading to even nullify the deformation work and the other, less advantageous, in which the cell can only minimize the work intensity. In the latter condition, it has also been found that optimal solutions coincide with the orientations of maximum extension for the cell, this tracing some results obtained by previous experimental works [14, 15, 34, 249].

With in mind sub-cellular components, the present work has finally examined the potential of multiscale models for the accurate mechanical description of living cell sub-units and, in general, of heterogeneous biological systems whose macroscopic behavior arises from structural kinematics evolving across different hierarchical (e.g. meso-, micro-, nano-) length scales [54, 162, 163, 181, 227]. In this regard, the theory of structured deformations has been recognized as a possible means to obtain augmented hyperelastic models able to interpret the smooth macroscopic deformation of biological bodies as the result of sub-macroscopic deformative processes possibly involving non-smooth geometrical changes, namely disarrangements [44, 47–49, 52, 159]. In this context, a first effective paradigm of augmented one-dimensional hyperelasticity lying on the structured deformation theory has been implemented, in this way laying the groundwork for building up further models oriented to biomechanical applications. Specifically, the overall elastic response of a one-dimensional multi-modular structure, incorporating possible imperfections and buckling instabilities at the discrete (sub-macroscopic) level, has been derived with respect to both tensile and compressive applied loads. With regard to the compressive loading, it has been found that the first bifurcation mode exhibited by the structure converges to the classical deformation provided by the Euler's elastica in the continuum limit, say in the limit case in which the system is made of an infinite number of infinitesimal modular constituents. On the other hand, in case of tensile loading, the continuum limit has been found to provide a (pos-

sibly threshold-activated) macroscopic uni-axial elongation that stores sub-macroscopic disarrangements, which would not have been traced by adopting a standard continuum theory. Also, associated to the tensile load case, by plotting the results in terms of nominal axial stress versus macroscopic stretch and by tuning internal microstructural parameters of the system, a wide family of standard nonlinear hyperelastic models (e.g. neo-Hookean, Hencky-like and others) often needed to describe both biological and man-made materials, has been obtained as a particular case of structural kinematics concealed at lower scales.

The issues addressed in this work represent all pieces of a greater puzzle on which mechanobiologists are working with the aim of achieving a whole and clear comprehension of the cell mechanics and of its implications into biological events at the level of both cells and tissues.

Despite the difficulties in completing the puzzle assembling, it is felt that the theoretical models presented in this thesis could be helpfully improved both by working on aspects that concern them as independent models and by integrating results borrowed by other approaches, to thus move further steps towards successful novel multiscale-multiphysics applications.

As a matter of fact, the one-dimensional multi-modular system here introduced as first paradigm of structured deformation-based augmented hyperelasticity could be redrawn by conceiving microstructures able to provide discrete kinematics properly catching the disarrangement-like phenomena that characterize actomyosin filaments at the level of their molecular architectures and, as a result, to trace their nonlinear macroscopic behavior in the continuum limit. Biochemically induced sliding mechanisms between actin segments and myosin heads are indeed known to affect the mechanics of actomyosin filaments embedded in the cytoskeleton apparatus by actively producing local contractile forces. Also, owing to the presence of crystal-like folded domains undergoing (disarrangement-like) unfolding phenomena when subject to certain levels of tensile forces, *saw-tooth* trends are known to typify the force-extension curves of single actin macromolecules, which in turn determine the nonlinear macroscopic behavior of the overall multi-modular macromolecular chain that makes up the actin filament [178, 227, 228, 252].

Biofilament-inspired structured deformations models, potentially obtained by following this rational, could be then *de facto* integrated within tensegrity-based cytoskeleton descriptions, say within the revised 30-element unit presented here, in place of the already adopted phenomeno-

logical nonlinear hyperelastic laws, in this way aiming for a more accurate modelling of the cell mechanical behavior, following a bottom-up logic. Such models should be furthermore enriched through the integration of mechanical elements (for example dash-pots) able to account for viscoelastic behaviors [50, 163, 164] that are also recognized in cytoskeleton as well as, in general, in actin networks, which have been neglected in this work by focusing the analyses at early-times of the cell response where it can be essentially assumed as elastic. Additionally, stress-mediated polymerization/depolymerization phenomena [210], continuously affecting *in vivo* cytoskeletal filaments and consequently influencing their mechanical properties, should be coherently involved. This could be done by introducing stress-influenced growth/resorption laws for individual filaments, modelled as inelastic contributions to the whole deformation [69, 140, 256, 257]. It is worth noting that, by following this way, the potential non-uniform occurrence of growth/resorption events within the cytoskeletal network, for example related to heterogeneous stress distributions, could be traced and would make eventually possible the detection of further related configurational switching deriving from the attempt of an overall elastic re-compatibilization [256, 257], which could be associated to those experienced by adherent cells during migration phases following the actin polymerization into lamellipodia at the cell leading edge.

On the other hand, the mechanical model here employed for investigating the principles of optimal orientation of adherent cells on deformable substrates could be improved too, by following different directions. In fact, the stationary force-dipole, adopted as physical equivalent of an highly stretched single-cell whose stress fibers bundle in parallel to form a fiber-shaped body, should be more faithfully modelled by involving the constitutive relationship existing between the cell extension and the level of contractile force that it can transmit to the substrate at the adhesion points. Since stress fibers arises from the assembling of actin filaments, this improvement could be achieved by implementing and combining structured deformation-based biofilament models as those envisaged above. In addition, the presented model predicts the preferential directions along with a cell would be aligned in order to minimize the work performed in deforming the underlying substrate, without taking into account a potential initial positioning of the cell and hence without tracing the eventual reorientation process. This however could represent an aspect to additionally consider in the perspective of employing the suggested theoretical strategy for building up novel experimental set up

aimed to the study of the cell mechanotropism, since, starting from a certain (say random) arrangement, the actual cell reorientation along a predicted optimal angle could be conditioned by a further expenditure of energy related to the same rotational motion that the cell has to perform during this process and to the demolition/reconstruction of focal adhesion sites that it can require.

By still focusing on cell orientation, the analytical results given by the proposed model have *de facto* revealed that, in case of isotropic and homogeneous linear elastic substrates, their Poisson ratio is the only relevant mechanical property, the Young modulus instead not directly affecting optimal solutions. Based on this observation as well as on the consolidated evidence that longitudinal gradients of substrate stiffness guide cell mechanotaxis [138], it would be of interest to study if angular variations of substrate Poisson ratio might induce (in absence of external loads) a complementary effect in driving cell mechanotropism.

In conclusion, it is worth to focus the attention on the capability that tensegrity systems intrinsically possess in explaining and tracing mechanical discrepancies experimentally observed between healthy and tumour cells, and, as a consequence, on their potential effectiveness in the theoretical modelling of novel mechano-driven therapeutic strategies for cancer diseases. This represents an ongoing research work that finds its starting point into some of the results obtained in the present thesis with regard to soft tensegrity systems, as briefly described below².

As a matter of fact, oncological treatments of solid tumours [27, 69] are to date based on therapeutic protocols that involve surgical techniques, chemotherapy and radiotherapy. These interventions are however often accompanied by side effects that compromise the quality of life of the patients since they damage cancer cells without preserving the surrounding healthy tissues. Several efforts are hence currently destined, in the oncological research context, to the development of mini-invasive techniques aimed to the recognition and to the therapeutic treatment of cancer diseases, able to induce death of malignant cells while safeguarding the healthy neighbourhood. In this framework, strategies relying on the use of low intensity therapeutic ultrasounds (LITUS) have been increasingly investigated [246]. In fact, owing to their low intensities (less

² In this regard, the research project ARS01-01384-PROSCAN, funded by the Italian Ministry of Education, Universities and Research (MIUR) and involving –among others– the University of Napoli "Federico II" and the University of Trento, is currently ongoing with the aim of applying strategies based on single-cell mechanics to *in vitro* and *in vivo* experiments.

than $5W/cm^2$), which can avoid tissue injuries due to the high thermal effects, LITUS have been considered for several procedures of cancer therapy, in which they are mainly employed as a mechanical input to trigger pharmaceutical or genetic events (e.g. ultrasound (US)-mediated chemotherapy) [128, 226, 246]. More interestingly from the mechanical point of view, recent studies have also been performed in order to understand the direct effects of US stimulation on living (human) cells. As an example, cell membrane damage has been observed after US treatment in human blood cells and leukaemic cell lines [61], other experimental studies having additionally demonstrated that malignant cells are sometimes much more susceptible and prone to be killed than normal cells when subjected to US exposure [125, 126]. Then, depending on the cell type and the sonication protocol, USs have been shown to be potentially able –if adequately modulated in terms of frequency and energy– to decrease proliferation of cancer cells and promote their apoptosis as well as to increase healthy cells proliferation and stimulate wound healing [193].

Despite the relation between US excitation and cell biological response is not completely clear yet, in this scenario, cytomechanics can be hypothesized to have a primary role in mediating US–cells interactions, LITUS-induced structural remodeling of the cytoskeleton having been also observed for human airway smooth muscle cells [145]. Among others, the mechanical effects promoted by the vibration of single-cells due to USs have been theoretically analyzed in a recent work by Fraldi et al. [68], in which LITUS-induced mechanical oscillations have been shown to produce in-frequency separated resonance-like phenomena for tumour and healthy cells, namely peaks of oscillation magnitude associated with distant critical frequencies (ranging between tens and hundreds of kilohertz) for the two cell phenotypes. On these bases, the authors have outlined the possibility to determine selective fatigue-like phenomena in cells by means of a properly in-frequency tuned pure mechanical action, a fact that could be helpfully utilized, at least in principle, to envisage novel and non-invasive mechano-based strategies for both targeting and selectively attacking tumour cells within localized solid tumours, without compromising healthy neighbours.

Importantly, the possibility of theoretically discriminating individual healthy and cancer cells in terms of harmonic response to mechanical solicitations *de facto* lies on the difference that the two cell phenotypes provide in terms of stiffness. Recent experimental evidences have indeed highlighted that healthy and malignant cells of the same line exhibit

a significant gap in elastic stiffness, the latter being about 70% more compliant than the normal counterpart [38, 68].

Within this context, since according to the cellular tensegrity paradigm cells deformability principally depends on cytoskeleton pre-stretch/stress, such discrepancy in elastic stiffness could be coherently explained as due to different levels of pre-stretch/stress related to alterations of cytoskeletal organization and cell adhesion that are associated with neoplastic transformations. As an example, cancer cells generally live in few adherent configurations –rather close to round-shaped arrangements– that make them prone to motion, while healthy cells highly adhere to the extra-cellular environment by assuming spread and more stable (i.e. less motile) forms. As a result, by interpreting the cell as a tensegrity system, the level of cytoskeleton pre-stretch in tumour cells should be significantly lower than the one attained by normal cells, this in turn affecting the value of the global cell elasticity and, thus, that of the related proper (resonance-like) frequency. On this basis, soft tensegrity units can be helpfully employed in the perspective of conceiving and implementing new biomechanical models aimed to a first theoretical analysis of the collective response of multi-cellular clusters composed by both tumour and healthy cells to LITUS-induced mechanical stimulation. Starting from this idea, three-dimensional tumour spheroids can be actually built up by combining different percentages of normal and tumour cells, each being modelled by including its main mechanical components –namely nucleus, cytoplasm, plasma membrane and cytoskeleton– and being properly characterized in terms of stiffness (hence of critical frequency) by *ad hoc* modulating the level of pre-stretch stored in its cytoskeletal tensegrity architecture. By then taking into account that the mechanical interaction among cells is mediated by the coupling with the ECM layer and by envisaging different percentages of normal and tumour cells to simulate multiple stages of tumour progression, harmonic analyses can be performed to study the possibility of selectively inducing resonance, and hence disruption, of the only cancer cells within the agglomerate by properly tuning the frequencies of the US stimulation on the tumour-specific band, in this way also predicting, for each tumour stage-specific scenario, the frequencies that simultaneously maximize the outcomes in terms of both destructive effects on tumour cells and healthy cells preservation. It is felt that, by adopting such multi-modular tensegrity-based models, it would be possible to pave the way for the first theoretical analyses testing the potentiality of LITUS-driven mechanical procedures in the

treatment of certain types of cancer diseases, performed at the length scale of cellular clusters.

BIBLIOGRAPHY

- [1] Crossley Dane A., Burggren Warren W., Reiber Carl L., Altimiras Jordi, and Rodnick Kenneth J. "Mass Transport: Circulatory System with Emphasis on Nonendothermic Species." In: *Comprehensive Physiology*. American Cancer Society, 2016, pp. 17–66. ISBN: 9780470650714. DOI: [10.1002/cphy.c150010](https://doi.org/10.1002/cphy.c150010).
- [2] Vivek C. Abraham, Vijaykumar Krishnamurthi, D. Lansing Taylor, and Frederick Lanni. "The Actin-Based Nanomachine at the Leading Edge of Migrating Cells." In: *Biophysical Journal* 77.3 (1999), pp. 1721–1732. DOI: [10.1016/s0006-3495\(99\)77018-9](https://doi.org/10.1016/s0006-3495(99)77018-9).
- [3] Steven K Akiyama. "Integrins in cell adhesion and signaling." In: *Human cell* 9.3 (1996), pp. 181–186.
- [4] L. Anand. "On H. Hencky's Approximate Strain-Energy Function for Moderate Deformations." In: *Journal of Applied Mechanics* 46.1 (1979), p. 78. DOI: [10.1115/1.3424532](https://doi.org/10.1115/1.3424532).
- [5] Ansys 15.0 User's Manual. *ANSYS Mechanical User's Guide*. Release 15.0. ANSYS, Inc. 2013.
- [6] Dan B., Roman Golkov, Yair Shokef, and Samuel A. Safran. "Response of adherent cells to mechanical perturbations of the surrounding matrix." In: *Soft Matter* 11.7 (2015), pp. 1412–1424. DOI: [10.1039/c4sm01817f](https://doi.org/10.1039/c4sm01817f).
- [7] Nathalie Q. Balaban et al. "Force and focal adhesion assembly: a close relationship studied using elastic micropatterned substrates." In: *Nature Cell Biology* 3.5 (2001), pp. 466–472. DOI: [10.1038/35074532](https://doi.org/10.1038/35074532).
- [8] Gang Bao and Subra Suresh. "Cell and molecular mechanics of biological materials." In: *Nature materials* 2.11 (2003), p. 715. DOI: [10.1038/nmat1001](https://doi.org/10.1038/nmat1001).
- [9] J. R. Barber. *Elasticity*. Springer Netherlands, 1992. DOI: [10.1007/978-94-011-2454-6](https://doi.org/10.1007/978-94-011-2454-6).

- [10] Andreas R. Bausch, Florian Ziemann, Alexei A. Boulbitch, Ken Jacobson, and Erich Sackmann. "Local Measurements of Viscoelastic Parameters of Adherent Cell Surfaces by Magnetic Bead Microrheometry." In: *Biophysical Journal* 75.4 (1998), pp. 2038–2049. DOI: [10.1016/s0006-3495\(98\)77646-5](https://doi.org/10.1016/s0006-3495(98)77646-5).
- [11] Barbara W. Bernstein and James R. Bamberg. "Actin-ATP Hydrolysis Is a Major Energy Drain for Neurons." In: *The Journal of Neuroscience* 23.1 (2003), pp. 1.2–6. DOI: [10.1523/jneurosci.23-01-00002.2003](https://doi.org/10.1523/jneurosci.23-01-00002.2003).
- [12] Alexander D Bershadsky, Nathalie Q Balaban, and Benjamin Geiger. "Adhesion-dependent cell mechanosensitivity." In: *Annual review of cell and developmental biology* 19.1 (2003), pp. 677–695.
- [13] Davide Bigoni. *Nonlinear Solid Mechanics - Bifurcation theory and material instability*. 2012.
- [14] I. B. Bischofs, S. A. Safran, and U. S. Schwarz. "Elastic interactions of active cells with soft materials." In: *Physical Review E* 69.2 (2004). DOI: [10.1103/physreve.69.021911](https://doi.org/10.1103/physreve.69.021911).
- [15] I. B. Bischofs and U. S. Schwarz. "Cell organization in soft media due to active mechanosensing." In: *Proceedings of the National Academy of Sciences* 100.16 (2003), pp. 9274–9279. DOI: [10.1073/pnas.1233544100](https://doi.org/10.1073/pnas.1233544100).
- [16] I. B. Bischofs and U. S. Schwarz. "Effect of Poisson Ratio on Cellular Structure Formation." In: *Physical Review Letters* 95.6 (2005). DOI: [10.1103/physrevlett.95.068102](https://doi.org/10.1103/physrevlett.95.068102).
- [17] Clifford P. Brangwynne, Frederick C. MacKintosh, Sanjay Kumar, Nicholas A. Geisse, Jennifer Talbot, L. Mahadevan, Kevin K. Parker, Donald E. Ingber, and David A. Weitz. "Microtubules can bear enhanced compressive loads in living cells because of lateral reinforcement." In: *J Cell Biol* 173.5 (2006), pp. 733–741. DOI: [10.1083/jcb.200601060](https://doi.org/10.1083/jcb.200601060).
- [18] G.W. Brodland and R. Gordon. "Intermediate Filaments May Prevent Buckling of Compressively Loaded Microtubules." In: *Journal of Biomechanical Engineering* 112.3 (1990), p. 319. DOI: [10.1115/1.2891190](https://doi.org/10.1115/1.2891190).
- [19] Peter Walter Julian Lewis Martin Raff Keith Roberts Bruce Alberts Alexander Johnson, ed. *Molecular Biology of the Cell*. 5th edition. Taylor & Francis, London, 2007.

- [20] Fuller Richard Buckminster. "Tensile-integrity structures." Pat. 3063521. US Patent 3063521. 1962.
- [21] James P. Butler, Iva Marija Tolić-Nørrelykke, Ben Fabry, and Jeffrey J. Fredberg. "Traction fields, moments, and strain energy that cells exert on their surroundings." In: *American Journal of Physiology-Cell Physiology* 282.3 (2002), pp. C595–C605. DOI: [10.1152/ajpcell.00270.2001](https://doi.org/10.1152/ajpcell.00270.2001).
- [22] PATRICK CAÑADAS, VALERIE M. LAURENT, CHRISTIAN ODDOU, DANIEL ISABEY, and SYLVIE WENDLING. "A Cellular Tensegrity Model to Analyse the Structural Viscoelasticity of the Cytoskeleton." In: *Journal of Theoretical Biology* 218.2 (2002), pp. 155–173. DOI: [10.1006/jtbi.2002.3064](https://doi.org/10.1006/jtbi.2002.3064).
- [23] B COOKE, N MOHANDAS, and R COPPEL. "The malaria-infected red blood cell: Structural and functional changes." In: *Advances in Parasitology Volume 50* (2001), pp. 1–86. DOI: [10.1016/s0065-308x\(01\)50029-9](https://doi.org/10.1016/s0065-308x(01)50029-9).
- [24] K. Caluwaerts, J. Despraz, A. Iscen, A. P. Sabelhaus, J. Bruce, B. Schrauwen, and V. SunSpiral. "Design and control of compliant tensegrity robots through simulation and hardware validation." In: *Journal of The Royal Society Interface* 11.98 (2014), pp. 20140520–20140520. DOI: [10.1098/rsif.2014.0520](https://doi.org/10.1098/rsif.2014.0520).
- [25] P. Cañadas, S. Wendling-Mansuy, and D. Isabey. "Structural contribution of the cytoskeleton to the dynamic response of adherent cells assessed by a viscoelastic tensegrity model." In: *Journal of Biomechanics* 39 (2006), S602. DOI: [10.1016/s0021-9290\(06\)85500-4](https://doi.org/10.1016/s0021-9290(06)85500-4).
- [26] Elizabeth P. Canović, D. Thomas Seidl, Samuel R. Polio, Assad A. Oberai, Paul E. Barbone, Dimitrije Stamenović, and Michael L. Smith. "Biomechanical imaging of cell stiffness and prestress with subcellular resolution." In: *Biomechanics and Modeling in Mechanobiology* 13.3 (2013), pp. 665–678. DOI: [10.1007/s10237-013-0526-8](https://doi.org/10.1007/s10237-013-0526-8).
- [27] A.R. Carotenuto, A. Cutolo, A. Petrillo, R. Fusco, C. Arra, M. Sansone, D. Larobina, L. Cardoso, and M. Fraldi. "Growth and in vivo stresses traced through tumor mechanics enriched with predator-prey cells dynamics." In: *Journal of the Mechanical Behavior of Biomedical Materials* 86 (2018), pp. 55–70. ISSN: 1751-6161. DOI: <https://doi.org/10.1016/j.jmbbm.2018.06.011>.

- [28] Bin Chen, Xiaofeng Chen, and Huajian Gao. "Dynamics of Cellular Reorientation on a Substrate under Biaxial Cyclic Stretches." In: *Nano Letters* 15.8 (2015), pp. 5525–5529. DOI: [10.1021/acs.nanolett.5b02095](https://doi.org/10.1021/acs.nanolett.5b02095).
- [29] Bin Chen, Baohua Ji, and Huajian Gao. "Modeling Active Mechanosensing in Cell-Matrix Interactions." In: *Annual Review of Biophysics* 44.1 (2015), pp. 1–32. DOI: [10.1146/annurev-biophys-051013-023102](https://doi.org/10.1146/annurev-biophys-051013-023102).
- [30] Bin Chen, Ralf Kemkemer, Martin Deibler, Joachim Spatz, and Huajian Gao. "Cyclic Stretch Induces Cell Reorientation on Substrates by Destabilizing Catch Bonds in Focal Adhesions." In: *PLoS ONE* 7.11 (2012). Ed. by Andrew Pelling, e48346. DOI: [10.1371/journal.pone.0048346](https://doi.org/10.1371/journal.pone.0048346).
- [31] Ting-Jung Chen, Chia-Ching Wu, and Fong-Chin Su. "Mechanical models of the cellular cytoskeletal network for the analysis of intracellular mechanical properties and force distributions: A review." In: *Medical Engineering & Physics* 34.10 (2012), pp. 1375–1386. DOI: [10.1016/j.medengphy.2012.08.007](https://doi.org/10.1016/j.medengphy.2012.08.007).
- [32] Y. Chen, A. M. Pasapera, A. P. Koretsky, and C. M. Waterman. "Orientation-specific responses to sustained uniaxial stretching in focal adhesion growth and turnover." In: *Proceedings of the National Academy of Sciences* 110.26 (2013), E2352–E2361. DOI: [10.1073/pnas.1221637110](https://doi.org/10.1073/pnas.1221637110).
- [33] Giancarlo Cicconofri and Antonio DeSimone. "A study of snake-like locomotion through the analysis of a flexible robot model." In: *Proceedings of the Royal Society A: Mathematical, Physical and Engineering Science* 471.2184 (2015), p. 20150054. DOI: [10.1098/rspa.2015.0054](https://doi.org/10.1098/rspa.2015.0054).
- [34] Amy M. Collinsworth, Carol E. Torgan, Suneel N. Nagda, Robert J. Rajalingam, William E. Kraus, and George A. Truskey. "Orientation and length of mammalian skeletal myocytes in response to a unidirectional stretch." In: *Cell and Tissue Research* 302.2 (2000), pp. 243–251. DOI: [10.1007/s004410000224](https://doi.org/10.1007/s004410000224).
- [35] M. F. Coughlin and D. Stamenovic. "A Tensegrity Structure With Buckling Compression Elements: Application to Cell Mechanics." In: *Journal of Applied Mechanics* 64.3 (1997), p. 480. DOI: [10.1115/1.2788918](https://doi.org/10.1115/1.2788918).

- [36] M. F. Coughlin and D. Stamenovic. "A Tensegrity Model of the Cytoskeleton in Spread and Round Cells." In: *Journal of Biomechanical Engineering* 120.6 (1998), p. 770. DOI: [10.1115/1.2834892](https://doi.org/10.1115/1.2834892).
- [37] Stephen C. Cowin and Stephen B. Doty, eds. *Tissue Mechanics*. Springer New York, 2007. DOI: [10.1007/978-0-387-49985-7](https://doi.org/10.1007/978-0-387-49985-7).
- [38] Sarah E. Cross, Yu-Sheng Jin, Jianyu Rao, and James K. Gimzewski. "Nanomechanical analysis of cells from cancer patients." In: *Nature Nanotechnology* 2.12 (2007), pp. 780–783. DOI: [10.1038/nnano.2007.388](https://doi.org/10.1038/nnano.2007.388).
- [39] Pan Dan, Émilie Velot, Véronique Decot, and Patrick Menu. "The role of mechanical stimuli in the vascular differentiation of mesenchymal stem cells." In: *Journal of Cell Science* 128.14 (2015), pp. 2415–2422. DOI: [10.1242/jcs.167783](https://doi.org/10.1242/jcs.167783).
- [40] Rumi De, Assaf Zemel, and Samuel A. Safran. "Dynamics of cell orientation." In: *Nature Physics* 3.9 (2007), pp. 655–659. DOI: [10.1038/nphys680](https://doi.org/10.1038/nphys680).
- [41] Rumi De, Assaf Zemel, and Samuel A. Safran. "Do Cells Sense Stress or Strain? Measurement of Cellular Orientation Can Provide a Clue." In: *Biophysical Journal* 94.5 (2008), pp. L29–L31. DOI: [10.1529/biophysj.107.126060](https://doi.org/10.1529/biophysj.107.126060).
- [42] Shinji Deguchi, Toshiro Ohashi, and Masaaki Sato. "Tensile properties of single stress fibers isolated from cultured vascular smooth muscle cells." In: *Journal of Biomechanics* 39.14 (2006), pp. 2603–2610. DOI: [10.1016/j.jbiomech.2005.08.026](https://doi.org/10.1016/j.jbiomech.2005.08.026).
- [43] Martin Deibler, Joachim P. Spatz, and Ralf Kemkemer. "Actin Fusion Proteins Alter the Dynamics of Mechanically Induced Cytoskeleton Rearrangement." In: *PLoS ONE* 6.8 (2011). Ed. by Laurent Kreplak, e22941. DOI: [10.1371/journal.pone.0022941](https://doi.org/10.1371/journal.pone.0022941).
- [44] Gianpietro Del Piero and David R. Owen. "Structured deformations of continua." In: *Archive for Rational Mechanics and Analysis* 124.2 (1993), pp. 99–155. DOI: [10.1007/bf00375133](https://doi.org/10.1007/bf00375133).
- [45] Gianpietro Del Piero and David R. Owen. "Structured Deformations, XXII Scuola Estiva di Fisica Matematica, Ravello - Settembre 1997." In: *Quaderni dell'Istituto Nazionale di Fisica Matematica* (2000).
- [46] Micah Dembo and Y. Wang. "Stresses at the Cell-to-Substrate Interface during Locomotion of Fibroblasts." In: *Biophysical Journal* 76.4 (1999), pp. 2307–2316. DOI: [10.1016/s0006-3495\(99\)77386-8](https://doi.org/10.1016/s0006-3495(99)77386-8).

- [47] L. Deseri and D. R. Owen. "Stable disarrangement phases of elastic aggregates: a setting for the emergence of no-tension materials with non-linear response in compression." In: *Meccanica* 49.12 (2014), pp. 2907–2932. ISSN: 1572-9648. DOI: [10.1007/s11012-014-0042-7](https://doi.org/10.1007/s11012-014-0042-7).
- [48] L. Deseri and D.R. Owen. "Invertible structured deformations and the geometry of multiple slip in single crystals." In: *International Journal of Plasticity* 18.7 (2002), pp. 833–849. DOI: [10.1016/s0749-6419\(01\)00010-9](https://doi.org/10.1016/s0749-6419(01)00010-9).
- [49] L. Deseri and D.R. Owen. "Stable disarrangement phases arising from expansion/contraction or from simple shearing of a model granular medium." In: *International Journal of Engineering Science* 96 (2015), pp. 111–130. DOI: [10.1016/j.ijengsci.2015.08.001](https://doi.org/10.1016/j.ijengsci.2015.08.001).
- [50] L. Deseri, P. Pollaci, M. Zingales, and K. Dayal. "Fractional hereditarity of lipid membranes: Instabilities and linearized evolution." In: *Journal of the Mechanical Behavior of Biomedical Materials* 58 (2016), pp. 11–27. DOI: [10.1016/j.jmbbm.2015.09.021](https://doi.org/10.1016/j.jmbbm.2015.09.021).
- [51] Luca Deseri and David R. Owen. "Toward a Field Theory for Elastic Bodies Undergoing Disarrangements." In: *Journal of Elasticity* 70.1-3 (2003), pp. 197–236. DOI: [10.1023/b:elas.0000005584.22658.b3](https://doi.org/10.1023/b:elas.0000005584.22658.b3).
- [52] Luca Deseri and David R. Owen. "Submacroscopically Stable Equilibria of Elastic Bodies Undergoing Disarrangements and Dissipation." In: *Mathematics and Mechanics of Solids* 15.6 (2010), pp. 611–638. DOI: [10.1177/1081286509106101](https://doi.org/10.1177/1081286509106101).
- [53] Luca Deseri and David R. Owen. "Submacroscopic Disarrangements Induce a Unique, Additive and Universal Decomposition of Continuum Fluxes." In: *Journal of Elasticity* 122.2 (2015), pp. 223–230. DOI: [10.1007/s10659-015-9542-5](https://doi.org/10.1007/s10659-015-9542-5).
- [54] Luca Deseri, Mario Di Paola, Massimiliano Zingales, and Pietro Pollaci. "Power-law hereditarity of hierarchical fractal bones." In: *International Journal for Numerical Methods in Biomedical Engineering* 29.12 (2013), pp. 1338–1360. DOI: [10.1002/cnm.2572](https://doi.org/10.1002/cnm.2572).
- [55] C. F. Dewey, S. R. Bussolari, M. A. Gimbrone, and P. F. Davies. "The Dynamic Response of Vascular Endothelial Cells to Fluid Shear Stress." In: *Journal of Biomechanical Engineering* 103.3 (1981), p. 177. DOI: [10.1115/1.3138276](https://doi.org/10.1115/1.3138276).

- [56] Ken Dill and Sarina Bromberg. *Molecular driving forces: statistical thermodynamics in biology, chemistry, physics, and nanoscience*. Garland Science, 2012.
- [57] Dennis E. Discher, Paul Janmey, and Yu-li Wang. "Tissue cells feel and respond to the stiffness of their substrate." In: *Science* 310.5751 (2005), pp. 1139–1143.
- [58] Kevin Doxzen, Sri Ram Krishna Vedula, Man Chun Leong, Hiroaki Hirata, Nir S. Gov, Alexandre J. Kabla, Benoit Ladoux, and Chwee Teck Lim. "Guidance of collective cell migration by substrate geometry." In: *Integrative Biology* 5.8 (2013), p. 1026. DOI: [10.1039/c3ib40054a](https://doi.org/10.1039/c3ib40054a).
- [59] M Eastwood, VC Mudera, DA McGrouther, and RA Brown. "Effect of precise mechanical loading on fibroblast populated collagen lattices: morphological changes." In: *Cell motility and the cytoskeleton* 40.1 (1998), pp. 13–21.
- [60] Paul Egan, Robert Sinko, Philip R. LeDuc, and Sinan Keten. "The role of mechanics in biological and bio-inspired systems." In: *Nature Communications* 6.1 (2015). DOI: [10.1038/ncomms8418](https://doi.org/10.1038/ncomms8418).
- [61] Joachim W. Ellwart, Hans Brettel, and Lorenz O. Kober. "Cell membrane damage by ultrasound at different cell concentrations." In: *Ultrasound in Medicine & Biology* 14.1 (1988), pp. 43–50. DOI: [10.1016/0301-5629\(88\)90162-7](https://doi.org/10.1016/0301-5629(88)90162-7).
- [62] Adam J Engler, Shamik Sen, H Lee Sweeney, and Dennis E Discher. "Matrix elasticity directs stem cell lineage specification." In: *Cell* 126.4 (2006), pp. 677–689.
- [63] E. Evans and A. Yeung. "Apparent viscosity and cortical tension of blood granulocytes determined by micropipet aspiration." In: *Biophysical Journal* 56.1 (1989), pp. 151–160. DOI: [10.1016/s0006-3495\(89\)82660-8](https://doi.org/10.1016/s0006-3495(89)82660-8).
- [64] Jeroen Eyckmans, Thomas Boudou, Xiang Yu, and Christopher S Chen. "A Hitchhiker's guide to mechanobiology." In: *Developmental cell* 21.1 (2011), pp. 35–47.
- [65] Ben Fabry, Geoffrey N. Maksym, James P. Butler, Michael Glogauer, Daniel Navajas, and Jeffrey J. Fredberg. "Scaling the Microrheology of Living Cells." In: *Physical Review Letters* 87.14 (2001). DOI: [10.1103/physrevlett.87.148102](https://doi.org/10.1103/physrevlett.87.148102).

- [66] Ben Fabry, Geoffrey N. Maksym, Stephanie A. Shore, Paul E. Moore, Reynold A. Panettieri, James P. Butler, and Jeffrey J. Fredberg. "Selected Contribution: Time course and heterogeneity of contractile responses in cultured human airway smooth muscle cells." In: *Journal of Applied Physiology* 91.2 (2001), pp. 986–994. DOI: [10.1152/jappl.2001.91.2.986](https://doi.org/10.1152/jappl.2001.91.2.986).
- [67] M. Fraldi, F. Carannante, and L. Nunziante. "Analytical solutions for n-phase Functionally Graded Material Cylinders under de Saint Venant load conditions: Homogenization and effects of Poisson ratios on the overall stiffness." In: *Composites Part B: Engineering* 45.1 (2013), pp. 1310–1324. ISSN: 1359-8368. DOI: <https://doi.org/10.1016/j.compositesb.2012.09.016>.
- [68] M. Fraldi, A. Cugno, L. Deseri, K. Dayal, and N. M. Pugno. "A frequency-based hypothesis for mechanically targeting and selectively attacking cancer cells." In: *J. R. Soc. Interface* 12.111 (2015), p. 20150656. DOI: [10.1098/rsif.2015.0656](https://doi.org/10.1098/rsif.2015.0656).
- [69] Massimiliano Fraldi and Angelo R. Carotenuto. "Cells competition in tumor growth poroelasticity." In: *Journal of the Mechanics and Physics of Solids* 112 (2018), pp. 345–367. ISSN: 0022-5096. DOI: <https://doi.org/10.1016/j.jmps.2017.12.015>.
- [70] Fernando Fraternali, Gerardo Carpentieri, and Ada Amendola. "On the mechanical modeling of the extreme softening/stiffening response of axially loaded tensegrity prisms." In: *Journal of the Mechanics and Physics of Solids* 74 (2015), pp. 136–157. ISSN: 00225096. DOI: [10.1016/j.jmps.2014.10.010](https://doi.org/10.1016/j.jmps.2014.10.010). eprint: [1406.1913](https://arxiv.org/abs/1406.1913).
- [71] Yuan-Cheng Fung. *Biomechanics*. Springer New York, 1993. DOI: [10.1007/978-1-4757-2257-4](https://doi.org/10.1007/978-1-4757-2257-4).
- [72] Sabato Fusco, Valeria Panzetta, and Paolo A. Netti. "Mechanosensing of substrate stiffness regulates focal adhesions dynamics in cell." In: *Meccanica* 52.14 (2017), pp. 3389–3398. ISSN: 1572-9648. DOI: [10.1007/s11012-017-0676-3](https://doi.org/10.1007/s11012-017-0676-3).
- [73] M. L. Gardel. "Elastic Behavior of Cross-Linked and Bundled Actin Networks." In: *Science* 304.5675 (2004), pp. 1301–1305. DOI: [10.1126/science.1095087](https://doi.org/10.1126/science.1095087).
- [74] Margaret L. Gardel, Karen E. Kasza, Clifford P. Brangwynne, Jiayu Liu, and David A. Weitz. "Mechanical Response of Cytoskeletal Networks." In: *Methods in Cell Biology* 89.08 (2008), pp. 487–519. ISSN: 0091679X. DOI: [10.1016/S0091-679X\(08\)00619-5](https://doi.org/10.1016/S0091-679X(08)00619-5).

- [75] Benjamin Geiger, Joachim P. Spatz, and Alexander D. Bershadsky. "Environmental sensing through focal adhesions." In: *Nature Reviews Molecular Cell Biology* 10.1 (2009), pp. 21–33. DOI: [10.1038/nrm2593](https://doi.org/10.1038/nrm2593).
- [76] Benjamin Geiger, Alexander Bershadsky, Roumen Pankov, and Kenneth M. Yamada. "Transmembrane crosstalk between the extracellular matrix and the cytoskeleton." In: *Nature Reviews Molecular Cell Biology* 2.11 (2001), pp. 793–805. DOI: [10.1038/35099066](https://doi.org/10.1038/35099066).
- [77] Marion Ghibaudo, Alexandre Saez, Lea Trichet, Alain Xayaphoumine, Julien Browaeys, Pascal Silberzan, Axel Buguin, and Benoit Ladoux. "Traction forces and rigidity sensing regulate cell functions." In: 4 (Aug. 2008).
- [78] F. Gittes. "Flexural rigidity of microtubules and actin filaments measured from thermal fluctuations in shape." In: *The Journal of Cell Biology* 120.4 (1993), pp. 923–934. DOI: [10.1083/jcb.120.4.923](https://doi.org/10.1083/jcb.120.4.923).
- [79] Zahra Goli-Malekabi, Mohammad Tafazzoli-Shadpour, Mohsen Rabbani, and Mohsen Janmaleki. "Effect of uniaxial stretch on morphology and cytoskeleton of human mesenchymal stem cells: static vs. dynamic loading." In: *Biomedizinische Technik/Biomedical Engineering* 56.5 (2011), pp. 259–265. DOI: [10.1515/bmt.2011.109](https://doi.org/10.1515/bmt.2011.109).
- [80] Roman Golkov and Yair Shokef. "Shape regulation generates elastic interaction between living cells." In: *New Journal of Physics* 19.6 (2017), p. 063011. DOI: [10.1088/1367-2630/aa70ef](https://doi.org/10.1088/1367-2630/aa70ef).
- [81] James Gray. *How Animals Move*. Cambridge University Press, 1953.
- [82] Marcelo Greco and Ivone Passos Ferreira. "Logarithmic strain measure applied to the nonlinear positional formulation for space truss analysis." In: *Finite Elements in Analysis and Design* 45.10 (2009), pp. 632–639. DOI: [10.1016/j.finel.2009.05.005](https://doi.org/10.1016/j.finel.2009.05.005).
- [83] Michael Greshko. *How Many Cells Are in the Human Body-And How Many Microbes?* 2016. URL: <https://news.nationalgeographic.com/2016/01/160111-microbiome-estimate-count-ratio-human-health-science/>.
- [84] Jochen Guck et al. "Optical Deformability as an Inherent Cell Marker for Testing Malignant Transformation and Metastatic Competence." In: *Biophysical Journal* 88.5 (2005), pp. 3689–3698. DOI: [10.1529/biophysj.104.045476](https://doi.org/10.1529/biophysj.104.045476).

- [85] Morton E. Gurtin, Eliot Fried, and Lallit Anand. *The Mechanics and Thermodynamics of Continua*. Cambridge University Press, 2009. DOI: [10.1017/cbo9780511762956](https://doi.org/10.1017/cbo9780511762956).
- [86] K. Haase and A. E. Pelling. "Investigating cell mechanics with atomic force microscopy." In: *Journal of The Royal Society Interface* 12.104 (2015), pp. 20140970–20140970. DOI: [10.1098/rsif.2014.0970](https://doi.org/10.1098/rsif.2014.0970).
- [87] Yuefeng Han, Stephen C. Cowin, Mitchell B. Schaffler, and Sheldon Weinbaum. "Mechanotransduction and strain amplification in osteocyte cell processes." In: *Proceedings of the National Academy of Sciences* 101.47 (2004), pp. 16689–16694. ISSN: 0027-8424. DOI: [10.1073/pnas.0407429101](https://doi.org/10.1073/pnas.0407429101).
- [88] A. Harris, P Wild, and D Stopak. "Silicone rubber substrata: a new wrinkle in the study of cell locomotion." In: *Science* 208.4440 (1980), pp. 177–179. DOI: [10.1126/science.6987736](https://doi.org/10.1126/science.6987736).
- [89] Albert K. Harris, David Stopak, and Patricia Wild. "Fibroblast traction as a mechanism for collagen morphogenesis." In: *Nature* 290.5803 (1981), pp. 249–251. DOI: [10.1038/290249a0](https://doi.org/10.1038/290249a0).
- [90] Kimihide Hayakawa, Naruki Sato, and Takashi Obinata. "Dynamic Reorientation of Cultured Cells and Stress Fibers under Mechanical Stress from Periodic Stretching." In: *Experimental Cell Research* 268.1 (2001), pp. 104–114. DOI: [10.1006/excr.2001.5270](https://doi.org/10.1006/excr.2001.5270).
- [91] Shijie He, Yewang Su, Baohua Ji, and Huajian Gao. "Some basic questions on mechanosensing in cell-substrate interaction." In: *Journal of the Mechanics and Physics of Solids* 70 (2014), pp. 116–135. DOI: [10.1016/j.jmps.2014.05.016](https://doi.org/10.1016/j.jmps.2014.05.016).
- [92] John Heddon. "Violin bow." Pat. 2252929. US Patent 2252929. 1941.
- [93] R. Hill. "On constitutive inequalities for simple materials-I." In: *Journal of the Mechanics and Physics of Solids* 16.4 (1968), pp. 229–242. DOI: [10.1016/0022-5096\(68\)90031-8](https://doi.org/10.1016/0022-5096(68)90031-8).
- [94] Anne Hoger. "The stress conjugate to logarithmic strain." In: *International Journal of Solids and Structures* 23.12 (1987), pp. 1645–1656. DOI: [10.1016/0020-7683\(87\)90115-6](https://doi.org/10.1016/0020-7683(87)90115-6).
- [95] G. A. Holzapfel. *Nonlinear Solid Mechanics: A Continuum Approach for Engineering*. Wiley, 2000.

- [96] Gerhard A. Holzapfel, Thomas C. Gasser, and Ray W. Ogden. "A New Constitutive Framework for Arterial Wall Mechanics and a Comparative Study of Material Models." In: *Journal of elasticity and the physical science of solids* 61.1 (2000), pp. 1–48. ISSN: 1573-2681. DOI: [10.1023/A:1010835316564](https://doi.org/10.1023/A:1010835316564).
- [97] Scott L. Hooper, Kevin H. Hobbs, and Jeffrey B. Thuma. "Invertebrate muscles: Thin and thick filament structure, molecular basis of contraction and its regulation, catch and asynchronous muscle." In: *Progress in Neurobiology* 86.2 (2008), pp. 72–127. DOI: [10.1016/j.pneurobio.2008.06.004](https://doi.org/10.1016/j.pneurobio.2008.06.004).
- [98] Hui-Ju Hsu, Chin-Fu Lee, and Roland Kaunas. "A dynamic stochastic model of frequency-dependent stress fiber alignment induced by cyclic stretch." In: *PloS one* 4.3 (2009), e4853.
- [99] Shaohua Hu, Jianxin Chen, and Ning Wang. "Cell spreading controls balance of prestress by microtubules and extracellular matrix." In: *Frontiers in bioscience : a journal and virtual library* 9 (Sept. 2004), pp. 2177–82. DOI: [10.2741/1352](https://doi.org/10.2741/1352).
- [100] J.D. Humphrey. "Review Paper: Continuum biomechanics of soft biological tissues." In: *Proceedings of the Royal Society of London. Series A: Mathematical, Physical and Engineering Sciences* 459.2029 (2003), pp. 3–46. DOI: [10.1098/rspa.2002.1060](https://doi.org/10.1098/rspa.2002.1060).
- [101] D. E. Ingber. "Cellular tensegrity: defining new rules of biological design that govern the cytoskeleton." In: *Journal of Cell Science* (1993).
- [102] D. E. Ingber. "TENSEGRITY: THE ARCHITECTURAL BASIS OF CELLULAR MECHANOTRANSDUCTION." In: *Annual Review of Physiology* 59.1 (1997), pp. 575–599. DOI: [10.1146/annurev.physiol.59.1.575](https://doi.org/10.1146/annurev.physiol.59.1.575).
- [103] D. E. Ingber. "Tensegrity I. Cell structure and hierarchical systems biology." In: *Journal of Cell Science* 116.7 (2003), pp. 1157–1173. DOI: [10.1242/jcs.00359](https://doi.org/10.1242/jcs.00359).
- [104] D. E. Ingber and J. D. Jamieson. "Cells as tensegrity structures: Architectural regulation of histodifferentiation by physical forces transduced over basement membrane." In: *Gene Expression during Normal and Malignant Differentiation*. (1985).

- [105] D. E. Ingber, J. A. Madri, and J. D. Jamieson. "Role of basal lamina in neoplastic disorganization of tissue architecture." In: *Proceedings of the National Academy of Sciences* 78.6 (1981), pp. 3901–3905. DOI: [10.1073/pnas.78.6.3901](https://doi.org/10.1073/pnas.78.6.3901).
- [106] Donald E Ingber, Ning Wang, and Dimitrije Stamenovic. "Tensegrity, cellular biophysics, and the mechanics of living systems." In: *Reports on progress in physics. Physical Society (Great Britain)* 77.4 (2014), p. 046603. ISSN: 1361-6633. DOI: [10.1088/0034-4885/77/4/046603](https://doi.org/10.1088/0034-4885/77/4/046603).
- [107] Thomas Iskratsch, Haguy Wolfenson, and Michael P. Sheetz. "Appreciating force and shape — the rise of mechanotransduction in cell biology." In: *Nature Reviews Molecular Cell Biology* 15.12 (2014), pp. 825–833. DOI: [10.1038/nrm3903](https://doi.org/10.1038/nrm3903).
- [108] P A Janmey, U Euteneuer, P Traub, and M Schliwa. "Viscoelastic properties of vimentin compared with other filamentous biopolymer networks." In: *The Journal of Cell Biology* 113.1 (1991), pp. 155–160. ISSN: 0021-9525. DOI: [10.1083/jcb.113.1.155](https://doi.org/10.1083/jcb.113.1.155). eprint: <http://jcb.rupress.org/content/113/1/155.full.pdf>.
- [109] K. L. Johnson. *Contact Mechanics*. Cambridge University Press, 1985. DOI: [10.1017/cbo9781139171731](https://doi.org/10.1017/cbo9781139171731).
- [110] Simon Jungbauer, Huajian Gao, Joachim P. Spatz, and Ralf Kemker. "Two Characteristic Regimes in Frequency-Dependent Dynamic Reorientation of Fibroblasts on Cyclically Stretched Substrates." In: *Biophysical Journal* 95.7 (2008), pp. 3470–3478. DOI: [10.1529/biophysj.107.128611](https://doi.org/10.1529/biophysj.107.128611).
- [111] Atsushi Kakogawa, Soo Jeon, and Shugen Ma. "Stiffness Design of a Resonance-Based Planar Snake Robot With Parallel Elastic Actuators." In: *IEEE Robotics and Automation Letters* 3.2 (2018), pp. 1284–1291. DOI: [10.1109/lra.2018.2797261](https://doi.org/10.1109/lra.2018.2797261).
- [112] Roland Kaunas and Hui-Ju Hsu. "A kinematic model of stretch-induced stress fiber turnover and reorientation." In: *Journal of Theoretical Biology* 257.2 (2009), pp. 320–330. ISSN: 0022-5193. DOI: <https://doi.org/10.1016/j.jtbi.2008.11.024>.
- [113] K. Kebiche, M.N. Kazi-Aoual, and R. Motro. "Geometrical non-linear analysis of tensegrity systems." In: *Engineering Structures* 21.9 (1999), pp. 864–876. DOI: [10.1016/s0141-0296\(98\)00014-5](https://doi.org/10.1016/s0141-0296(98)00014-5).

- [114] Alperen N. Ketene, Eva M. Schmelz, Paul C. Roberts, and Masoud Agah. "The effects of cancer progression on the viscoelasticity of ovarian cell cytoskeleton structures." In: *Nanomedicine: Nanotechnology, Biology and Medicine* 8.1 (2012), pp. 93–102. DOI: [10.1016/j.nano.2011.05.012](https://doi.org/10.1016/j.nano.2011.05.012).
- [115] Taeyoon Kim, Wonmuk Hwang, Hyungsuk Lee, and Roger D. Kamm. "Computational Analysis of Viscoelastic Properties of Crosslinked Actin Networks." In: *PLOS Computational Biology* 5.7 (July 2009), pp. 1–13. DOI: [10.1371/journal.pcbi.1000439](https://doi.org/10.1371/journal.pcbi.1000439).
- [116] Tyler J. Kirby and Jan Lammerding. "Emerging views of the nucleus as a cellular mechanosensor." In: *Nature Cell Biology* 20.4 (2018), pp. 373–381. ISSN: 1476-4679.
- [117] P. Kollmannsberger, C. M. Bidan, J. W. C. Dunlop, and P. Fratzl. "The physics of tissue patterning and extracellular matrix organisation: how cells join forces." In: *Soft Matter* 7.20 (2011), p. 9549. DOI: [10.1039/c1sm05588g](https://doi.org/10.1039/c1sm05588g).
- [118] Dong Kong, Baohua Ji, and Lanhong Dai. "Stability of adhesion clusters and cell reorientation under lateral cyclic tension." In: *Biophysical journal* 95.8 (2008), pp. 4034–4044.
- [119] Roderic Lakes. "Foam Structures with a Negative Poisson's Ratio." In: *Science* 235.4792 (1987), pp. 1038–1040. ISSN: 0036-8075. DOI: [10.1126/science.235.4792.1038](https://doi.org/10.1126/science.235.4792.1038).
- [120] Lev D Landau and EM Lifshitz. *Theory of Elasticity*. Vol. 7. Pergamon, 1970.
- [121] Janina R. Lange, Julian Steinwachs, Thorsten Kolb, Lena A. Lautscham, Irina Harder, Graeme Whyte, and Ben Fabry. "Microconstriction Arrays for High-Throughput Quantitative Measurements of Cell Mechanical Properties." In: *Biophysical Journal* 109.1 (2015), pp. 26–34. DOI: [10.1016/j.bpj.2015.05.029](https://doi.org/10.1016/j.bpj.2015.05.029).
- [122] K. A. Lazopoulos and N. K. Lazopoulou. "On the elastica solution of a tensegrity structure: Application to cell mechanics." In: *Acta Mechanica* 182.3-4 (2006), pp. 253–263. DOI: [10.1007/s00707-005-0288-1](https://doi.org/10.1007/s00707-005-0288-1).
- [123] K.A. Lazopoulos. "Stability of an elastic cytoskeletal tensegrity model." In: *International Journal of Solids and Structures* 42.11-12 (2005), pp. 3459–3469. DOI: [10.1016/j.ijsolstr.2004.11.008](https://doi.org/10.1016/j.ijsolstr.2004.11.008).

- [124] Konstantinos A. Lazopoulos and Dimitrije Stamenović. "Durotaxis as an elastic stability phenomenon." In: *Journal of Biomechanics* 41.6 (2008), pp. 1289–1294. DOI: [10.1016/j.jbiomech.2008.01.008](https://doi.org/10.1016/j.jbiomech.2008.01.008).
- [125] Flavio Lejbkowicz and Samuel Salzberg. "Distinct Sensitivity of Normal and Malignant Cells to Ultrasound in Vitro." In: *Environmental Health Perspectives* 105 (1997), p. 1575. DOI: [10.2307/3433673](https://doi.org/10.2307/3433673).
- [126] Flavio Lejbkowicz, Mordechai Zwiran, and Samuel Salzberg. "The response of normal and malignant cells to ultrasound in vitro." In: *Ultrasound in Medicine and Biology* 19.1 (1993), pp. 75–82. DOI: [10.1016/0301-5629\(93\)90020-o](https://doi.org/10.1016/0301-5629(93)90020-o).
- [127] M. Lekka, P. Laidler, D. Gil, J. Lekki, Z. Stachura, and A. Z. Hryniewicz. "Elasticity of normal and cancerous human bladder cells studied by scanning force microscopy." In: *European Biophysics Journal* 28.4 (1999), pp. 312–316. DOI: [10.1007/s002490050213](https://doi.org/10.1007/s002490050213).
- [128] Fan Li, Lifang Jin, Huiping Wang, Fang Wei, Min Bai, Qiusheng Shi, and Lianfang Du. "The dual effect of ultrasound-targeted microbubble destruction in mediating recombinant adeno-associated virus delivery in renal cell carcinoma: transfection enhancement and tumor inhibition." In: *The Journal of Gene Medicine* 16.1-2 (2014), pp. 28–39. DOI: [10.1002/jgm.2755](https://doi.org/10.1002/jgm.2755).
- [129] Teng Li. "A mechanics model of microtubule buckling in living cells." In: *Journal of Biomechanics* 41.8 (2008), pp. 1722–1729. DOI: [10.1016/j.jbiomech.2008.03.003](https://doi.org/10.1016/j.jbiomech.2008.03.003).
- [130] C. T. Lim, A. Bershadsky, and M. P. Sheetz. "Mechanobiology." In: *Journal of The Royal Society Interface* 7 (2010), S291–S293. DOI: [10.1098/rsif.2010.0150.focus](https://doi.org/10.1098/rsif.2010.0150.focus).
- [131] C.T. Lim, E.H. Zhou, and S.T. Quek. "Mechanical models for living cells - a review." In: *Journal of Biomechanics* 39.2 (2006), pp. 195–216. DOI: [10.1016/j.jbiomech.2004.12.008](https://doi.org/10.1016/j.jbiomech.2004.12.008).
- [132] Jung Yul Lim and Henry J. Donahue. "Cell Sensing and Response to Micro- and Nanostructured Surfaces Produced by Chemical and Topographic Patterning." In: *Tissue Engineering* 13.8 (2007), pp. 1879–1891. DOI: [10.1089/ten.2006.0154](https://doi.org/10.1089/ten.2006.0154).

- [133] Feng Lin, Feng Du, Jianyong Huang, Alicia Chau, Yongsheng Zhou, Huiling Duan, Jianxiang Wang, and Chunyang Xiong. "Substrate effect modulates adhesion and proliferation of fibroblast on graphene layer." In: *Colloids and Surfaces B: Biointerfaces* 146 (2016), pp. 785–793. DOI: [10.1016/j.colsurfb.2016.07.008](https://doi.org/10.1016/j.colsurfb.2016.07.008).
- [134] C. Liu, S. Baek, J. Kim, E. Vasko, R. Pyne, and C. Chan. "Effect of Static Pre-stretch Induced Surface Anisotropy on Orientation of Mesenchymal Stem Cells." In: *Cellular and Molecular Bioengineering* 7.1 (2013), pp. 106–121. DOI: [10.1007/s12195-013-0300-0](https://doi.org/10.1007/s12195-013-0300-0).
- [135] Ke Liu, Jiangtao Wu, Glaucio H. Paulino, and H. Jerry Qi. "Programmable Deployment of Tensegrity Structures by Stimulus-Responsive Polymers." In: *Scientific Reports* 7.1 (2017). DOI: [10.1038/s41598-017-03412-6](https://doi.org/10.1038/s41598-017-03412-6).
- [136] Xiumei Liu and Gerald H. Pollack. "Mechanics of F-Actin Characterized with Microfabricated Cantilevers." In: *Biophysical Journal* 83.5 (2002), pp. 2705–2715. DOI: [10.1016/s0006-3495\(02\)75280-6](https://doi.org/10.1016/s0006-3495(02)75280-6).
- [137] Ariel Livne, Eran Bouchbinder, and Benjamin Geiger. "Cell re-orientation under cyclic stretching." In: *Nature Communications* 5 (2014). DOI: [10.1038/ncomms4938](https://doi.org/10.1038/ncomms4938).
- [138] C. Lo, H. Wang, Micah Dembo, and Y. Wang. "Cell Movement Is Guided by the Rigidity of the Substrate." In: *Biophysical Journal* 79.1 (2000), pp. 144–152. DOI: [10.1016/s0006-3495\(00\)76279-5](https://doi.org/10.1016/s0006-3495(00)76279-5).
- [139] Augustus Edward Hough Love. *A treatise on the mathematical theory of elasticity*. Cambridge university press, 1982.
- [140] V.A. Lubarda and A. Hoger. "On the mechanics of solids with a growing mass." In: *International Journal of Solids and Structures* 39.18 (2002), pp. 4627–4664. DOI: [10.1016/s0020-7683\(02\)00352-9](https://doi.org/10.1016/s0020-7683(02)00352-9).
- [141] Yaozhi Luo, Xian Xu, Tanmay Lele, Sanjay Kumar, and Donald E. Ingber. "A multi-modular tensegrity model of an actin stress fiber." In: *Journal of Biomechanics* 41.11 (2008), pp. 2379–2387. DOI: [10.1016/j.jbiomech.2008.05.026](https://doi.org/10.1016/j.jbiomech.2008.05.026).
- [142] Timothy M. Maul, Douglas W. Chew, Alejandro Nieponice, and David A. Vorp. "Mechanical stimuli differentially control stem cell behavior: morphology, proliferation, and differentiation." In: *Biomechanics and Modeling in Mechanobiology* 10.6 (2011), pp. 939–953. DOI: [10.1007/s10237-010-0285-8](https://doi.org/10.1007/s10237-010-0285-8).

- [143] Jakob M. A. Mauritz, Alessandro Esposito, Teresa Tiffert, Jeremy N. Skepper, Alice Warley, Young-Zoon Yoon, Pietro Cicuta, Virgilio L. Lew, Jochen R. Guck, and Clemens F. Kaminski. "Biophotonic techniques for the study of malaria-infected red blood cells." In: *Medical & Biological Engineering & Computing* 48.10 (2010), pp. 1055–1063. DOI: [10.1007/s11517-010-0668-0](https://doi.org/10.1007/s11517-010-0668-0).
- [144] Ron Milo and Rob Phillips. *Cell Biology by the Numbers*. Garland Science, 2015.
- [145] Natalya Mizrahi, Enhua H. Zhou, Guillaume Lenormand, Ramaswamy Krishnan, Daphne Weihs, James P. Butler, David A. Weitz, Jeffrey J. Fredberg, and Eitan Kimmel. "Low intensity ultrasound perturbs cytoskeleton dynamics." In: *Soft Matter* 8.8 (2012), p. 2438. DOI: [10.1039/c2sm07246g](https://doi.org/10.1039/c2sm07246g).
- [146] Mohammad R. K. Mofrad and Roger D. Kamm, eds. *Cellular Mechanotransduction*. Cambridge University Press (CUP), 2009. DOI: [10.1017/cbo9781139195874](https://doi.org/10.1017/cbo9781139195874).
- [147] Mohammad RK Mofrad and Roger D Kamm. *Cytoskeletal mechanics: models and measurements in cell mechanics*. Cambridge University Press, 2006.
- [148] Hamid Mohammadi and Erik Sahai. "Mechanisms and impact of altered tumour mechanics." In: *Nature Cell Biology* 20.7 (2018), pp. 766–774. ISSN: 1476-4679.
- [149] R. Motro. *Tensegrity: structural systems for the future*. Kogan Page Science, 2003.
- [150] Ingo Müller. "Two instructive instabilities in non-linear elasticity: Biaxially loaded membrane, and rubber balloons." In: *Mechanica* 31.4 (1996), pp. 387–395. ISSN: 1572-9648. DOI: [10.1007/BF00429927](https://doi.org/10.1007/BF00429927).
- [151] H. Murakami and Y. Nishimura. "Static and Dynamic Characterization of Some Tensegrity Modules." In: *Journal of Applied Mechanics* 68.1 (2001), p. 19. DOI: [10.1115/1.1331058](https://doi.org/10.1115/1.1331058).
- [152] Francesco Nappi, Angelo Rosario Carotenuto, Donato Di Vito, Cristiano Spadaccio, Cristophe Acar, and Massimiliano Fraldi. "Stress-shielding, growth and remodeling of pulmonary artery reinforced with copolymer scaffold and transposed into aortic position." In: *Biomechanics and Modeling in Mechanobiology* 15.5 (2015), pp. 1141–1157. DOI: [10.1007/s10237-015-0749-y](https://doi.org/10.1007/s10237-015-0749-y).

- [153] C. M. Nelson, R. P. Jean, J. L. Tan, W. F. Liu, N. J. Sniadecki, A. A. Spector, and C. S. Chen. "Emergent patterns of growth controlled by multicellular form and mechanics." In: *Proceedings of the National Academy of Sciences* 102.33 (2005), pp. 11594–11599. DOI: [10.1073/pnas.0502575102](https://doi.org/10.1073/pnas.0502575102).
- [154] Siavouche Nemat-Nasser and Muneo Hori. *Micromechanics: Overall Properties of Heterogeneous Materials*. Elsevier, 1999.
- [155] R. M. Nerem. "Vascular Endothelial Morphology as an Indicator of the Pattern of Blood Flow." In: *Journal of Biomechanical Engineering* 103.3 (1981), p. 172. DOI: [10.1115/1.3138275](https://doi.org/10.1115/1.3138275).
- [156] Kendra D. Nyberg, Kenneth H. Hu, Sara H. Kleinman, Damir B. Khismatullin, Manish J. Butte, and Amy C. Rowat. "Quantitative Deformability Cytometry: Rapid, Calibrated Measurements of Cell Mechanical Properties." In: *Biophysical Journal* 113.7 (2017), pp. 1574–1584. DOI: [10.1016/j.bpj.2017.06.073](https://doi.org/10.1016/j.bpj.2017.06.073).
- [157] I.J. Oppenheim and W.O. Williams. "Geometric Effects in an Elastic Tensegrity Structure." In: *Journal of elasticity and the physical science of solids* 59.1 (2000), pp. 51–65. ISSN: 1573-2681. DOI: [10.1023/A:1011092811824](https://doi.org/10.1023/A:1011092811824).
- [158] David R. Owen. "Structured deformations and the refinements of balance laws induced by microslip." In: *International Journal of Plasticity* 14.1-3 (1998), pp. 289–299. DOI: [10.1016/s0749-6419\(97\)00057-0](https://doi.org/10.1016/s0749-6419(97)00057-0).
- [159] David R. Owen. "Elasticity with Disarrangements." In: *Multiscale Modeling in Continuum Mechanics and Structured Deformations*. Ed. by Gianpietro Del Piero and David R. Owen. Vol. 447. CISM Courses and Lectures. Springer Vienna, 2004, pp. 231–275. DOI: [10.1007/978-3-7091-2770-4_7](https://doi.org/10.1007/978-3-7091-2770-4_7).
- [160] David R. Owen. "Elasticity with Gradient-Disarrangements: A Multiscale Perspective for Strain-Gradient Theories of Elasticity and of Plasticity." In: *Journal of Elasticity* 127.1 (2016), pp. 115–150. DOI: [10.1007/s10659-016-9599-9](https://doi.org/10.1007/s10659-016-9599-9).
- [161] M. Pachenari, S.M. Seyedpour, M. Janmaleki, S. Babazadeh Shayan, S. Taranejoo, and H. Hosseinkhani. "Mechanical properties of cancer cytoskeleton depend on actin filaments to microtubules content: Investigating different grades of colon cancer cell lines." In: *Journal of Biomechanics* 47.2 (2014), pp. 373–379. DOI: [10.1016/j.jbiomech.2013.11.020](https://doi.org/10.1016/j.jbiomech.2013.11.020).

- [162] Anna Pandolfi. "The Influence of the Collagen Architecture on the Mechanical Response of the Human Cornea." In: *Computational Methods in Applied Sciences*. Springer International Publishing, 2017, pp. 337–355. DOI: [10.1007/978-3-319-60885-3_16](https://doi.org/10.1007/978-3-319-60885-3_16).
- [163] Anna Pandolfi, Alessio Gizzi, and Marcello Vasta. "Visco-electro-elastic models of fiber-distributed active tissues." In: *Meccanica* 52.14 (2017), pp. 3399–3415. DOI: [10.1007/s11012-017-0622-4](https://doi.org/10.1007/s11012-017-0622-4).
- [164] Mario Di Paola, Francesco Paolo Pinnola, and Massimiliano Zingales. "Fractional differential equations and related exact mechanical models." In: *Computers & Mathematics with Applications* 66.5 (2013), pp. 608–620. DOI: [10.1016/j.camwa.2013.03.012](https://doi.org/10.1016/j.camwa.2013.03.012).
- [165] Amit Pathak, Christopher S. Chen, Anthony G. Evans, and Robert M. McMeeking. "Structural Mechanics Based Model for the Force-Bearing Elements Within the Cytoskeleton of a Cell Adhered on a Bed of Posts." In: *Journal of Applied Mechanics* 79.6 (2012), p. 061020. DOI: [10.1115/1.4006452](https://doi.org/10.1115/1.4006452).
- [166] C. Paul, F.J. Valero-Cuevas, and H. Lipson. "Design and control of tensegrity robots for locomotion." In: *IEEE Transactions on Robotics* 22.5 (2006), pp. 944–957. DOI: [10.1109/tro.2006.878980](https://doi.org/10.1109/tro.2006.878980).
- [167] R. J. Pelham and Yuli Wang. "Cell locomotion and focal adhesions are regulated by substrate flexibility." In: *Proceedings of the National Academy of Sciences* 94.25 (1997), pp. 13661–13665. DOI: [10.1073/pnas.94.25.13661](https://doi.org/10.1073/pnas.94.25.13661).
- [168] Nicoletta I. Petridou, Zoltán Spiró, and Carl-Philipp Heisenberg. "Multiscale force sensing in development." In: *Nature Cell Biology* 19 (May 2017), p. 581.
- [169] Rob Phillips, Jane Kondev, Julie Theriot, and Hernan Garcia. *Physical Biology of the Cell*. Garland Science, 2012. DOI: [10.1201/9781134111589](https://doi.org/10.1201/9781134111589).
- [170] Athanassios P. Pirentis and Konstantinos A. Lazopoulos. "On the orientation of plane tensegrity cytoskeletons under biaxial substrate stretching." In: *Advances in Bioscience and Biotechnology* 01.01 (2010), pp. 12–25. DOI: [10.4236/abb.2010.11003](https://doi.org/10.4236/abb.2010.11003).
- [171] J. Plešek and A. Kruisová. "Formulation, validation and numerical procedures for Hencky's elasticity model." In: *Computers & Structures* 84.17-18 (2006), pp. 1141–1150. DOI: [10.1016/j.compstruc.2006.01.005](https://doi.org/10.1016/j.compstruc.2006.01.005).

- [172] Marija Plodinec et al. "The nanomechanical signature of breast cancer." In: *Nature Nanotechnology* 7 (Oct. 2012), p. 757.
- [173] Marija Plodinec et al. "The nanomechanical signature of breast cancer." In: *Nature Nanotechnology* 7.11 (2012), pp. 757–765. DOI: [10.1038/nnano.2012.167](https://doi.org/10.1038/nnano.2012.167).
- [174] Sergey V. Plotnikov, Benedikt Sabass, Ulrich S. Schwarz, and Clare M. Waterman. "High-Resolution Traction Force Microscopy." In: *Methods in Cell Biology*. Elsevier, 2014, pp. 367–394. DOI: [10.1016/b978-0-12-420138-5.00020-3](https://doi.org/10.1016/b978-0-12-420138-5.00020-3).
- [175] Thomas D Pollard and Gary G Borisy. "Cellular Motility Driven by Assembly and Disassembly of Actin Filaments." In: *Cell* 113.4 (2003), p. 549. DOI: [10.1016/s0092-8674\(03\)00357-x](https://doi.org/10.1016/s0092-8674(03)00357-x).
- [176] Masha Prager-Khoutorsky, Alexandra Lichtenstein, Ramaswamy Krishnan, Kavitha Rajendran, Avi Mayo, Zvi Kam, Benjamin Geiger, and Alexander D. Bershadsky. "Fibroblast polarization is a matrix-rigidity-dependent process controlled by focal adhesion mechanosensing." In: *Nature Cell Biology* 13.12 (2011), pp. 1457–1465. DOI: [10.1038/ncb2370](https://doi.org/10.1038/ncb2370).
- [177] Robyn H Pritchard, Yan Yan Shery Huang, and Eugene M Terentjev. "Mechanics of biological networks: from the cell cytoskeleton to connective tissue." In: *Soft matter* 10.12 (2014), pp. 1864–84. DOI: [10.1039/c3sm52769g](https://doi.org/10.1039/c3sm52769g).
- [178] H. Jerry Qi, Christine Ortiz, and Mary C. Boyce. "Mechanics of Biomacromolecular Networks Containing Folded Domains." In: *Journal of Engineering Materials and Technology* 128.4 (2006), p. 509. DOI: [10.1115/1.2345442](https://doi.org/10.1115/1.2345442).
- [179] Jin Qian, Haipei Liu, Yuan Lin, Weiqiu Chen, and Huajian Gao. "A Mechanochemical Model of Cell Reorientation on Substrates under Cyclic Stretch." In: *PLoS ONE* 8.6 (2013). Ed. by Neil A. Hotchin, e65864. DOI: [10.1371/journal.pone.0065864](https://doi.org/10.1371/journal.pone.0065864).
- [180] Sisi Qin, Vincent Ricotta, Marcia Simon, Richard A. F. Clark, and Miriam H. Rafailovich. "Continual Cell Deformation Induced via Attachment to Oriented Fibers Enhances Fibroblast Cell Migration." In: *PLOS ONE* 10.3 (Mar. 2015), pp. 1–16. DOI: [10.1371/journal.pone.0119094](https://doi.org/10.1371/journal.pone.0119094).

- [181] Charles B. Reilly and Donald E. Ingber. "Multi-scale modeling reveals use of hierarchical tensegrity principles at the molecular, multi-molecular, and cellular levels." In: *Extreme Mechanics Letters* 20 (2018), pp. 21–28. DOI: [10.1016/j.eml.2018.01.001](https://doi.org/10.1016/j.eml.2018.01.001).
- [182] Julian J. Rimoli. "A reduced-order model for the dynamic and post-buckling behavior of tensegrity structures." In: *Mechanics of Materials* 116 (2018). IUTAM Symposium on Dynamic Instabilities in Solids, pp. 146–157. ISSN: 0167-6636. DOI: <https://doi.org/10.1016/j.mechmat.2017.01.009>.
- [183] Julian J. Rimoli and Raj Kumar Pal. "Mechanical response of 3-dimensional tensegrity lattices." In: *Composites Part B: Engineering* 115 (2017). Composite lattices and multiscale innovative materials and structures, pp. 30–42. ISSN: 1359-8368. DOI: <https://doi.org/10.1016/j.compositesb.2016.10.046>.
- [184] Daniel Riveline, Eli Zamir, Nathalie Q Balaban, Ulrich S Schwarz, Toshimasa Ishizaki, Shuh Narumiya, Zvi Kam, Benjamin Geiger, and Alexander D Bershadsky. "Focal contacts as mechanosensors: externally applied local mechanical force induces growth of focal contacts by an mDia1-dependent and ROCK-independent mechanism." In: *The Journal of cell biology* 153.6 (2001), pp. 1175–1186. DOI: [10.1083/jcb.153.6.1175](https://doi.org/10.1083/jcb.153.6.1175).
- [185] R. S. Rivlin. "Large elastic deformations of isotropic materials. I. Fundamental concepts." In: *Philosophical Transactions of the Royal Society of London A: Mathematical, Physical and Engineering Sciences* 240.822 (1948), pp. 459–490. ISSN: 0080-4614. DOI: [10.1098/rsta.1948.0002](https://doi.org/10.1098/rsta.1948.0002).
- [186] Pere Roca-Cusachs, Vito Conte, and Xavier Trepac. "Quantifying forces in cell biology." In: *Nature Cell Biology* 19 (June 2017), p. 742.
- [187] D. F. Rolfe and G. C. Brown. "Cellular energy utilization and molecular origin of standard metabolic rate in mammals." In: *Physiological Reviews* 77.3 (1997), pp. 731–758. DOI: [10.1152/physrev.1997.77.3.731](https://doi.org/10.1152/physrev.1997.77.3.731).
- [188] Michael J. Rosenbluth, Wilbur A. Lam, and Daniel A. Fletcher. "Analyzing cell mechanics in hematologic diseases with microfluidic biophysical flow cytometry." In: *Lab on a Chip* 8.7 (2008), p. 1062. DOI: [10.1039/b802931h](https://doi.org/10.1039/b802931h).

- [189] J. Rosing and E.C. Slater. "The value of ΔG^0 for the hydrolysis of ATP." In: *Biochimica et Biophysica Acta (BBA) - Bioenergetics* 267.2 (1972), pp. 275–290. ISSN: 0005-2728. DOI: [https://doi.org/10.1016/0005-2728\(72\)90116-8](https://doi.org/10.1016/0005-2728(72)90116-8).
- [190] DIMITRIJE STAMENOVIC and MARK F COUGHLIN. "The Role of Prestress and Architecture of the Cytoskeleton and Deformability of Cytoskeletal Filaments in Mechanics of Adherent Cells: a Quantitative Analysis." In: *Journal of Theoretical Biology* 201.1 (1999), pp. 63–74. DOI: [10.1006/jtbi.1999.1014](https://doi.org/10.1006/jtbi.1999.1014).
- [191] Benedikt Sabass, Margaret L. Gardel, Clare M. Waterman, and Ulrich S. Schwarz. "High Resolution Traction Force Microscopy Based on Experimental and Computational Advances." In: *Biophysical Journal* 94.1 (2008), pp. 207–220. DOI: [10.1529/biophysj.107.113670](https://doi.org/10.1529/biophysj.107.113670).
- [192] Maike Schmelter, Bernadette Ateghang, Simone Helmig, Maria Wartenberg, and Heinrich Sauer. "Embryonic stem cells utilize reactive oxygen species as transducers of mechanical strain-induced cardiovascular differentiation." In: *The FASEB Journal* 20.8 (2006), pp. 1182–1184. DOI: [10.1096/fj.05-4723fje](https://doi.org/10.1096/fj.05-4723fje).
- [193] A. Schuster, T. Schwab, M. Bischof, M. Klotz, R. Lemor, C. Degel, and K.H. Schafer. "Cell specific ultrasound effects are dose and frequency dependent." In: *Annals of Anatomy - Anatomischer Anzeiger* 195.1 (2013), pp. 57–67. DOI: [10.1016/j.aanat.2012.03.008](https://doi.org/10.1016/j.aanat.2012.03.008).
- [194] U. S. Schwarz and S. A. Safran. "Elastic Interactions of Cells." In: *Physical Review Letters* 88.4 (2002). DOI: [10.1103/physrevlett.88.048102](https://doi.org/10.1103/physrevlett.88.048102).
- [195] U.S. Schwarz, N.Q. Balaban, D. Rivelino, A. Bershadsky, B. Geiger, and S.A. Safran. "Calculation of Forces at Focal Adhesions from Elastic Substrate Data: The Effect of Localized Force and the Need for Regularization." In: *Biophysical Journal* 83.3 (2002), pp. 1380–1394. DOI: [10.1016/s0006-3495\(02\)73909-x](https://doi.org/10.1016/s0006-3495(02)73909-x).
- [196] Ulrich S. Schwarz and Ilka B. Bischofs. "Physical determinants of cell organization in soft media." In: *Medical Engineering & Physics* 27.9 (2005), pp. 763–772. DOI: [10.1016/j.medengphy.2005.04.007](https://doi.org/10.1016/j.medengphy.2005.04.007).
- [197] Ulrich S. Schwarz and Samuel A. Safran. "Physics of adherent cells." In: *Reviews of Modern Physics* 85.3 (2013), pp. 1327–1381. DOI: [10.1103/revmodphys.85.1327](https://doi.org/10.1103/revmodphys.85.1327).

- [198] J. P. Shelby, J. White, K. Ganesan, P. K. Rathod, and D. T. Chiu. "A microfluidic model for single-cell capillary obstruction by Plasmodium falciparum-infected erythrocytes." In: *Proceedings of the National Academy of Sciences* 100.25 (2003), pp. 14618–14622. DOI: [10.1073/pnas.2433968100](https://doi.org/10.1073/pnas.2433968100).
- [199] Craig A. Simmons, Sean Matlis, Amanda J. Thornton, Shaoqiong Chen, Cun-Yu Wang, and David J. Mooney. "Cyclic strain enhances matrix mineralization by adult human mesenchymal stem cells via the extracellular signal-regulated kinase (ERK1/2) signaling pathway." In: *Journal of Biomechanics* 36.8 (2003), pp. 1087–1096. DOI: [10.1016/s0021-9290\(03\)00110-6](https://doi.org/10.1016/s0021-9290(03)00110-6).
- [200] J.R. Sims, S. Karp, and D.E. Ingber. "Altering the cellular mechanical force balance results in integrated changes in cell, cytoskeletal and nuclear shape." In: *Journal of Cell Science* 103.4 (1992), pp. 1215–1222. ISSN: 0021-9533.
- [201] R.E. Skelton, R. Adhikari, J.-P. Pinaud, Waileung Chan, and J.W. Helton. "An introduction to the mechanics of tensegrity structures." In: *Proceedings of the 40th IEEE Conference on Decision and Control (Cat. No.01CH37228)*. IEEE. DOI: [10.1109/.2001.980861](https://doi.org/10.1109/.2001.980861).
- [202] Robert E. Skelton and Mauricio C. Oliveira. *Tensegrity Systems*. Springer Nature, 2009. DOI: [10.1007/978-0-387-74242-7](https://doi.org/10.1007/978-0-387-74242-7).
- [203] Kenneth D Snelson. "Continuous tension, discontinuous compression structures." Pat. US Patent 3169611. 1965.
- [204] Mohammad Soheilypour, Mohaddeseh Peyro, Stephen J. Peter, and Mohammad R.K. Mofrad. "Buckling Behavior of Individual and Bundled Microtubules." In: *Biophysical Journal* 108.7 (2015), pp. 1718–1726. DOI: [10.1016/j.bpj.2015.01.030](https://doi.org/10.1016/j.bpj.2015.01.030).
- [205] D. Stamenović. "Rheological behavior of mammalian cells." In: *Cellular and Molecular Life Sciences* 65.22 (2008), pp. 3592–3605. DOI: [10.1007/s00018-008-8292-y](https://doi.org/10.1007/s00018-008-8292-y).
- [206] D. Stamenovic and D. E. Ingber. "Models of cytoskeletal mechanics of adherent cells." In: *Biomechanics and Modeling in Mechanobiology* 1.1 (2002), pp. 95–108. DOI: [10.1007/s10237-002-0009-9](https://doi.org/10.1007/s10237-002-0009-9).
- [207] D. Stamenovic, S. M. Mijailovich, I. M. Tolic-Norrelykke, J. Chen, and N. Wang. "Cell prestress. II. Contribution of microtubules." In: *AJP: Cell Physiology* 282.3 (2001), pp. C617–C624. DOI: [10.1152/ajpcell.00271.2001](https://doi.org/10.1152/ajpcell.00271.2001).

- [208] Dimitrije Stamenović. "Effects of cytoskeletal prestress on cell rheological behavior." In: *Acta Biomaterialia* 1.3 (2005), pp. 255–262. DOI: [10.1016/j.actbio.2005.01.004](https://doi.org/10.1016/j.actbio.2005.01.004).
- [209] Dimitrije Stamenovic and Mark F. Coughlin. "A Quantitative Model of Cellular Elasticity Based on Tensegrity." In: *Journal of Biomechanical Engineering* 122.1 (2000), p. 39. DOI: [10.1115/1.429631](https://doi.org/10.1115/1.429631).
- [210] Dimitrije Stamenović and Donald E. Ingber. "Tensegrity-guided self assembly: from molecules to living cells." In: *Soft Matter* 5.6 (2009), pp. 1137–1145. DOI: [10.1039/b806442c](https://doi.org/10.1039/b806442c).
- [211] Dimitrije Stamenović, Jeffrey J. Fredberg, Ning Wang, James P. Butler, and Donald E. Ingber. "A Microstructural Approach to Cytoskeletal Mechanics based on Tensegrity." In: *Journal of Theoretical Biology* 181.2 (1996), pp. 125–136. DOI: [10.1006/jtbi.1996.0120](https://doi.org/10.1006/jtbi.1996.0120).
- [212] Dimitrije Stamenović, Zhuangli Liang, Jianxin Chen, and Ning Wang. "Effect of the cytoskeletal prestress on the mechanical impedance of cultured airway smooth muscle cells." In: *Journal of Applied Physiology* 92.4 (2002), pp. 1443–1450. DOI: [10.1152/jappphysiol.00782.2001](https://doi.org/10.1152/jappphysiol.00782.2001).
- [213] Robert L. Steward, Chao-Min Cheng, Danny L. Wang, and Philip R. LeDuc. "Probing Cell Structure Responses Through a Shear and Stretching Mechanical Stimulation Technique." In: *Cell Biochemistry and Biophysics* 56.2-3 (2009), pp. 115–124. DOI: [10.1007/s12013-009-9075-2](https://doi.org/10.1007/s12013-009-9075-2).
- [214] Robert W. Style, Rostislav Boltanskiy, Guy K. German, Callen Hyland, Christopher W. MacMinn, Aaron F. Mertz, Larry A. Wilen, Ye Xu, and Eric R. Dufresne. "Traction force microscopy in physics and biology." In: *Soft Matter* 10 (23 2014), pp. 4047–4055. DOI: [10.1039/C4SM00264D](https://doi.org/10.1039/C4SM00264D).
- [215] Cornel Sultan, Dimitrije Stamenović, and Donald E. Ingber. "A Computational Tensegrity Model Predicts Dynamic Rheological Behaviors in Living Cells." In: *Annals of Biomedical Engineering* 32.4 (2004), pp. 520–530. DOI: [10.1023/b:abme.0000019171.26711.37](https://doi.org/10.1023/b:abme.0000019171.26711.37).
- [216] S. Suresh, J. Spatz, J.P. Mills, A. Micoulet, M. Dao, C.T. Lim, M. Beil, and T. Seufferlein. "Connections between single-cell biomechanics and human disease states: gastrointestinal cancer and malaria." In: *Acta Biomaterialia* 1.1 (2005), pp. 15–30. DOI: [10.1016/j.actbio.2004.09.001](https://doi.org/10.1016/j.actbio.2004.09.001).

- [217] Subra Suresh. "Biomechanics and biophysics of cancer cells." In: *Acta Biomaterialia* 3.4 (2007), pp. 413–438. DOI: [10.1016/j.actbio.2007.04.002](https://doi.org/10.1016/j.actbio.2007.04.002).
- [218] Tatyana M. Svitkina, Alexander B. Verkhovskiy, Kyle M. McQuade, and Gary G. Borisy. "Analysis of the Actin–Myosin II System in Fish Epidermal Keratocytes: Mechanism of Cell Body Translocation." In: *The Journal of Cell Biology* 139.2 (1997), pp. 397–415. DOI: [10.1083/jcb.139.2.397](https://doi.org/10.1083/jcb.139.2.397).
- [219] Chiara Tamiello, Antonetta B. C. Buskermolen, Frank P. T. Baaijens, Jos L. V. Broers, and Carlijn V. C. Bouten. "Heading in the Right Direction: Understanding Cellular Orientation Responses to Complex Biophysical Environments." In: *Cellular and Molecular Bioengineering* 9.1 (2015), pp. 12–37. DOI: [10.1007/s12195-015-0422-7](https://doi.org/10.1007/s12195-015-0422-7).
- [220] J. L. Tan, J. Tien, D. M. Pirone, D. S. Gray, K. Bhadriraju, and C. S. Chen. "Cells lying on a bed of microneedles: An approach to isolate mechanical force." In: *Proceedings of the National Academy of Sciences* 100.4 (2003), pp. 1484–1489. DOI: [10.1073/pnas.0235407100](https://doi.org/10.1073/pnas.0235407100).
- [221] Yee Han Tee et al. "Cellular chirality arising from the self-organization of the actin cytoskeleton." In: *Nature Cell Biology* 17.4 (2015), pp. 445–457. DOI: [10.1038/ncb3137](https://doi.org/10.1038/ncb3137).
- [222] Gawain Thomas, Nancy A. Burnham, Terri Anne Camesano, and Qi Wen. "Measuring the Mechanical Properties of Living Cells Using Atomic Force Microscopy." In: *Journal of Visualized Experiments* 76 (2013). DOI: [10.3791/50497](https://doi.org/10.3791/50497).
- [223] D'Arcy Wentworth Thompson. *On growth and form*. University press, 1917. DOI: [10.5962/bhl.title.11332](https://doi.org/10.5962/bhl.title.11332).
- [224] Gunnar Tibert and Sergio Pellegrino. "Deployable Tensegrity Masts." In: *44th AIAA/ASME/ASCE/AHS/ASC Structures, Structural Dynamics, and Materials Conference*. American Institute of Aeronautics and Astronautics, 2003. DOI: [10.2514/6.2003-1978](https://doi.org/10.2514/6.2003-1978).
- [225] SP Timoshenko and JN Goodier. *Theory of Elasticity 3rd ed.* 1967, p. 142.
- [226] Minoru Tomizawa, Masaaki Ebara, Hiromitsu Saisho, Shigeru Sakiyama, and Masatoshi Tagawa. "Irradiation with ultrasound of low output intensity increased chemosensitivity of subcutaneous solid tumors to an anti-cancer agent." In: *Cancer Letters* 173.1

(2001), pp. 31–35. ISSN: 0304-3835. DOI: [https://doi.org/10.1016/S0304-3835\(01\)00687-5](https://doi.org/10.1016/S0304-3835(01)00687-5).

- [227] D. De Tommasi, G. Puglisi, and G. Saccomandi. “Multiscale mechanics of macromolecular materials with unfolding domains.” In: *Journal of the Mechanics and Physics of Solids* 78 (2015), pp. 154–172. DOI: [10.1016/j.jmps.2015.02.002](https://doi.org/10.1016/j.jmps.2015.02.002).
- [228] D. De Tommasi, N. Millardi, G. Puglisi, and G. Saccomandi. “An energetic model for macromolecules unfolding in stretching experiments.” In: *Journal of The Royal Society Interface* 10.88 (2013), pp. 20130651–20130651. DOI: [10.1098/rsif.2013.0651](https://doi.org/10.1098/rsif.2013.0651).
- [229] Abhishek Tondon and Roland Kaunas. “The Direction of Stretch-Induced Cell and Stress Fiber Orientation Depends on Collagen Matrix Stress.” In: *PLoS ONE* 9.2 (2014). Ed. by Sanjay Kumar, e89592. DOI: [10.1371/journal.pone.0089592](https://doi.org/10.1371/journal.pone.0089592).
- [230] Caroline Uhler and G. V. Shivashankar. “Regulation of genome organization and gene expression by nuclear mechanotransduction.” In: *Nature Reviews Molecular Cell Biology* 18 (Oct. 2017), p. 717.
- [231] Michael J. Unterberger, Kurt M. Schmoller, Christine Wurm, Andreas R. Bausch, and Gerhard A. Holzapfel. “Viscoelasticity of cross-linked actin networks: Experimental tests, mechanical modeling and finite-element analysis.” In: *Acta Biomaterialia* 9.7 (2013), pp. 7343–7353. DOI: [10.1016/j.actbio.2013.03.008](https://doi.org/10.1016/j.actbio.2013.03.008).
- [232] K.Yu. Volokh, O. Vilnay, and M. Belsky. “Tensegrity architecture explains linear stiffening and predicts softening of living cells.” In: *Journal of Biomechanics* 33.12 (2000), pp. 1543–1549. DOI: [10.1016/S0021-9290\(00\)00157-3](https://doi.org/10.1016/S0021-9290(00)00157-3).
- [233] Huicong Wang, Wallace Ip, Raymond Boissy, and Edward S. Grood. “Cell orientation response to cyclically deformed substrates: Experimental validation of a cell model.” In: *Journal of Biomechanics* 28.12 (1995), pp. 1543–1552. DOI: [10.1016/0021-9290\(95\)00101-8](https://doi.org/10.1016/0021-9290(95)00101-8).
- [234] James H.-C. Wang, Pascal Goldschmidt-Clermont, Jeremiah Wille, and Frank C.-P. Yin. “Specificity of endothelial cell reorientation in response to cyclic mechanical stretching.” In: *Journal of Biomechanics* 34.12 (2001), pp. 1563–1572. DOI: [10.1016/S0021-9290\(01\)00150-6](https://doi.org/10.1016/S0021-9290(01)00150-6).

- [235] N Wang, J. Butler, and D. Ingber. "Mechanotransduction across the cell surface and through the cytoskeleton." In: *Science* 260.5111 (1993), pp. 1124–1127. DOI: [10.1126/science.7684161](https://doi.org/10.1126/science.7684161).
- [236] N. Wang and D.E. Ingber. "Control of cytoskeletal mechanics by extracellular matrix, cell shape, and mechanical tension." In: *Biophysical Journal* 66.6 (1994), pp. 2181–2189. DOI: [10.1016/s0006-3495\(94\)81014-8](https://doi.org/10.1016/s0006-3495(94)81014-8).
- [237] N. Wang, I. M. Tolic-Norrelykke, J. Chen, S. M. Mijailovich, J. P. Butler, J. J. Fredberg, and D. Stamenovic. "Cell prestress. I. Stiffness and prestress are closely associated in adherent contractile cells." In: *AJP: Cell Physiology* 282.3 (2001), pp. C606–C616. DOI: [10.1152/ajpcell.00269.2001](https://doi.org/10.1152/ajpcell.00269.2001).
- [238] N. Wang, K. Naruse, D. Stamenovic, J. J. Fredberg, S. M. Mijailovich, I. M. Tolic-Norrelykke, T. Polte, R. Mannix, and D. E. Ingber. "Mechanical behavior in living cells consistent with the tensegrity model." In: *Proceedings of the National Academy of Sciences* 98.14 (2001), pp. 7765–7770. DOI: [10.1073/pnas.141199598](https://doi.org/10.1073/pnas.141199598).
- [239] Ning Wang, Jessica D. Tytell, and Donald E. Ingber. "Mechanotransduction at a distance: mechanically coupling the extracellular matrix with the nucleus." In: *Nature Reviews Molecular Cell Biology* 10.1 (2009), pp. 75–82. DOI: [10.1038/nrm2594](https://doi.org/10.1038/nrm2594).
- [240] Clare M. Waterman-Storer and E.D. Salmon. "Actomyosin-based Retrograde Flow of Microtubules in the Lamella of Migrating Epithelial Cells Influences Microtubule Dynamic Instability and Turnover and Is Associated with Microtubule Breakage and Treadmilling." In: *The Journal of Cell Biology* 139.2 (1997), pp. 417–434. DOI: [10.1083/jcb.139.2.417](https://doi.org/10.1083/jcb.139.2.417).
- [241] Zhensong Wei, Vikram S Deshpande, Robert M McMeeking, and Anthony G Evans. "Analysis and interpretation of stress fiber organization in cells subject to cyclic stretch." In: *Journal of biomechanical engineering* 130.3 (2008), p. 031009.
- [242] Sylvie Wendling, Christian Oddou, and Daniel Isabey. "Stiffening Response of a Cellular Tensegrity Model." In: *Journal of Theoretical Biology* 196.3 (1999), pp. 309–325. DOI: [10.1006/jtbi.1998.0841](https://doi.org/10.1006/jtbi.1998.0841).
- [243] H. M. Westergaard. *Theory of Elasticity and Plasticity*. Harvard University Press, 1952. DOI: [10.4159/harvard.9780674436923](https://doi.org/10.4159/harvard.9780674436923).
- [244] Inc. Wolfram Research. *Mathematica*. Wolfram Research, Inc., 2015.

- [245] Charles W. Wolgemuth and Pilhwa Lee. "Crawling Cells Can Close Wounds Without Purse Strings or Signaling." In: *Biophysical Journal* 100.3 (2011), 440a–441a. DOI: [10.1016/j.bpj.2010.12.2594](https://doi.org/10.1016/j.bpj.2010.12.2594).
- [246] Andrew K.W. Wood and Chandra M. Sehgal. "A Review of Low-Intensity Ultrasound for Cancer Therapy." In: *Ultrasound in Medicine & Biology* 41.4 (2015), pp. 905–928. DOI: [10.1016/j.ultrasmedbio.2014.11.019](https://doi.org/10.1016/j.ultrasmedbio.2014.11.019).
- [247] Wang Xi, Christine K. Schmidt, Samuel Sanchez, David H. Gracias, Rafael E. Carazo-Salas, Richard Butler, Nicola Lawrence, Stephen P. Jackson, and Oliver G. Schmidt. "Molecular Insights into Division of Single Human Cancer Cells in On-Chip Transparent Microtubes." In: *ACS Nano* 10.6 (2016), pp. 5835–5846. DOI: [10.1021/acsnano.6b00461](https://doi.org/10.1021/acsnano.6b00461).
- [248] H Xiao and LS Chen. "Hencky's elasticity model and linear stress-strain relations in isotropic finite hyperelasticity." In: *Acta Mechanica* 157.1 (2002), pp. 51–60.
- [249] Guang-Kui Xu, Xi-Qiao Feng, and Huajian Gao. "Orientations of Cells on Compliant Substrates under Biaxial Stretches: A Theoretical Study." In: *Biophysical Journal* 114.3 (2018), pp. 701–710. DOI: [10.1016/j.bpj.2017.12.002](https://doi.org/10.1016/j.bpj.2017.12.002).
- [250] Guang-Kui Xu, Bo Li, Xi-Qiao Feng, and Huajian Gao. "A Tensegrity Model of Cell Reorientation on Cyclically Stretched Substrates." In: *Biophysical Journal* 111.7 (2016), pp. 1478–1486. DOI: [10.1016/j.bpj.2016.08.036](https://doi.org/10.1016/j.bpj.2016.08.036).
- [251] Wenwei Xu, Roman Mezencev, Byungkyu Kim, Lijuan Wang, John McDonald, and Todd Sulchek. "Cell Stiffness Is a Biomarker of the Metastatic Potential of Ovarian Cancer Cells." In: *PLoS ONE* 7.10 (2012). Ed. by Surinder K. Batra, e46609. DOI: [10.1371/journal.pone.0046609](https://doi.org/10.1371/journal.pone.0046609).
- [252] Hidetaka Yamaoka, Shinji Matsushita, Yoshitaka Shimada, and Taiji Adachi. "Multiscale modeling and mechanics of filamentous actin cytoskeleton." In: *Biomechanics and Modeling in Mechanobiology* 11.3-4 (2011), pp. 291–302. DOI: [10.1007/s10237-011-0317-z](https://doi.org/10.1007/s10237-011-0317-z).
- [253] Osman N. Yagurtcu, Jin Seob Kim, and Sean X. Sun. "A Mechanochemical Model of Actin Filaments." In: *Biophysical Journal* 103.4 (2012), pp. 719–727. DOI: [10.1016/j.bpj.2012.07.020](https://doi.org/10.1016/j.bpj.2012.07.020).

- [254] D. Zaccaria, D. Bigoni, G. Noselli, and D. Misseroni. "Structures buckling under tensile dead load." In: *Proceedings of the Royal Society A: Mathematical, Physical and Engineering Sciences* 467.2130 (2011), pp. 1686–1700. DOI: [10.1098/rspa.2010.0505](https://doi.org/10.1098/rspa.2010.0505).
- [255] Hu Zhang and Kuo-Kang Liu. "Optical tweezers for single cells." In: *Journal of The Royal Society Interface* 5.24 (2008), pp. 671–690. DOI: [10.1098/rsif.2008.0052](https://doi.org/10.1098/rsif.2008.0052).
- [256] Giuseppe Zurlo and Lev Truskinovsky. "Printing Non-Euclidean Solids." In: *Phys. Rev. Lett.* 119 (4 2017), p. 048001. DOI: [10.1103/PhysRevLett.119.048001](https://doi.org/10.1103/PhysRevLett.119.048001).
- [257] Giuseppe Zurlo and Lev Truskinovsky. "Inelastic surface growth." In: *Mechanics Research Communications* 93 (2018), pp. 174–179. DOI: [10.1016/j.mechrescom.2018.01.007](https://doi.org/10.1016/j.mechrescom.2018.01.007).